DEVELOPMENT OF A MICROFLUIDIC CAPILLARY ELECTROPHORESIS-MASS SPECTROMETRY PLATFORM FOR THE CHARACTERIZATION OF BIOTHERAPEUTIC PROTEINS

Erin Anne Redman

A dissertation submitted to the faculty at the University of North Carolina at Chapel Hill in partial fulfillment of the requirements for the degree of Doctor of Philosophy in the Department of Chemistry.

Chapel Hill
2016

Approved by:

J. Michael Ramsey

James W. Jorgenson

Leslie M. Hicks

Anne M. Taylor

Glenn M. Walker

ABSTRACT

Erin Anne Redman: Development of a Microfluidic Capillary Electrophoresis-Mass Spectrometry Platform for the Characterization of Biotherapeutic Proteins
(Under the direction of J. Michael Ramsey)

This work describes the development of a mass spectrometry (MS) compatible microfluidic capillary electrophoresis (CE) analysis platform capable of characterizing large biomolecules. Initial efforts focused on developing a method for performing highly efficient CE separations of intact proteins with on-line MS analysis. Surface coating technology was optimized for the analysis of intact proteins. The ability to reproducibly generate uniform surface coatings for CE separations of biomolecules was paramount to achieving efficient separations of these large molecules. The effectiveness of the intact protein coating was demonstrated by analyzing whole blood lysate. The microfluidic CE-MS method proved to be a simple and rapid way to assess hemoglobin glycation and the results compared well with a commercially available technique used to measure glycated hemoglobin. Further application of this technology involved characterizing monoclonal antibody (mAb) based biotherapeutics at the intact level. The size and complexity of these molecules makes them difficult to analyze at the intact level. It was determined that maintaining some of the structural conformation of the mAbs was vital to achieving separation of intact variants. Thus, a background electrolyte was optimized to balance preserving antibody conformation and maximizing MS signal. In conjunction with the optimized surface chemistry, this resulted in the first MS compatible liquid phase separation of intact charge variants of mAbs. This technology was then adapted to perform other levels of antibody

characterization. Both limited proteolysis and disulfide bond reduction were evaluated for a middle-up analysis of mAbs. Analysis of mAb fragments generated through disulfide bond reduction resulted in more reliable characterization of the molecules analyzed. Although the surface chemistry described in this work was developed for analyzing intact proteins, it has also proven effective for analyzing smaller molecules. The technology was used to perform bottom-up mapping experiments to generate in-depth information about biomolecules. It was determined that in many cases the resulting microfluidic CE-MS data was comparable to that achieved through LC-MS analysis, but with significantly shorter analysis times. The overall result of this work is a single microfluidic CE-MS analysis platform that is capable of rapidly performing multiple levels of protein characterization.

TABLE OF CONTENTS

LIST OF ABBREVIATIONS

ADC	Antibody Drug Conjugate
APDIPES	3-(aminopropyl)di-isopropyl-ethoxysilane
APS	Aminopropylsilane
APTES	3-aminopropyltriethoxysilane
BGE	Background Electrolyte
CE	Capillary Electrophoresis
CGE	Capillary Gel Electrophoresis
CVD	Chemical Vapor Deposition
CZE	Capillary Zone Electrophoresis
D	Molecular Diffusion Coefficient
Da	Dalton
D_{app}	Apparent Diffusion Coefficient
DAR	Drug-to-Antibody Ratio
Δ	Efficiency Coefficient
DTT	Dithiothreitol
EACA	ε-amino-caproic acid
EDTA	ethylenediaminetetraacetic acid
EI	Extracted Ion
EK	Electrokinetic
EOF	Electroosmotic Flow
ESI	Electrospray Ionization
F	Fucose

Fab	Antigen Binding Fraction
Fc	Crystallizable Fraction
FWHH	Full Width at Half Height
G	Galactose
GlcNAc	N-acetylhexosamine
HSA	Human Serum Albumin
Hb	Hemoglobin
HbA1c	Glycated Hemoglobin
HC	Antibody Heavy Chain
HCP	Host Cell Protein
HD	Hydrodynamic
HDX	Hydrogen Deuterium Exchange
HIC	Hydrophobic Interaction Chromatography
HPLC	High Performance Liquid Chromatography
IAM	Iodoacetamide
iCE	Imaging Capillary Electrophoresis
IEF	Isoelectric Focusing
IEX	Ion Exchange Chromatography
IgG	γ-immunoglobulins
IMS	Ion Mobility Spectroscopy
K	Lysine (single letter amino acid code)
LC	Antibody Light Chain
LIF	Laser Induced Fluorescence

M	Mannose
m/z	Mass to Charge Ratio
mAb	Monoclonal Antibody
MALDI	Matrix Assisted Laser Desorption Ionization
MS	Mass Spectrometry
N	Number of Theoretical Plates
n_c	Peak Capacity
NHS	n-hydroxysuccinimide
NHS-PEG_{450}	methyl-terminated polyethylene glycol n-hydroxy succinimide ester
PEG	Polyethylene Glycol
PTM	Post Translational Modification
RPLC	Reverse Phase Liquid Chromatography
Rs	Resolution
SPE	Solid Phase Extraction
TCEP	*tris*(2-carboxyethyl)phosphine
TETA	triethylenetetramine
tITP	Transient Isotachophoresis
μ_{app}	Apparent Electrophoretic Mobility
μ_{EOF}	Magnitude of Electroosmotic Flow
μ_{EP}	Electrophoretic Mobility
v	linear velocity
σ_s^2	Spatial Variance
σ_t^2	Temporal Variance

LIST OF FIGURES

LIST OF TABLES

CHAPTER 1: INTRODUCTION

1.1 Project History and Motivation

In the early 1990s, Professor Ramsey's group at Oak Ridge National Lab was one of the pioneering labs developing microfluidic capillary electrophoresis (CE) technology. Efforts to interface this separation technology with mass spectrometry (MS) carried over to the University of North Carolina in 2004. The success of this was dependent on creating a reliable device design for interfacing with mass spectrometry and then developing surface chemistry to optimize separation performance. The basic device design used for the work presented here was developed in the late 2000s and was shown to effectively couple the CE separation with electrospray ionization (ESI) and mass spectrometry.[1] With a successful CE-ESI chip design in place, research efforts shifted to creating stable surface chemistries to optimize the performance of the CE separation. A gas phase surface treatment strategy depositing a cationic coating on the device channels resulted in separation efficiencies that approached the theoretical limit of CE separations.[2] Subsequent functionalization of this cationic surface with polyethylene glycol chains generates the ability to affect the separation resolution by tuning the electroosmotic flow. Much of my work focused on further developing one of these polyethylene glycol surface coatings to perform CE separations of intact proteins.

Separating intact proteins can be a very useful approach to analyzing biological systems. One of the major challenges associated with performing intact protein separations is that proteins exist as a heterogeneous population. These variants are usually due to post translational

modifications (PTMs) that occur in a biological system. Often the modifications do not result in a drastic change in net charge or mass so separating the different protein variants is quite challenging. Many commonly used analytical techniques are not well suited to this type of analysis, or do not always generate sufficient selectivity and specificity. While reversed-phase liquid chromatography is regularly employed for a wide range of applications, when used for intact protein analysis it suffers from poor reproducibility, carry over, and poor peak shape. Extreme measures such as high column temperatures, high pressures, and harsh solvents can improve the analysis, but can be detrimental to the proteins.[3–5] This limits its effectiveness as a technique for separating large biomolecules. CE is particularly well suited for this because its separation mechanism is based partly on analyte charge, does not rely on a stationary phase, and can generate very high quality separations. Further integration of this separation technique with mass spectrometry through electrospray ionization represents an incredibly powerful platform for analyzing biomolecules. The following sections outline the principles of CE, the motivation for using microfluidic technology to interface CE with mass spectrometry, and its utility in analyzing biological samples.

1.2 Theory of Capillary Zone Electrophoresis

1.2.1 Separation mechanism

Electrophoresis can be briefly defined as the motion of charged analytes in a liquid when exposed to an electric field. The phenomenon of electrophoresis has been exploited in various separation techniques such as gel electrophoresis, paper electrophoresis, and isoelectric focusing (IEF).[6] Perhaps the simplest version of an electrophoretic separation is zone electrophoresis where ions are separated in free solution. However, one of the major problems encountered with

this technique is the generation of thermal gradients in the solution due to Joule heating. This significantly limits the separation performance by causing band broadening. A solution to this problem was not realized until the 1980s when zone electrophoresis was performed in a narrow-bore glass capillary which proved to dissipate heat more effectively.[7–9] Higher voltages could be used to increase the separation performance and capillary zone electrophoresis (CZE) was demonstrated as an impactful analytical technique. Since then CZE has become an important tool in industrial labs as well as research labs.

The basic experimental set-up for CZE can be very simple and is often amenable to customization in labs. As illustrated in Figure 1.1, the technique utilizes a capillary that connects inlet and outlet reservoirs containing a buffer solution, a voltage source, and a mode of detection. When a potential is applied to the reservoirs an electric field is generated within the capillary. Once sample is injected, analyte ions separate according to their electrophoretic mobility. The electrophoretic mobility (μ_{EP}) of an analyte is a function of the charge on the molecule and its hydrodynamic radius, and is described by the following equation[6,10,11]:

$$\mu_{EP} = \frac{q}{6\pi\eta a} \tag{1.1}$$

where q is the charge on the molecule, η is the viscosity of the buffer, and a is the hydrodynamic radius of the molecule. Thus, the separation mechanism is based on the charge of the analytes in addition to their conformation in solution.

Another phenomenon that factors into CZE separations is electroosmosis. As illustrated in Figure 1.2, an ionic layer forms at the inner wall of the capillary. In the case of a bare silica surface, negatively charged silanol groups attract cationic buffer components to form the

relatively static Stern layer. A second layer of mobile cations forms above the Stern layer creating a positive charge density that dissipates exponentially into the bulk solution. This is termed the diffuse layer, and together the Stern layer and diffuse layer are referred to as the double layer.[6,10,11] When a potential is applied as indicated in Figure 1.2, cations in the diffuse layer will migrate toward the cathode. This mass migration of ions generates bulk fluid flow in the capillary that is called electroosmotic flow (EOF). The movement of analytes during the separation is a function of not only the magnitude of their μ_{EP}, but also the magnitude of the EOF (μ_{EOF}). This is represented as apparent mobility (μ_{app}) and defined as[6,7,10]:

$$\mu_{app} = \mu_{EP} + \mu_{EOF} \tag{1.2}$$

Because it affects how analytes migrate during analysis, the EOF magnitude can have significant effects on the CE separation. Thus, characterizing and optimizing EOF is an important factor during CE method development.

1.2.2 Performance of CE as a separation technique

A metric for describing the performance of a separation technique is to describe the separation efficiency, which is often represented by the number of theoretical plates (*N*) available for separation.[9,12] This term is derived from the use of fractionating columns where the number of physical plates in the distillation column directly impacted the distillation process; a higher number of plates resulted in a better distillation. With current separation technology, N refers to a theoretical reaction site within a separating medium rather than a physical entity. N can be

determined from a peak in a separation based on the migration time (t) and the variance of the peak:

$$N = \frac{t^2}{\sigma_t^2} \tag{1.3}$$

where σ_t^2 is the temporal variance of the band.[6,13,14]

According to CE theory, analyte diffusion is the only source of band broadening for a theoretically optimal CE separation.[8,9,12] Therefore, CE should be able to produce very narrow analyte bands and, as a result, very high efficiency separations. According to the Einstein-Smoluchowski equation,[6,11] band broadening in a diffusion limited CE separation can be described as:

$$\sigma_s^2 = 2Dt \tag{1.4}$$

where σ_s^2 is the spatial variance of the analyte band, D is the molecular diffusion coefficient, and t is the migration time of the analyte. An apparent diffusion coefficient (D_{app}) can be calculated from a peak in a CE separation. After measuring the *FWHH* of the peak, Equation 1.5 is used to calculate the temporal variance:

$$\sigma_t^2 = \left(\frac{FWHH}{2\sqrt{2\ln 2}}\right) \tag{1.5}$$

where *FWHH* is the width of the peak at half its height and σ_t^2 is temporal variance. The migration time, velocity, and temporal variance are then used to determined D_{app} according to Equation 1.6:

$$D_{app} = \frac{\sigma_t^2 v^2}{2t} \tag{1.6}$$

where *t* is the migration time and *v* is the linear velocity of the analyte. The ratio of D_{app} to *D* can be a useful metric for evaluating CE performance which has been defined as Δ:[2]

$$\Delta = \frac{D_{app}}{D} \tag{1.7}$$

As compared to using N, the Δ value is more indicative of the actual CE separation performance relative to the theoretical optimum as it is independent of variable experimental parameters, such as capillary length, applied voltage, and analyte mobility. For a theoretically optimal CE separation, D_{app} is equal to the molecular diffusion coefficient of the analyte and the Δ value equals 1. Any additional band broadening in the separation would result in a D_{app} value greater than the molecular diffusion coefficient and a Δ value >1.[11,15,16] Some of these sources of band broadening include injection broadening, areas of dead volume, analyte adsorption to the capillary wall, and poorly applied surface coatings.

Δ can be related back to N through the following relationship:

$$N_{optimal} = \Delta N_{observed} \tag{1.8}$$

Thus, the optimal separation efficiency is decreased by a factor of $1/\Delta$ when excess band broadening is present in the CE system. The following outlines the solutions developed to minimize sources of band broadening and achieve near diffusion limited CE separations.

1.3 Microfluidic platforms for electrophoretic separations

The first demonstrations of zone electrophoresis separations in microfluidic channels occurred little more than 10 years after Jorgenson, et al. first demonstrated CZE, and was referred to as "capillary electrophoresis on a chip."[15–22] As with capillaries, the reduced dimensions of the microfluidic channels effectively dissipated heat resulting from Joule heating and devices could be operated at higher field strengths to improve separation efficiency.[17,19,23] The devices were fabricated from planar silicon or glass substrates and described as micro-total analysis systems because they incorporated several functions into the device design including injection, separation, and detection.[16–18,22,24] This ability to incorporate multiple functional elements into the device design is a notable benefit of using a microfluidic platform.

1.3.1 Microfluidic CE-ESI device design

A typical channel architecture for the microfluidic CE-ESI devices is provided in Figure 1.3. The devices are fabricated from planar glass substrates using standard photolithography techniques and wet chemical etching. This creates a flat, almost rectangular channel cross section as compared to the circular cross section of capillaries. This planar channel shape, however, is more effective at dissipating heat from Joule heating. Further details about the fabrication process can be found in Appendix 1. A completed device is pictured in Figure 1.4a. The device design incorporates several functional elements including sample handling, a serpentine

separation channel, and an integrated ESI emitter. These elements have all been optimized to minimize on-column and extra-column band broadening.

The functional element for performing sample handling takes the form of a simple injection cross. This is a very common strategy used in microfluidics and has been proven effective in performing rapid, reproducible injections of narrow sample bands.[1,20,23] The speed of the injection is a key factor in preserving separation efficiency. For instance, capillary electrophoresis systems usually rely on physically moving the inlet of the capillary in and out of vials containing buffer and sample. This can result in band broadening because the injected sample plug has time to broaden in the capillary via longitudinal diffusion before voltage is re-applied for the separation. However, with this microfluidic system the time between injection and separation is significantly smaller because fluid is being manipulated directly on the device. This minimizes distortion of the injection plug and band broadening due to injection.

The length of the separation channel in Figure 1.3 from the injection cross to the ESI emitter is 23 cm. To maintain a small footprint, the channel takes six turns before reaching the ESI emitter. The small radius of curvature of these turns can lead to additional band broadening from geometric dispersion of the analyte bands. This is sometimes referred to as the racetrack effect. Briefly, molecules closer to the internal radius of curvature travel around the curve faster than those closer to the exterior radius of curvature. To compensate for this, the turns are asymmetrically tapered in width to minimize band broadening contributions from varying path lengths around the turn.[19,20,23,25] The inset of Figure 1.3 (Asymmetrically tapered turns) shows the mask design for the tapered turns. After isotropic etching, the channel width differential between the straight channels and the curvature of the turn is 2.8x. Shortly before the ESI emitter, the separation channel intersects the pumping channel (Integrated ESI emitter inset).

This channel serves to establish bulk fluid flow for sustaining ESI. Additionally, reservoir 4 contains the terminating electrode to complete the electric circuit for the CZE separation.

Perhaps the greatest benefit of the microfluidic platform is the ability to directly integrate the ESI emitter into the device design. Integrating CZE separations with ESI-MS is not straightforward. The interface must supply the necessary potential to generate a field strength for the separation while also satisfying conditions for effective ESI. Most importantly it must maintain the efficiency of the separation. Fulfilling the first two criteria involves establishing electrical contact with the liquid in the capillary. Since the capillary itself is not conductive, the electrical connection must be made with some other conductive medium. This could be a metal fitting or an electrolyte solution. With inner diameters typically on the order of ≤100 μm making these connections is not trivial. The total column volume could easily be less than 10 μL and, therefore, any connection to the capillary must be extremely precise to avoid introducing significant dead volume. Strategies for interfacing capillary zone electrophoresis to ESI-MS have utilized sheath flow interfaces,[26–28] metal coated ESI emitters,[29–31] liquid junctions,[32] and porous tip emitters.[33] However many of these suffer from poor stability and short lifetimes, or result in extra column band broadening from areas of dead-volume in the interface or dilution with the sheath liquid. There are many examples in the literature of using microfluidic CE devices with ESI needles or pulled capillary emitter tips glued to the channel terminus.[34–37] While functional, these approaches do not necessarily solve the issues encountered with capillary interfaces and also complicate device fabrication.

An elegant alternative to this utilizes channel architecture and the exterior surface of the device to form the ESI emitter.[1,38] After the separation channel intersects the pumping channel, it terminates at the corner of the device and is open to atmosphere. Bulk fluid flow for establishing

ESI can either be generated through an electroosmotic pump or by simply applying a head pressure to the pumping reservoir. When voltage is applied to the chip, this channel terminus is held at a potential that can be optimized for establishing ESI. Experimentally we have found this potential to be optimal at approximately 3.5 kV. A photograph of ESI generated off the corner of a microfluidic CE-ESI device is provided in Figure 1.4b. Initial characterization of the integrated ESI interface determined that it performs comparably in terms of signal intensity and stability to a commercial nanospray emitter powered by a syringe pump.[1] Because the channels are seamlessly interconnected in the microfluidic platform, the only dead volume associated with this interface is the space between the intersection of the separation and pumping channels and the exterior surface of the device. This channel segment is typically ≤100 μm in length, which equates to a 70 pL or less area of dead volume. This is less than 0.05% of the total column volume and does not significantly contribute to band broadening. Thus the seamless incorporation of multiple functional elements in the device design through unique channel architectures resulted in the development of a highly efficient microfluidic CE-ESI-MS interface.

1.3.2 Injection strategies for microfluidic CE-MS

A variety of sample injection methods have been developed for microfluidic devices. Both electrokinetic and hydrodynamic flow based injection methods are common and have been demonstrated for a variety of channel architectures. These include valve-less electrokinetic switching,[16–18] gated,[15,20,23] pinched,[39–41] multi tee and offset tee[42,43] electrokinetic injections, hydrostatic injections,[44–46] and off-chip pumping to name a few.[22,47–51] The injection schemes used most frequently in the Ramsey lab for performing microfluidic CE-MS analysis are gated

electrokinetic injections and hydrodynamic flow based injections. Both strategies are utilized in the work described in this document and will be briefly discussed here.

Electrokinetic injections (EK) are performed through electrical manipulation of ions in the sample and back ground electrolyte (BGE). As depicted in Figure 1.5a, when voltage is applied, ions in the sample migrate from the top reservoir and are diverted to waste to form the gate. Analyte ions are injected by balancing the potentials of the side arms, directing the ions into the separation channel. A sample plug is formed by switching the electric potentials back to the gated position and the analyte ions then separate via zone electrophoresis. The amount injected can be varied by simply adjusting the duration for which the voltages remain in the "inject" configuration. This injection strategy has the benefit of being able to be performed very rapidly. Distortion of the sample plug is minimized so very high separation efficiencies can be achieved. One of the limitations of the gated EK injection is that it is biased based on the electrophoretic mobility of the analyte ions. For analytes that have very similar mobilities, this bias may not be significant enough to affect the analysis, but it becomes more pronounced with more heterogeneous samples whose analytes span a wide range of mobilities, such as tryptic digests of proteins or small molecule metabolites. Another limitation of the gated EK injection is the limited ability to utilize concentration enhancement techniques. Without this capability, CE-MS analysis can suffer from poor sensitivity due to the small amounts of sample injected.

An alternative to the gated EK injection is a hydrodynamic (HD) flow based injection. This injection approach relies on pressure driven flow rather than voltage to manipulate sample ions. As seen in Figure 1.5b, when pressure is applied to the top and side reservoirs, sample solution is forced down the separation channel and to the waste reservoir. Isolation of the sample plug is accomplished by applying head pressure to just the top reservoir and then voltage is

applied to perform the CZE separation. The amount injected is controlled by increasing the duration of the loading step or increasing the pressure used for injection. Because the sample plug is delivered through hydrodynamic flow there is no electrophoretic mobility based bias. Another significant advantage of HD injections is that they make online sample concentration techniques feasible, such as transient isotachophoresis (tITP).

1.4 Surface Coatings for CE-MS.

Surface coatings are extremely important for CE analysis to prevent analyte adsorption and control the EOF. An issue affecting separation efficiency of CE is adsorption of biomolecules to the channel wall through electrostatic and hydrophobic interactions. A common approach to assuage this is to use a surface coating.[52–55] For CE-MS analysis of biomolecules these coatings are often neutral polymers or cationic in nature to prevent analyte adsorption through electrostatic repulsion. Polybrene, polyethyleneimine, polyacrylamide, cellulose, dextran, poly(vinyl alcohol), and silane based coatings have been reported in the literature for use with CE-MS.[55–63] However, when compared with theoretical separation performance for CE, it can be determined that most separations presented in the literature could be improved several fold.[2] For instance, a polyacrylamide based coating was recently reported.[62] Δ values were calculated from the electropherograms and the average Δ was found to be 5.5. This indicates that there is significant band broadening in the CE system. If surface coatings are not applied uniformly, electroosmosis will be inconsistent throughout the capillary. This creates pressure gradients during the CE separation which degrades the separation efficiency through Taylor dispersion. Therefore, the ideal surface coating for CE-MS prevents analyte adsorption, is easily and reproducibly applied to generate uniform electroosmosis, and will not introduce background during MS analysis.

1.4.1 Coating technology for microfluidic CE-MS

Around 2010 the Ramsey group began experimenting with applying surface coatings for CE-MS in the gas phase. A method was developed based on previously published work[64] to deposit cationic aminopropylsilanes (APS) on the microfluidic channel surfaces via chemical vapor deposition (CVD). This technique proved to produce highly uniform, dense coatings. APS coatings using trifunctional 3-aminopropyltriethoxysilane (APTES) and monofunctional 3-aminopropyldiisopropylethoxysilane (APDIPES) have generated near diffusion limited separations of fluorescent dyes with Δ values of 1.2 and 1.09 for APTES and APDIPES, respectively.[2] Analyses of peptide and protein standards using an APDIPES coating indicate that the APS surface prevents adsorption of biomolecules and maintains separation efficiency. Figure 1.6 shows the separation of bradykinin, methionine-enkephalin, thymopentin, and angiotensin II, four peptides commonly used to characterize the performance of our devices. The average Δ value for the peptides is 1.4 with an average efficiency of 6.8×10^5 plates, and according to Equation 1.8 theoretically this could be further improved to 9.5×10^5 plates. In comparison, most CE separations reported in the literature using coatings generate efficiencies below 200,000 plates for small molecules and in the tens of thousands for intact proteins.[54,56] Thus, the gas phase APS coating generates superior CE performance for biomolecules.

A characteristic of these coatings is that there is a high level of EOF. This reduces analysis time, but the resulting resolution is often insufficient to separate similar species. For CE analysis the resolution between analyte species can be characterized by the following equation[7]:

$$R_s = 0.177(\mu_{EP1} - \mu_{EP2})\sqrt{\frac{V}{\bar{D}(\bar{\mu}_{EP} + \mu_{EOF})}} \quad (1.9)$$

where $\mu_{EP1,2}$ are the electrophoretic mobilities of the analyte ions, $\bar{\mu}_{EP}$ is the average electrophoretic mobility, μ_{EOF} is the EOF magnitude, $\bar{D}$ is the average diffusion coefficient of the analytes and V is the applied voltage for separation. Based on this equation, R_s is maximized when the product μ_{EP} and μ_{EOF} is 0. However, this results in impractical migration times. An alternative approach is to suppress the EOF. The EOF magnitude can be affected by several factors including buffer ionic strength and pH, or through the use of buffer additives, such as surfactants. However, with CE-MS many of these approaches cannot be utilized due to the need to maintain MS compatibility.

In the Ramsey lab, the approach to reduce the EOF in the separation channel is to use surface chemistry rather than modifying the separation buffer so that it can remain simple and MS compatible. A novel modification to the APS coating has been developed to achieve EOF reduction. The APS coatings are reacted with polyethyleneglycol (PEG) chains as illustrated in Figure 1.7. The PEG chains are available in various lengths and terminate with an N-hydroxysuccinimide (NHS) ester that reacts spontaneously with the primary amine of the APS coating, forming an amide bond between the APS and PEG chain. Previous work determined that the degree of EOF suppression is dependent on the length of the PEG chain used; the longer the chain, the lower the EOF (unpublished data).[65]

As mentioned previously, a significant amount of separation resolution is necessary to successfully resolve proteins at the intact level since protein variants are often very similar in structure and net charge. Thus, as described by Equation 1.9, the EOF should be reduced to

maximize the R_s between similar species. Using this strategy, the APS-PEG combination that resulted in the highest degree of EOF reduction was chosen to be optimized for intact protein separations. The EOF reduction was characterized through microfluidic CE separations of fluorescent dyes using laser induced fluorescence (LIF) detection and chips without integrated ESI and 3 cm long separation channels. The APS-PEG_{450} coating was been found to reduce the EOF from approximately $9.5x10^{-4}$ cm^2/Vs to $0.8x10^{-4}$ cm^2/Vs. However, this coating scheme had not yet been successfully applied to microfluidic CE-ESI devices with longer separation channels. A modified coating procedure was developed that has successfully been used to coat microfluidic CE-ESI devices with separation channel lengths of up to 46 cm. The optimized coating procedure can be found in Appendix 2.

Figure 1.8 compares the separation of a five protein mixture (carbonic anhydrase I, hemoglobin, human serum albumin, cytochrome c, and lysozyme) using the APS and the optimized APS-PEG_{450} coating for intact protein separations. It should be noted that due to the EOF suppression, the APS-PEG_{450} separations were performed in reverse polarity in order to direct cations into the separation channel. As such, the migration times of the proteins are reversed compared to the separations performed with the APS coating. As theorized, suppressing the EOF increased the separation resolution by enhancing differences in apparent analyte mobility. From the separations in Figure 1.8a and b, a significant improvement in resolution can be seen between neighboring peaks. The APS-PEG_{450} device generated a resolution of 2.9 between cyt-c (Peak 5) and HSA (Peak 4) while the APS coated device resulted in a resolution of 1.5. Unresolved Hb species can be detected in the mass spectra of the β-Hb peak from the APS separation. As seen in Figure 1.8c the mass spectra of peaks 2a-2c spectrally combine to give the spectrum obtained from peak 2 of the APDIPES-based separation, indicating that these are the

unresolved charge variants detected in peak 2. Overall, the APS-PEG_{450} coating resulted in fast, highly efficient separations of intact proteins with improved resolution as compared to APDIPES. Additionally, as will be discussed later in the text, this low EOF coating has proven useful for a variety of analyte molecules ranging in size from large intact proteins to small metabolites.

1.5 Protein Biotherapeutics

Monoclonal antibody (mAb) based biotherapeutics are the specific targets for developing an analysis platform capable of performing high efficiency intact protein separations with on-line MS analysis. There are several analytical techniques available for separating intact mAb variants, but most are not MS compatible which makes identification of the variants difficult. In order to be used as a therapeutic agent the mAb must be rigorously characterized in order to ensure safety, efficacy, and potency. Post translational modifications can introduce a significant amount of heterogeneity in the final product, and it is likely that mixtures of multiple modifications will co-exist in finished products that may ultimately increase upon storage or degradation.[66–69] Consequently, it is critical to characterize mAbs at multiple levels (amino acid sequence to intact structure) to ensure clinically significant bioactivity, drug effectiveness, and quality.

Most therapeutic mAbs are γ-immunoglobulins (IgGs) with molecular weights of approximately 150 kDa.[66,67,70–72] IgGs have the familiar Y shaped structure depicted in Figure 1.9. This is formed by two light chains (LC) and two heavy chains (HC) at ~25 kDa and ~50 kDa, respectively. These chains are linked through noncovalent interactions as well as covalent disulfide bonds and the arrangement of these chains forms two main regions of the mAb: the crystallizable fraction (Fc) and the antigen-binding fraction (Fab).[66,67,70,73] IgGs are further

classified into four groups (IgG1-4) based on alterations in the Fc domain that typically manifest as differences in the pattern of disulfide linkages.[67,70,73] IgGs 1, 2 and 4 are commonly used as biotherapeutics.

Throughout cell culture production, purification, and storage, variations in the mAb structure can result from modifications at the primary and secondary structure level.[72,74] Such modifications may include disulfide bond scrambling, glycosylation, deamidation, pyroglutamate formation, C-terminal lysine truncation, oxidation, and amino acid substitutions/misincorporations, in addition to others. These can potentially impact the immunogenic properties of the mAb. Table 1.1 lists several of the common post translational modifications discussed in this document along with characteristic mass shifts and the effect on the net charge of the biomolecule at acidic pH. mAbs have not only charge heterogeneity, but also a significant amount of mass heterogeneity due to glycosylation. Glycosylation is an expected modification of antibodies that can significantly impact their immunogenic properties. A majority of IgG molecules will be glycosylated at a highly conserved site in the Fc domain. Glycosylation in the Fab domain is possible, but is less common.[70,75] These structures are often represented with colored shapes and letter abbreviations to more easily visualize and discuss the glycans. Figure 1.10 provides block diagrams as well as the abbreviations for some common glycan structures used throughout this document. IgG glycans are typically biantennary structures with a core fucose (F) residue and branches made up of mannose (M) and N-acetylhexosamine (GlcNAc) residues with 0, 1, or 2 terminal galactose residues (G).[66,67,70,75] The addition of sialic acids to the glycan structure is possible although it is relatively uncommon for Fc glycans.[66]

1.6 Summary

The following Chapters detail the use of the microfluidic CE-MS analysis platform for separating and analyzing intact proteins in addition to performing multiple levels of mAb characterization. Although the characterization of biotherapeutics was the overall goal, initial work focused on evaluating the separation quality with smaller blood proteins. From there intact mAb separations were investigated and methods developed to characterize the molecules at different levels of complexity. The results as a whole demonstrate that the analysis platform initially developed just for intact protein separations is capable of protein characterization from the peptide to intact level.

1.7 Figures and Tables

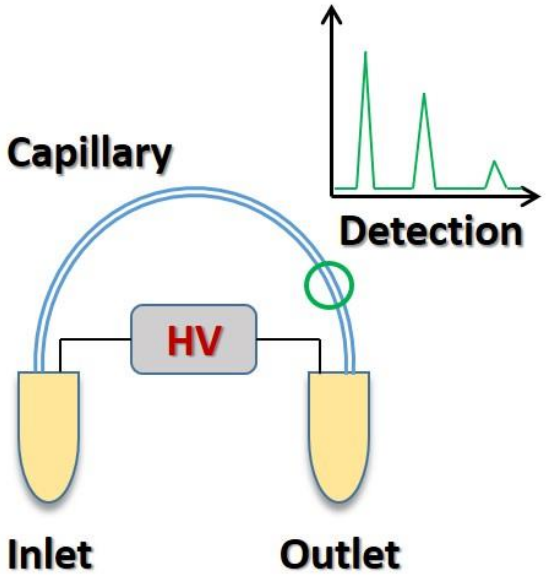

Figure 1.1: Schematic of a basic capillary electrophoresis experimental set-up. An inlet and outlet reservoir are required that are connected by a capillary and a high voltage power supply (HV). A detection window (green circle) is positioned shortly before the capillary terminates in the outlet reservoir.

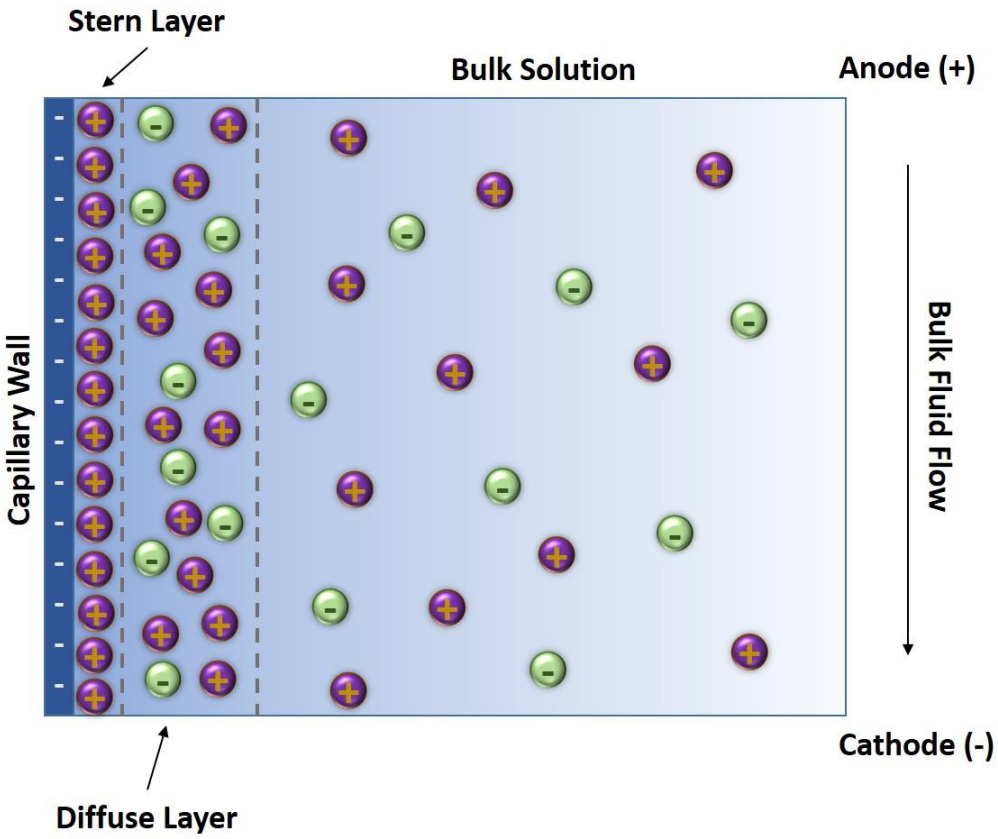

Figure 1.2: Diagram of the electric double layer formed at the wall of the capillary. An ionic layer forms at the inner wall of the capillary. For a bare silica surface, negatively charged silanol groups attract cationic buffer components to form the static Stern layer. A layer of cations forms above the Stern layer creating a positive charge density called the diffuse layer. Together the Stern layer and diffuse layer are referred to as the double layer. When a voltage is applied as cations in the diffuse layer migrate toward the cathode generating bulk fluid flow called electroosmotic flow (EOF).

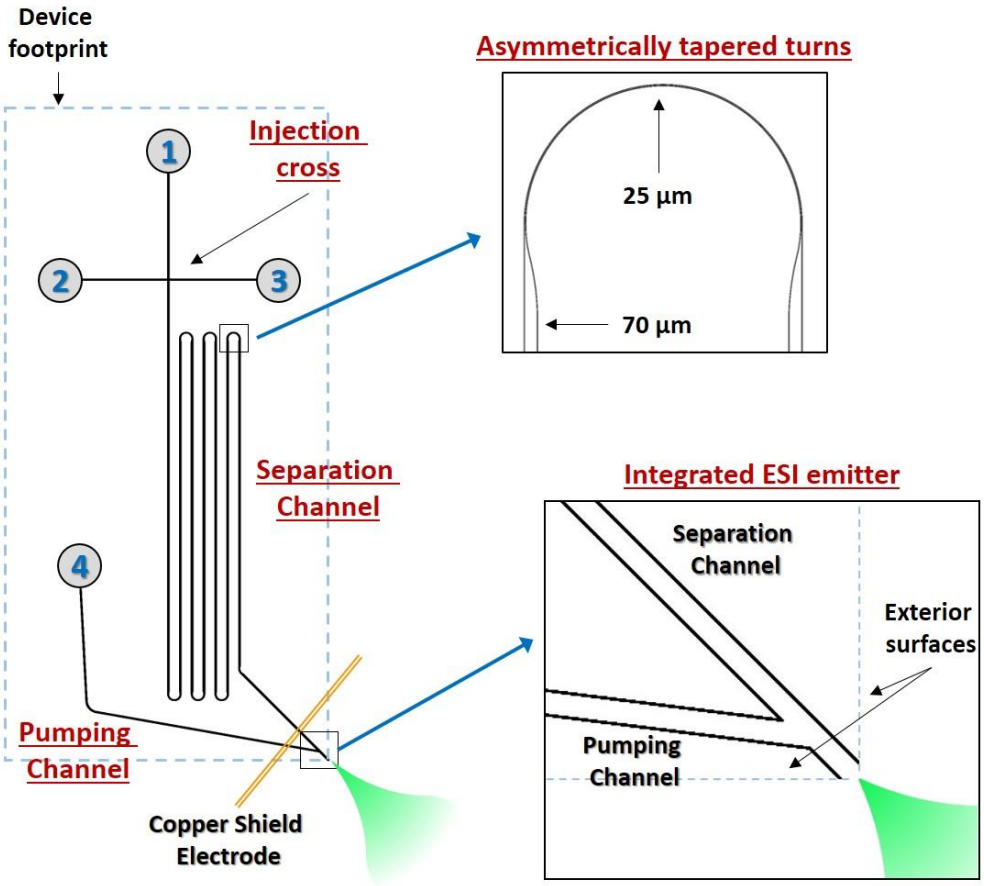

Figure 1.3: Diagram of the microfluidic CE device with integrated ESI. The insets show enlarged views of the turn tapering in the separation channel and the channel junctions that form the integrated ESI emitter.

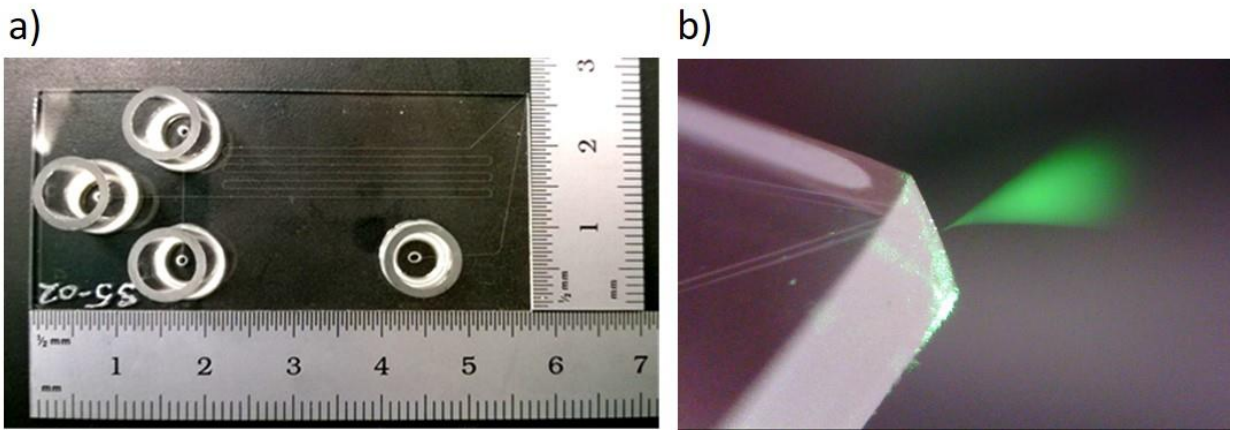

Figure 1.4: Photographs of microfluidic CE-ESI devices. a) Photograph of a completed device. The final device footprint is comparable to that of a microscope slide. b) Photograph of ESI generated off the corner of the device. The spray is visualized with green laser light.

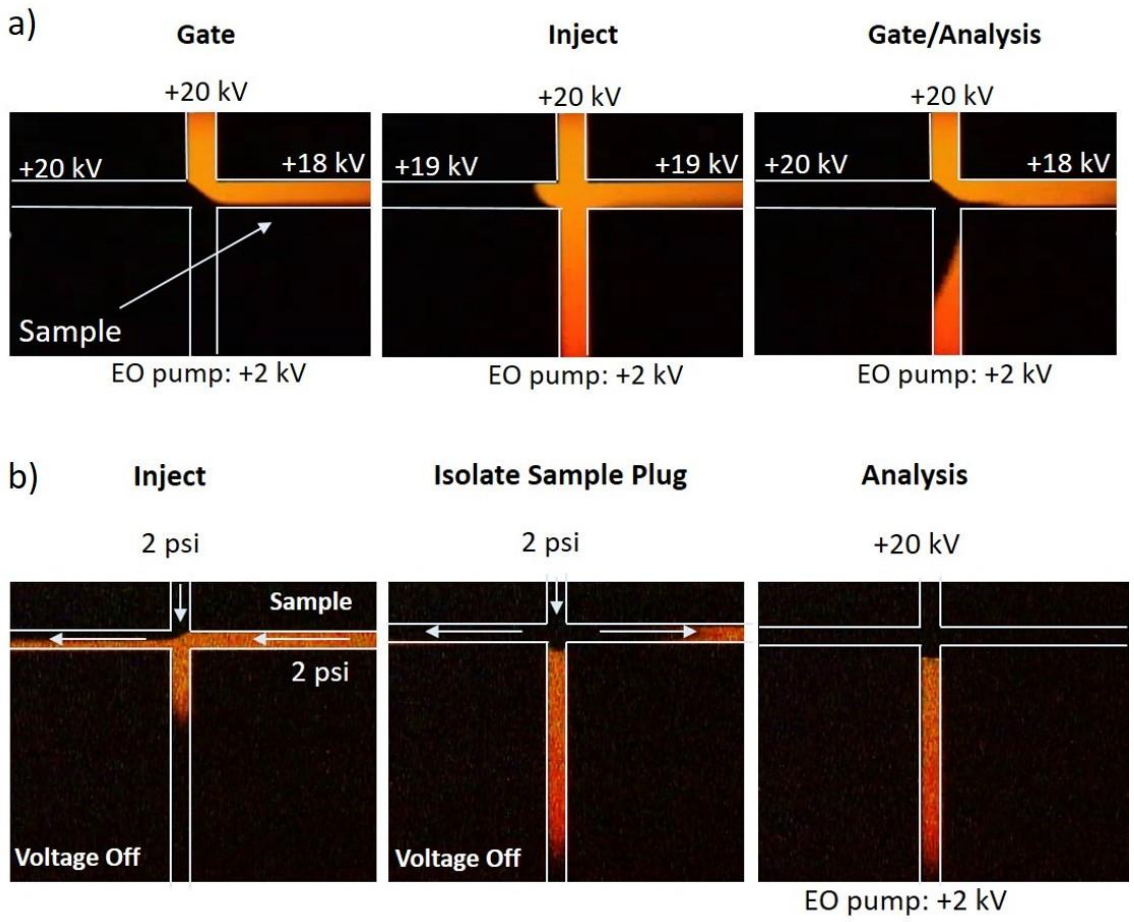

Figure 1.5: Injections schemes used in the Ramsey lab for microfluidic CE-MS analysis. Sample ions are visualized using Rhodamine 6G. a) Gated electrokinetic injection. Using different voltage potentials, the sample is diverted to waste (Gate image). Sample is injected by balancing the potentials of the side arms (Inject image) and separated by returning to the gate potentials (Gate/Analysis image) . b) Hydrodynamic injections. Solution is manipulated by applying head pressure to the solvent reservoirs. The arrows indicate the direction of pressure driven flow. To inject sample, a head pressure is applied to the reservoirs containing the sample and BGE (Inject image). The sample is then isolated by applying a head pressure to just the reservoir containing BGE (Isolate Sample Plug image). Voltage is then applied to perform the separation (Analysis image).

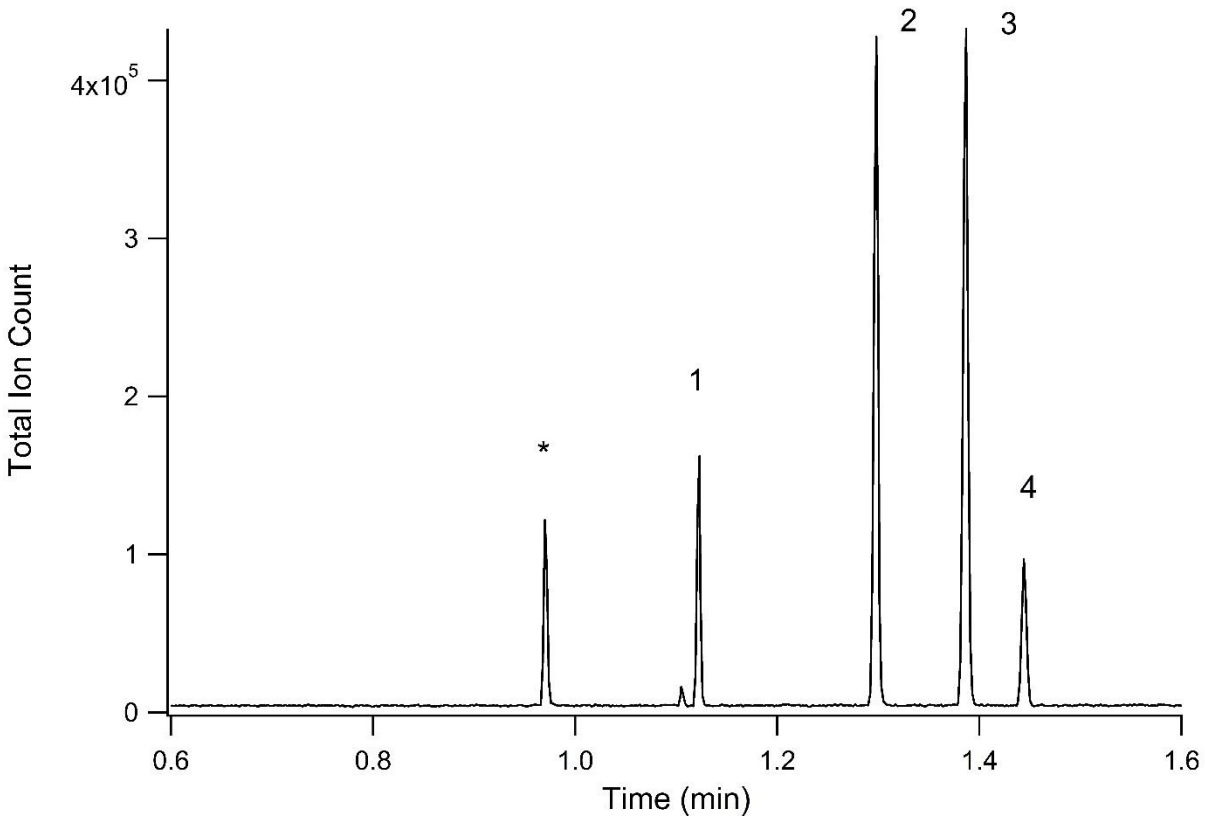

Figure 1.6: Separation of standard peptides using an APS surface coating. An average Δ value of 1.4 was achieved with an average efficiency of 680,000 theoretical plates. Fluorescein (*), Methionine enkephalin (1), Bradykinin (2), Angiotensin II (3), Thymopentin (4)

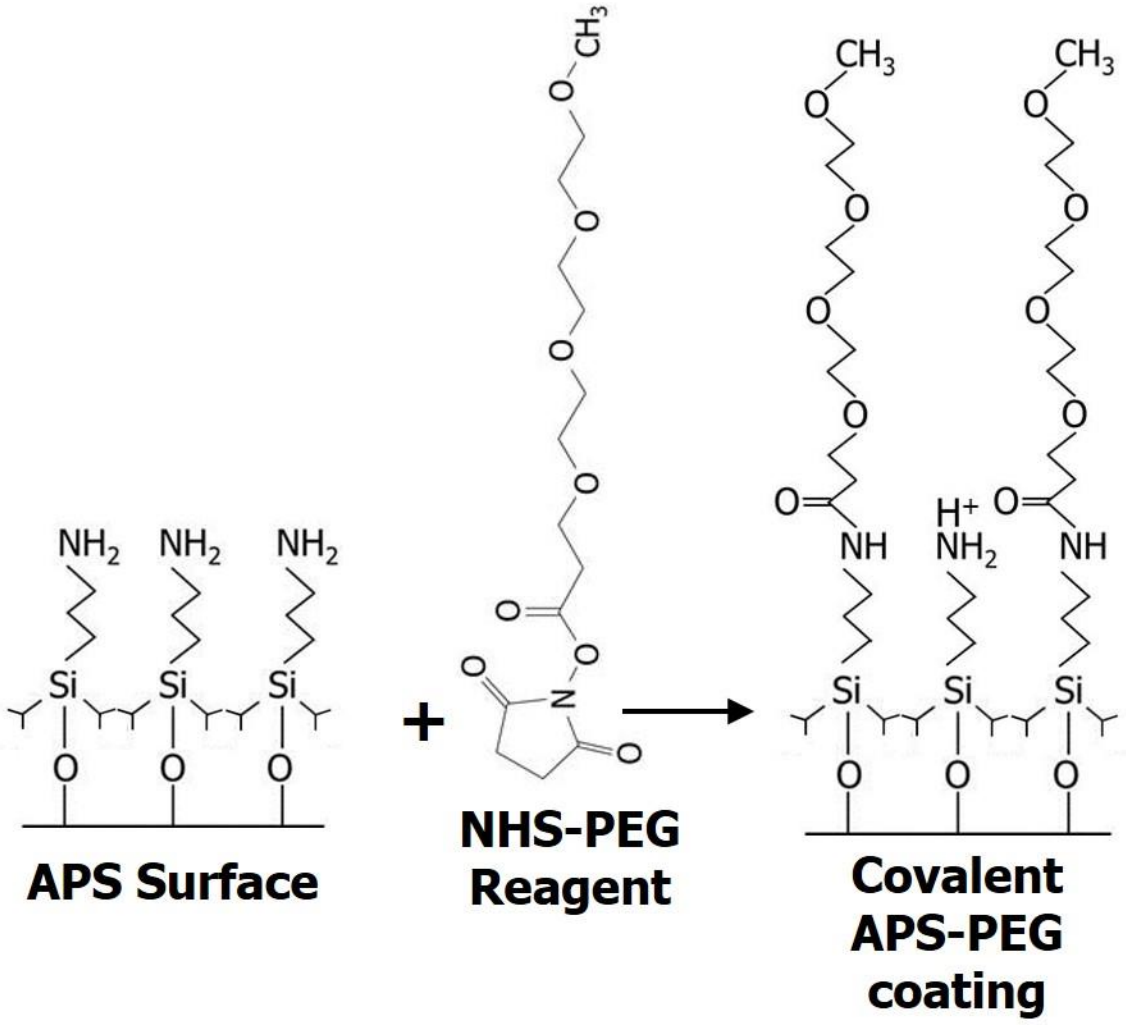

Figure 1.7: Reaction scheme for applying PEG reagents to microfluidic CE-ESI devices. The APS coating is first applied in the gas phase. The NHS functionalized PEG is reacted with the primary amines of the silane reagent in the liquid phase. This results in a covalently bound APS-PEG coating.

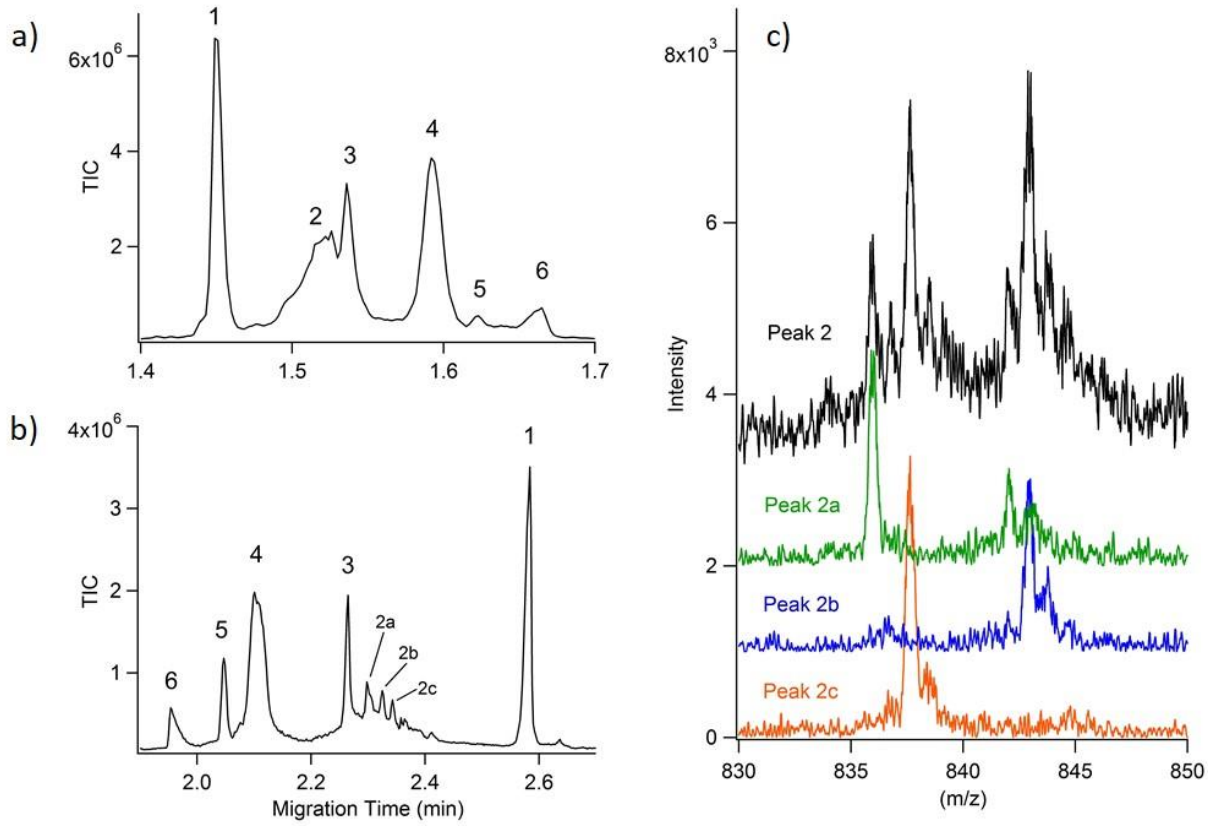

Figure 1.8: Comparison between intact protein separations performed with a) an APS coated microfluidic CE-ESI device and b) an APS-PEG_{450} coated microfluidic CE-ESI device. Note that the polarity of the separation is reversed for the APS-PEG_{450} coated devices so the migration order of the proteins is also reversed. The protein mixture contained carbonic anhydrase I (1), β-hemoglobin (2), α-hemoglobin (3), human serum albumin (4) cytochrome c (5) and lysozyme (6). c) Comparison between the most abundant charge state in the mass spectra for the hemoglobin variants (peak 2 in electropherogram (a) and peaks 2a-2c in electropherogram (b)). Mass spectra were generated by manually summing data points across the width of each peak.

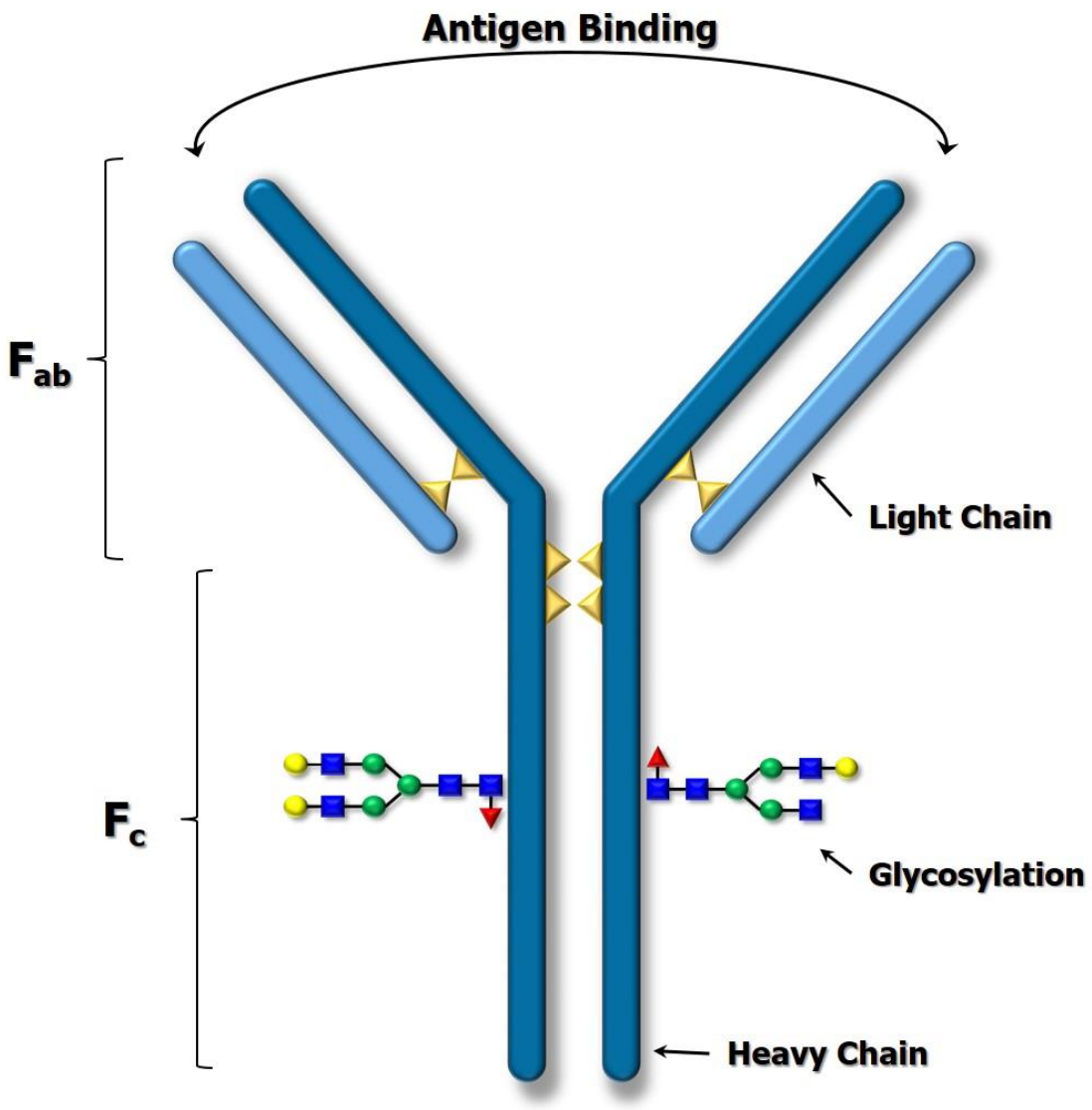

Figure 1.9: Diagram of an IgG mAb. The structure consists of two identical LCs and HCs covalently bound together through disulfide linkages (yellow triangles). The molecule pictured here is an IgG-1. Antigen binding occurs in the Fab domain while the Fc region dictates important immunogenicity functions of the mAb.

Table 1.1: Protein modifications commonly encountered with intact protein analysis

Modification	Monoisotopic Mass Change (Da)	Net Charge Change
C-terminal lysine truncation	-128.09496	-1
Pyroglutamic acid formed from Gln	-17.02655	-1
Disulphide bond formation	-2.01565	
Deamidation of Asn and Gln	0.98402	-1
Methylation	14.01565	
Oxidation of Met	15.99491	variable
Carboxylation of Asp and Glu	43.98983	-1
Carboxyamidomethylcysteine (Cam) from Cys (iodoacetamide)	57.02146	
Phosphorylation	79.96633	-1
Cysteinylation	119.0041	
Deoxyhexoses (Fuc, Rha)	146.05791	
Hexoses (Fru, Gal, Glc, Man)	162.05282	-1 for glycation
N-acetylhexosamines (GalNAc, GlcNAc)	203.07937	
N-acetylneuraminic acid (Sialic acid, NeuAc, NANA, SA)	291.09542	-1

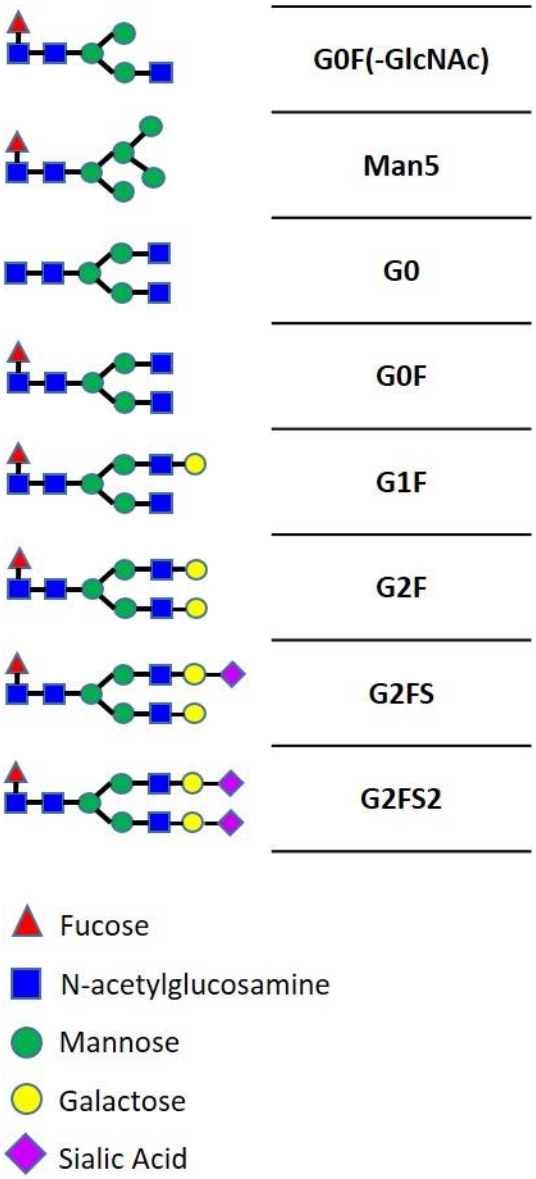

Figure 1.10: Common N-linked glycan structures encountered with IgG based mAbs. Typical IgG glycans are biantennary structures constituted from fucose, N-acetylglucosamine, mannose, and galactose residues. Sialylation is typically not seen with Fc glycans, but can occur under certain cell culture production conditions.

REFERENCES

(1) Mellors, J. S.; Gorbounov, V.; Ramsey, R. S.; Ramsey, J. M. *Anal. Chem.* **2008**, *80* (18), 6881–6887.

(2) Batz, N. G.; Mellors, J. S.; Alarie, J. P.; Ramsey, J. M. *Anal. Chem.* **2014**, *86*, 3493–3500.

(3) Vlasak, J.; Ionescu, R. *MAbs* **2011**, *3* (3), 253–263.

(4) Fekete, S.; Guillarme, D. *LC-GC Eur.* **2012**, *25* (10), 540–550.

(5) Fekete, S.; Guillarme, D.; Sandra, P.; Sandra, K. *Anal. Chem.* **2016**, *88* (1), 480–507.

(6) Landers, J. P. *Handbook of Capillary Electrophoresis*, 2nd ed.; CRC Press: New York, NY, 1997.

(7) Jorgenson, J. W.; Lukacs, K. D. *Anal. Chem.* **1981**, *53* (8), 1298–1302.

(8) Jorgenson, J. W.; Lukacs, K. D. *Clin. Chem.* **1981**, *27* (9), 1551–1553.

(9) Jorgenson, J. W.; Lukacs, K. D. *Science (80-.).* **1983**, *222* (4621), 266–272.

(10) Altria, K. D. *Capillary Electrophoresis Guidebook*; Altria, K. D., Ed.; Humana Press: Totowa, NJ, 1996.

(11) Li, S. F. Y. *Capillary Electrophoresis: principles, practice and applications*; Elsevier Science: Amsterdam, 1993.

(12) Giddings, J. C. *Sep. Sci.* **1969**, *4* (3), 181–189.

(13) Guiochon, G.; Felinger, A.; Shirazi, D. G.; Katti, A. M. *Fundamentals of preparative and nonlinear chromatography*, 2nd ed.; Elsevier: San Diego, CA, 2006.

(14) Felinger, A.; Cavazzini, A. *Liquid Chromatography*; Elsevier, 2013.

(15) Jacobson, S. C.; Koutny, L. B.; Hergenroder, R.; Moore, A. W.; Ramsey, J. M. *Anal. Chem.* **1994**, *66* (20), 3472–3476.

(16) Seiler, K.; Harrison, D. J.; Manz, A. *Anal. Chem.* **1993**, *65* (10), 1481–1488.

(17) Manz, A.; Harrison, D. J.; Verpoorte, E. M. J.; Fettinger, J. C.; Paulus, A.; Lüdi, H.; Widmer, H. M. *J. Chromatogr. A* **1992**, *593* (1-2), 253–258.

(18) Harrison, D. J.; Manz, A.; Fan, Z.; Luedi, H.; Widmer, H. M. *Anal. Chem.* **1992**, *64* (17),

1926–1932.

(19) Jacobson, S. C.; Hergenroder, R.; Koutny, L. B.; Ramsey, J. M. *Anal. Chem.* **1994**, *66*, 1114–1118.

(20) Jacobson, S. C.; Hergenroder, R.; Koutny, L. B.; Warmack, R. J.; Ramsey, J. M. *Anal. Chem.* **1994**, *66*, 1107–1113.

(21) Jacobson, S. C.; Hergenruder, R.; Moore, A. W.; Ramsey, J. M. *Anal. Chem.* **1994**, *66* (23), 4127–4132.

(22) Kutter, J. P.; Fintschenko, Y. *Separation Methods in Microanalytical Systems*; Taylor and Francis Group, LLC: Boca Raton, FL, 2006.

(23) Culbertson, C. T.; Jacobson, S. C.; Ramsey, J. M. *Anal. Chem.* **2000**, *72* (23), 5814–5819.

(24) Harrison, D. J.; Seiler, K.; Manz, A.; Zhonghui Fan. In *Technical Digest IEEE Solid-State Sensor and Actuator Workshop*; IEEE, 1992; Vol. 64, pp 110–113.

(25) Culbertson, C. T.; Jacobson, S. C.; Ramsey, J. M. *Anal. Chem.* **1998**, *70*, 3781–3789.

(26) Kirby, D. P.; Thorne, J. M.; Götzinger, W. K.; Karger, B. L. *Anal. Chem.* **1996**, *68* (24), 4451–4457.

(27) Wojcik, R.; Dada, O. O.; Sadilek, M.; Dovichi, N. J. *Rapid Commun. Mass Spectrom.* **2010**, *24* (17), 2554–2560.

(28) Liu, C. C.; Zhang, J.; Dovichi, N. J. *Rapid Commun. Mass Spectrom.* **2005**, *19* (2), 187–192.

(29) Valaskovic, G. A.; Kelleher, N. L.; McLafferty, F. W. *Science (80-.).* **1996**, *273* (5279), 1199–1202.

(30) Smith, R. D.; Olivares, J. A.; Nguyen, N. T.; Udseth, H. R. *Anal. Chem.* **1988**, *60* (5), 436–441.

(31) Olivares, J. A.; Nguyen, N. T.; Yonker, C. R.; Smith, R. D. *Anal. Chem.* **1987**, *59* (8), 1230–1232.

(32) Foret, F.; Zhou, H.; Gangl, E.; Karger, B. L. *Electrophoresis* **2000**, *21* (7), 1363–1371.

(33) CAO, P.; MOINI, M. *J. Am. Soc. Mass Spectrom.* **1997**, *8* (5), 561–564.

(34) Zhang, B.; Liu, H.; Karger, B. L.; Foret, F. *Anal. Chem.* **1999**, *71* (15), 3258–3264.

(35) Lazar, I. M.; Ramsey, R. S.; Sundberg, S.; Ramsey, J. M. *Anal. Chem.* **1999**, *71* (17), 3627–3631.

(36) Lazar, I. M.; Ramsey, R. S.; Jacobson, S. C.; Foote, R. S.; Ramsey, J. M. *J. Chromatogr.*

A **2000**, *892* (1-2), 195–201.

(37) Lazar, I. M.; Ramsey, R. S.; Ramsey, J. M. *Anal. Chem.* **2001**, *73* (8), 1733–1739.

(38) Ramsey, R. S.; Ramsey, J. M. *Anal. Chem.* **1997**, *69* (13), 2617.

(39) Alarie, J. P.; Jacobson, S. C.; Ramsey, J. M. *Electrophoresis* **2001**, *22* (2), 312–317.

(40) Alarie, J. P.; Jacobson, S. C.; Culbertson, C. T.; Ramsey, J. M. *Electrophoresis* **2000**, *21* (1), 100–106.

(41) Fu, L.-M.; Yang, R.-J.; Lee, G.-B. *Anal. Chem.* **2003**, *75* (8), 1905–1910.

(42) Fu, L.-M.; Yang, R.-J.; Lee, G.-B.; Pan, Y.-J. *Electrophoresis* **2003**, *24* (17), 3026–3032.

(43) Backofen, U.; Matysik, F.-M.; Lunte, C. E. *Anal. Chem.* **2002**, *74* (16), 4054–4059.

(44) Gai, H.; Yu, L.; Dai, Z.; Ma, Y.; Lin, B. *Electrophoresis* **2004**, *25* (12), 1888–1894.

(45) Luo, Y.; Wu, D.; Zeng, S.; Gai, H.; Long, Z.; Shen, Z.; Dai, Z.; Qin, J.; Lin, B. *Anal. Chem.* **2006**, *78* (17), 6074–6080.

(46) Gong, M.; Wehmeyer, K. R.; Stalcup, A. M.; Limbach, P. A.; Heineman, W. R. *Electrophoresis* **2007**, *28* (10), 1564–1571.

(47) Bai, X.; Lee, H. J.; Rossier, J. S.; Reymond, F.; Schafer, H.; Wossner, M.; Girault, H. H. *Lab Chip* **2002**, *2* (1), 45–49.

(48) Chen, C.-C.; Yen, S.-F.; Makamba, H.; Li, C.-W.; Tsai, M.-L.; Chen, S.-H. *Anal. Chem.* **2007**, *79* (1), 195–201.

(49) Dossi, N.; Toniolo, R.; Susmel, S.; Pizzariello, A.; Bontempelli, G. *Electrophoresis* **2010**, *31* (15), 2541–2547.

(50) Fu, L.-M.; Yang, R.-J.; Lee, G.-B.; Liu, H.-H. *Anal. Chem.* **2002**, *74* (19), 5084–5091.

(51) Karlinsey, J. M. *Anal. Chim. Acta* **2012**, *725*, 1–13.

(52) Haselberg, R.; de Jong, G. J.; Somsen, G. W. *J. Chromatogr. A* **2007**, *1159* (1-2), 81–109.

(53) Sassi, A. P.; Andel, F.; Bitter, H.-M. L.; Brown, M. P. S.; Chapman, R. G.; Espiritu, J.; Greenquist, A. C.; Guyon, I.; Horchi-Alegre, M.; Stults, K. L.; Wainright, A.; Heller, J. C.; Stults, J. T. *Electrophoresis* **2005**, *26* (7-8), 1500–1512.

(54) Herrero, M.; Bernal, J.; Velasco, D.; Elvira, C.; Cifuentes, A. *J. Chromatogr. A* **2010**, *1217* (48), 7586–7592.

(55) Haselberg, R.; de Jong, G. J.; Somsen, G. W. *Electrophoresis* **2013**, *34* (1), 99–112.

(56) Huhn, C.; Ramautar, R.; Wuhrer, M.; Somsen, G. W. *Anal. Bioanal. Chem.* **2010**, *396* (1), 297–314.

(57) Hardenborg, E.; Zuberovic, A.; Ullsten, S.; Söderberg, L.; Heldin, E.; Markides, K. E. *J. Chromatogr. A* **2003**, *1003* (1-2), 217–221.

(58) Ullsten, S.; Zuberovic, A.; Wetterhall, M.; Hardenborg, E.; Markides, K. E.; Bergquist, J. *Electrophoresis* **2004**, *25* (13), 2090–2099.

(59) Martma, K.; Lindenburg, P. W.; Habicht, K. L.; Vulla, K.; Resik, K.; Kuut, G.; Shimmo, R. *J. Chromatogr. A* **2013**, *1317*, 193–198.

(60) Pattky, M.; Huhn, C. *Anal. Bioanal. Chem.* **2013**, *405* (1), 225–237.

(61) Zhang, Y. W.; Zhao, M. Z.; Liu, J. X.; Zhou, Y. L.; Zhang, X. X. *J. Sep. Sci.* **2015**, *38* (3), 475–482.

(62) Zhu, G.; Sun, L.; Dovichi, N. J. *Talanta* **2016**, *146*, 839–843.

(63) Acunha, T.; Simó, C.; Ibáñez, C.; Gallardo, A.; Cifuentes, A. *J. Chromatogr. A* **2016**, *1428*, 326–335.

(64) Zhang, F.; Sautter, K.; Larsen, A. M.; Findley, D. a; Davis, R. C.; Samha, H.; Linford, M. R. *Langmuir* **2010**, *26* (18), 14648–14654.

(65) Batz, N. G. Development and Application of Surface Coatings for Microchip Capillary Electrophoresis-Electrospray Ionization-Mass Spectrometry Analysis of Biological Analytes, University of North Carolina at Chapel Hill, 2014.

(66) Liu, H.; Gaza-bulseco, G.; Faldu, D.; Chumsae, C.; Sun, J. *J. Pharm. Sci.* **2008**, *97*, 2426–2447.

(67) Zhang, H.; Cui, W.; Gross, M. L. *FEBS Lett.* **2014**, *588* (2), 308–317.

(68) Chelius, D.; Jing, K.; Lueras, A.; Rehder, D. S.; Dillon, T. M.; Vizel, A.; Rajan, R. S.; Li, T.; Treuheit, M. J.; Bondarenko, P. V. *Anal. Chem.* **2006**, *78* (7), 2370–2376.

(69) Jones, L. M.; Zhang, H.; Cui, W.; Kumar, S.; Sperry, J. B.; Carroll, J. A.; Gross, M. L. *J. Am. Soc. Mass Spectrom.* **2013**, *24* (6), 835–845.

(70) Fekete, S.; Gassner, A.-L.; Rudaz, S.; Schappler, J.; Guillarme, D. *TrAC Trends Anal. Chem.* **2013**, *42*, 74–83.

(71) Macht, M. *TrAC Trends Anal. Chem.* **2013**, *48*, 62–71.

(72) Arnold, J. N.; Wormald, M. R.; Sim, R. B.; Rudd, P. M.; Dwek, R. A. *Annu. Rev. Immunol.* **2007**, *25*, 21–50.

(73) Liu, H.; May, K. *MAbs* **2012**, *4* (1), 17–23.

(74) Zhang, Z.; Pan, H.; Chen, X. *Mass Spectrom. Rev.* **2009**, *28*, 147–176.

(75) Raju, T. S.; Scallon, B. J. *Biochem. Biophys. Res. Commun.* **2006**, *341* (3), 797–803.

CHAPTER 2: ANALYSIS OF HEMOGLOBIN GLYCATION USING MICROFLUIDIC CAPILLARY ELECTROPHORESIS-MASS SPECTROMETRY

2.1 Introduction

Glycated hemoglobin (HbA1c) is characterized by the nonenzymatic addition of a glucose moiety to an amino group in the protein structure.[1–4] This modification to hemoglobin (Hb) is more prevalent when blood glucose levels are elevated; as is often the case with diabetes. Due to the lifetime of human erythrocytes (~120 days) HbA1c levels can be used as an indicator of long-term glycemic control in diabetic patients and have become essential to the management of this condition.[1,5] A wide variety of methods are available for measuring HbA1c in the clinical setting. Current analysis techniques are typically based on either separation methods or immunoassays with optical detection, such as ion exchange high performance liquid chromatography (HPLC), boronate affinity HPLC, or immunoturbidimetry.[1,5,6]

Several studies have been performed evaluating mass spectrometry as an alternative method for assessing Hb glycation.[4,7,8] Because a discrete mass is generated for all hemoglobin species introduced into the mass spectrometer, it was theorized that this approach may be less susceptible to common interferences, such as genetic variants and modifications to amino acid side chains under conditions of uremia, aspirin therapy, or improper sample handling.[6,9–11] Both matrix assisted laser desorption ionization mass spectrometry (MALDI)-MS[12–14] and electrospray ionization (ESI)-MS[9,15–20] were independently evaluated for the direct analysis of blood lysates. The levels of glycated Hb calculated from the mass spectra using both ionization methods were found to correlate well with HbA1c levels measured using established techniques.

These studies established mass spectrometry as a potential method for assessing Hb glycation, but the technique has not been adopted clinically due to the high cost of instrumentation and the need for specially trained technicians. These limitations are, however, becoming less significant over time due to the development of small, low cost, and simple to operate mass spectrometers which have the potential to make mass spectrometry more accessible to the clinical lab.[21–25]

One of the limitations of directly introducing complex mixtures into a mass spectrometer is the high resolving power required to adequately characterize analyte ions in the mass domain. A strategy to simplify the sample mixture before ESI-MS analysis is to use an in-line separation technique. The separation techniques that are currently used in clinics are not compatible with ESI-MS due to the high ionic strength buffers needed for the analysis. However, capillary electrophoresis (CE) has been demonstrated as an MS-compatible alternative to ion exchange HPLC for the separation of protein variants differing in net charge. Previously, CE-MS has been used to analyze proteins from human erythrocytes without enzymatic digestion including hemoglobin, carbonic anhydrase, and blood protein complexes.[26–29] While α-Hb and β-Hb were resolved from each other, resolution between glycated forms of Hb was not achieved in the CE domain and glycation was not evaluated.

Performing CE on a microfluidic platform offers several advantages over a capillary format because multiple functional elements can be integrated in the design, providing a means to perform sample handling, separation, and direct coupling of the CE separation to MS analysis with minimal added dead volume.[30–32] This results in rapid, highly efficient separations.[32] Recently, this analysis platform has been applied to the separation of peptide fragments for hydrogen/deuterium exchange experiments and intact biotherapeutic monoclonal antibodies.[33,34] Described here is a method for assessing Hb glycation in whole blood lysates using microfluidic

CE-MS. The analysis is performed under denaturing conditions with minimal sample preparation required and is complete in less than 3 minutes. The method is tested by analyzing whole blood samples with known HbA1c levels and assessing the correlation between the microfluidic CE-MS method and the clinical technique.

2.2 Experimental

2.2.1 Materials and Reagents

Deionized water was generated with a Nanopure Diamond water purifier (Barnstead International, Dubuque, IA). Optima LC/MS grade acetonitrile and acetic acid (99% purity) were obtained from Fisher Scientific (Fairlawn, NJ). The silane coating reagent 3-(aminopropyl)di-isopropyl-ethoxysilane (APDIPES) was purchased from Gelest (Morrisville, PA) and the methyl-terminated polyethylene glycol n-hydroxy succinimide ester (NHS-PEG_{450}) was purchased from Nanocs Inc. (Boston, MA). Trichloro-(1H,1H,2H,2H-perfluorooctyl)-silane was purchased from Sigma-Aldrich (St. Louis, MO). Myoglobin, lysozyme, human serum albumin, human hemoglobin, and human carbonic anhydrase I were obtained from Sigma-Aldrich (St. Louis, MO). HbA1c standard was purchased from BBI Solutions (Cardiff, UK). De-identified blood samples were obtained from McLendon Clinical Laboratories (University of North Carolina, USA).

2.2.2 Sample Preparation

Whole blood samples were collected in EDTA-containing tubes and analyzed for HbA1c levels using a Vitros 5600 immuno-assay (Ortho Clinical Diagnostics, Inc.). For the 12 samples collected, the HbA1c levels ranged between 4.7-12.9 % HbA1c. Samples were stored at 4 ºC

until analysis by microfluidic CE-MS. To prepare samples for microfluidic CE-MS analysis, 10 µL of whole blood was diluted to 1 mL with a 50% acetonitrile 3% acetic acid 47% water solution resulting in a 100x dilution of the blood sample. An aliquot of the 100x blood dilution stock was diluted an addition 10x with the same solution to achieve a final dilution level of 1000x. The sample was then filtered using a Costar Spin-X 0.45 µm nylon centrifugal filter before loading 100 µL into the reservoir of the microfluidic device. It should be noted that a much smaller volume of blood could be used, provided that a final 1000x dilution is achieved.

2.2.3 CE-ESI-MS Device Preparation and Operation

The APS-PEG_{450} surface coating described in the introduction was used for this analysis and applied according to the procedures in Appendix 2. Bulk fluid flow for sustaining ESI was supplied via electroosmotic pumping.

An aqueous solution of 50/50 acetonitrile/water with 3% acetic acid was used for all analyses. CE-ESI devices were operated by applying and controlling voltages as described in Appendix 3. For this analysis +20kV and +1.5kV were applied to reservoirs 1 and 4, respectively, which resulted in a field strength of approximately 685 V/cm. A pressure based injection scheme was used for sample manipulation and injection. The samples were injected for 3 seconds at 2 psi, which corresponds to an injection volume of ~0.5 nL.

2.2.4 Data Analysis

MS analysis was performed using a Waters Synapt G2 quadrupole time-of-flight mass spectrometer (Waters Corporation, Milford, MA) operated in sensitivity mode with the source at 105 °C. Data were acquired over a mass range of 500-2500 m/z with a 0.1 s scan time. A mass

spectrum was generated for each species by averaging mass scans across the width of the peak at its base. Deconvolution of the resulting mass spectra was performed based on maximum entropy analysis using the MaxEnt1 deconvolution algorithm in the MassLynx software as described previously.[33,35–37] The deconvoluted masses were used to identify the protein species. Extracted ion (EI) electropherograms were generated by selecting the two most abundant charge state m/z values with a 1.0 Da selection window. Peak areas in the EI electropherograms were generated through integration in the MassLynx software.

2.3 Results and Discussion

2.3.1 Analysis of whole blood lysate

To assess the application of the APS-PEG_{450} coated devices to more complex biological matrices, whole blood lysate was analyzed as a representative real-world sample. Microfluidic CE-MS analysis of whole blood lysate samples achieved significantly better separation performance than previously described methods. A representative electropherogram is shown in Figure 2.1Figure 2.1 Microfluidic CE-MS separation of whole blood lysate from a patient with a 5.6% HbA1c. The separation is complete in less than 3 minutes. The inset shows an enlarged view of the separation window with identified protein species.. The complete separation finished in less than 2.2 minutes, with all protein peaks detected in a migration time window between 1.6 and 2.2 minutes with an average width at base of 0.8 seconds. Peaks corresponding to the major blood proteins serum albumin and hemoglobin were easily identified by mass. Under these analysis conditions, the Hb tetramer dissociates into two alpha and two beta subunits, which are separated from each other with a resolution of 1.1. The observed masses for the subunits (15126 Da and 15867 Da) agree with the expected masses for α-Hb and β-Hb based on linear amino acid

sequences: 15126.4 Da and 15867.2 Da, respectively.[20] Whole blood contains a wide range of protein concentrations and while this method was optimized for Hb analysis, several blood proteins of lower abundance were detected, such as carbonic anhydrase I. Not all minor species were identified and unidentified proteins are labeled by mass only. To achieve better signal for minor blood components additional sample preparation is needed, such as protein concentration or hemoglobin and albumin depletion.

In addition to the main Hb subunit peaks, modified forms of the subunits are detected during analysis. These peaks have lower electrophoretic mobilities than the unmodified subunits, indicating that the modifications to the protein induce a decrease in net charge. Upon deconvolution, the first variant peak was found to have a mass of 16029 Da. This corresponds to the mass of glycated β-Hb where a sugar moiety is non-enzymatically attached to the globin structure at a primary amine. Although this modification only induces a decrease in net charge of 1, glycated β-Hb is easily separated from the unmodified β-Hb with a resolution of 1.0. As seen in Figure 2.2, generating an extracted ion electropherogram reveals that there is an additional isomer of glycated β-Hb that is not fully resolved from the β-Hb peak. Studies have shown that glycation of the β-Hb subunit occurs preferentially at the N-terminal valine, but can also occur on other amino acid side chains.[3,13,17] Due to the relative abundances of the species it was hypothesized that the more abundant, slower migrating peak is due to glycation at the N-terminal valine (β-Hb_{V1}), and the faster migrating, minor peak is due to glycation at a different residue on the β-Hb subunit. To confirm this, a HbA1c standard was spiked into a blood sample pre-determined to have low HbA1c levels (Figure 2.3) and analyzed. The slower migrating glycated β-Hb_{V1} peak increased in intensity without a significant increase in the more quickly migrating isomer, further suggesting that this species is β-Hb_{V1}. Glycation of the α-Hb subunit is also

detectable in the mass spectrum of the unmodified subunit at 15288 Da, but is not resolved as a separate peak (Figure 2.2c). Although the species is of low abundance, as seen in Figure 2.2a the glycated α-Hb is separated from the unmodified subunit with a resolution of 0.4. Current methods for measuring HbA1c using optical detection do not provide specific information about glycation on the α-Hb. However, with the microfluidic CE-MS method, information about glycation on both subunits is simultaneously generated without additional analysis steps.

Other modifications of β-Hb were observed in addition to glycation. Protein species of masses 15924 Da, 15909 Da and 16086 Da are detected as minor peaks of lower electrophoretic mobility. The 15924 Da and 16086 Da species correspond to a 57 Da increase to the mass of unmodified and glycated β-Hb as designated in Figure 2.1. According to literature, a +57 Da mass shift can be indicative of the addition of a glyoxal moiety to the protein structure. The 15909 Da species was identified as acetylated β-Hb by a +42 Da mass shift. Glyoxal is a reactive oxoaldehyde that will modify proteins, typically at lysine and arginine residues, and has been found to be at increased levels in diabetic patients.[4,12,38–40] The reaction of glycated proteins with glyoxal and similar compounds forms advanced glycation end products and advanced oxidation protein products, which have been linked to the development of complications such as nephropathy, retinopathy, neuropathy, and cardiovascular disease.[38,41]

2.3.2 Measurement of HbA1c Levels

With the ability to resolve the glycated forms of β-Hb, 12 whole blood samples were analyzed using microfluidic CE-MS to assess their %glycated Hb and compared to HbA1c levels determined through an immunoassay standard. Because the hemoglobin tetramer dissociates under these analysis conditions, glycation on both the alpha and beta subunit can be measured

simultaneously. This is information that is not necessarily obtained using methods where the tetramer structure is preserved or the technique is targeted to a specific glycation site.[1,5] To calculate the glycated Hb levels from the microfluidic CE-MS data, extracted ion electropherograms were generated for α-Hb, glycated α-Hb, β-Hb, and glycated β-Hb. The areas of the peaks were used to calculate the %glycated subunit according to Equations 2.1 and 2.2 below where A indicates the area of the peak corresponding to the subscript ID. The peak area of beta hemoglobin glycated at the N-terminal valine was used to calculate the %glycated β-Hb_{V1}.

$$\text{glycated } \alpha\text{Hb } \% = \frac{A_{\text{glycated } \alpha\text{Hb}}}{A_{\alpha\text{Hb}} + A_{\text{glycated } \alpha\text{Hb}}} \times 100 \qquad (2.10)$$

$$\text{glycated } \beta\text{Hb}_{V1}\% = \frac{A_{\text{glycated } \beta\text{Hb}_{V1}}}{A_{\beta\text{Hb}} + A_{\text{glycated } \beta\text{Hb}_{V1}} + A_{\text{glycated } \beta\text{Hb isomer}}} \times 100 \qquad (2.11)$$

A correlation plot was generated for the clinically derived %HbA1c values and %glycated subunit values derived using the microfluidic CE-MS method and a linear correlation was obtained. As illustrated in Figure 2.4, for %glycated β-Hb a slope of 1.20 and an R^2 value of 0.99 was seen. The amount of %glycated α-Hb also increased linearly as %HbA1c increased, but was consistently lower.

While other studies have evaluated the use of ESI-MS for assessing hemoglobin glycation, they did not incorporate a separation step prior to MS analysis.[9,18,20] Blood samples were often centrifuged and rinsed to remove the serum proteins and other interfering species, such as salts. During the microfluidic CE separation other proteins and salt ions are effectively removed from the hemoglobin species and do not interfere with ionization or MS analysis. Thus, with this

approach the only sample processing required is dilution and filtration. Additionally, the separation prior to MS analysis simplifies the sample entering the mass spectrometer. This alleviates some of the resolving requirements of the instrument making it an option to use a mass spectrometer with limited resolving capabilities for this analysis.

Hemoglobin variants, such as HbAS, HbAC, HbAE, and HbAD, are known to interfere with HbA1c measurements.[1,6] These variants are characterized by single point mutations in the amino acid backbone of the β-Hb subunit, and in the case of variants C, E, and D can alter the net charge of the subunit by +1 or +2, and the mass by 1 Da. Separation techniques or mass spectrometry alone may struggle to detect the presence of these variants. Elevated levels of these variants can be misinterpreted as HbA1c peaks with separation techniques that rely on optical detection[6], and 1 Da differences are challenging to resolve by mass spectrometry without an MS instrument with high resolving power. However, uniting these two approaches via microfluidic CE-MS provides two means of identification for detecting the presence of the Hb variants: changes in electrophoretic mobility due to charge differences and mass shifts due to structural modifications. Thus, it is possible that the microfluidic CE-MS method could be optimized so that the common Hb variants do not interfere with the measurement of glycated Hb. Additional experiments are needed to assess this using blood containing these Hb variants.

2.3.3 Human Serum Albumin Glycation

As seen in Figure 2.1, human serum albumin (HSA) was clearly detected during the same analysis used to quantify Hb glycation. Glycated albumin has also been found to be an informative biomarker for diabetes management. The lifetime of albumin is shorter than that of erythrocytes, so it can be used to evaluate short-term glycemic control.[4,42–44] While the

sensitivity of the mass spectrometer used for this analysis made it difficult to identify glycated albumin from the separations optimized for Hb glycation analysis, glycated albumin can be assessed using the same method by simply increasing the injection volume. This overloads the Hb peaks causing broadening and loss of resolution, but the HSA signal nearly triples in intensity. Thus, both HSA and Hb glycation can be easily assessed by performing back-to-back injections of the sample using injection volumes optimized for each biomarker. To demonstrate this, the patient samples 2, 4, 8, and 12 were reanalyzed with the injection volume increased from 3 seconds to 9 seconds. The spectra associated with the albumin peaks were deconvoluted and are provided in Figure 2.5. Although the glycated forms of albumin are not resolved as separate species, they can still be detected by a mass shift of 162 Da in the deconvoluted spectrum. Glycated albumin species are detected in patient samples 8 and 12, and at trace levels for patient sample 4. Interestingly, the greatest amount of albumin glycation was not seen in the sample with the highest levels of glycated Hb. Since albumin glycation provides more information about glycemic control over the previous 1-2 weeks, this could indicate that the patient with greater amounts of albumin glycation experienced a lapse in glycemic control shortly before the blood was collected. Thus, measuring both biomarkers simultaneously could provide a more complete picture of diabetes management leading up to the blood collection. It is possible that a more sensitive MS instrument would allow both biomarkers to be measured using the same injection volume. Future work will further explore the use of microfluidic CE-MS for simultaneous measurements of HSA and Hb glycation.

2.3.4 Integration with Portable Mass Spectrometer

While mass spectrometry offers several advantages for diagnostics, it is still not a routinely used technology in a point-of-care or clinical setting. This can be partly attributed to the high cost and level of expertise required to maintain and operate MS instruments, which necessitates that they remain in a designated laboratory. Currently in the Ramsey lab, research is being performed to miniaturize ion trap based mass spectrometers to create small, simple, and portable instruments that can be taken out of the laboratory setting.[45–47] Preliminary work in this field focused on volatile analytes, but efforts are being made to modify these systems to analyze nonvolatile analytes via ESI. Thus, there is the potential for a small, lower cost mass spectrometer that could be used in a clinical setting by users with modest expertise. To explore this possibility, the microfluidic CE-ESI method for hemoglobin glycation analysis was interfaced with an ESI compatible miniature MS prototype system. An image of the prototype is provided in Figure 2.6. Figure 2.7a shows the electropherogram generated using the prototype MS as a detector for the CE separation. The alpha and beta subunits of hemoglobin are clearly visible along with smaller peaks corresponding to glycated beta hemoglobin and another beta chain variant. Serum albumin was not detected because it is beyond the current upper limit of detectable m/z values for the prototype. The mass spectra for the alpha and beta subunits are provided in Figure 2.7b. Although the prototype MS generates only modest mass resolution as compared to commercial instruments there are measureable differences between the m/z values in the protein envelopes. When these measurements were taken there was not sufficient sensitivity to generate a mass spectrum for glycated beta hemoglobin and adequately detect it. Nevertheless, these preliminary results interfacing microfluidic CE-ESI with the portable MS

prototype for intact protein analysis are promising, and efforts are being made to further optimize the prototype system for the analysis of intact proteins.

2.4 Conclusions

We have demonstrated a rapid and simple method for analyzing hemoglobin and HSA glycation in whole blood samples using microfluidic CE-MS. The microfluidic CE separation simplifies the sample mixture entering the MS instrument, reducing the potential for ionization suppression and the formation of adducts with salts in the sample matrix. Additionally, it lessens the resolving requirements for MS analysis providing the option of using an instrument with less resolving power than state of the art mass spectrometers. The α-Hb and β-Hb are separated in the CE domain with a resolution of 1.1. The glycated forms of the β-Hb are separated from the unmodified subunit and can be additionally identified by the 162 Da mass shift characteristic of glycation events. Two isomers of glycated β-Hb are visible in an extracted ion electropherogram. The slower migrating species was identified as glycation at the N-terminal valine through spiking experiments with an HbA1c standard. Glycation of α-Hb is detectable in the mass domain though it does not appear as a discrete peak in the CE electropherogram due to its low intensity and close proximity to the main alpha Hb peak. Glycation levels for each subunit were calculated using peak areas from integrated extracted ion electropherograms. The %glycated β-Hb_{V1} values correlated favorably with clinically derived %HbA1c levels for all 12 patient samples. Glycation of α-Hb was also found to increase linearly with increasing %HbA1c although the species was consistently of lower abundance than glycated β-Hb_{V1}. Larger injection volumes of four samples were analyzed to obtain greater signal intensity for serum albumin. The patient samples with elevated levels of glycated Hb also had greater amounts of glycated

albumin species. However, the highest level of albumin glycation did not correspond to the highest level of glycated hemoglobin, which could indicate a more recent lapse in glycemic control. The ability to measure both Hb and HSA glycation has the potential to provide more information about diabetes management in the months leading up to blood collection and both can be easily measured using this technique. Preliminary work interfacing this analysis method with a portable MS prototype generated very promising results. Although there was not enough sensitivity to confidently detect glycated beta hemoglobin at the time of the analysis, further optimization of the prototype system should easily resolve this issue. The work presented here demonstrates that microfluidic CE-MS could be a useful technique for analyzing hemoglobin glycation, and to thoroughly evaluate this method for robustness, a larger population of patient sample must be analyzed.

Acknowledgements

I would like to thank Maria Ramos-Payan, PhD for being instrumental in obtaining the clinical blood samples used for this work. Mac Gilliland developed the ESI compatible miniature MS prototype and graciously provided a tremendous amount of assistance integrating the microfluidic CE-ESI analysis platform with his instrument.

2.5 Figures and Tables

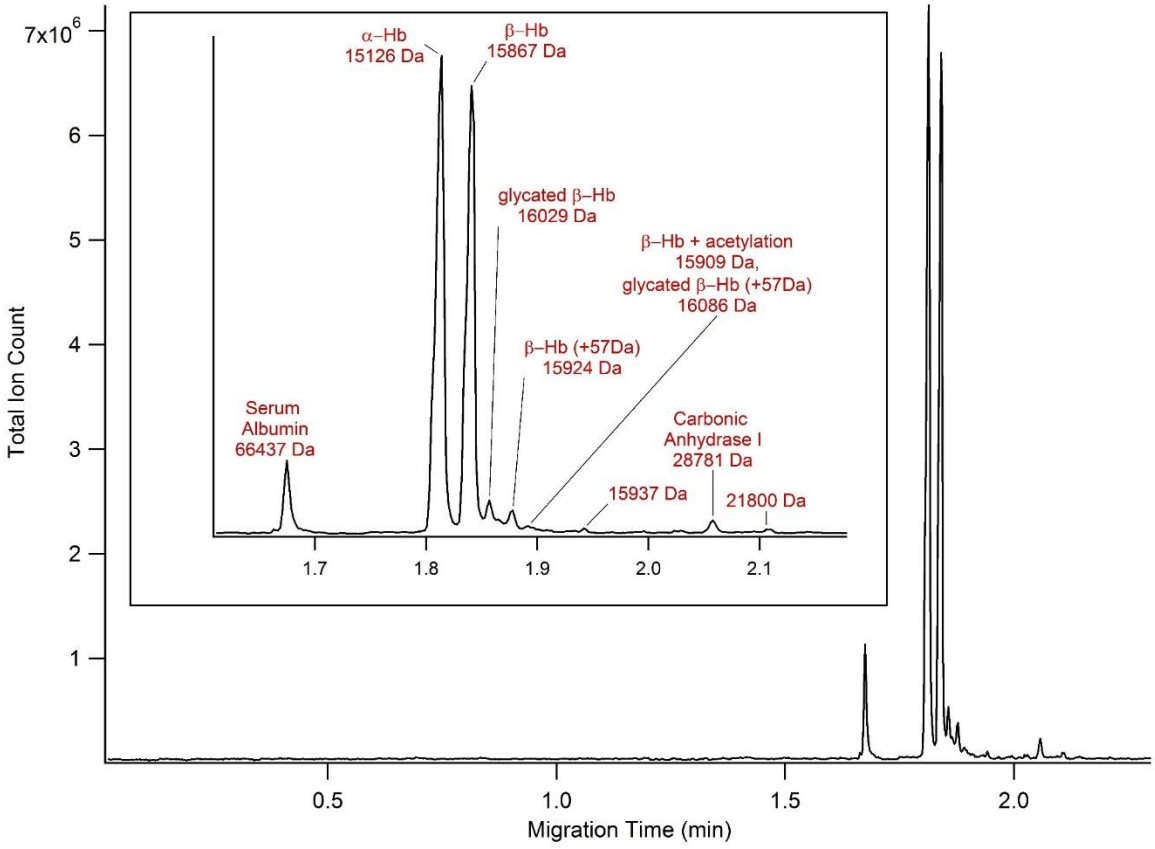

Figure 2.1 Microfluidic CE-MS separation of whole blood lysate from a patient with a 5.6% HbA1c. The separation is complete in less than 3 minutes. The inset shows an enlarged view of the separation window with identified protein species.

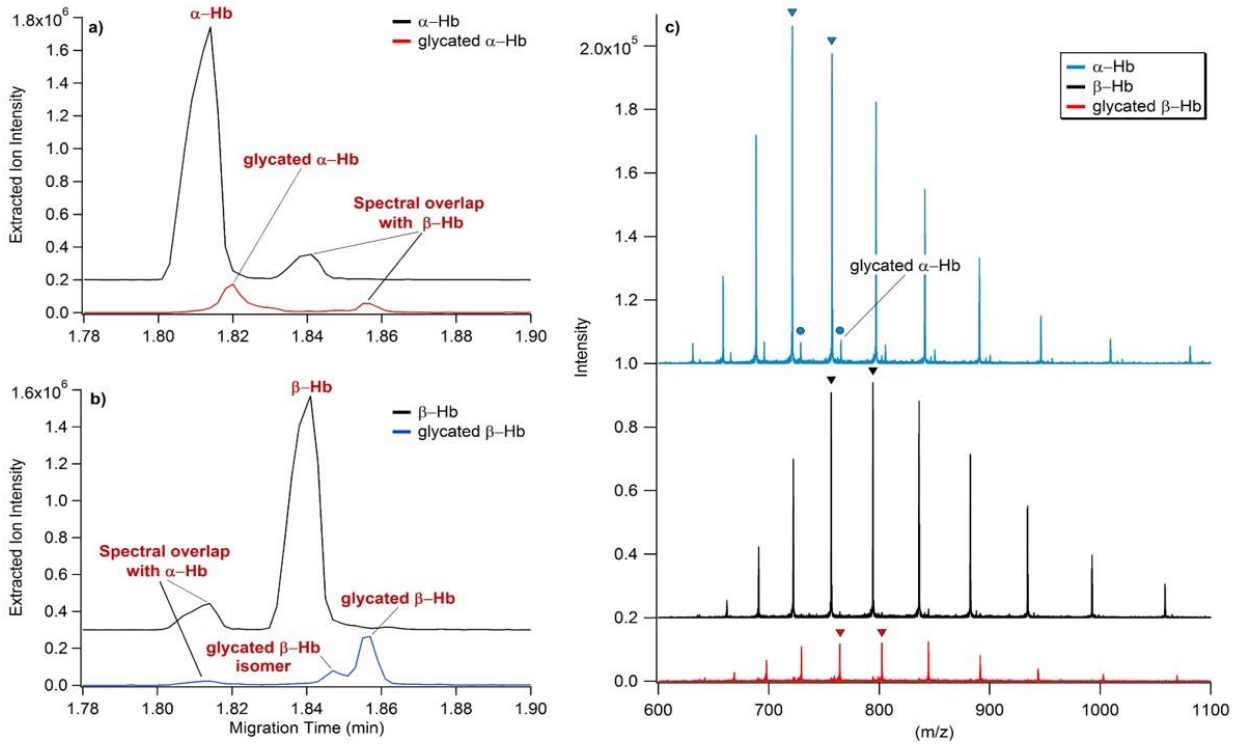

Figure 2.2: a) Extracted ion electropherogram for glycated and non-glycated α-Hb. b) extracted ion electropherogram for glycated and non-glycated β-Hb. c) Mass spectra for hemoglobin subunits. The charge states used to generate the extracted ion electropherograms are indicated with markers.

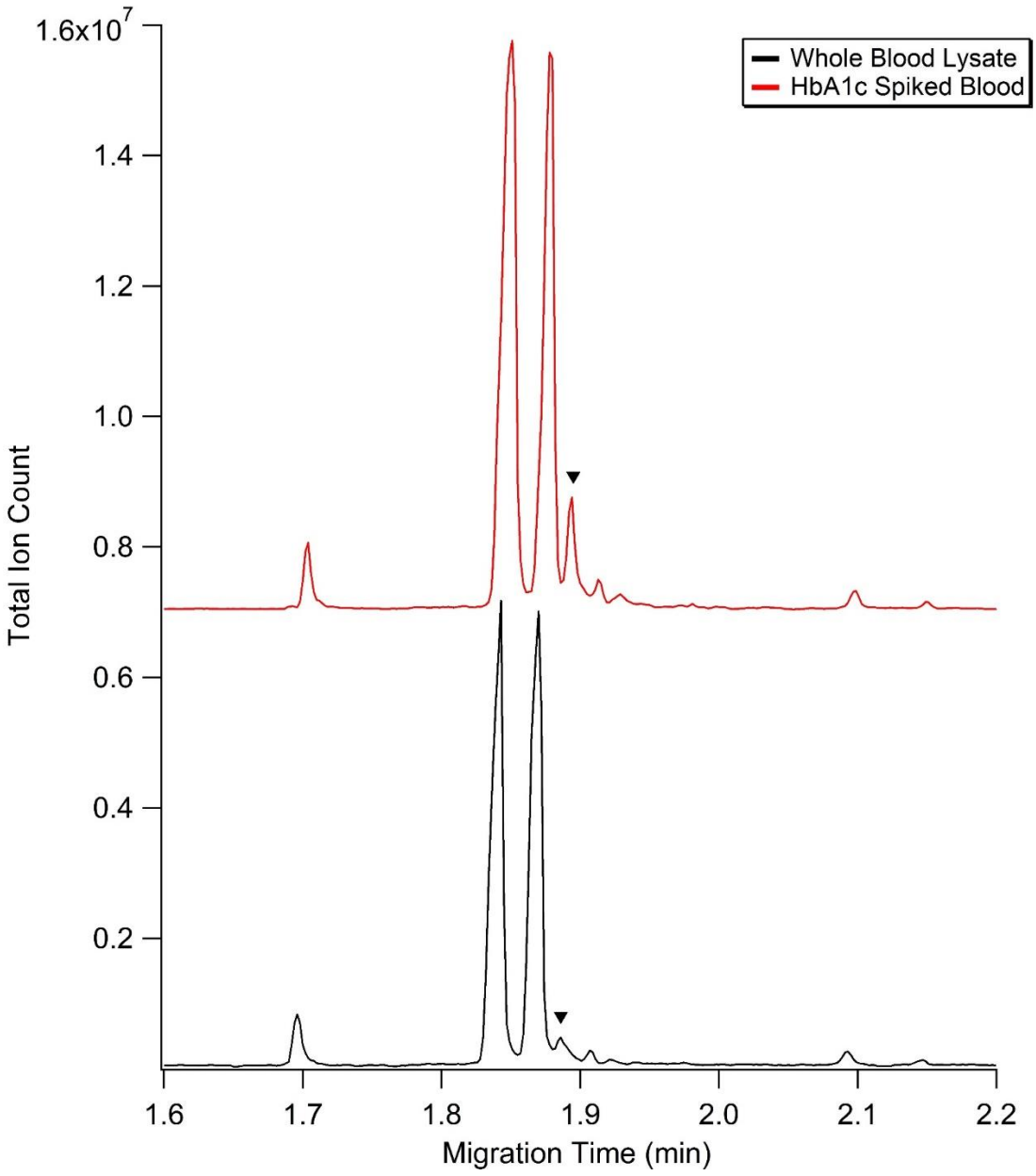

Figure 2.3: Whole blood sample spiked with HbA1c standard. Only the slower migrating glycated β-Hb peak increases after spiking, indicating that it is the glycated β-Hb_{V1} isomer.

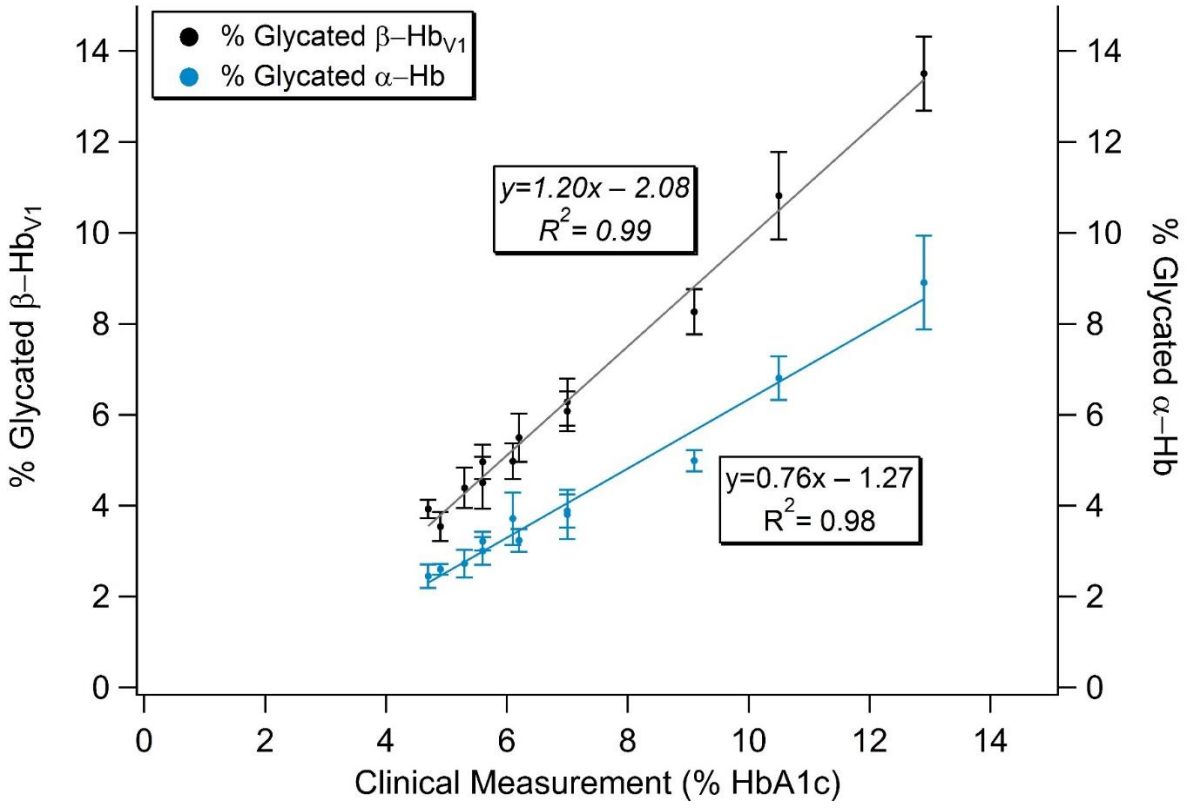

Figure 2.4: Correlation plot between clinical HbA1c levels and glycated α-Hb and β-Hb measured by microfluidic CE-MS. The %glycated β-Hb$_{V1}$ and %glycated α-Hb correlate linearly with the %HbA1c values measured clinically.

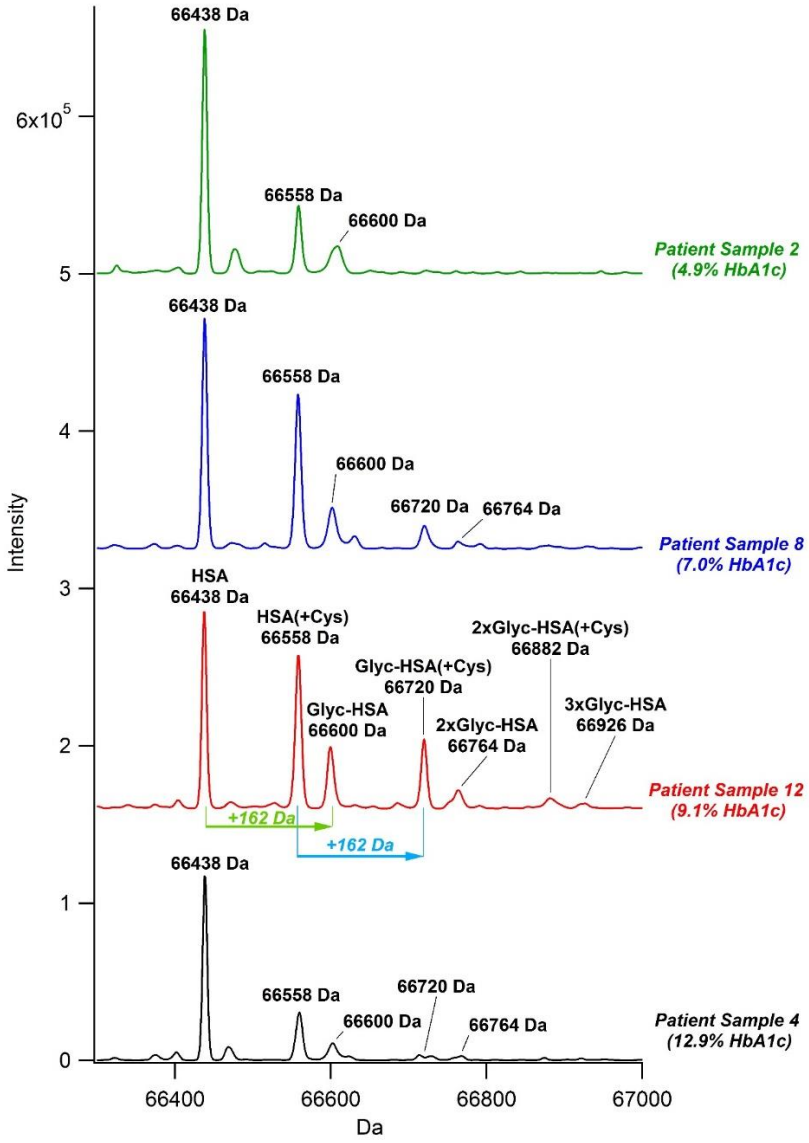

Figure 2.5: Deconvoluted mass spectra for human serum albumin from patient samples 2, 4, 8, and 12. The traces are arranged with increasing HbA1c from top to bottom. The patients with elevated HbA1c levels also have an increased number of glycated HSA species. However, the highest level of albumin glycation did not correspond to the highest level of glycated hemoglobin, which could indicate a more recent lapse in glycemic control. Identified glycated albumin species are labeled in the spectrum for patient 12. The spectra were offset for viewing purposes.

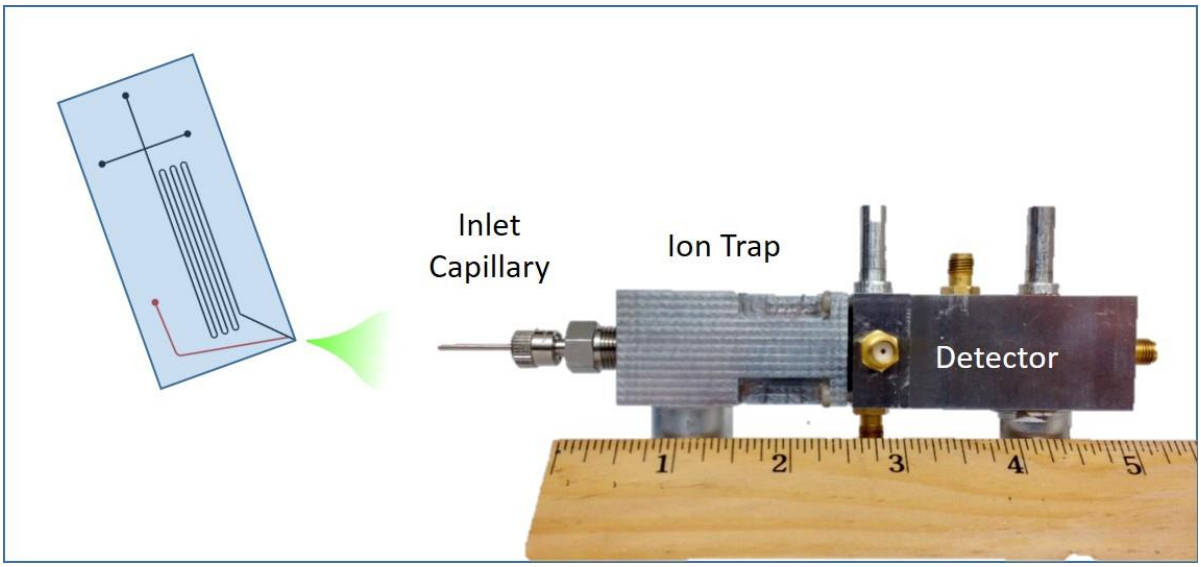

Figure 2.6: Photograph of the miniature MS prototype system. The regions accounting for ion transfer, mass analysis, and detection are approximately 6 inches in length. Analyte ions are transferred through the inlet capillary to the ion trap where they are trapped, ejected, and then detected in the detector region. It should be noted that the electronics and pumps needed to operate the prototype are not shown in this image.

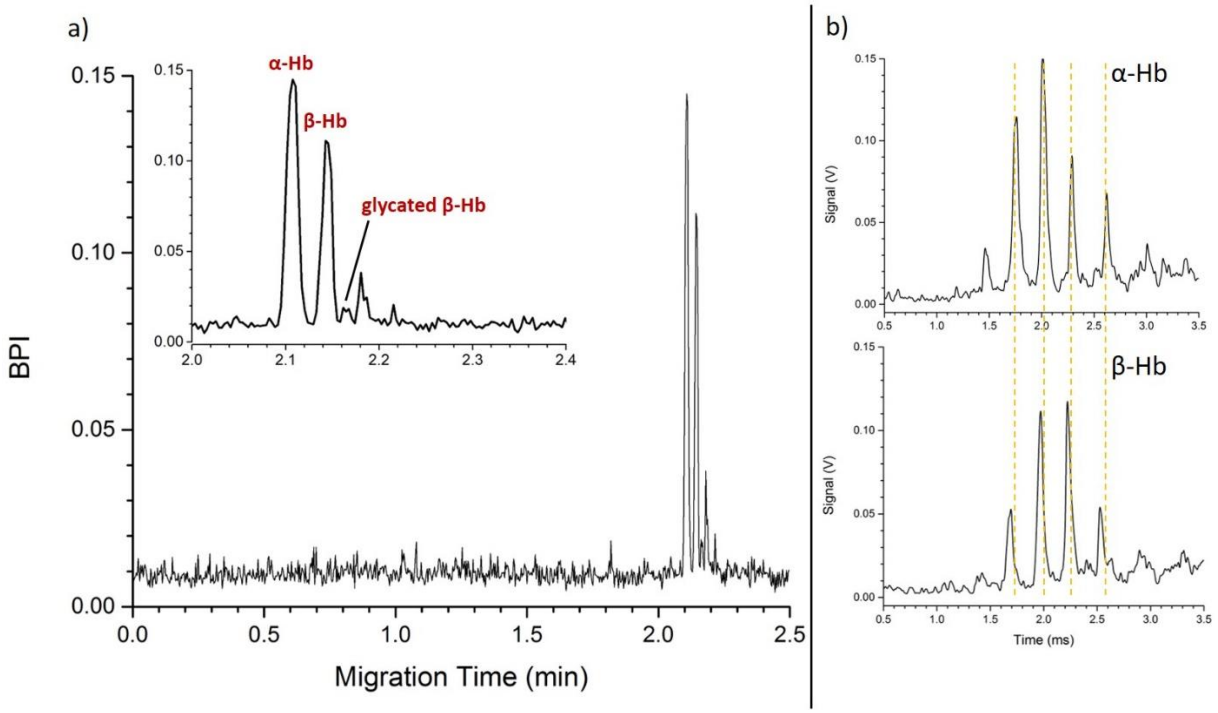

Figure 2.7: Microfluidic CE-MS analysis of hemoglobin glycation using the prototype miniature MS. a) Electropherogram showing the separation of the hemoglobin subunits. The alpha and beta subunits are easily detected with small peaks corresponding to glycated beta hemoglobin and a beta hemoglobin variant. b) Raw mass spectra for the alpha and beta hemoglobin subunits. Although the mass resolution is much lower than that achieved with the commercial instruments, there are still measureable differences between the two charge envelopes. The time axis of the mass spectra corresponds to ion ejection time during the mass scan. These values are directly correlated to the m/z value of the ion and can be reflected as m/z if the instrument if properly calibrated before analysis.

REFERENCES

(1) Little, R. R.; Sacks, D. B. *Curr. Opin. Endocrinol. Diabetes Obes.* **2009**, *16* (2), 113–118.

(2) Mao, P.; Wang, D. *J. Proteome Res.* **2014**, *13* (3), 1560–1569.

(3) Wang, S.-H.; Wang, T.-F.; Wu, C.-H.; Chen, S.-H. *J. Am. Soc. Mass Spectrom.* **2014**, *25*, 758–766.

(4) Lapolla, A.; Molin, L.; Traldi, P. *Int. J. Endocrinol.* **2013**, *2013*.

(5) Goodall, I. *Clin. Biochem.* **2005**, *26* (February).

(6) Bry, L.; Chen, P. C.; Sacks, D. B. *Clin. Chem.* **2001**, *47* (2), 153–163.

(7) Woodi, M.; Mondal, A. K.; Padmanabhan, B.; Rajagopalan, K. P. *Indian J. Clin. Biochem.* **2009**, *24* (1), 23–29.

(8) Lapolla, A.; Fedele, D.; Traldi, P. *Diabetes. Metab. Res. Rev.* **2001**, *17* (2), 99–112.

(9) Roberts, N. B.; Green, B. N.; Morris, M. *Clin. Chem.* **1997**, *43* (5), 771–778.

(10) Wild, B. J.; Green, B. N.; Cooper, E. K.; Lalloz, M. R.; Erten, S.; Stephens, a D.; Layton, D. M. *Blood Cells, Mol. Dis.* **2001**, *27* (3), 691–704.

(11) Miyazaki, A.; Kohzuma, T.; Kasayama, S.; Koga, M. *Ann. Clin. Biochem.* **2012**, *49* (5), 441–444.

(12) Lapolla, A.; Tubaro, M.; Fedele, D.; Reitano, R.; Aricò, N. C.; Ragazzi, E.; Seraglia, R.; Vogliardi, S.; Traldi, P. *Rapid Commun. Mass Spectrom.* **2005**, *19* (2), 162–168.

(13) Lapolla, A.; Fedele, D.; Aronica, R.; Garbeglio, M.; D'Alpaos, M.; Plebani, M.; Seraglia, R.; Traldi, P. *Rapid Commun. Mass Spectrom.* **1997**, *11* (6), 613–617.

(14) Lapolla, A.; Fedele, D.; Plebani, M.; Garbeglio, M.; Traldi, P. *Rapid Commun. Mass Spectrom.* **1999**, *13*, 8–14.

(15) Davison, A. S.; Green, B. N.; Roberts, N. B. *Clin. Chem. Lab. Med.* **2008**, *46* (9), 1230–1238.

(16) Rai, D. K.; Landin, B.; Alvelius, G.; Griffiths, W. J. *Anal. Chem.* **2002**, *74* (9), 2097–2102.

(17) Zhang, X.; Medzihradszky, K. F.; Cunningham, J.; Lee, P. D. K.; Rognerud, C. L.; Ou, C. N.; Harmatz, P.; Witkowska, H. E. *J. Chromatogr. B Biomed. Sci. Appl.* **2001**, *759* (1), 1–15.

(18) Roberts, N. B.; Amara, A. B.; Morris, M.; Green, B. N. *Clin. Chem.* **2001**, *47* (2), 316–321.

(19) Peterson, K. P.; Pavlovich, J. G.; Goldstein, D.; Little, R.; England, J.; Peterson, C. M. *Clin. Chem.* **1998**, *44* (9), 1951–1958.

(20) Nakanishi, T.; Miyazaki, A.; Kishikawa, M.; Yasuda, M.; Tokuchi, Y.; Kanada, Y.; Shimizu, A. *J. Mass Spectrom.* **1997**, *32* (November 1996), 773–778.

(21) Bu, X.; Yang, J.; Gong, X.; Welch, C. J. *J. Pharm. Biomed. Anal.* **2014**, *94*, 139–144.

(22) Taha, M. N.; Krawinkel, M. B.; Morlock, G. E. *J. Chromatogr. A* **2015**, *1394*, 137–147.

(23) Spaggiari, D.; Mehl, F.; Desfontaine, V.; Grand-Guillaume Perrenoud, A.; Fekete, S.; Rudaz, S.; Guillarme, D. *J. Chromatogr. A* **2014**, *1371*, 244–256.

(24) Browne, D. L.; Wright, S.; Deadman, B. J.; Dunnage, S.; Baxendale, I. R.; Turner, R. M.; Ley, S. V. *Rapid Commun. Mass Spectrom.* **2012**, *26* (17), 1999–2010.

(25) Ouyang, Z.; Cooks, R. G. *Annu. Rev. Anal. Chem.* **2009**, *2*, 187–214.

(26) Nguyen, A.; Moini, M. *Anal. Chem.* **2008**, *80* (18), 7169–7173.

(27) Moini, M.; Demars, S. M.; Huang, H. *Anal. Chem.* **2002**, *74* (15), 3772–3776.

(28) Cao, P.; Moini, M. *J. Am. Soc. Mass Spectrom.* **1999**, No. 10, 184–186.

(29) Cao, P.; Moini, M. *J Am Soc Mass Spectrom* **1998**, *9*, 1081–1088.

(30) Mellors, J. S.; Gorbounov, V.; Ramsey, R. S.; Ramsey, J. M. *Anal. Chem.* **2008**, *80* (18), 6881–6887.

(31) Mellors, J. S.; Jorabchi, K.; Smith, L. M.; Ramsey, J. M. *Anal. Chem.* **2010**, *82* (3), 967–973.

(32) Batz, N. G.; Mellors, J. S.; Alarie, J. P.; Ramsey, J. M. *Anal. Chem.* **2014**, *86*, 3493–3500.

(33) Redman, E. A.; Batz, N. G.; Mellors, J. S.; Ramsey, J. M. *Anal. Chem.* **2015**, *87* (4), 2264–2272.

(34) Black, W. A.; Stocks, B. B.; Mellors, J. S.; Engen, J. R.; Ramsey, J. M. *Anal. Chem.* **2015**, *87*, 6280–6287.

(35) Zhang, Z.; Pan, H.; Chen, X. *Mass Spectrom. Rev.* **2009**, *28*, 147–176.

(36) Berger, S. J.; Chen, W. *Waters Corporation Application Note*. 2008, p Number APNT10094155.

(37) Ferrige, A. G.; Seddon, M. J.; Green, B. N.; Jarvix, S. A.; Skilling, J. *Rapid Commun. Mass Spectrom.* **1992**, *6*, 707–711.

(38) Lopez-Clavijo, A. F.; Duque-Daza, C. A.; Romero Canelon, I.; Barrow, M. P.; Kilgour, D.; Rabbani, N.; Thornalley, P. J.; O'Connor, P. B. *J. Am. Soc. Mass Spectrom.* **2014**, *25* (4), 673–683.

(39) Banerjee, S.; Chakraborti, A. S. *Int. J. Biol. Macromol.* **2014**, *66*, 311–318.

(40) Zhang, Q.; Ames, J. M.; Smith, R. D.; Baynes, J. W.; Metz, T. O. *J. Proteome Res.* **2008**, *8* (2), 754–769.

(41) Gradinaru, D.; Borsa, C.; Ionescu, C.; Margina, D. *J. Proteomics* **2013**, *92*, 313–322.

(42) Koga, M. *Clin. Chim. Acta* **2014**, *433*, 96–104.

(43) Koga, M.; Kasayama, S. *Endocr. J.* **2010**, *57* (9), 751–762.

(44) Regazzoni, L.; Del Vecchio, L.; Altomare, A.; Yeum, K.-J.; Cusi, D.; Locatelli, F.; Carini, M.; Aldini, G. *Free Radic. Res.* **2013**, *47* (3), 172–180.

(45) Wolfe, D. High-pressure Cylindrical Ion Trap Mass Spectrometry, University of North Carolina at Chapel Hill, 2012.

(46) Schultze, K. Advanced System Components for the Development of a Handheld Ion Trap Mass Spectrometer, University of North Carolina at Chapel Hill, 2014.

(47) Blakeman, K. Development of High Pressure Mass Spectrometry for Handheld Instruments, University of North Carolina at Chapel Hill, 2015.

CHAPTER 3: DEVELOPMENT OF AN INTEGRATED MICROFLUIDIC CE-MS PLATFORM FOR THE SEPARATION AND CHARACTERIATION OF INTACT MONOCLONAL ANTIBODY VARIANTS

3.1 Introduction

Common techniques used to analyze monoclonal antibodies (mAbs) include chromatographic methods such as size exclusion chromatography, ion-exchange chromatography, reversed-phase liquid chromatography, and electrophoresis based methods such as isoelectric focusing, gel electrophoresis, and capillary zone electrophoresis. Each technique contributes complementary information to the overall characterization of the mAb, but currently there is no single technique capable of generating all of the desired information about mAb heterogeneity.

Electrospray ionization mass spectrometry (ESI-MS) is a powerful technique for mAb characterization due to the ability to assign mass values to many structural variants. An average mass as well as significant mass shifts (such as those arising from glycosylation) can often be determined by direct infusion into a mass spectrometer. But, as the heterogeneity of the mAb population increases so does the complexity of the mass spectrum; and the isotopic distribution of an intact mAb (~25 Da at half height) combined with additional mass spectral peak broadening obscures minor mass variations such as those due to deamidation and oxidation unless unit mass resolution can be achieved. [2–4,6,9] . It has been shown that a resolving power in excess of 400,000 is required to achieve unit mass baseline resolution of molecules of the size

and complexity of mAbs.[10] A more accessible solution to the problem of spectral overlap is to include a separation step prior to MS analysis

Many mAb modifications induce a change in net charge, and therefore mAb variants can be separated based on charge differences. However, the most common analysis techniques for assessing mAb charge heterogeneity, such as ion-exchange chromatography (IEC) and isoelectric focusing, do not directly interface well with MS. To separate charge variants, these techniques typically require mobile phases or background electrolytes that are not compatible with ESI.[2,9,11–13] Thus, they are almost exclusively relegated to optical detection methods, requiring additional analysis to identify the observed peaks. Efforts have been made to develop MS compatible methodology for these techniques, but they have yet to result in the successful separation of intact mAb charge variants with identification by online MS analysis.[14–16]

Capillary electrophoresis (CE) is another method that can be used to separate intact mAb variants that is potentially compatible with MS detection. The CE separation mechanism is based on differences in electrophoretic mobility, which is determined by the charge and size of analyte molecules. All successful CE methods must control analyte adsorption, maintain solubility, and enhance mobility differences between species; all of which tend to become more challenging as the size and complexity of the analyte increases.[2,17–20] While CE-MS has been successfully demonstrated for the analysis of enzymatically digested mAbs and substantially smaller intact proteins[21–28], previous work using CE for intact mAb analysis has been limited to optical detection. Consequently, MS compatibility was not a consideration during method development. Consequently, separation background electrolytes (BGEs) have included mixtures of components that facilitate the separation, but preclude the use of ESI. For instance, triethylenetetramine (TETA) and high levels of ε-amino-caproic acid (EACA) are often added to

the BGE. TETA acts as a dynamic coating to prevent analyte adsorption, and EACA is a zwitterion that can be used to create high ionic strength, low conductivity buffers that reduce electroosmotic flow (EOF) and enhance electrophoretic mobility differences.[29–33] This strategy results in the separation of charge variants, but the complexity and nature of the BGE components render it incompatible with ESI-MS. Thus, the same problems encountered with ion-exchange chromatography and isoelectric focusing exist.

Our strategy for performing CE-ESI-MS has been to use microfluidic technology to eliminate sources of extra-column band broadening, and surface coatings to control analyte adsorption; this has resulted in highly efficient separations of biomolecules using ESI compatible BGEs.[34–38] For mAb analysis, a surface coating method utilizing chemical vapor deposition (CVD) of an aminopropylsilane (APS) base layer[38] and covalent modification with polyethyleneglycol (PEG) is used to prevent analyte adsorption and reduce the EOF. The uniformity and stability of this surface coating yields highly efficient separations. Additionally, the EOF reduction enhances differences in the electrophoretic mobility of the charge variants and increases the resolution of the separation without the use of surfactants or high ionic strength buffers. This eliminates the need for additives such as TETA and EACA so a simple MS compatible BGE can be used without sacrificing separation performance. The APS-PEG surface coating strategy in conjunction with the zero dead volume integration of microfluidic CE-ESI devices results in the successful separation of intact mAb charge variants with online MS analysis. The device performance is demonstrated by characterizing C-terminal lysine variants of a commercial biotherapeutic IgG as well as two additional mAbs.

3.2 Experimental

3.2.1 Materials and Reagents

Deionized water was generated with a Nanopure Diamond water purifier (Barnstead International, Dubuque, IA). Optima LC/MS grade 2-propanol, methanol, acetonitrile, formic acid, and acetic acid (99% purity) were obtained from Fisher Scientific (Fairlawn, NJ). The silane coating reagent 3-(aminopropyl)di-isopropyl-ethoxysilane (APDIPES) was purchased from Gelest (Morrisville, PA) and the methyl-terminated polyethylene glycol *n*-hydroxy succinimide ester (NHS-PEG_{450}) was purchased from Nanocs Inc.(Boston, MA). The number designation 450 denotes the number of PEG units in the reagent. Trichloro(1H,1H,2H,2H-perfluorooctyl)silane was purchased from Sigma-Aldrich (St. Louis, MO). Infliximab was provided by Waters Corporation (Milford, MA) and mAb-A and mAb-B were provided by Pfizer Inc. (St. Louis, MO).

3.2.2 Sample Preparation

Monoclonal antibody samples were stored in their respective formulation buffers at -20° C until analysis. Samples were thawed at room temperature and diluted to 0.1 mg/mL for infusion-MS or 1.0 mg/mL for microfluidic CE-MS with BGE. For Infliximab no additional sample preparation was necessary. mAb-A and mAb-B were buffer exchanged with BGE using an Amicon Ultra Ultracel 50 kDa centrifugal filter (Millipore, Billerica, MA) prior to analysis. The final sample volume was 100 µL for all three mAbs.

3.2.3 CE-ESI-MS Device Preparation and Operation

CE-ESI devices were prepared by applying a two stage APS-PEG coating. Detailed coating procedures are described in Appendix 2. For this analysis an electroosmotic pump was used to sustain ESI. Voltage application to the devices and voltage control was performed as described in Appendix 3. For this analysis a gated injection scheme was used for sample handling. A 200 ms injection was performed for each mAb analyzed, which resulted in ~175 pg of mAb injected. For this work the full 100 µL of sample solution was put in reservoir 1. However, it should be noted that only a small fraction of this is consumed during analysis and a significantly smaller sample volume could be used. Infusions of mAbs were performed using a simplified version of this device that utilizes just two channels to create an electroosmotic pump. A schematic of this device is provided in Figure 2 of Appendix 3.

3.2.4 Data Analysis

MS analysis was performed using either a Waters LCT-Premier time-of-flight mass spectrometer or Synapt G2 quadruple time-of-flight mass spectrometer (Waters Corporation, Milford, MA). The particular instrument used will be provided in the figure caption. Information about the MS instrument settings used is provided in Appendix 4. Deconvolution of the mass spectra was performed based on maximum entropy analysis using the MaxEnt1 deconvolution algorithm in the MassLynx software. Resolution was set at 1.00 Da with minimum intensity ratios at 50%, and the software was set to perform 15 iterations to reduce the occurrence of deconvolution artifacts in the resulting spectrum.[6] The mass range and uniform Gaussian width at half height were adjusted to best match the specific set of data.[6,44] As described previously for deconvolution of intact mAbs spectra, the 5-6 most abundant charge state peaks were used to

provide high signal-to-noise data for processing and reduce the potential side effects of adducts on high m/z ions.[45]

3.3 Results and Discussion

3.3.1 Optimization of Background Electrolytes for mAb Analysis

Infusion of mAbs is a simple way to assess the effect of different background electrolytes on the antibody and to obtain an average MW. Characteristics of the most abundant charge state and charge envelope can provide information about the conformation of the antibody (denatured or natured), whether there is significant aggregation, or other detrimental effects. An added benefit is that waste is minimized because a much lower concentration of antibody is suitable for infusion experiments. The commercially available mAb, Infliximab, was selected for method development because it has been characterized in the literature[32,33] and has a distinct charge variant profile due to relatively equal abundances of C-terminal lysine variants.

It has been shown that protein conformation can significantly impact ESI spectra: an unfolded protein becomes more highly charged during ESI and exhibits lower m/z values.[46–48] Based on the poor separation results obtained initially for Infliximab (data not shown), it was hypothesized that high levels of organic modifier partially denature the antibody, muddling subtle differences in electrophoretic mobility induced by post translational modifications (PTMs). To confirm this, Infliximab was infused into a MS using a variety of background electrolytes of different organic modifiers at varying percentages to identify the effect of changing these parameters. The first step in this study was to characterize the appearance of the antibody MS signal in a background electrolyte suspected to greatly denature the molecule: 50% acetonitrile 0.1% formic acid. The resulting mass spectrum contained a very convoluted charge

envelope centered on ~2750 m/z, which is given in Figure 3.1. There is little definition within the individual charge state peaks that would otherwise provide information about glycosylation, and the signal deconvolutes with low certainty to a mass of 149 kDa. Additionally, there is a second charge envelope appearing below 1750 m/z that deconvolutes to approximately 23.5 kDa, which is in agreement with the mass of a typical IgG1 light chain. This supports the idea that the 50% acetonitrile 0.1% formic acid background electrolyte is detrimental to the mAb structure.

Following this characterization, the focus centered on reducing the organic content and changing the type of organic modifier; background electrolytes of 10% acetonitrile, 2-propanol, and methanol were used. The results of this experiment are given in Figure 3.2. The appearance and m/z values of the charge envelopes generated by the low organic content background electrolytes are very similar to the charge envelope seen with the 50% acetonitrile background electrolyte. Although there is not a significant signal for dissociated light chain, it can be concluded that the antibody is also denatured under these conditions. Thus, the organic modifier content is not the only factor contributing to mAb denaturation.

Additional experiments determined that the acid used in the background electrolyte has just as much of an impact as the organic modifier. Acetic acid is another volatile acid commonly used for MS analysis and upon replacing the formic acid with acetic acid, very different results were obtained. As seen in Figure 4b, with a 10% methanol 0.2% acetic acid BGE, rather than a single charge envelope at fairly low m/z values, a bimodal distribution of charge states spanning a range of ~3500-6000 m/z is obtained with the most intense occurring at the higher end of this range. This indicates a lower degree of protonation, which could be attributed to the antibody remaining in a more folded state. These envelopes could be interpreted as two difference species, but both envelopes deconvolute to the same mass, indicating that they are the same mAb species.

The difference in charge state, therefore, could potentially be due to differences in conformation. Overall, it appears that the acetic acid better preserves the native conformation of the antibody while formic acid denatures it. It is evident that this low organic, acetic acid background electrolyte has benefits in terms of conformation preservation.

Once the methanol/acetic acid based background electrolyte was identified as a potential solution, the methanol composition was varied to examine the impact of altering this parameter with the different acid component. Infliximab was infused using four background electrolytes ranging from 0%-50% methanol all with 0.2% acetic acid. As is evident in Figure 3.3, the higher the organic content, the more the antibody is denatured and eventually dissociated light chain was visible in the mass spectrum. The major differences between the 10% methanol BGE and the purely aqueous BGE seem to be signal intensity and clarity. Though the same charge states appear in both mass spectra, the signal intensity is greater with organic modifier present and the charge state peaks appear narrower and more defined. Thus, it seems that the presence of low levels of suitable organic modifier do not have a significant effect on the conformation of the antibody, but act to enhance the antibody signal. Additional experiments utilizing 2-propanol revealed no significant difference between methanol and 2-propanol based BGEs and the organic solvents could be used interchangeably.

Based on the results of the infusion studies, it was concluded that high levels of organic modifiers or the use of formic acid will denature the antibody and can dissociate the light and heavy chains. However, in combination with acetic acid, methanol and 2-propanol are suitable organic modifiers provided their concentration is kept below approximately 10%. Adding an organic modifier to the background electrolyte may not be absolutely necessary, but there are benefits in terms of MS signal and peak resolution. This could become a more significant issue

when separations are performed. It is necessary to gain as much signal as possible since averaged mass spectra are generated from a seconds wide peak rather than a minutes long infusion study.

3.3.2 Separation of Intact mAb Charge Variants

3.3.2.1 Separation Optimization with Infliximab

The initial strategy used for the separation of the mAbs was to attempt to maintain the native conformation as much as possible while still employing a MS compatible background electrolyte. The 10% methanol 0.2% acetic acid background electrolyte identified in the infusion studies was used for the preliminary separation of Infliximab. The analysis was performed using a 23 cm APDIPES coated device and the results are provided in Figure 3.4. It is evident that there is little definition to the mAb peak and at face value it appears that there is no separation of variants. However, the MS data corresponding to the first half and second half of the peak show a distinct difference in the m/z values associated with the charge states (Figure 3.4b). Thus, separation is occurring, but it is very slight. This subtle difference insinuating the beginning of a separation is more significant than any of the previous separation attempts performed up to this point. It implies that the 10% methanol 0.2% acetic acid background electrolyte has a definite impact on the separation and there is a feasible potential for improving the resolution.

As stated before, PEG coating technology developed in the lab can suppress the EOF which, according to CE theory, can improve resolution between analyte species. The longest chain PEG reagent, PEG_{450}, was previously shown to reduce the EOF by approximately 90% and used to increase the resolution between similar protein species in a standard mixture. An APS-PEG450 coated device was used to analyze a sample of Infliximab. Figure 3.5a shows the microfluidic CE separation of Infliximab with ESI-MS detection. The separation profile is similar to CE separations of Infliximab reported in the literature using TETA and EACA BGE

additives with optical detection.[32,33] However, with this analysis platform these additives were unnecessary to achieve a comparable separation, and for the first time intact mAb charge variants have been separated and identified by MS analysis using a single experiment. There are three nearly baseline resolved peaks along with smaller peaks to the left and right, indicating the presence of minor basic and acidic variants, respectively. The three largest peaks are on average 1.2 s duration at half height (~2 s duration at the base.) Mass spectra were generated by summing an approximately 2 s window of MS data points from the center of each peak in the electropherogram.

Deconvolution of each charge variant mass spectrum generated multiple masses, corresponding to the expected presence of neutral glycosylation variants. To facilitate discussion of the charge variants, the most abundant mass variant is used to describe the mass of the charge variant band. The less intense mass peaks present between the labeled mass peaks in the deconvoluted spectrum are believed to be deconvolution artifacts. Thus as seen in Figure 3.5b, the masses ascribed to the three most abundant charge variant bands are 148,633 Da, 148,506 Da, and 148,380 Da. The difference in mass between these bands is similar to the expected mass shift associated with the addition of a lysine residue. Based on the MW information, the earliest band corresponds to the 2-lysine variant (2-K), the middle band corresponds to the 1-lysine variant (1-K), and the last band corresponds to the 0-lysine variant (0-K). This assignment is also supported by the change in apparent mobility (μ_{app}) of the variants. Based on three replicate electropherograms, the three bands correspond to μ_{app} values and relative standard deviations of 2.28×10^{-4} (±0.83%) cm^2/Vs, 2.25×10^{-4} (±0.82%) cm^2/Vs, and 2.22×10^{-4} (±0.83%) cm^2/Vs. The addition of each lysine residue increased the electrophoretic mobility by the same amount (0.03×10^{-4} cm^2/Vs), implying that the variation between the charge variants is of the same nature.

In addition to the major lysine variants, there are also minor basic and acidic variants visible to the left and right of the three major peaks. These minor peaks deconvolute to masses of 148,642 Da and 148,378 Da for the basic and acidic regions, respectively. Relating these minor variants to their nearest lysine variant peak equates to a 9 Da increase for the basic variant and a 2 Da decrease for the acidic variant. Although further work is required to identify these modifications, it is plausible that the mass shifts are a result of several cumulative modifications. For instance, two deamidations would cause a decrease in mass of 2 Da and also reduce the net charge of the mAb causing a μ_{app} decrease.[1] This is in agreement with the characteristics of the minor acidic variant and is a potential explanation for its modification. The low signal to noise ratio of the mass spectra associated with these low-abundance variants introduces error into the deconvolution process and a more sensitive mass spectrometer with greater resolving power would improve the identification of these species.

The addition of galactose moieties to the glycan structure is associated with a mass increase of 162 Da/moiety, but does not induce a change in net charge.[1,5,49] While changes in mass have the potential to affect mobility, the mass of a galactose moiety accounts for only ~0.1% of the total mass of the antibody. To induce a μ_{app} shift on par to that associated with a change in net charge, the mass increase would have to be much greater or induce a significant change in conformation. Although there is not a mobility shift between mAb glycoforms, glycosylation patterns are visible in the mass spectra of the major charge variants of Infliximab. Glycoforms are labeled in Figure 6b above the associated mass peak. The addition of 0 to 2 galactose moieties per glycan structure is visible and the various glycoforms are present in similar abundances for each lysine variant. While not observed here, it is worth noting that CE

has the potential to resolve glycoforms with acidic glycans, due to a reduction in net charge from the addition of negatively charged sialic acid groups.[1]

The same separation was performed using different background electrolytes to determine if changing the organic modifier content causes a significant improvement in resolution or signal quality. The organic content was varied from 0% to 20% 2-propanol and the results of this are presented in Figure 3.6. Decreasing the 2-propanol content from 10% reduces the separation window from approximately 0.2 min (12s) to 0.14 min (8s). Though the decrease is not drastic, it is sufficient to lose definition of the minor acidic and basic variants. The intensity of the mass spectra also decreases with decreasing organic. Increasing the 2-propanol content has a much more obvious effect on the antibody separation. This begins to partially denature the antibody, which is evidenced by the large, broad peak appearing after the three lysine variant peaks. The mass spectrum associated with this peak is similar to that seen with background electrolytes that denature the antibody: there is a single major charge envelope centered around a relatively low m/z value. Based on the results of this study where 2-propanol and acetic acid content was varied, it was determined that no other combination of those two reagents yielded significant improvement of the separation of the Infliximab charge variants. Thus, 10% 2-propanol 0.2% acetic acid became the predominant background electrolyte used for mAb characterization.

The advantage of a separation prior to MS analysis is obvious when comparing the mass spectrum of Infliximab generated by direct infusion-MS to the mass spectra of the individual variant peaks produced by CE-ESI-MS. The infusion mass spectrum for the +31 charge state is given in Figure 3.7 and the comparable charge states of the three lysine variants are overlaid beneath the infusion spectrum. The overlaid lysine variant spectra depict how the mAb species overlap and combine to obscure individual mass signals if they are not separated prior to MS

analysis. As described in Figure 3.5b, at least 4 mAb glycoforms can be identified per lysine variant, resulting in at least 12 mAb species identified. However, there are only six distinct features in the infusion spectrum due to spectral overlap of the lysine variants. The result of this is a more convoluted mass spectrum with wider m/z peaks (FWHH ~5 m/z) as opposed to the separated variant spectra (FWHH ~2 m/z). The deconvolution algorithm is incapable of generating masses for the different glycoforms of each lysine variant from the infusion mass spectrum. Only seven masses are generated that are not easily interpreted because they are a combination of multiple mAb mass signals (data not shown). Additionally, the minor acidic and basic variants are completely obscured due to their low abundance and small mass shifts. Having a CE separation in line with MS detection results in simpler mass spectra and, in turn, the identification of more mAb species. While an instrument with state of the art resolving power will resolve more mass species during an infusion experiment than the instrument used for this work, the simplification of the mAb population achieved through separation reduces the requirements for MS resolving power. The microfluidic CE-ESI-MS approach, in turn, renders this type of mAb analysis available to laboratories with modest MS resolving power, i.e., a few thousand.

3.3.2.2 Analysis of Biotherapeutic mAbs to Assess General Method Applicability

One the difficulties associated with analyzing these large, complex molecules is that different mAb species can respond quite differently to the same analysis parameters. The value of a method decreases if it only works well for a specific molecule, so to test the general applicability of the microfluidic CE-ESI-MS method for the characterization biotherapeutics, additional mAbs were analyzed.

The mAb-A molecule is an IgG2 type antibody and a separation of this mAb is given in Figure 3.8a. There are four distinct product related bands present in the electropherogram. The masses generated from deconvoluting the mass spectra associated with each band are 146,407 Da, 146,277 Da, 146,146 Da, and 146,169 Da for bands 1-4 respectively. The mass differences between the first three bands are approximately 130 Da, corresponding to a shift associated with a C-terminal lysine residue. The 2-3 Da difference between the expected and observed mass shifts is likely due to both the signal intensity of the smaller charge variant peaks and error associated with the deconvolution process. To support the identification of these as lysine variants, the μ_{app} of each species was calculated. Bands 1-3 have μ_{app} values of $2.09x10^{-4}$ (±0.023%) cm^2/Vs, $2.06x10^{-4}$ (±0.057%) cm^2/Vs, and $2.03x10^{-4}$ (±0.043%) cm^2/Vs, respectively. The trend of decreasing μ_{app} with decreasing masses that was seen with Infliximab is also followed with mAb-A. Additionally, the difference in mobility of the mAb-A charge variants under these conditions is $0.03x10^{-4}$ cm^2/Vs, which is identical to the μ_{app} shift between the lysine variants of Infliximab. Bands 1-3 can therefore be characterized as 2-K, 1-K, and 0-K, respectively. This strategy of using electrophoretic mobility shifts to support identification could potentially be applied as a metric for analyzing other mAb modifications. Although both mAb-A and Infliximab have C-terminal lysine variants, the relative variant abundances are very different. The mAb-A material is perhaps more indicative of a typical biotherapeutic mAb in that the partial C-terminal lysine truncation variants account for a relatively small percentage of the total mAb population. The mAb-A and Infliximab data were analyzed using the Igor Pro Multipeak Fitting 2 analysis package and the results of the fit were used to approximate the relative abundance of C-terminal lysine variants for each molecule. Based on peak areas from the total ion electropherogram for the C-terminal lysine variants it was determined that mAb-A is

comprised of 2% 2-K variant, 6% 1-K variant, and 92% 0-K variant, while Infliximab is approximately 34% 2-K variant, 28% 1-K variant, and 38% 0-K variant. Glycosylation patterns are also visible in the mass spectra associated with the identified lysine variants for mAb-A. Glycoform labels are designated above the peak masses in Figure 3.8b. The addition of up to four galactose residues is visible in the mass spectrum for the major 0-K charge variant peak. The most acidic variant, peak 4, differs in mass from the 0-K variant (peak 3) by 23 Da. The nature of this modification is not immediately obvious, and therefore could be a combination of variations to the structure that also results in a net charge reduction as supported by the observable shift in μ_{app}.

The monoclonal antibody mAb-B is also an IgG-2 type antibody. Intact analysis of mAb-B charge variants via microfluidic CE-ESI-MS revealed three main variants of the mAb (labeled 1, 2, and 3) as seen in Figure 3.9a. To generate mass spectra for the charge variants, the mass scans were averaged over the width of the CE bands. The mass spectrum of the most abundant charge variant in the separation is provided in Figure 3.9b. Masses for the charge variants were obtained through deconvolution of the mass spectra and are provided above their respective bands in Figure 10a.

Identification of the charge variants was accomplished by considering both the mass shift and relative change in electrophoretic mobility between variants. The mass difference between the two most abundant charge variants, 2 and 3, is 18 Da, which is similar to the mass shift attributed with multiple common modifications including oxidation and pyroglutamic acid formation at the N-terminus of the heavy chain.[1] While both modifications are plausible, pyroglutamic acid formation is more consistent with the observed shift in electrophoretic mobility because there is a reduction in charge associated with the cyclization reaction with the

N-terminus amine. The presence of this modification was confirmed using conventional peptide mapping with MS detection by collaborators at Pfizer (data not shown). With this analysis strategy where mobile cations are sampled, the most mobile variants in the electropherogram (those with the lowest migration time) are more positively charged, or more basic, than those with longer migration times. Thus, the mAb-B charge variant 2 is more basic than the more abundant variant 3. The apparent mobility of variants 2 and 3 are $2.47x10^{-4}$ cm^2/Vs and $2.44x10^{-4}$ cm^2/Vs, respectively. This is a mobility decrease of $0.03x10^{-4}$ cm^2/Vs. Considered with respect to pyroglutamic acid formation the decrease in mass of 18 Da is consistent with the decrease in mobility due to the loss of +1 charge. As discussed above, the same mobility shift of $0.03x10^{-4}$ cm^2/Vs between mAb bands was observed for C-terminal lysine variants, which also differ by 1 charge unit.[50] Thus, this mobility shift has twice been found to be characteristic of mAb modifications that alter the net charge by 1 with relatively minor mass changes.

The most basic variant at 149135 Da (band 1 in Figure 3.9a) is lower in mass than both other charge variants. There is a mass shift of 44 Da between this variant and its more acidic neighbor (band 2) and the magnitude of the mobility shift suggests that the modification also induces a change in net charge of 1. These properties agree with the mass and charge modifications characteristic of a decarboxylation event; removal of a carboxylic acid group as carbon dioxide results in a mass decrease of ~44 Da and elimination of a negative charge. A mAb species with this modification would present as more basic and 44 Da lighter in mass. Thus, the most basic variant of mAb-B is a decarboxylated form of the molecule.

Again, a sufficient level of sensitivity and resolution was obtained in the mass domain to identify several glycoforms of mAb-B. Identified mAb-B glycoforms are labeled in the deconvoluted mass spectrum in Figure 3.9c. It should be noted that the glycoform masses

generated during intact analysis account for the glycans on both heavy chains of the mAb. As such, it is not possible to differentiate between some glycoforms that have identical masses, such as G0F/G2F and G1F/G1F. The glycoforms identified are characteristic of Chinese hamster ovary expressed monoclonal antibodies. Based on the areas of the mass peaks in the deconvoluted spectrum, mAb-A is primarily G0F/G0F and G0F/G1F at 77.2% and 18.3%, respectively. The remaining glycoforms account for less than 5% each: 2.5% G2F, 1.7% G0, 0.2% G0F(-GlcNAc), and 0.1% partially aglyco mAb. Results from conventional glycan cleavage and derivatization analysis performed at Pfizer support the identification of the intact glycoforms. However, as seen in Table 3.1, there are low abundance glycans (less than 0.15% of total population) detected through the cleaved glycan analysis that are not identified in the deconvoluted mass spectrum. These species differ in mass from one of the identified glycoforms by less than 50 Da and are spectrally obscured by the more abundant species. For instance, Man 5 differs in mass by 23 Da from G0F(-GlnNAc) and G1F(-GlnNAc) differs from G0F by 36 Da. At such low abundances these species will not be resolved in the mass domain without a mass spectrometer with higher resolving power. Although some minor glycoforms are not resolved in the mass domain, this method is able to detect aglyco isoforms of the mAb, which is information that is not generated through cleaved glycan analysis. Additionally, this glycoform information can be generated in minutes with minimal sample preparation as no enzymatic digestion and labeling is required.

3.4 Conclusions

Here we have demonstrated a microfluidic CE-ESI-MS method for the separation of intact mAb charge variants. Through method development it was determined that the BGE

composition and the surface chemistry have significant impact on the separation of the mAbs. A BGE with low levels of methanol or 2-propanol and acetic was found to preserve some of the native structure of the mAb. Additionally, PEGylation of the APS coating in the separation channel proved vital to achieving significant resolution between the mAb charge variants. This surface chemistry suppressed the EOF and prevented analyte adsorption which eliminated the need for complex BGE additives commonly used in CE analysis of mAbs. The microfluidic ESI interface proved vital to the successful ionization and resulting MS analysis by maintaining fluid flow to generate stable ESI. The use of an ESI compatible BGE and the efficient microfluidic ESI interface enabled MS analysis of the intact mAb charge variants. Molecular weights were determined for five charge variants detected in the separation of Infliximab through deconvolution of the mass spectra. Three C-terminal lysine variants were identified by characteristic 128 Da mass shifts, and this identification was supported by the increase in cationic μ_{app} with the addition of a lysine residue to the mAb species. Thus, this analysis platform yields two criteria to aid in the identification of mAb charge variants: mass and electrophoretic mobility. The advantage of adding a separation step prior to MS analysis of intact monoclonal antibodies is evident when comparing direct infusion mass spectra to spectra generated from separation data. Individually analyzing mAb variants results in simplified MS data and increases the number of mAb species that can be identified from the analysis. The separation of Infliximab charge variants allowed the glycoforms of the variants to be characterized; the addition of 0 to 4 galactose residues to the glycan structure were identified in the deconvoluted spectra of the major variant bands.

Two additional mAbs were analyzed to demonstrate the general applicability of our approach. The antibody, mAb-A, proved to bear similar modifications to Infliximab. Three C-

terminal lysine residues were identified by mass and confirmed by the same electrophoretic mobility shift observed for the Infliximab sample. While the lysine variants of Infliximab were of roughly equal abundance, the 1-K and 2-K variants of mAb-A were estimated to account for only 6% and 2% of the total population of mAb-A. For mAb-B, it was determined that the charge heterogeneity was due to pyroglutamic acid formation and decarboxylation rather than C-terminal lysine truncation. Further, it was confirmed that the identified glycoforms from the intact analysis agree very well the results of a cleaved glycan experiment. Many of the same glycan species can be detected and in similar abundances. However, those of very low abundance or very similar masses are difficult to detect at the intact level.

These results demonstrate that the microfluidic CE-ESI device strategy described here is a rapid, generic strategy for the separation of intact mAb charge variants and allows direct coupling to MS analysis. This approach generates multiple pieces of information in a single analysis step. The mass of intact mAb variants, an assessment of charge heterogeneity, and glycoform information are all obtained with little to no sample preparation and total analysis times of less than four minutes. The electrophoretic separation of mAb variants prior to MS analysis reduces the performance requirements of the MS instrument needed to characterize the mAb. MS instrumentation with greater mass accuracy and sensitivity would indeed facilitate the identification of mAb variants while using the separation device, but is not a requirement for successful analysis. The CE separation could also be improved by utilizing higher voltages or longer separation channels to increase the resolution between mAb charge variants.

3.5 Figures and Tables

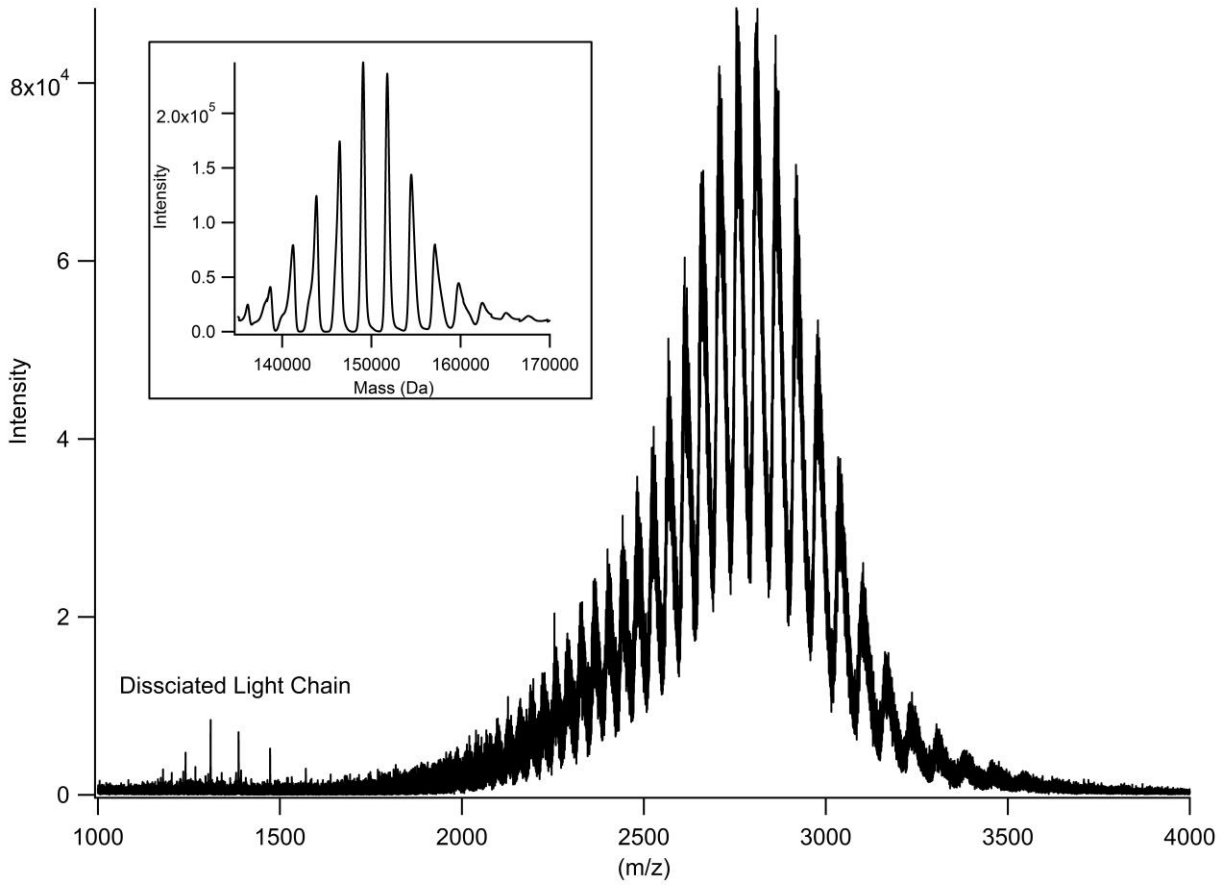

Figure 3.1: Infusion of Infliximab in 50% Acetonitrile 0.1% Formic Acid. Inset: deconvoluted mass spectrum providing an approximate MW. Instrument: Waters Synapt G2

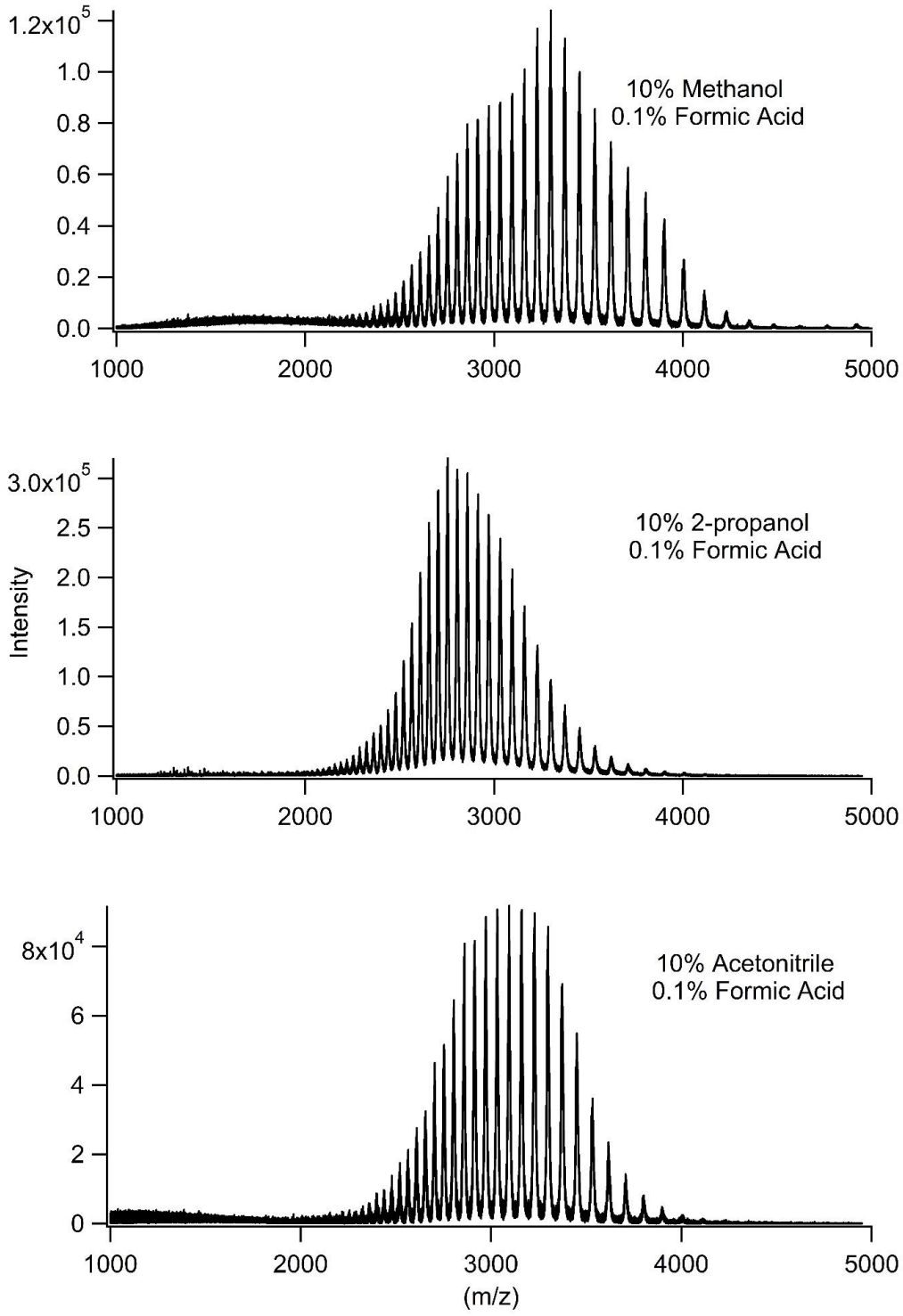

Figure 3.2: Infliximab infusions using 10% 2-propanol 0.1% Formic Acid, 10% Acetonitrile 0.1% Formic Acid, and 10% Methanol 0.2% Acetic Acid. Instrument: Waters Synapt G2

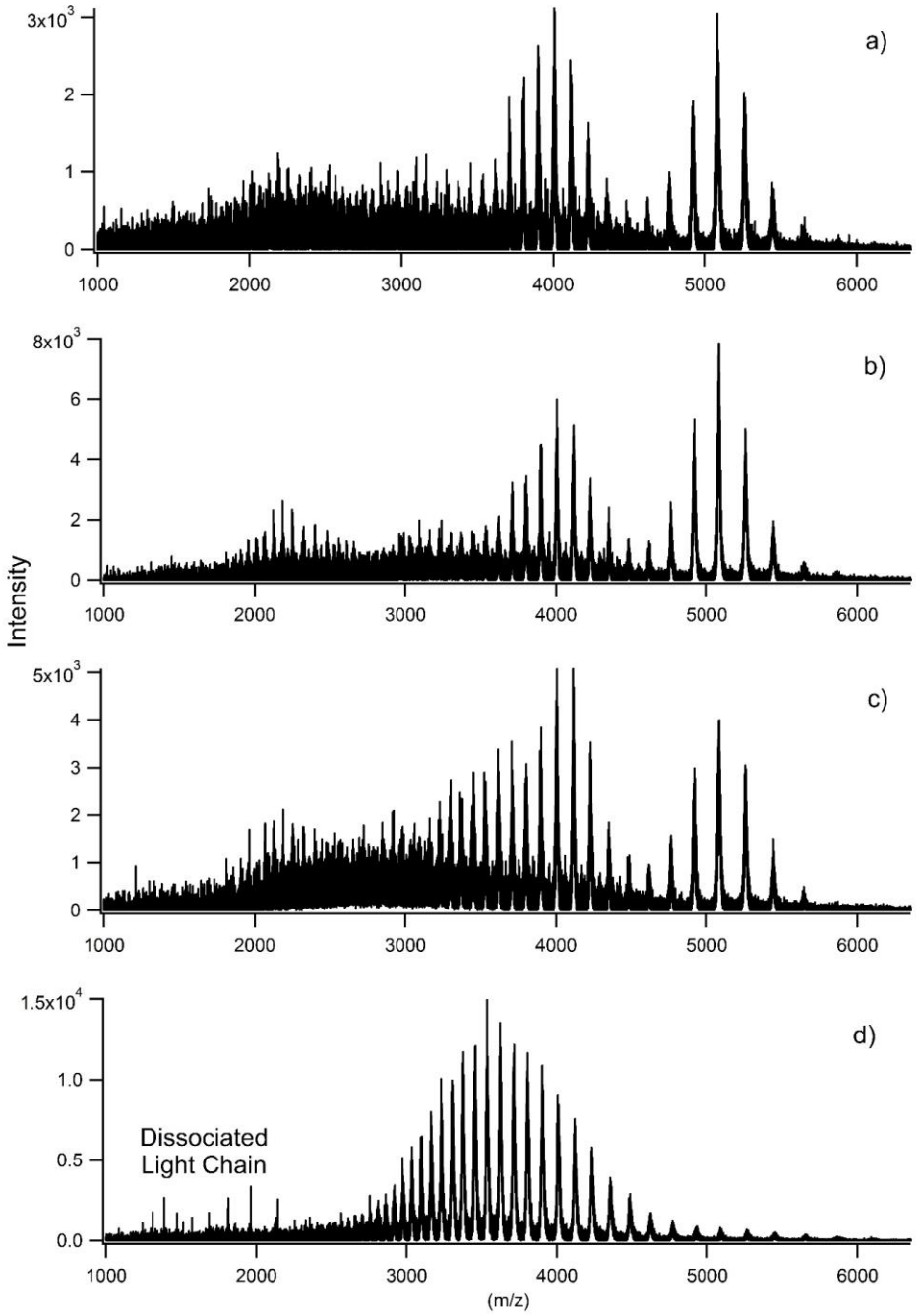

Figure 3.3: Infliximab infused with increasing levels of methanol in the background electrolyte. The acid content of 0.2% acetic acid remained constant for all of the background electrolytes used. a) aqueous 0.2% acetic acid, b) 10% methanol, c) 20% methanol, d) 50% methanol. The mAb begins to dissociate at 20% methanol and evidence of dissociated light chain is seen in (d). Instrument: Waters Synapt G2

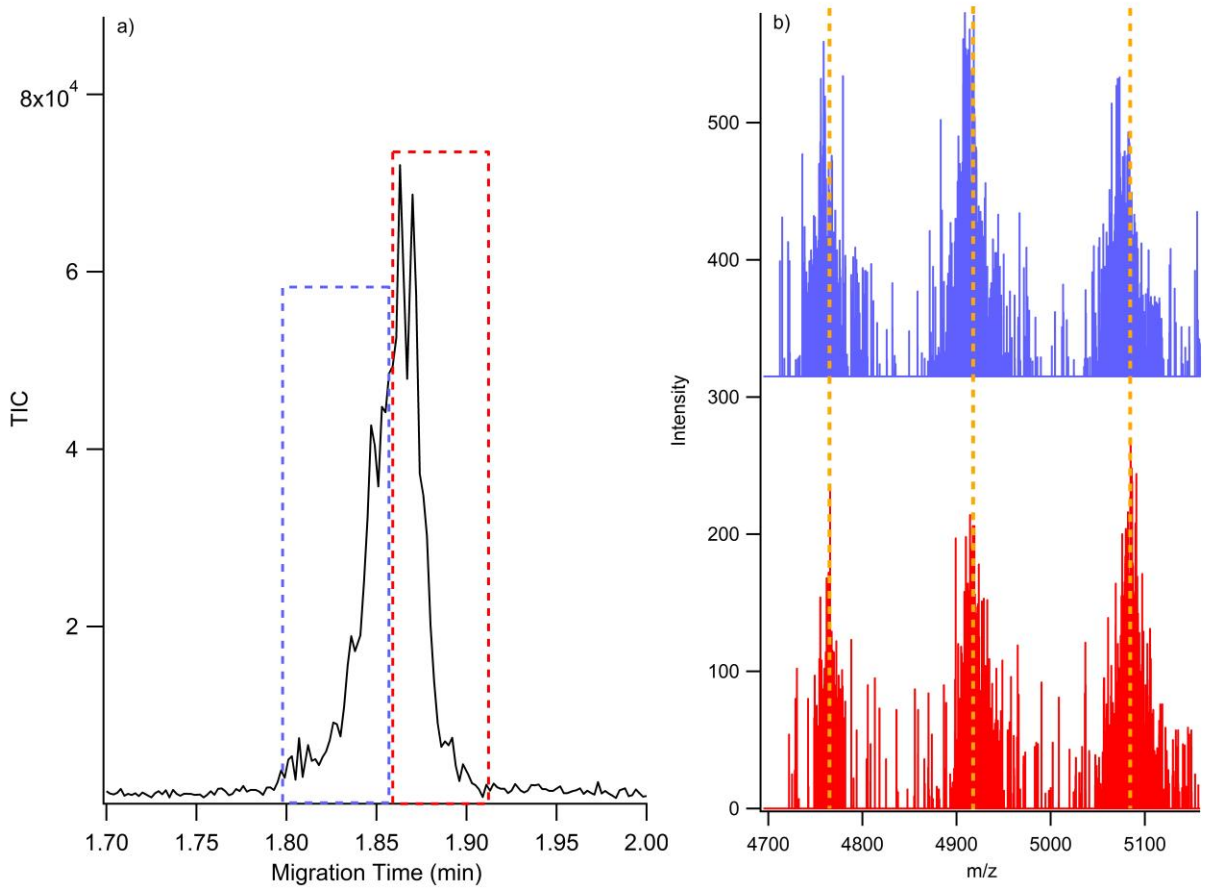

Figure 3.4: a) Separation of 2 mg/mL Infliximab using 10% methanol 0.2% acetic acid and a 23 cm APS coated device. Little to no separation of charge variants resulted from this strategy. b) Mass spectra associated with the first half and second half of the antibody peaks. Differences in the m/z values of the charge states indicate slight separation within the peak. Instrument: Waters Synapt G2

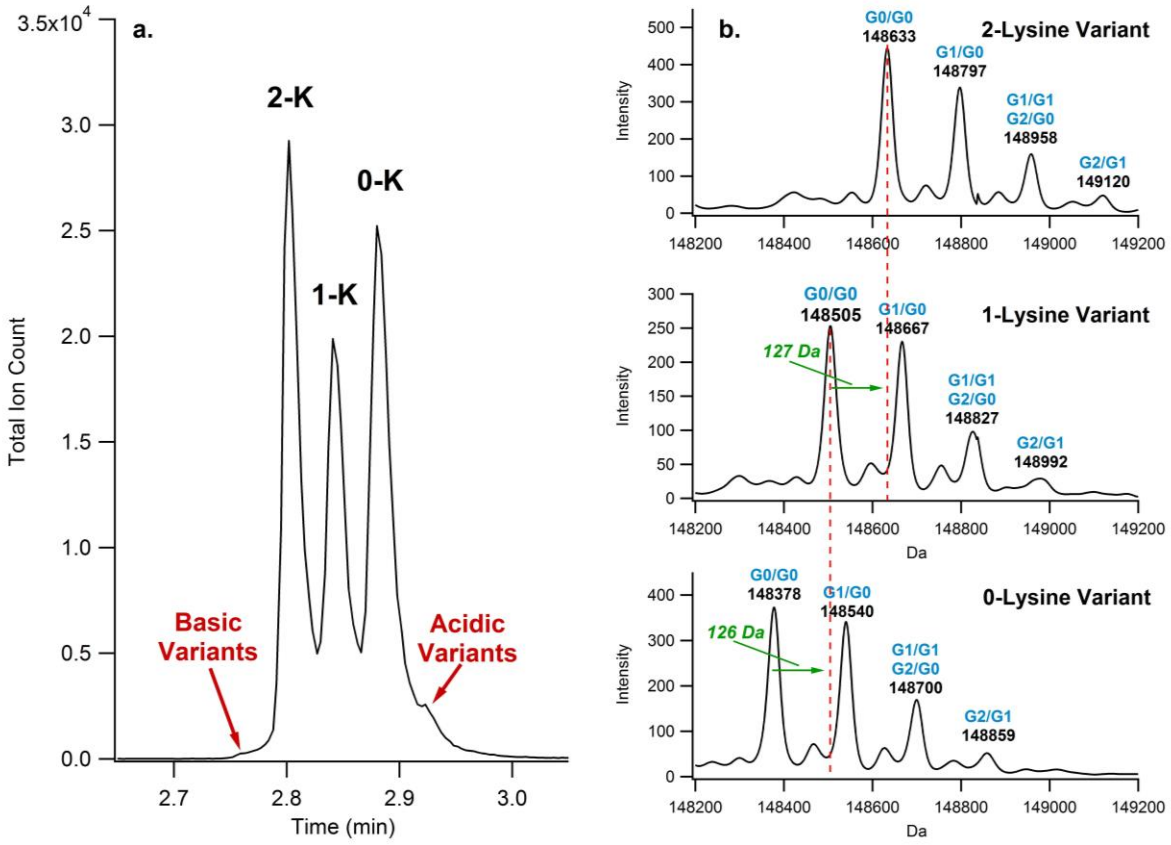

Figure 3.5: a) Separation of intact Infliximab charge variants using a 23-cm APS-PEG_{450} coated device at approximately 600 V/cm. Identified lysine variant bands are labeled as 2-K, 1-K, and 0-K. b) Deconvoluted mass spectra for each lysine variant. Glycosylation structures are labeled above the mass of each peak. Instrument: Waters LCT-Premier

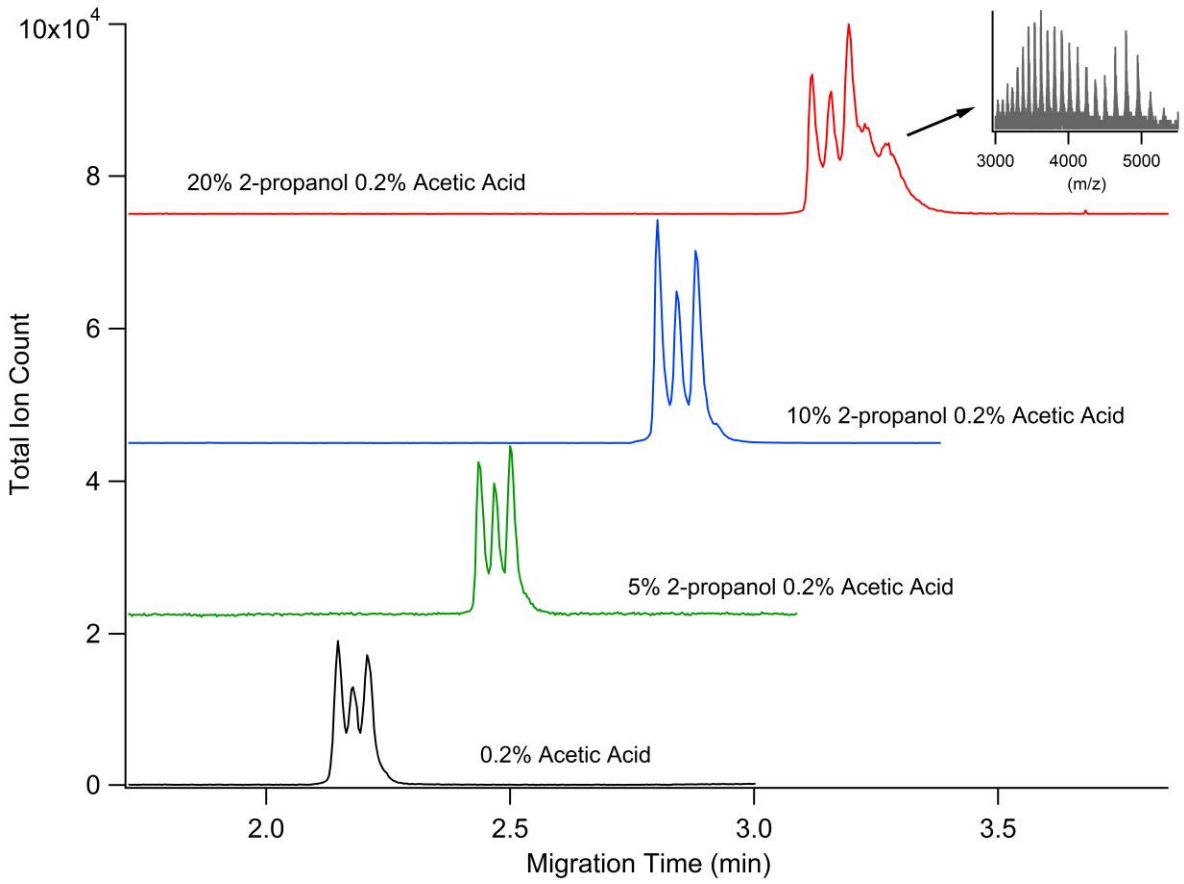

Figure 3.6: Separation of 1mg/mL Infliximab at varying 2-propanol contents. The separation resolution and signal intensity increases up to 10% 2-propanol. At 20% 2-propanol the mAb begins to denature. Waters LCT-Premier.

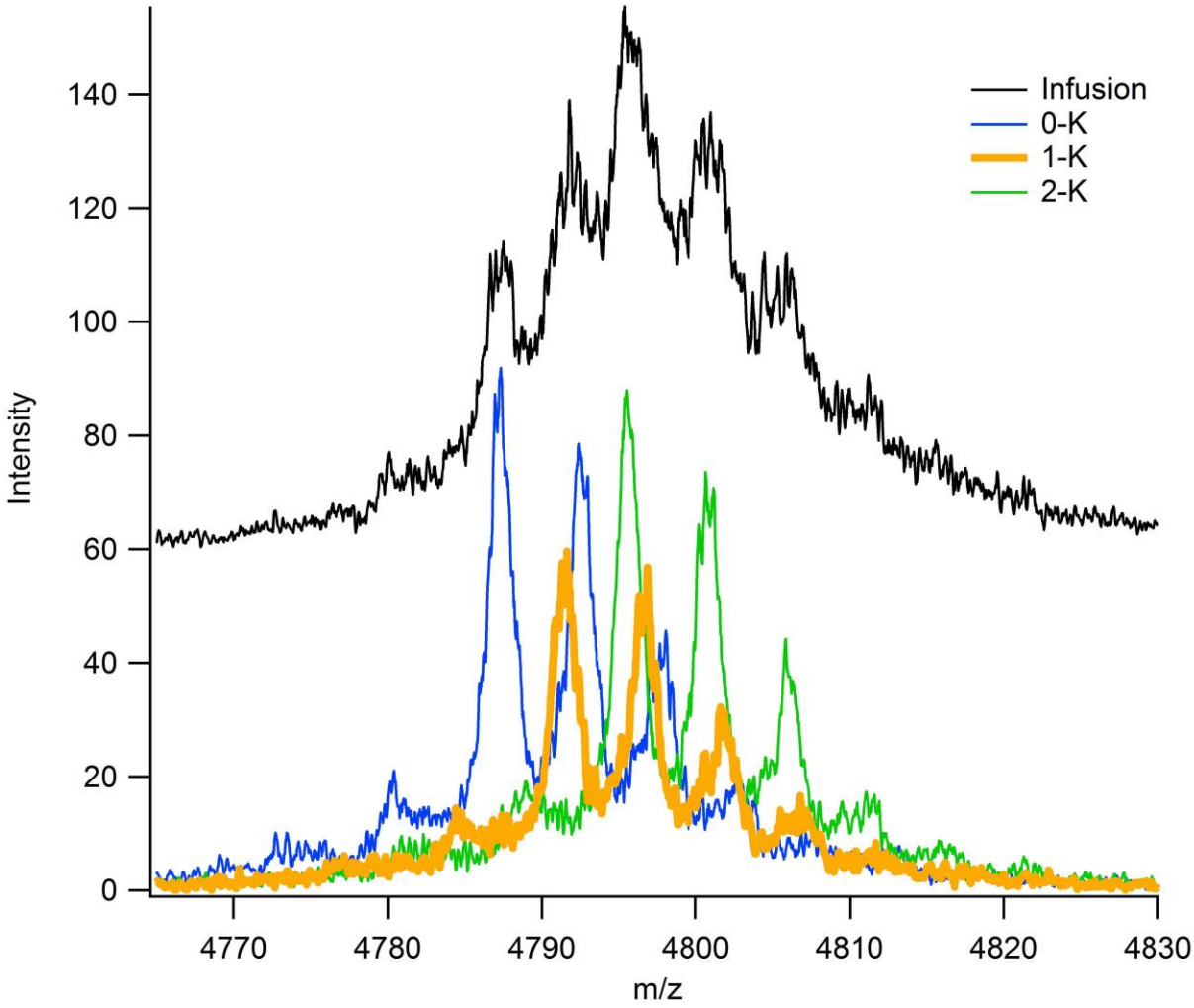

Figure 3.7: Direct infusion of Infliximab compared to overlaid spectra of the 0K-2K variants generated from the separation in Figure 2a. The 1-K variant spectrum is bolded to show detail. Instrument: Waters LCT-Premier

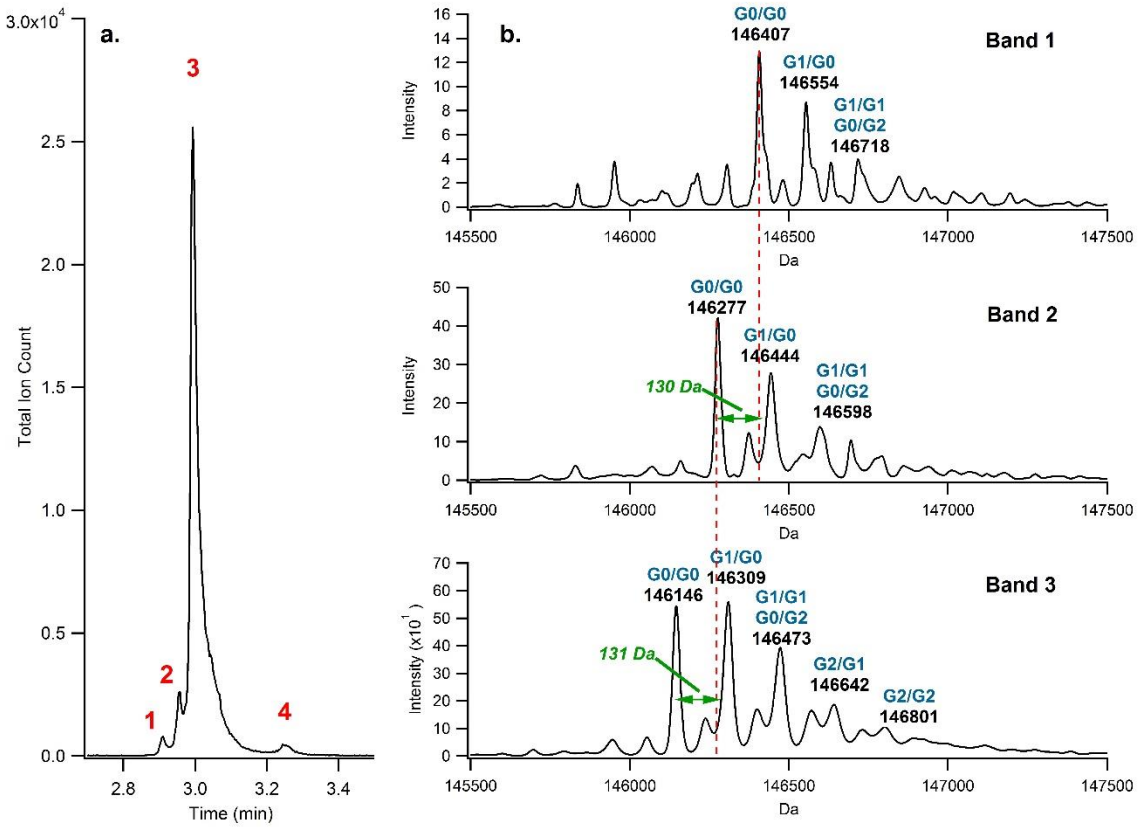

Figure 3.8: a) Separation of 1 mg/mL mAb-A using a 23-cm APS-PEG_{450} coated device at approximately 600 V/cm. b) Deconvoluted mass spectra for each major variant band. Glycosylation structures are labeled above each mass spectral peak. Instrument: Waters LCT-Premier

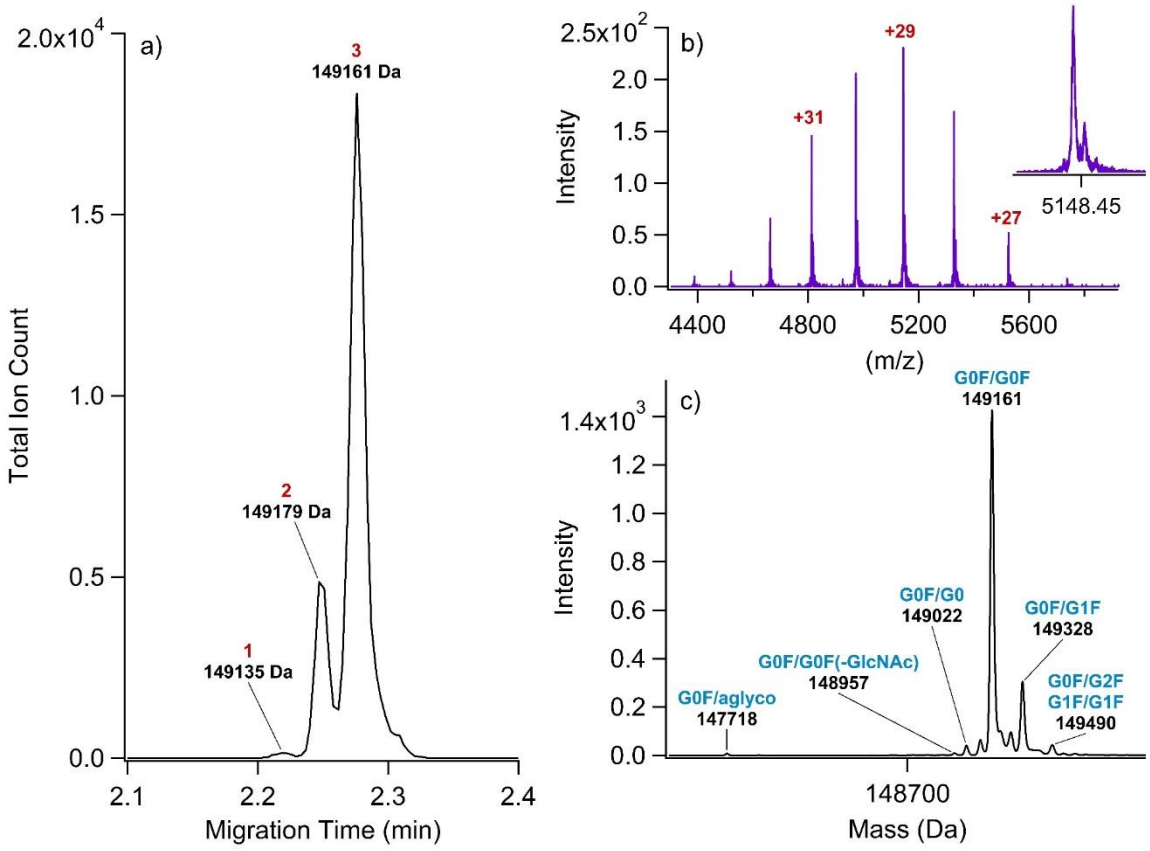

Figure 3.9: Characterization of mAb-B: a) Electropherogram of intact charge variants generated via microfluidic CE-ESI-MS. Peaks are labeled with the mass obtained through deconvolution of that variants' mass spectra. b) Raw mass spectrum corresponding to the most abundant charge variant, c) Deconvolution of the mass spectrum in b with identifiable glycoforms labeled. Instrument: Waters LCT-Premier

Table 3.1: Glycans and glycoforms of mAb-A identified through cleaved glycan analysis and intact microfluidic CE-MS separation. Released glycans were 2-AB labeled and separated using liquid chromatography.

Glycan ID	Cleaved Glycan	Glycoform ID	Intact mAb
G0F	87.35%	**G0F/G0F**	77.22%
G1Fb	5.88%	**G0F/G1F**	18.35%
G1Fa	4.95%	**G0F/G2F or G1F/G1F**	2.46%
G0	0.97%	**G0F/G0**	1.75%
G2F	0.25%	**G0F/G0F(-GlnNAc)**	0.15%
G0F-GlnNAc	0.21%	**G0F/aglyco**	0.07%
G1-GlcNAc	0.14%		
Man 5	0.14%		
G0-GlnNAc-Fuc	0.11%		

REFERENCES

(1) Liu, H.; Gaza-bulseco, G.; Faldu, D.; Chumsae, C.; Sun, J. *J. Pharm. Sci.* **2008**, *97*, 2426–2447.

(2) Fekete, S.; Gassner, A.-L.; Rudaz, S.; Schappler, J.; Guillarme, D. *TrAC Trends Anal. Chem.* **2013**, *42*, 74–83.

(3) Macht, M. *TrAC Trends Anal. Chem.* **2013**, *48*, 62–71.

(4) Zhang, H.; Cui, W.; Gross, M. L. *FEBS Lett.* **2014**, *588* (2), 308–317.

(5) Arnold, J. N.; Wormald, M. R.; Sim, R. B.; Rudd, P. M.; Dwek, R. A. *Annu. Rev. Immunol.* **2007**, *25*, 21–50.

(6) Zhang, Z.; Pan, H.; Chen, X. *Mass Spectrom. Rev.* **2009**, *28*, 147–176.

(7) Chelius, D.; Jing, K.; Lueras, A.; Rehder, D. S.; Dillon, T. M.; Vizel, A.; Rajan, R. S.; Li, T.; Treuheit, M. J.; Bondarenko, P. V. *Anal. Chem.* **2006**, *78* (7), 2370–2376.

(8) Jones, L. M.; Zhang, H.; Cui, W.; Kumar, S.; Sperry, J. B.; Carroll, J. A.; Gross, M. L. *J. Am. Soc. Mass Spectrom.* **2013**, *24* (6), 835–845.

(9) Beck, A.; Diemer, H.; Ayoub, D.; Debaene, F.; Wagner-Rousset, E.; Carapito, C.; Van Dorsselaer, A.; Sanglier-Cianférani, S. *TrAC Trends Anal. Chem.* **2013**, *48*, 81–95.

(10) Valeja, S. G.; Kaiser, N. K.; Xian, F.; Hendrickson, C. L.; Rouse, J. C.; Marshall, A. G. *Anal. Chem.* **2011**, No. 83, 8391–8395.

(11) Rea, J. C.; Moreno, G. T.; Lou, Y.; Farnan, D. *J. Pharm. Biomed. Anal.* **2011**, *54* (2), 317–323.

(12) Farnan, D.; Moreno, G. T. *Anal. Chem.* **2009**, *81* (21), 8846–8857.

(13) Rozhkova, A. *J. Chromatogr. A* **2009**, *1216* (32), 5989–5994.

(14) Talebi, M.; Nordborg, A.; Gaspar, A.; Lacher, N. A.; Wang, Q.; He, X. Z.; Haddad, P. R.; Hilder, E. F. *J. Chromatogr. A* **2013**, *1317* (2013), 148–154.

(15) Mokaddem, M.; Gareil, P.; Varenne, A. *Electrophoresis* **2009**, *30* (23), 4040–4048.

(16) Alvarez, M.; Tremintin, G.; Wang, J.; Eng, M.; Kao, Y.-H.; Jeong, J.; Ling, V. T.; Borisov, O. V. *Anal. Biochem.* **2011**, *419*, 17–25.

(17) Lucy, C. A.; MacDonald, A. M.; Gulcev, M. D. *J. Chromatogr. A* **2008**, *1184* (1-2), 81–105.

(18) Stutz, H. *Electrophoresis* **2009**, *30* (12), 2032–2061.

(19) Huhn, C.; Ramautar, R.; Wuhrer, M.; Somsen, G. W. *Anal. Bioanal. Chem.* **2010**, *396* (1), 297–314.

(20) Haselberg, R.; de Jong, G. J.; Somsen, G. W. *Electrophoresis* **2013**, *34* (1), 99–112.

(21) Gahoual, R.; Busnel, J.; Beck, A.; Leize-wagner, E. *Anal. Chem.* **2014**, *86*, 9074–9081.

(22) Gahoual, R.; Burr, A.; Busnel, J.-M.; Kuhn, L.; Hammann, P.; Beck, A.; François, Y.-N.; Leize-Wagner, E. *MAbs* **2013**, *5* (3), 1–12.

(23) Whitmore, C. D.; Gennaro, L. a. *Electrophoresis* **2012**, *33* (11), 1550–1556.

(24) Sun, L.; Knierman, M. D.; Zhu, G.; Dovichi, N. J. *Anal. Chem.* **2013**, *85*, 5989–5995.

(25) Haselberg, R.; de Jong, G. J.; Somsen, G. W. *J. Sep. Sci.* **2009**, *32* (14), 2408–2415.

(26) Haselberg, R.; Jong, G. J. De; Somsen, G. W. *Anal. Biochem.* **2013**, *85*, 2289–2296.

(27) Ramautar, R.; Jong, G. J. De; Somsen, G. W. *Electrophoresis* **2012**, *33* (1), 243–250.

(28) Haselberg, R.; Brinks, V.; Hawe, A.; de Jong, G. J.; Somsen, G. W. *Anal. Bioanal. Chem.* **2011**, *400* (1), 295–303.

(29) He, Y.; Isele, C.; Hou, W.; Ruesch, M. *J. Sep. Sci.* **2011**, *34* (5), 548–555.

(30) Shi, Y.; Li, Z.; Qiao, Y.; Lin, J. *J. Chromatogr. B* **2012**, *906* (2012), 63–68.

(31) He, Y.; Lacher, N. A.; Hou, W.; Wang, Q.; Isele, C.; Starkey, J.; Ruesch, M. *Anal. Chem.* **2010**, *82* (8), 3222–3230.

(32) Gassner, A.-L.; Rudaz, S.; Schappler, J. *Electrophoresis* **2013**, *34* (18), 2718–2724.

(33) Espinosa-de la Garza, C. E.; Perdomo-Abúndez, F. C.; Padilla-Calderón, J.; Uribe-Wiechers, J. M.; Pérez, N. O.; Flores-Ortiz, L. F.; Medina-Rivero, E. *Electrophoresis* **2013**, *34*, 1133–1140.

(34) Chambers, A. G.; Mellors, J. S.; Henley, W. H.; Ramsey, J. M. *Anal. Chem.* **2011**, *83*, 842–849.

(35) Mellors, J. S.; Black, W. A.; Chambers, A. G.; Starkey, J. A.; Lacher, N. A.; Ramsey, J. M. *Anal. Chem.* **2013**, *85*, 4100–4106.

(36) Mellors, J. S.; Gorbounov, V.; Ramsey, R. S.; Ramsey, J. M. *Anal. Chem.* **2008**, *80* (18), 6881–6887.

(37) Mellors, J. S.; Jorabchi, K.; Smith, L. M.; Ramsey, J. M. *Anal. Chem.* **2010**, *82* (3), 967–973.

(38) Batz, N. G.; Mellors, J. S.; Alarie, J. P.; Ramsey, J. M. *Anal. Chem.* **2014**, *86*, 3493–3500.

(39) Culbertson, C. T.; Jacobson, S. C.; Ramsey, J. M. *Anal. Chem.* **2000**, *72* (23), 5814–5819.

(40) Culbertson, C. T.; Jacobson, S. C.; Ramsey, J. M. *Anal. Chem.* **1998**, *70*, 3781–3789.

(41) Jacobson, S. C.; Hergenroder, R.; Koutny, L. B.; Ramsey, J. M. *Anal. Chem.* **1994**, *66*, 1114–1118.

(42) Jacobson, S. C.; Mcknight, T. E.; Ramsey, J. M. *Anal. Chem.* **1999**, *71* (20), 5172–5176.

(43) Jacobson, S. C.; Hergenroder, R.; Koutny, L. B.; Warmack, R. J.; Ramsey, J. M. *Anal. Chem.* **1994**, *66*, 1107–1113.

(44) Ferrige, A. G.; Seddon, M. J.; Green, B. N.; Jarvix, S. A.; Skilling, J. *Rapid Commun. Mass Spectrom.* **1992**, *6*, 707–711.

(45) Berger, S. J.; Chen, W. *Waters Corporation Application Note*. 2008, p Number APNT10094155.

(46) Chowdhury, S. K.; Katta, V.; Chait, B. T. *J. Am. Chem. Soc.* **1990**, *112*, 9012–9013.

(47) Testa, L.; Brocca, S.; Grandori, R. *Anal. Chem.* **2011**, *83*, 6459–6463.

(48) Grandori, R. *J. Mass Spectrom.* **2003**, *38* (1), 11–15.

(49) Raju, T. S.; Scallon, B. J. *Biochem. Biophys. Res. Commun.* **2006**, *341* (3), 797–803.

(50) Redman, E. A.; Batz, N. G.; Mellors, J. S.; Ramsey, J. M. *Anal. Chem.* **2015**, *87* (4), 2264–2272.

CHAPTER 4: CHARACTERIZATION OF INTACT ANTIBODY DRUG CONJUGATE VARIANTS USING MICROFLUIDIC CE-MS

4.1 Introduction

Antibody drug conjugates (ADCs) are monoclonal antibodies (mAbs) decorated with highly potent small molecule drugs that generally have anti-tumor activity. This class of biotherapeutic has drawn particular interest in the biopharmaceutical industry due to their potential ability to harness the specificity of a mAb and the therapeutic value of a chemotherapeutic drug.[1–5] The importance of and challenges associated with characterizing biotherapeutic mAbs have been thoroughly described and the difficulty and complexity of these challenges are further exacerbated in the case of ADCs due to their increased heterogeneity.[1,6–9]

Typically, ADCs are manufactured in a process that couples a smaller drug molecule to a mAb, via a linker.[1,5] The primary mAb by itself will exhibit heterogeneity due to post translational modifications and degradation that commonly occurs during cellular expression, processing, and storage. This complexity increases further following conjugation to generate the ADC. Various approaches and technologies have been demonstrated to couple the mAb and drug molecule. Commonly conjugation is performed at the primary amine of lysine residues or sulfhydryl groups of cysteine residues, but regardless of the conjugation chemistry used, the resulting ADC population is often a diverse mixture of species in terms of the drug-to-antibody ratio (DAR) and their isoforms.[1,10–13] Thus, the variants in the ADC population include the initial variants of the primary mAb molecule layered with additional heterogeneity introduced as a result of the conjugation process.

The various DAR species of an ADC can potentially exhibit very different pharmacokinetic properties.[1,3,14,15] As such, the DAR and often the distribution are deemed as being critical quality attributes of an ADC. At the intact level, analyses of these species is often accomplished using separation techniques such as hydrophobic interaction chromatography (HIC), ion exchange chromatography (IEC), reverse phase liquid chromatography (RPLC), capillary electrophoresis (CE), or capillary isoelectric focusing.[1,2,16–21] Generally these approaches are coupled to absorbance based detection techniques and are incompatible with mass spectrometry generally due to the high salt content required for analysis. RPLC can be interfaced with a mass spectrometer as a desalting technique to generate an infusion-like spectrum of the intact ADC sample, but separation of variants does not occur.[19] Recently, several studies have been published using native spray ion mobility spectroscopy (IMS) with MS detection for characterizing ADCs.[22–24] With this approach, DAR and distribution can be determined from the mass spectrum and some resolution between DAR species is obtained during the IMS separation. However, several sample preparation techniques are required to simplify the ADC in order to reduce spectral overlap in the mass domain, such as deglycosylation or C-terminal lysine removal, which significantly lengthens the analysis.

Recently we described a method for assessing the charge heterogeneity of intact mAbs using microfluidic CE-ESI with online MS analysis. With very little sample preparation, charge variants of mAbs can be separated and introduced directly into the mass spectrometer via ESI. Having the CE separation prior to MS analysis generates electrophoretic mobility data that can be used in conjunction with mass data as criteria for identifying mAb charge variants. Additionally, the CE separation prior to MS analysis simplifies the resulting mass spectra. Demonstrated here is the use of this method for measuring both charge variant heterogeneity and

DAR distribution of an ADC at the intact level. While DAR and distribution have been characterized using infusion-MS or separation techniques coupled to optical detection, this is the first example of the separation of intact ADC species with direct MS detection to characterize charge variant heterogeneity, and DAR distribution.

4.2 Experimental

4.2.1 Materials and Reagents

Deionized water was generated with a Nanopure Diamond water purifier (Barnstead International, Dubuque, IA). Optima LC/MS grade 2-propanol and acetic acid (99% purity) were obtained from Fisher Scientific (Fairlawn, NJ). The silane coating reagent 3-(aminopropyl)di-isopropyl-ethoxysilane (APDIPES) was purchased from Gelest (Morrisville, PA) and the methyl-terminated polyethylene glycol *n*-hydroxy succinimide ester (NHS-PEG_{450}) was purchased from Nanocs Inc. (Boston, MA). Trichloro-(1H,1H,2H,2H-perfluorooctyl)-silane was purchased from Sigma-Aldrich (St. Louis, MO). The monoclonal antibody conjugates ADC-B, mAb-C, and ADC-C were provided by Pfizer Inc. (St. Louis, MO). T-DM1 was provided by 908 Devices, Inc. (Boston, MA).

4.2.2 Sample Preparation

Monoclonal antibody samples were stored in their respective formulation buffers at - 20 °C until analysis. Samples were thawed at room temperature and diluted to 0.5 mg/mL for mAb-A and 1.0 mg/mL for ADC-B with an aqueous solution of 10% 2-propanol 0.2% acetic acid (pH 3.17). TDM-1 was diluted in a similar manner to 1 mg/mL. The stock solution of mAb-

C was diluted to 1.125 mg/mL and ADC-C was diluted to 2.5 mg/mL with 2.5% methanol 0.1% acetic acid. The final sample volume was 100 µL for all analytes.

4.2.3 CE-ESI-MS Device Preparation and Operation

As described in Appendix 2, CE-ESI devices were coated with an aminopropylsilane reagent and a polyethylene glycol (PEG) reagent to reduce analyte adsorption and suppress EOF.[25,26,34] An electroosmotic pump was used to provide the bulk fluid flow for ESI. CE-ESI devices were operated by applying and controlling voltages to the solvent reservoirs according to the parameters in Appendix 3. A gated injection scheme was used for sample manipulation and injection.[25,35] Injection of the sample was performed by switching the voltage profile from the gated state to the injection state for 200 ms and back again. For this work infusion of ADC-B was performed by allowing the voltages to remain in the injection state.

4.2.4 Data Analysis

MS analysis was performed using a Waters LCT-Premier time-of-flight mass spectrometer (Waters Corporation, Milford, MA) operated in V-mode with the source at 105 °C with ion transfer settings as described in Appendix 4. Data were acquired over a mass range of 4000-6000 m/z with a 0.2 s scan time. Deconvolution of the mass spectra was performed based on maximum entropy analysis using the MaxEnt1 deconvolution algorithm in the MassLynx software as described previously.[9,26,36,37]

4.3 Results and Discussion

4.3.1 Separation of Intact Lysine Linked ADC Charge Variants

ADC-B was created by collaborators at Pfizer using previously described conjugation chemistry that attaches the drug compound to the sidechain of lysine residues in mAb-B.[10] The drug conjugated to the antibody is primarily neutral, and therefore the main shifts in the pI of the intact ADC are associated with the loss of available ε-amino groups in the lysine residues that are conjugated. As such, this reaction would decrease the mobility as the DAR increases. Additionally, it is reasonable to expect each ADC-B conjugate species to maintain the initial charge variant and glycoform profile of the starting molecule, mAb-B (Chapter 2, Figure 10). Intact charge variant analysis of ADC-B is provided in Figure 4.1 along with the identified glycoforms from the deconvoluted mass spectrum of the most abundant charge variant. Five DAR species are detected and labeled with the mass obtained from deconvoluting the mass spectrum generated from each band. The minor basic variants associated with each are the previously identified pyroglutamic acid variants found in mAb-B.

The deconvoluted mass spectra from each of the separated DAR species and the mass shift between each species is provided in Figure 4.2. The average mass shift due to an increase in DAR is 3145 Da, which agrees very well with the known mass of the drug load. Migration times and mobilities for the ADC-B DAR species can be found in Table 4.1.

Although the addition of a drug load should only decrease the net charge on the mAb by 1 unit, a more substantial shift in mobility of 0.1×10^{-4} cm^2/Vs is observed than previously calculated for modifications causing a similar change in net charge.[26] This is most likely due to the size of the drug load. At 3145 Da, this mass accounts for approximately 2% of the total mAb mass per drug load. This is a much larger mass shift compared to those associated with C-terminal lysine truncations or pyroglutamic acid formation. It can be surmised that the presence

of a drug load(s) on the mAb structure affects the hydrodynamic radius of the molecule in solution, which in turn affects the mobility of the mAb.

The mass of DAR 0 in Figure 4.1 and Figure 4.2 is similar to the mass calculated for mAb-B (Chapter 2, Figure 10a) but are not identical and the migration times vary slightly. To determine whether these minor variations are caused by additional modification to the mAb-B structure during the conjugation reaction or simply the result of experimental variability, 5 µg of mAb-B was spiked into the ADC-B sample. Multiple bands would be expected in the region of DAR 0 if this species differed from mAb-B. However, as seen in Figure 4.3, DAR 0 and its associated variants increased in intensity after mAb-B was spiked into the sample. Additionally, there are no partially resolved variants appearing as shoulders in the area of DAR 0 or protein envelopes present in the mass spectrum that were not there previously. Thus, DAR 0 in ADC-B can be confirmed to be residual mAb-B in the sample.

To establish that the dynamic range of the mass spectrometer was sufficient to calculate DAR distribution, a range of ADC-B concentrations were analyzed using the microfluidic CE-MS method. The areas for each DAR species were calculated using MassLynx software and plotted against the sample concentration (Figure 4.4). The MS response was found to be linear for all DAR species at less than 1.5 mg/mL ADC-B. The relative area percent was calculated for each DAR species in the separation and is provided in Table 4.2. The measurements were corrected for injection bias by multiplying the area of the peak by its migration time:

$$Area\ \% = \frac{t_m Area_{DARn}}{Total\ Area} \tag{4.12}$$

where t_m is the migration time of the species and $Area_{DARn}$ is the area of DAR species with n drug loads. The average DAR was calculated using the equation below and found to be 1.7:

$$\overline{DAR} = \frac{\sum nA_{\%}}{100} \tag{4.13}$$

where *n* is the number of drug loads and $A_{\%}$ is the area % of the species. An infusion of ADC-B performed by opening the microchip gate valve as mentioned above and the relative area percent of the DAR species is provided in Table 4.2. The results of the infusion also yielded an average DAR of 1.7. Both the CE-MS and infusion values are in relative agreement with conventional analytical methods that measure the DAR of ADCs. Table 4.2 also lists the distribution of DAR species calculated from imaging CE (iCE) data collected by collaborators at Pfizer where an average DAR value of 1.8 was obtained. The similarity between the average DAR calculations indicates that the three methods are in agreement with one another.

While the drug load distribution generated using both methods is similar, more information is generated about the charge heterogeneity of the ADC-B population through the intact charge variant analysis. Figure 4.5 compares the raw mass spectra for the DAR 2 variants in the infusion data and the separation in Figure 4.1. The mass difference of 18 Da associated with the pyroglutamic acid variants was not resolved in the mass domain during the ADC-B infusion experiment. As indicated in Figure 4.5b, there is a slight mass shift discernable between the spectra for the 2 load variant with and without pyroglutamic acid, but this shift only manifests as spectral broadening in the infusion spectrum. When deconvoluted, the mass obtained from the infusion data is a function of the mass of both pyroglutamic acid variants.

It is evident from the data provided that at least four sites on the intact mAb-B structure readily undergo conjugation during the reaction. Although IgG type antibodies consist of two heavy chains and two light chains, the overall molecule is not conformationally symmetric.[6] The occurrence of a drug load at the same residue but on different chains may have different structural effects that could affect the mobility. Thus, there are positional isomers determined by

the location and identity of the conjugation site accessed, which could perturb the mAb structure enough to affect the mobility on the basis of conformation. Potential evidence for this is present as reproducible shoulder features on DAR species 1 and 2 in the electropherogram for ADC-B. These features are marked with asterisks in Figure 4.1. The mass spectra are homogenous throughout the width of both bands indicating that the partially resolved shoulder species do not differ in mass. If the resolution of the CE separation were increased, it is possible that these isomers could be separated and used to further assess the conjugation reaction based on drug load location in addition to DAR.

Since ADCs are designed to deliver a drug payload to a specific target, the stability of the drug load is of vital importance. Degradation of the drug load can significantly reduce the potency of the ADC as a therapeutic molecule. The drug load on ADC-B is subject to a characteristic degradation. Collaborators at Pfizer have determined the pathway of this degradation to be catalyzed by a residual host cell protein (HCP). The HCP cleaves the peptide based drug load at a specific residue, causing a decrease in mass of ~575 Da. This reaction occurs in solution over time and during product characterization at Pfizer it was observed as an increase in acidic variants due to exposure of a carboxylic acid group on the drug load. To mimic the degradation of the drug load over a long period of time, ADC-B was incubated in formulation buffer at 45 ºC over a period of 3 days and an aliquot was taken each day. Intact analysis via microfluidic CE-MS did not reveal additional acidic variants in the electropherogram. However, the presence of degraded species is detectable in the deconvoluted mass spectra and as seen in Figure 4.6a. For species with more than one drug load, degradation of multiple drug loads is detected. Residual amounts of degraded ADC-B are present in the sample prior to heat stressing the molecule, but the amount increases quickly during the forced

degradation process. As seen in Figure 4.6b, by the third day of incubation up to approximately 45% drug load degradation was seen for some DAR species.

4.3.2 Analysis of T-DM1

The ability to separate lysine conjugated DAR variants is limited if the conjugate molecule has a net charge of +1. Although the conjugation chemistry removes a positive charge at the lysine side chain, the net charge on the mAb does not change overall. Thus, any separation is dependent on changes in electrophoretic mobility due to conformational differences between the DAR species from the size of the drug load or its effect on mAb folding. Often these mobility shifts are quite minor and in these instances the presence of the DAR species is mainly visible in the mass spectra of the ADC rather than the electropherogram.

The ADC T-DM1 is an illustrative example of this. The drug load conjugated to the mAb bears a positive charge at acidic pHs negating any change in net charge due to reaction at the lysine residues. As seen in Figure 4.7a, there is no visible separation of charge variants in the electropherogram. A mass spectrum for the ADC was generated by averaging the mass scans across the base width of the CE peak. The ADC generates a very complex spectrum and when deconvoluted many different mass species are seen (Figure 4.7b, 7c). The different DAR species are shifted by an average of 958 Da and up to four drug loads per mAb are detected in the deconvoluted spectrum. For each DAR species various glycoforms are also detectable by a mass shift of 162 Da with the most abundant glycoform being G0F/G1F. In addition to the glycoform distribution, a subspecies is detected that corresponds to an error during the conjugation process where a linker molecule is attached to the mAb, but not a drug load.[22] These species are marked with an asterisk.

Overall, T-DM1 is an exceedingly complex molecule in terms of charge and mass heterogeneity making analysis difficult in both the separation and MS domain. Recently, native spray IMS-MS has been used to analyze ADCs for drug load distribution and average DAR.[22–24] Researchers were able to achieve some resolution between DAR species of T-DM1 through the IMS separation.[22] While it initially appears that there is no separation occurring in the CE domain of the microfluidic CE-MS analysis, the mass spectrum across the width of the peak is not homogenous, indicating that there is a slight amount of charge variant separation. Extracted ion electropherograms can be generated for the various DAR species. When overlaid as in the inset of Figure 4.7a they reveal slight separation between the DAR species of T-DM1. The separation resolution and MS information generated here with the microfluidic CE separation is similar to that obtained in the IMS studies. However, using the microfluidic CE-MS approach a specialized MS instrument with IMS capabilities is not needed to achieve similar results.

4.3.3 Separation of Intact Cysteine Linked ADCs

An alternative mode of mAb conjugation is to modify cysteine residues in the antibody structure. Briefly, to produce a cysteine linked ADC, disulfide bonds in a mAb are reduced to generate reactive sulfhydryl groups that are then functionalized with maleimide based components.[11–14,38–40] Conjugation tends to occur in pairs so DAR species increase in multiples of 2, i.e. DAR 0, DAR 2, DAR 4, etc. Thus, as compared to lysine based conjugation where any solvent accessible lysine can be functionalized, cysteine conjugation is more site specific and tends to produce a less heterogeneous ADC population.

Although potentially less heterogeneous, analyzing cysteine linked ADCs can be challenging because the disulfide bond structure of the mAb is disrupted. This could potentially render non-covalent interactions between the light and heavy chains the predominant force

holding the ADC together. It has been seen that cysteine linked ADCs tend to dissociate under the conditions often used for LC-MS analysis: high levels of organic modifier and acidic pH.[1] As such, HIC has emerged as a useful technique for separating the DAR species because the separation can be performed at neutral pH to preserve the ADC structure.[1,41–43] The BGE used for microfluidic CE-MS analysis of mAbs and ADCs is not as harsh as typical LC-MS conditions and appears to preserve a certain amount of mAb structure. Therefore, it is possible that a cysteine linked ADC could be analyzed at the intact level using our method. To evaluate this, a mAb/ADC pair was analyzed at the intact level via microfluidic CE-MS.

Charge variants of the naked mAb (mAb-C) were characterized via microfluidic CE-MS. As illustrated in Figure 4.8, a main isoform and two basic variants were detected and identified as C-terminal lysine variants. The glycosylation profile of mAb-C was fairly complex with 6 different glycoforms identified. mAb-C was conjugated with a small molecule drug load (~376 Da) using *tris*(2-carboxyethyl)phosphine (TCEP) reduction and conjugation chemistry developed at Pfizer, Inc. to create ADC-C. Figure 4.9a shows the intact analysis of ADC-C. The same lysine variants of mAb-C are separated and detected, but deconvolution of the main isoform of ADC-C reveals multiple species generated from the conjugation reaction. There is a mass shift of ~757 Da between the groupings of peaks in the deconvoluted spectrum. This mass agrees with the addition of two drug loads to mAb-C when disulfide bonds are reduced to generate two reactive sulfhydryl groups.

As is evident in Figure 4.9a, the separation efficiency appears to have decreased during intact analysis of ADC-C. However, closer inspection of the CE and MS data reveals partial separation of the DAR species. This is easily visualized by generating an extracted ion electropherogram for each DAR species (Figure 4.9c). Because the resolution generated between

the DAR species is less than 1.0, it manifests as artificial band broadening in the separation. The integrated peak areas from the extracted ion electropherograms were used to calculated the relative abundance of the DAR species. It was determined that the ADC population consisted of 5.27% DAR 0, 31.46% DAR 2, 45.41% DAR 4, and 17.86% DAR 6 with an average DAR of 3.52. This value does not agree with the average DAR of 4.55 calculated from data generated by collaborators at Pfizer. HIC analysis of the molecule at Pfizer detected DAR species ranging 0-8, but DAR 8 is not detected to any degree during microfluidic CE-MS analysis. It is possible that DAR 8 is degrading due to the degree to which the disulfide structure is disrupted. This hypothesis is potentially supported by the presence of dissociated light chain in the intact separation of ADC-C (Figure 4.9a). Additionally, widening the m/z range used for data acquisition reveals another protein species at much higher m/z values than the intact ADC. As seen in Figure 4.10, deconvolution of this protein envelope generates a mass that agrees with the loss of a light chain from the ADC. Thus, degradation of the ADC does in fact appear to be occurring, but it is not obvious where. If the ADC was dissociating throughout the separation, the light chain would appear as a broad trailing signal in the electropherogram. However, it is being detected as a discrete peak. Therefore, in an attempt to pinpoint where the degradation is occurring, an aliquot of ADC-C stock was diluted in a 50 mM ammonium carbonate buffer at neutral pH and filtered through a 100 kDa MWCO filter. The solution containing components <100 kDa was reduced and alkylated to prevent disulfide scrambling, and analyzed via microfluidic CE-MS. Analysis of the filtrate is given in Figure 4.11a. Peaks for mAb light chain (LC) and heavy chain (HC) were detected in the electropherogram. Deconvolution of the mass spectrum associated with the heavy chain reveals glycoforms of the HC and also mass species corresponding to the addition of a drug load to a cysteine residue (Figure 4.11b). It is worth

noting that after alkylation the observed mass shift for a drug load is ~57 Da less than the nominal mass of the drug molecule. Thus, there are two forms of the HC that differ in the amount of drug conjugated to the molecules. Similar patterns are observed in the deconvoluted mass spectra for the two LC peaks in the electropherogram (Figure 4.11c), but the LC appears to have more conjugation heterogeneity than the HC. Based on the observed species in the filtrate, it appears that ADC-C is degrading in the formulation buffer to a certain degree. This could potentially be the reason that DAR 8 is not observed in the intact separation. Analysis of the LC and HC generated from the total ADC-C population could be helpful in determining whether DAR 8 is not present or is just degrading too much for analysis. If the average DAR calculated from this data more closely agrees with the value determined at Pfizer, it would indicate that DAR 8 is present, but is not being detected at the intact level during microfluidic CE-MS analysis.

4.4 Conclusions

To assess the utility of the microfluidic CE-MS method for characterizing ADCs three ADCs differing in terms of conjugation chemistry or drug load characteristics were analyzed. The first ADC, ADC-B, was generated from mAb-C (discussed in Chapter 2) using lysine-based conjugation chemistry to attach a peptide based drug load to the mAb structure. Post conjugation, in addition to DAR variants, the same charge variants were present in the resulting ADC-B sample as were observed in the mAb-C. The average DAR and DAR distribution for ADC-B was assessed based on the electropherogram. Five separate ADC-B species with different DARs were detected from the separation and mass spectral data with an average mass shift of 3145 Da. It was determined that a maximum of 4 drug loads were present on the mAb with an average DAR of 1.7. While the addition of a drug load should theoretically only reduce the mAb net charge by

1 unit, a relatively large decrease in mobility was seen due to conjugation. This is most likely attributable to changes in the hydrodynamic radius of the molecule induced by the size of the drug load. It was postulated that partial separation of conformational isomers was seen due to the band widths of DAR species 1-3 and reproducible shoulder features in the electropherogram. The mobility differences between such conformational isomers would be less than those caused by charge differences and more difficult to resolve in the CE domain. Altering the background electrolyte, raising the operating voltage, or increasing separation channel length could potentially increase the separation resolution and confirm or refute the presence of structural isomers.

The properties of the ADC drug load and the type of conjugation chemistry used can significantly affect the charge heterogeneity of the ADC species. For instance, a cationic drug load negates the decrease in net charge associated with lysine conjugation and separation of DAR species would be dependent on conformational changes. For smaller drug loads this makes separation of the DAR species quite challenging. T-DM1 was analyzed via microfluidic CE-MS to assess the utility of this method for analyzing such ADCs. Six DAR species were detected in the deconvoluted mass spectrum in addition to glycoforms of the mAb and species that correspond to errors in the conjugation reaction. As expected, the resolution between the DAR species in the CE domain was lower than what was observed for ADC-B, but extracted ion electropherograms revealed that there was some separation of the DAR species occurring. The CE resolution generated for T-DM1 using this technique was comparable to that generated using IMS, but a specialized MS instrument is not required for microfluidic CE-MS analysis.

The third ADC, ADC-C, analyzed was generated using conjugation chemistry based on functionalization of cysteine residues. While this conjugation strategy produces a less

heterogeneous ADC population, analysis can be difficult because the conjugation process reduces the structural stability of the mAb. Similar to T-DM1, separation of the DAR species was mainly observed through generating extracted ion electropherograms for the DAR species. From the CE and MS data, DAR species 0-6 were detected during intact analysis with an average DAR of 3.52. This is not in agreement with values reported by Pfizer most likely due to the fact that the DAR 8 species was not observed. Subsequent experiments suggest that ADC-C could be degrading in the formulation buffer causing the highly conjugated DAR 8 to not be detectable at the intact level. Further experiments analyzing the LC and HC of the ADC population are needed to determine if the degradation is due to the microfluidic CE-MS analysis or poor sample stability.

In this work we have demonstrated the use of microfluidic CE-ESI with online MS analysis for the characterization of intact antibody drug conjugates. This analysis method appears to be a simple, generic strategy for characterizing the charge heterogeneity of mAbs and ADCs with direct MS analysis. The method is particularly well suited for conjugation that produces a change in net charge of at least 1 due to lysine conjugation, a cationic drug load, a large drug load, or a combination of these factors. For ADCs with minimal changes in net charge, DAR distribution and average DAR can still be determined from the MS data even though resolution in the CE domain is limited. However, it may be possible to improve the CE resolution by increasing the length of the separation channel in the CE device or altering the BGE for certain molecules.

4.5 Figures and Tables

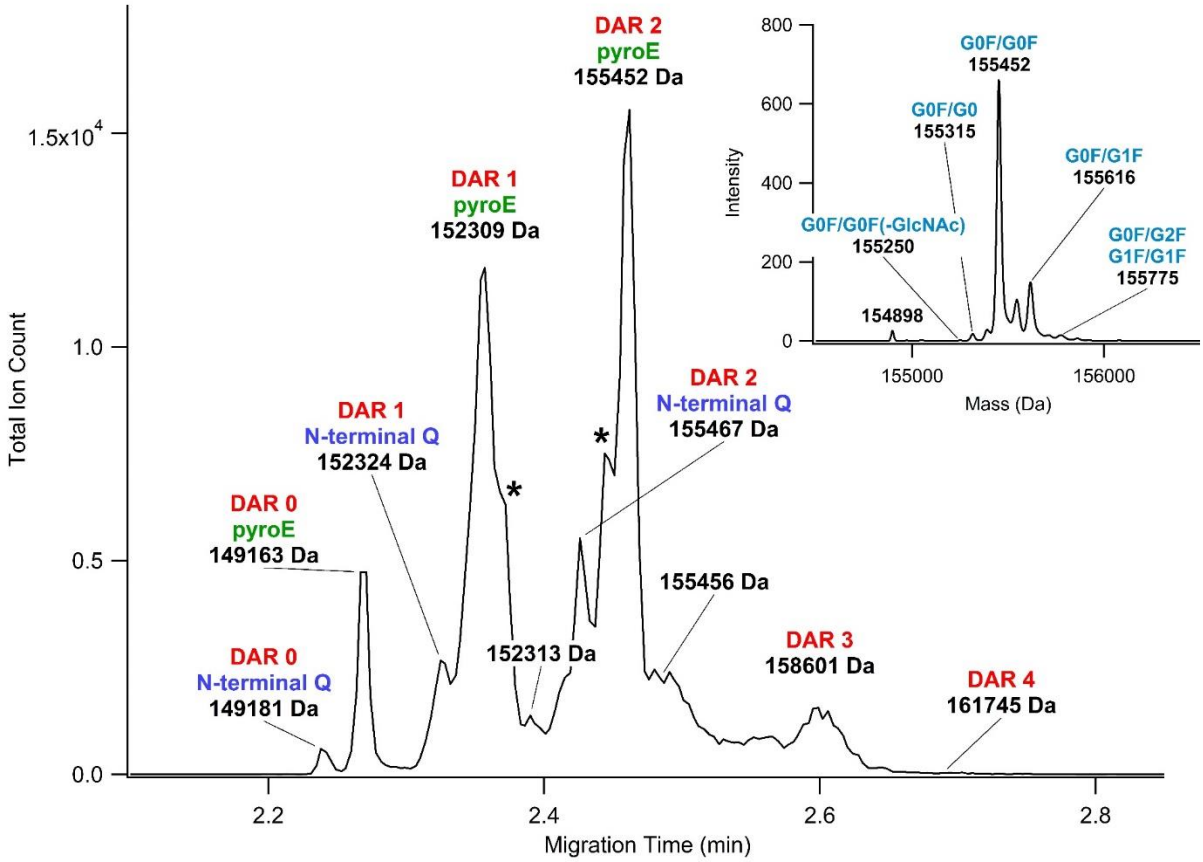

Figure 4.1: Intact charge variant separation of ADC-B. Peaks are labeled with masses obtained by deconvolution of the mass spectrum associated with that peak. Pyroglutamic acid variants of each DAR species are labeled as having either an N-terminal Q or pyroE. (*) indicate reproducible shoulder features on the main peaks. The inset shows the deconvoluted mass spectrum for DAR 2 with identified glycoforms labeled.

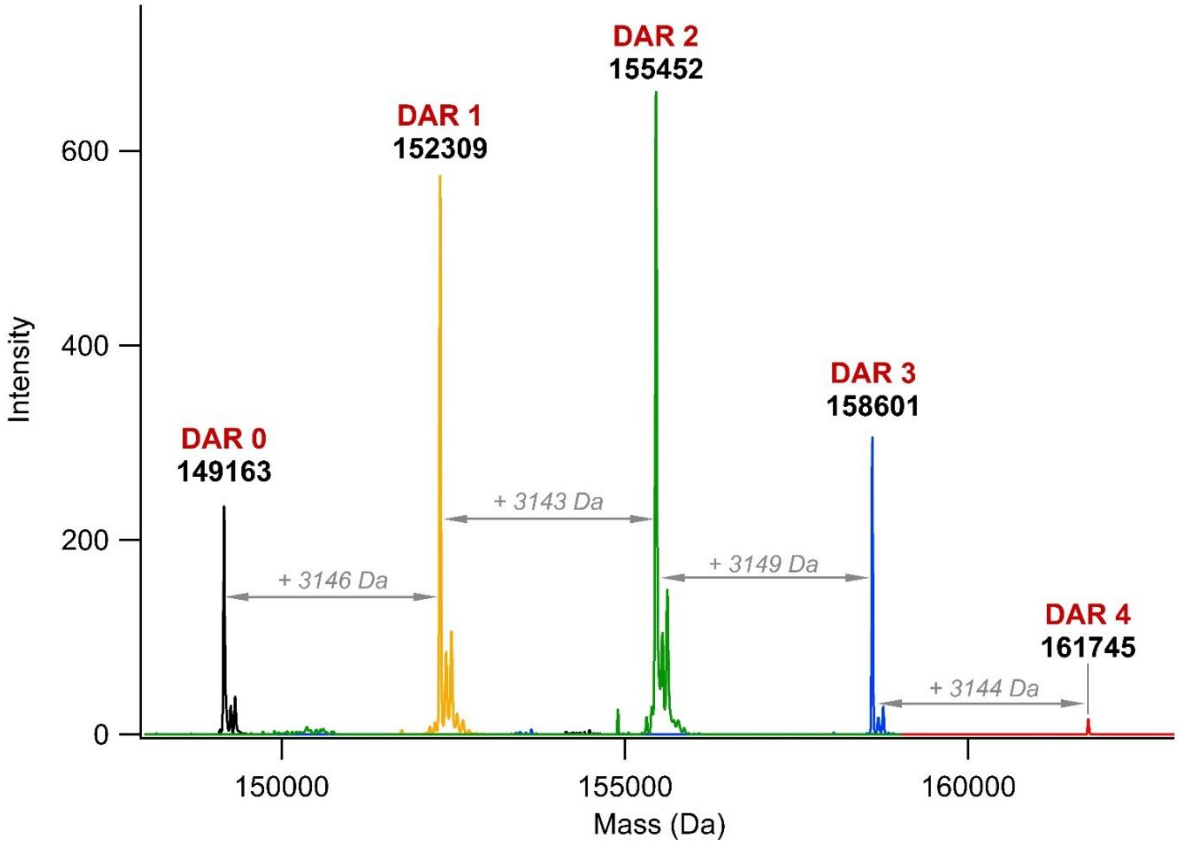

Figure 4.2: Overlaid deconvoluted mass spectra for DAR species 0-4 generated from the electropherogram shown in Figure 1. The mass shift between neighboring DAR species is shown with an average mass shift calculated at 3145 Da.

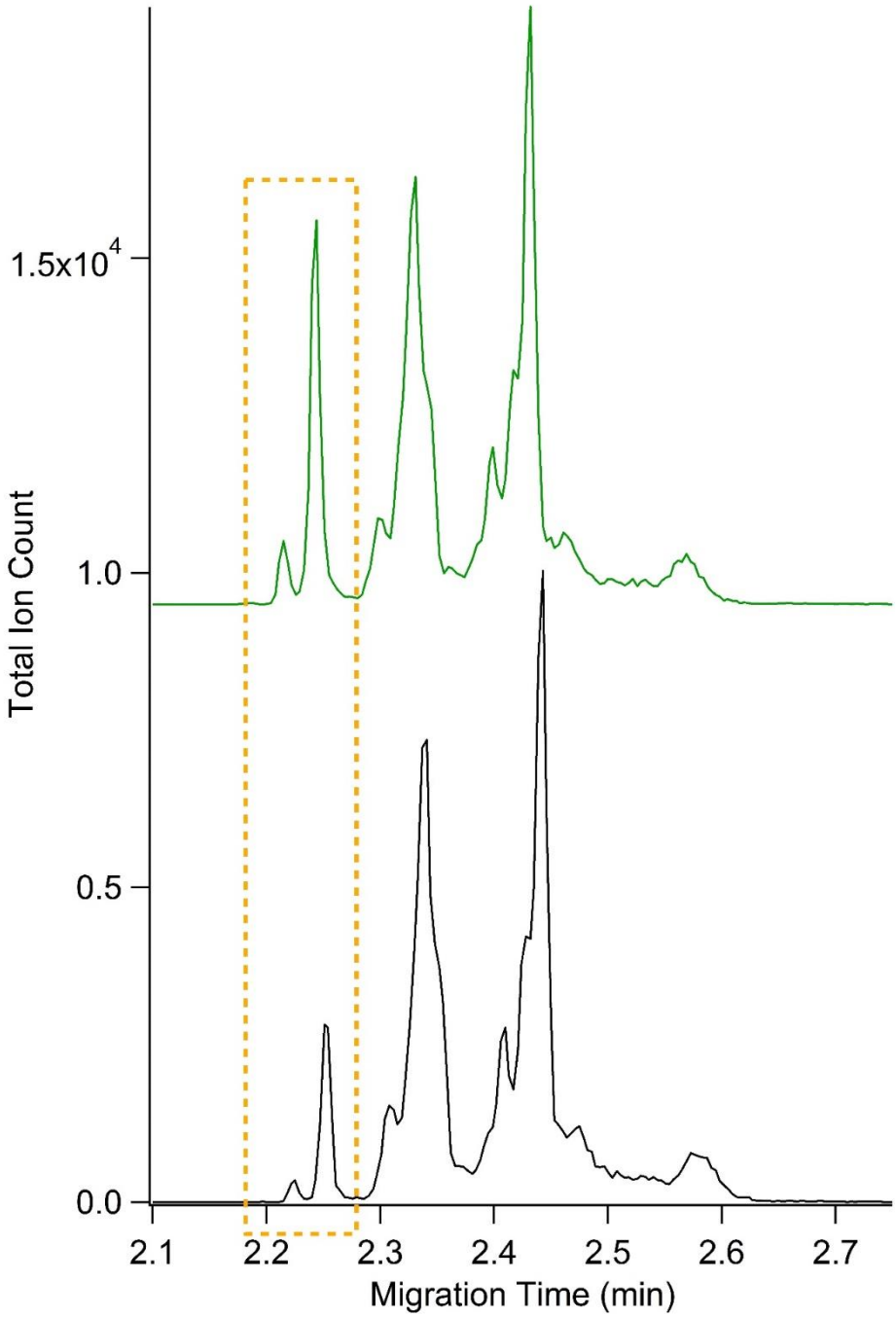

Figure 4.3: Intact charge variant analysis of ADC-B (bottom) and ADC-B spiked with mAb-A (top). The intensity of the peaks highlighted in the box increases after the sample is spiked with mAb-A.

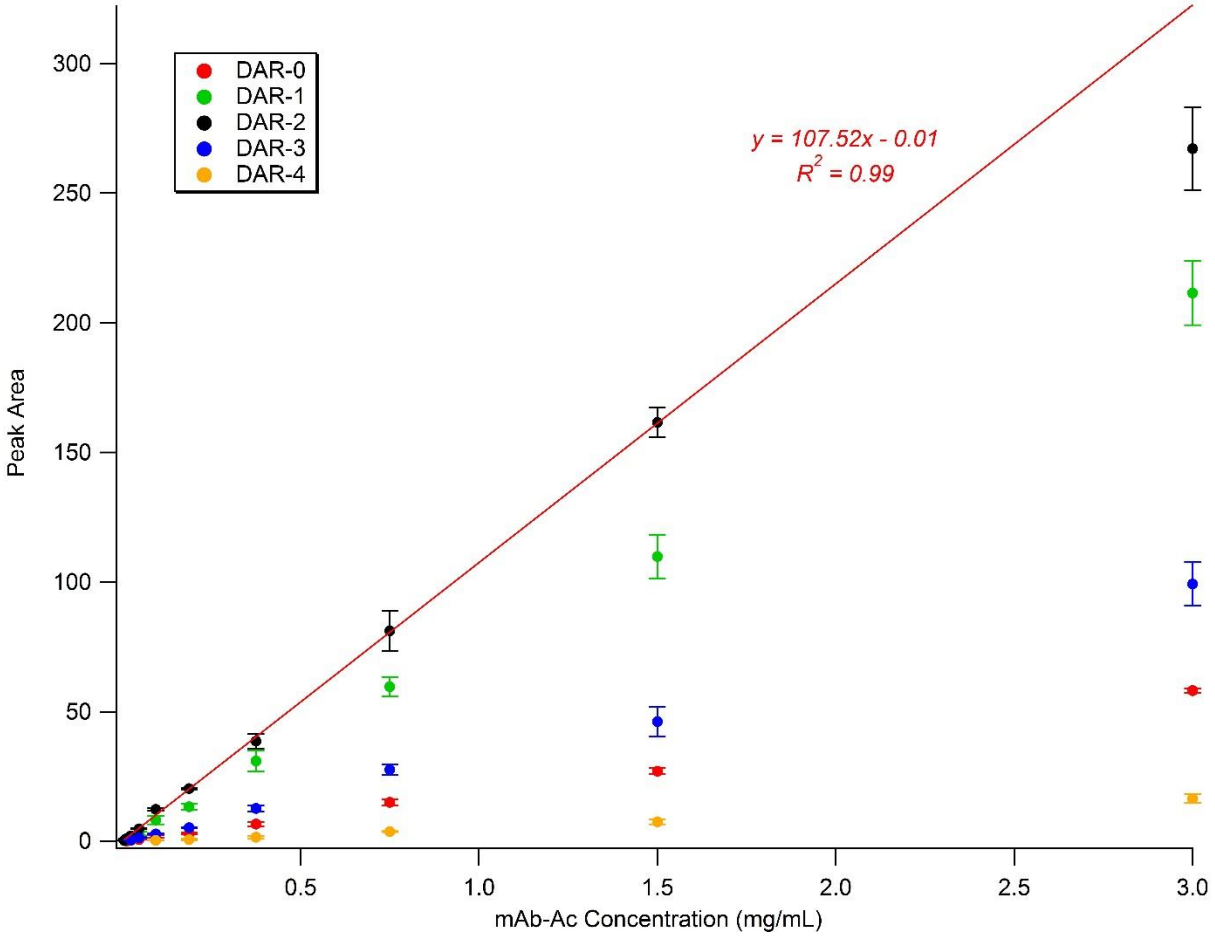

Figure 4.4: Plot of peak areas with respect to ADC-B concentration. Data points from concentrations 0.006 mg/mL to 1.5 mg/mL were used to generate the linear trend line for the most abundant DAR species, DAR-2. It was determined that the MS response remained linear when the concentration is less than or equal to 1.5 mg/mL ADC-B. Detector saturation occurs at higher concentrations. Data was generated from three replicate separations.

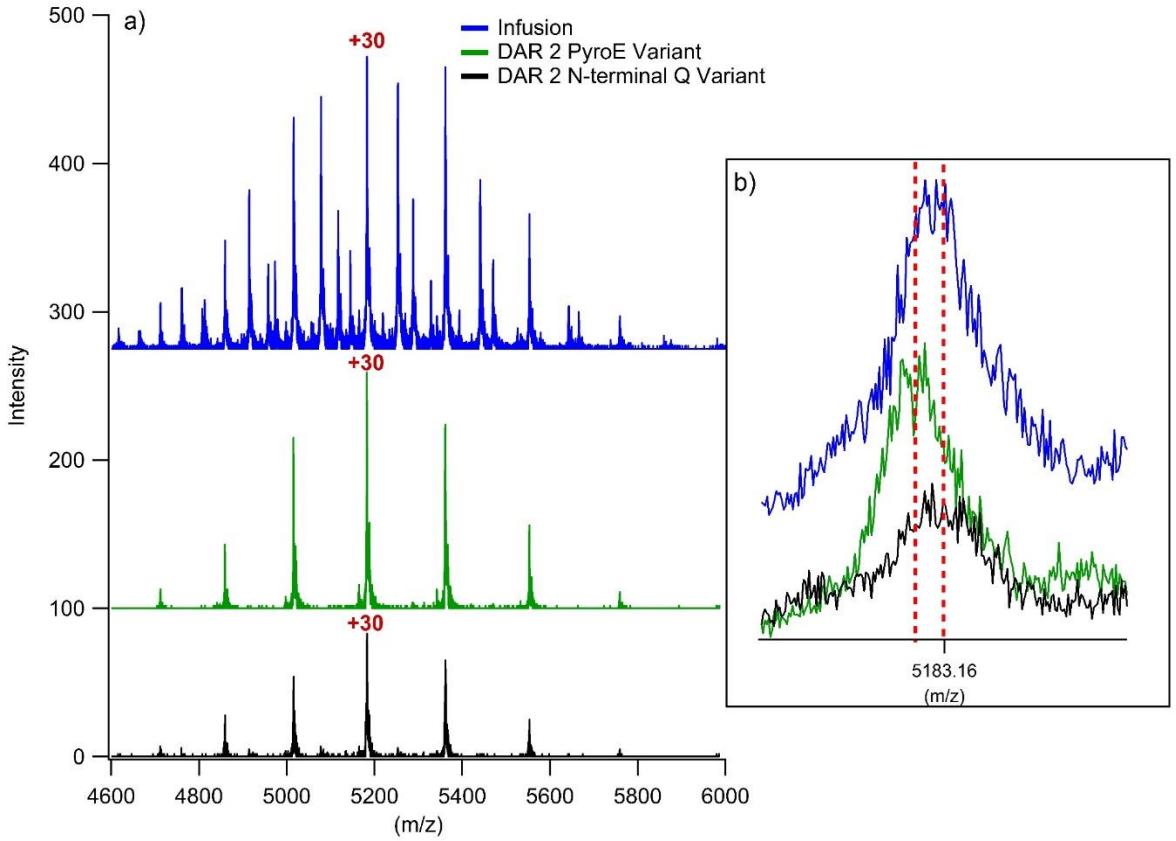

Figure 4.5: Comparison of infusion-MS and intact CE-ESI-MS analysis: a) mass spectrum of the pyroglutamic acid and N-terminal Q variants of the DAR 2 species (green, black) compared to an infusion of ADC-B containing all DAR species (blue). b) comparison of the +30 charge states of the DAR 2 species in the infusion spectrum and separation spectra. The 18 Da mass shift due to the cyclization of glutamine is not resolved in the infusion spectrum.

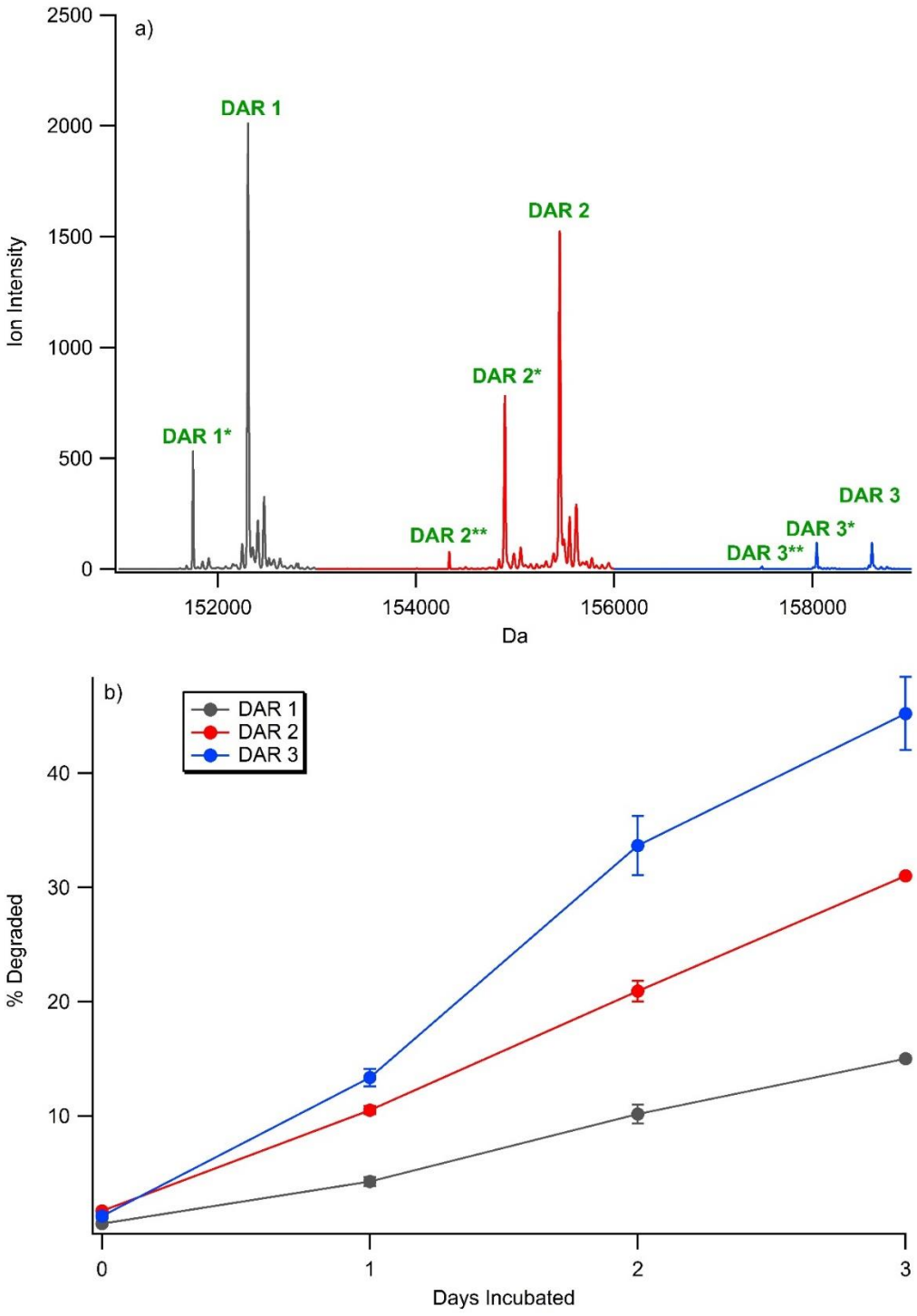

Figure 4.6: Degradation of the ADC drug load. a) Deconvoluted mass spectra for DAR species 1-3 after three days of incubation at 45 °C. (*) indicates a degraded drug load. b) Plot of %degraded ADC species versus incubation time.

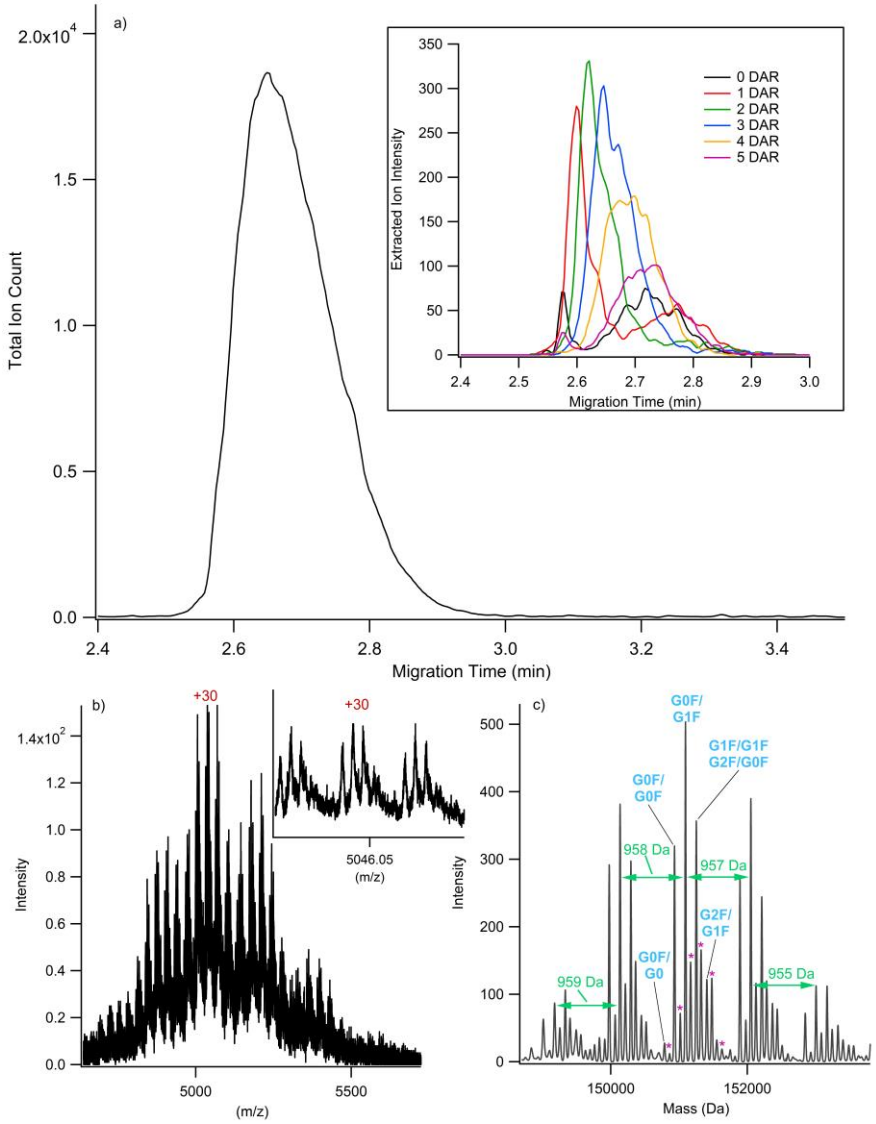

Figure 4.7: Intact microfluidic CE-MS analysis of T-DM1. a) Intact separation of T-DM1. It initially appears as though no separation of charge variants has been achieved. The inset shows overlaid extracted ion electropherograms for the DAR species revealing the partial separation of the ADC population. b) Raw mass spectrum for T-DM1 generated by averaging the mass scans across the width of the peak in (a). c) Deconvolution of the spectrum in (b). Five DAR species are detected along with glycoforms of the ADC and species due to incomplete conjugation (marked with *).

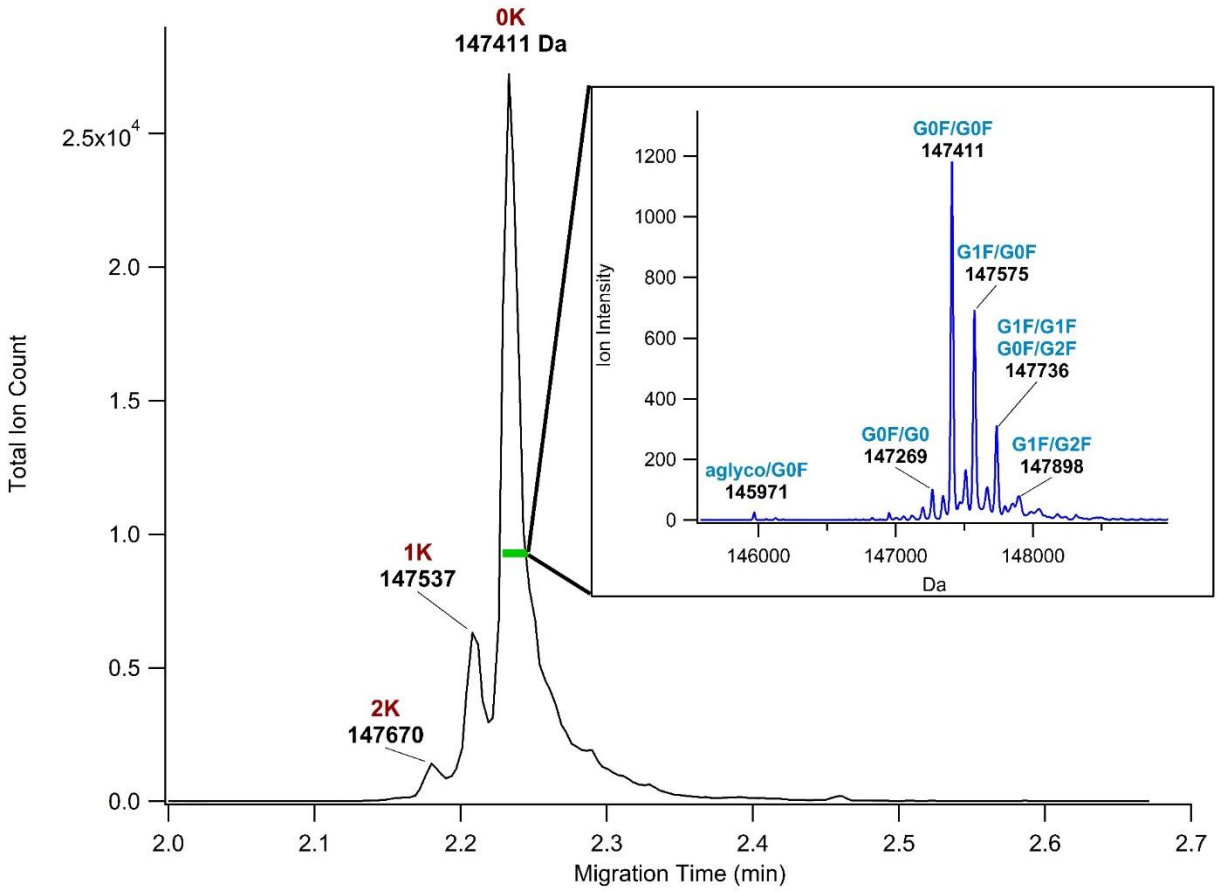

Figure 4.8: Intact analysis of mAb-C. Three main forms of the mAb are separated in the CE domain and identified as C-terminal lysine variants. Deconvolution of main isoform's mass spectrum reveals several glycoforms of the mAb.

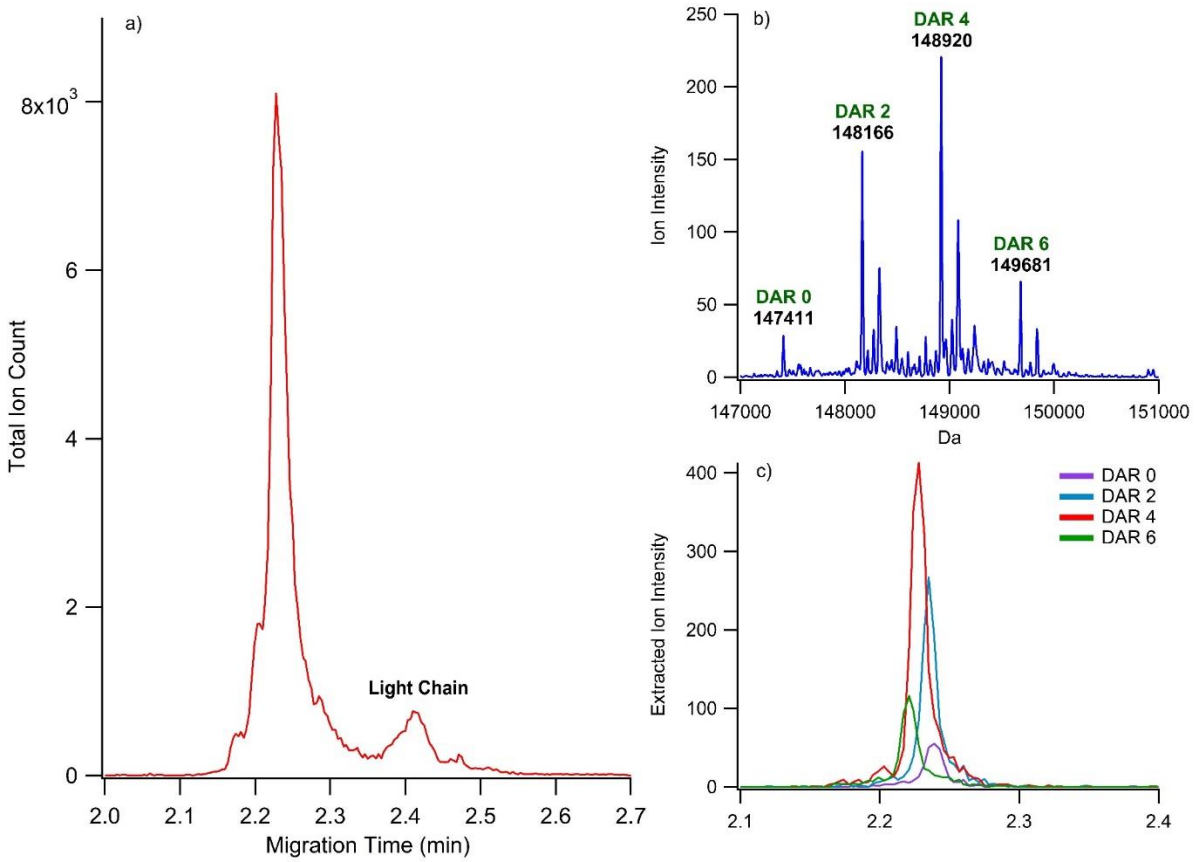

Figure 4.9: Intact analysis of ADC-C. a) Separation of intact charge variants. The same C-terminal lysine variants are detected post conjugation. b) Deconvolution of the main isoform's mass spectrum. DAR species ranging from 0-6 are detected. c) Extracted ion electropherograms reveals partial separation of the DAR species.

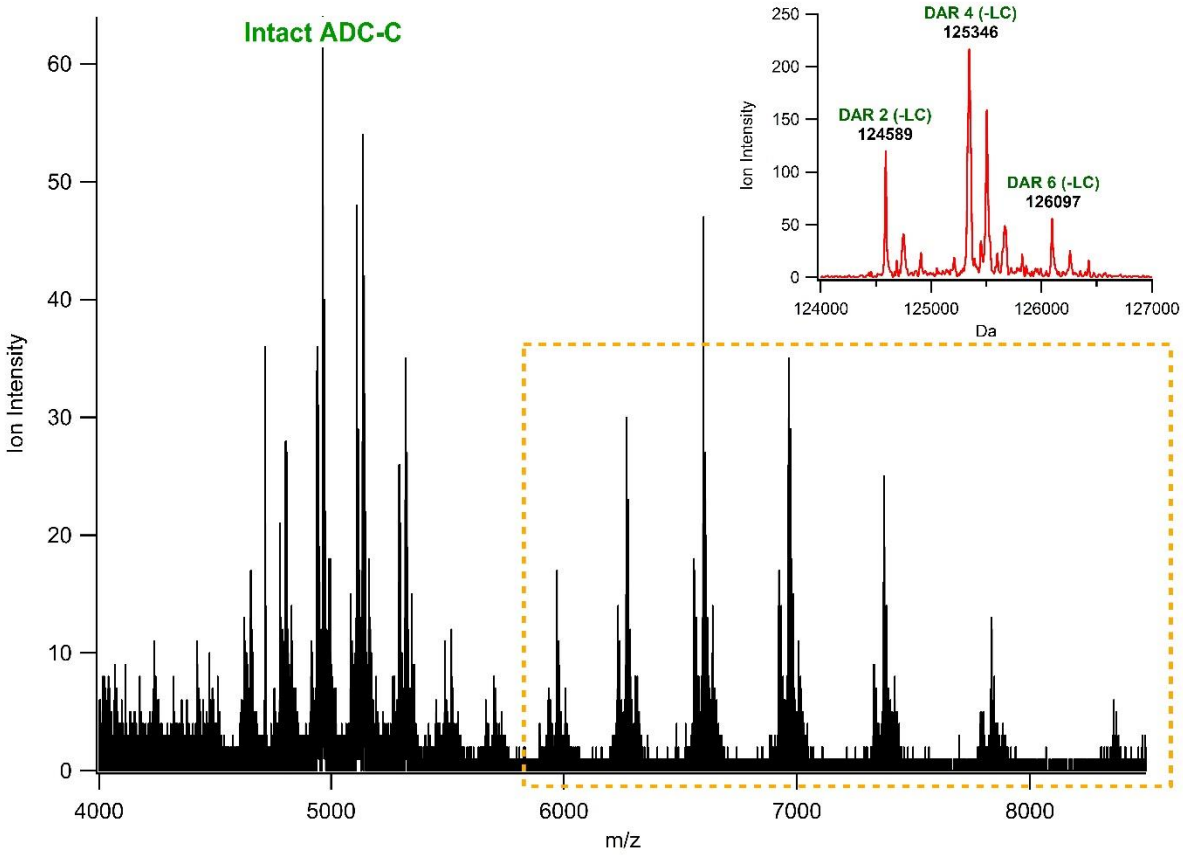

Figure 4.10: Raw and deconvoluted mass spectra for the ADC-C fragment. The charge envelope for intact ADC-C is centered around ~5000 m/z. In contrast, the ADC-C fragment indicated by the orange box appears at much higher m/z values. The inset shows the deconvolution of the ADC-C fragment. The deconvoluted masses agree with the loss of a light chain (LC) from the DAR species 2-6.

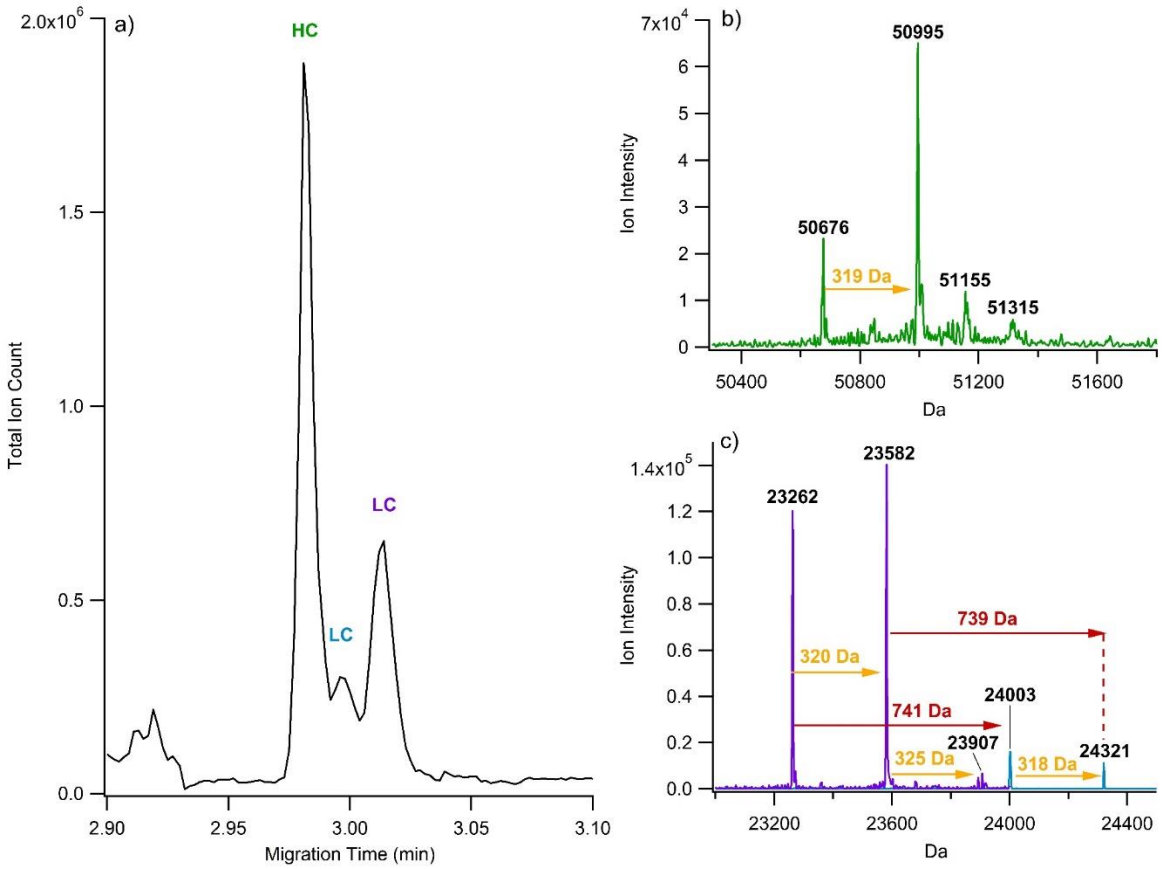

Figure 4.11: Analysis of ADC-C filtrate after filtering with a 100 kDa MWCO filter. a) Microfluidic CE-MS analysis reveals the separation of HC and LC species from ADC-C. b) deconvolution of the mass spectrum generated from the HC peak in the electropherogram. The mass shift of 319 Da between the two most abundant species is indicative of a drug load. Glycoforms of the more abundant HC species are also visible in the spectrum. c) overlay of the deconvoluted mass spectra for the two LC peaks in the separation.

Table 4.1: Migration times and apparent mobilities for DAR species. Data was generated from three replicate separations.

ADC-B Band	Migration Time (min)	μ_{app} (cm^2/Vs)
DAR 0	2.268 (±0.002)	$2.449x10^{-4}$ ($\pm 0.002x10^{-4}$)
DAR 1	2.357 (±0.002)	$2.357x10^{-4}$ ($\pm 0.002x10^{-4}$)
DAR 2	2.461 (±0.002)	$2.258x10^{-4}$ ($\pm 0.002x10^{-4}$)
DAR 3	2.602 (±0.002)	$2.135x10^{-4}$ ($\pm 0.002x10^{-4}$)
DAR 4	2.684 (±0.004)	$2.070x10^{-4}$ ($\pm 0.003x10^{-4}$)

Table 4.2: Area percent of DAR species generated via microfluidic CE-MS, infusion-MS, and iCE.

Species	CE-MS Area %	Infusion Area %	iCE Area %
DAR-0	7.7%	8.6%	5.8%
DAR-1	31.2%	33.2%	29.1%
DAR-2	45.9%	39.0%	44.8%
DAR-3	13.1%	16.5%	16.7%
DAR-4	2.1%	2.7%	3.6%

REFERENCES

(1) Wakankar, A.; Chen, Y.; Gokarn, Y.; Jacobson, F. S. *MAbs* **2011**, *3* (2), 161–172.

(2) Alley, S. C.; Anderson, K. E. *Curr. Opin. Chem. Biol.* **2013**, *17* (3), 406–411.

(3) Teicher, B. a.; Chari, R. V. J. *Clin. Cancer Res.* **2011**, *17* (20), 6389–6397.

(4) Le, L. N.; Moore, J. M. R.; Ouyang, J.; Chen, X.; Nguyen, M. D. H.; Galush, W. J. *Anal. Chem.* **2012**, *84* (17), 7479–7486.

(5) Ducry, L. *Antibody-Drug Conjugates*; Springer: New York, NY, 2013.

(6) Liu, H.; Gaza-bulseco, G.; Faldu, D.; Chumsae, C.; Sun, J. *J. Pharm. Sci.* **2008**, *97*, 2426–2447.

(7) Macht, M. *TrAC Trends Anal. Chem.* **2013**, *48*, 62–71.

(8) Zhang, H.; Cui, W.; Gross, M. L. *FEBS Lett.* **2014**, *588* (2), 308–317.

(9) Zhang, Z.; Pan, H.; Chen, X. *Mass Spectrom. Rev.* **2009**, *28*, 147–176.

(10) Doppalapudi, V. R.; Huang, J.; Liu, D.; Jin, P.; Liu, B.; Li, L.; Desharnais, J.; Hagen, C.; Levin, N. J.; Shields, M. J.; Parish, M.; Murphy, R. E.; Del Rosario, J.; Oates, B. D.; Lai, J.-Y.; Matin, M. J.; Ainekulu, Z.; Bhat, A.; Bradshaw, C. W.; Woodnutt, G.; Lerner, R. a; Lappe, R. W. *Proc. Natl. Acad. Sci. U. S. A.* **2010**, *107* (52), 22611–22616.

(11) Alley, S. C.; Okeley, N. M.; Senter, P. D. *Curr. Opin. Chem. Biol.* **2010**, *14* (4), 529–537.

(12) Panowski, S.; Bhakta, S.; Raab, H.; Polakis, P.; Junutula, J. R. *MAbs* **2014**, *6* (1), 34–45.

(13) Sochaj, A. M.; Świderska, K. W.; Otlewski, J. *Biotechnol. Adv.* **2015**, *33* (6), 775–784.

(14) Strop, P.; Delaria, K.; Foletti, D.; Witt, J. M.; Hasa-Moreno, A.; Poulsen, K.; Casas, M. G.; Dorywalska, M.; Farias, S.; Pios, A.; Lui, V.; Dushin, R.; Zhou, D.; Navaratnam, T.; Tran, T.-T.; Sutton, J.; Lindquist, K. C.; Han, B.; Liu, S.-H.; Shelton, D. L.; Pons, J.; Rajpal, A. *Nat. Biotechnol.* **2015**, *33* (7), 694–696.

(15) Lyon, R. P.; Bovee, T. D.; Doronina, S. O.; Burke, P. J.; Hunter, J. H.; Neff-LaFord, H. D.; Jonas, M.; Anderson, M. E.; Setter, J. R.; Senter, P. D. *Nat. Biotechnol.* **2015**, *33* (7), 733–735.

(16) Fekete, S.; Beck, A.; Veuthey, J.-L.; Guillarme, D. *J. Pharm. Biomed. Anal.* **2015**, 1–13.

(17) Harrington, S.; Varro, R.; Li, T. *J. Chromatogr.* **1991**, *559*, 385–390.

(18) Krull, I. S.; Liu, X.; Dai, J.; Gendreau, C.; Li, G. *J. Pharm. Biomed. Anal.* **1997**, *16* (3), 377–393.

(19) Xu, K.; Liu, L.; Saad, O. M.; Baudys, J.; Williams, L.; Leipold, D.; Shen, B.; Raab, H.; Junutula, J. R.; Kim, A.; Kaur, S. *Anal. Biochem.* **2011**, *412* (1), 56–66.

(20) Michels, D. a.; Salas-Solano, O.; Felten, C. *Bioprocess Int.* **2011**, *9* (10), 48–54.

(21) Chen, X.; Nguyen, M.; Jacobson, F.; Ouyang, J. *MAbs* **2009**, *1* (6), 563–571.

(22) Marcoux, J.; Champion, T.; Colas, O.; Wagner-Rousset, E.; Corvaïa, N.; Van Dorsselaer, A.; Beck, A.; Cianférani, S. *Protein Sci.* **2015**.

(23) Debaene, F.; Wagner-rousset, E.; Colas, O.; Ayoub, D.; Corva, N.; Dorsselaer, A. Van; Beck, A.; Cianferani, S. *Anal. Chem.* **2013**, *85*, 9785–9792.

(24) Debaene, F.; Amandine, B.; Wagner-rousset, E.; Colas, O.; Ayoub, D.; Corva, N.; Dorsselaer, A. Van; Beck, A.; Cianfe, S. *Anal. Chem.* **2014**, *86*, 10674–10683.

(25) Batz, N. G.; Mellors, J. S.; Alarie, J. P.; Ramsey, J. M. *Anal. Chem.* **2014**, *86*, 3493–3500.

(26) Redman, E. A.; Batz, N. G.; Mellors, J. S.; Ramsey, J. M. *Anal. Chem.* **2015**, *87* (4), 2264–2272.

(27) Culbertson, C. T.; Jacobson, S. C.; Ramsey, J. M. *Anal. Chem.* **2000**, *72* (23), 5814–5819.

(28) Culbertson, C. T.; Jacobson, S. C.; Ramsey, J. M. *Anal. Chem.* **1998**, *70*, 3781–3789.

(29) Jacobson, S. C.; Hergenroder, R.; Koutny, L. B.; Ramsey, J. M. *Anal. Chem.* **1994**, *66*, 1114–1118.

(30) Jacobson, S. C.; Mcknight, T. E.; Ramsey, J. M. *Anal. Chem.* **1999**, *71* (20), 5172–5176.

(31) Jacobson, S. C.; Hergenroder, R.; Koutny, L. B.; Warmack, R. J.; Ramsey, J. M. *Anal. Chem.* **1994**, *66*, 1107–1113.

(32) Mellors, J. S.; Gorbounov, V.; Ramsey, R. S.; Ramsey, J. M. *Anal. Chem.* **2008**, *80* (18), 6881–6887.

(33) Mellors, J. S.; Jorabchi, K.; Smith, L. M.; Ramsey, J. M. *Anal. Chem.* **2010**, *82* (3), 967–973.

(34) Black, W. a.; Stocks, B. B.; Mellors, J. S.; Engen, J. R.; Ramsey, J. M. *Anal. Chem.* **2015**, *87*, 6280–6287.

(35) Jacobson, S. C.; Koutny, L. B.; Hergenroder, R.; Moore, A. W.; Ramsey, J. M. *Anal.*

Chem. **1994**, *66* (20), 3472–3476.

(36) Berger, S. J.; Chen, W. *Waters Corporation Application Note*. 2008, p Number APNT10094155.

(37) Ferrige, A. G.; Seddon, M. J.; Green, B. N.; Jarvix, S. A.; Skilling, J. *Rapid Commun. Mass Spectrom.* **1992**, *6*, 707–711.

(38) McDonagh, C. F.; Turcott, E.; Westendorf, L.; Webster, J. B.; Alley, S. C.; Kim, K.; Andreyka, J.; Stone, I.; Hamblett, K. J.; Francisco, J. a.; Carter, P. *Protein Eng. Des. Sel.* **2006**, *19* (7), 299–307.

(39) Strop, P.; Liu, S.-H.; Dorywalska, M.; Delaria, K.; Dushin, R. G.; Tran, T.-T.; Ho, W.-H.; Farias, S.; Casas, M. G.; Abdiche, Y.; Zhou, D.; Chandrasekaran, R.; Samain, C.; Loo, C.; Rossi, A.; Rickert, M.; Krimm, S.; Wong, T.; Chin, S. M.; Yu, J.; Dilley, J.; Chaparro-Riggers, J.; Filzen, G. F.; O'Donnell, C. J.; Wang, F.; Myers, J. S.; Pons, J.; Shelton, D. L.; Rajpal, A. *Chem. Biol.* **2013**, *20* (2), 161–167.

(40) Shen, B.-Q.; Xu, K.; Liu, L.; Raab, H.; Bhakta, S.; Kenrick, M.; Parsons-Reponte, K. L.; Tien, J.; Yu, S.-F.; Mai, E.; Li, D.; Tibbitts, J.; Baudys, J.; Saad, O. M.; Scales, S. J.; McDonald, P. J.; Hass, P. E.; Eigenbrot, C.; Nguyen, T.; Solis, W. a; Fuji, R. N.; Flagella, K. M.; Patel, D.; Spencer, S. D.; Khawli, L. a; Ebens, A.; Wong, W. L.; Vandlen, R.; Kaur, S.; Sliwkowski, M. X.; Scheller, R. H.; Polakis, P.; Junutula, J. R. *Nat. Biotechnol.* **2012**, *30* (2), 184–189.

(41) Hamblett, K. J.; Senter, P. D.; Chace, D. F.; Sun, M. M. C.; Lenox, J.; Cerveny, C. G.; Kissler, K. M.; Bernhardt, S. X.; Kopcha, A. K.; Zabinski, R. F.; Meyer, D. L.; Francisco, J. a. *Clin. Cancer Res.* **2004**, *10* (425), 7063–7070.

(42) Doronina, S. O.; Toki, B. E.; Torgov, M. Y.; Mendelsohn, B. a; Cerveny, C. G.; Chace, D. F.; DeBlanc, R. L.; Gearing, R. P.; Bovee, T. D.; Siegall, C. B.; Francisco, J. a; Wahl, A. F.; Meyer, D. L.; Senter, P. D. *Nat. Biotech.* **2003**, *21* (7), 778–784.

(43) Junutula, J. R.; Raab, H.; Clark, S.; Bhakta, S.; Leipold, D. D.; Weir, S.; Chen, Y.; Simpson, M.; Tsai, S. P.; Dennis, M. S.; Lu, Y.; Meng, Y. G.; Ng, C.; Yang, J.; Lee, C. C.; Duenas, E.; Gorrell, J.; Katta, V.; Kim, A.; McDorman, K.; Flagella, K.; Venook, R.; Ross, S.; Spencer, S. D.; Lee Wong, W.; Lowman, H. B.; Vandlen, R.; Sliwkowski, M. X.; Scheller, R. H.; Polakis, P.; Mallet, W. *Nat. Biotechnol.* **2008**, *26* (8), 925–932.

CHAPTER 5: MIDDLE-UP APPROACHES TO BIOTHERAPEUTIC MONOCLONAL ANTIBODY CHARACTERIZATION VIA MICROFLUIDIC CE-MS

5.1 Introduction

One of the goals of analytically characterizing monoclonal antibody (mAb) based therapeutics is to identify major and minor modifications to the molecules and ascertain if they affect drug potency or pharmacokinetic properties. A thorough characterization of mAb therapeutics generally involves analyzing the molecule at different levels ranging from intact analysis to amino acid composition. Each level provides different pieces of information that are necessary for obtaining a clear picture of the state of the molecule. For instance, top-down analysis of intact mAbs provides a broad view of the mAb population heterogeneity while a bottom-up mapping experiment can generate very specific information about modification sites.

A common approach that can provide information about the general localization of modifications involves sectioning the mAb into moderately sized fragments either enzymatically or chemically. This is often referred to as a middle-up approach or middle-down if further fragmentation is performed in a mass spectrometer (MS).[1–5] The benefits of this approach are two-fold: the challenges of intact mAb analysis are mitigated with the smaller mAb fragments and it can be ascertained if modifications are occurring in a location of the mAb that may affect its efficacy, such as the antigen binding region. Enzymatic fragmentation, or limited proteolysis, is often performed using Lys-C, papain, or IdeS to cleave the mAb in the hinge region.[1,3,6] As illustrated in Figure 5.1, depending on the location of the cleavage site either Fab and Fc fragments (~50 kDa each) or $F(ab')_2$ (~100 kDa) and Fc fragments are generated. mAbs can also

be fragmented chemically to the light chains (LC) and heavy chains (HC) (~25 kDa and ~50 kDa, respectively) using reducing agents such as dithiothreitol (DTT) or *tris*(2-carboxyethyl)phosphine **(**TCEP). Both modes of fragmentation bring the size of the mAb analytes to be measured into a regime that is more manageable for many separation techniques.

Both chromatographic and electrophoretic separation techniques have been used to analyze mAb LC, HC, Fc, Fab, and F(ab´)$_2$ fragments. At these reduced sizes minor modifications, such as oxidation or deamidation, can be separated from unmodified counterparts. Reversed phase liquid chromatography (RPLC) and ion exchange chromatography (IEC) have been shown to be effective in separating mAb fragments.[6–10] RPLC methods for this analysis have also been effectively coupled to MS analysis for added levels of characterization.[11–18] However, it has been shown that without proper care, the harsh solvent conditions in combination with the elevated column temperatures needed to achieve efficient RPLC separations can induce artificial degradation.[1,19,20] Common electrophoretic approaches to analyzing mAb fragments are capillary zone electrophoresis (CZE) or capillary gel electrophoresis (CGE). Successful demonstrations of both techniques for middle up analysis can be found in the literature although as is typical with electrophoretic techniques, these methods are not MS compatible.[21–27]

The potential benefits of using CZE coupled to MS analysis for protein separations have been thoroughly described.[28,29] Although recently there has been much interest in CE-MS techniques for characterizing biopharmaceuticals there have been few reports demonstrating the analysis of mAb fragments in the middle-up/down regime.[30] In this work, a middle-up approach is utilized for analyzing biotherapeutic mAbs and ADCs. Both limited proteolysis and chemical reduction were evaluated. While both fragmentation strategies resulted in mAb fragments that

were able to be separated and detected with MS, microfluidic CE-MS analysis of the LC and HC from chemical reduction of the mAbs proved to be a more robust method.

5.2 Experimental

5.2.1 Materials and Reagents

Deionized water was generated with a Nanopure Diamond water purifier (Barnstead International, Dubuque, IA). Optima LC/MS grade 2-propanol, acetonitrile, formic acid, acetic acid, and cysteine were obtained from Fisher Scientific (Fairlawn, NJ). The silane coating reagent 3-(aminopropyl)di-isopropyl-ethoxysilane (APDIPES) was purchased from Gelest (Morrisville, PA) and the methyl-terminated polyethylene glycol n-hydroxy succinimide ester (NHS-PEG450) was purchased from Nanocs Inc. (Boston, MA). Trichloro-(1H,1H,2H,2H-perfluorooctyl)-silane, the papain protease, ethylenediaminetetraacetic acid (EDTA), ammonium bicarbonate, dithiothreitol (DTT), and iodoacetamide (IAM) was purchased from Sigma-Aldrich (St. Louis, MO). The monoclonal antibodies and antibody drug conjugates mAb-B, ADC-B, mAb-C, ADC-C, and mAb-D were provided by Pfizer Inc. (St. Louis, MO). Infliximab was provided by Waters Corporation (Milford, MA).

5.2.2 Sample Preparation

Infliximab and mAb-D were diluted to 5 mg/mL and 3 mg/mL, respectively, and papain digested in phosphate buffered saline with 20 mM cysteine and 20 mM EDTA at an enzyme to protein ratio of 1:50. It was found that the Infliximab digestion was complete in approximately 3 hours at 37 °C while digestion of mAb-D required at least 5 hours. The digested mAbs were buffer exchanged to 0.2% acetic acid using 25 kDa molecular weight cutoff filters.

For analysis of the LC and HC via reduction and alkylation, antibodies in formulation buffer were diluted to a concentration of 1 mg/mL with 50 mM ammonium bicarbonate buffer. Reduction of the disulfide bonds was performed with 20 mM DTT for ~30 minutes at 37 °C. The cysteine residues were alkylated with 40 mM IAM. The mAb samples were incubated with the IAM in the dark at room temperature for ~30 minutes. For microfluidic CE-MS analysis, the reduced and alkylated mAbs were diluted with 50 mM ammonium bicarbonate to 0.25 mg/mL.

5.2.3 CE-ESI-MS Device Preparation and Operation

The APS-PEG_{450} surface coating described in the introduction was used for this analysis and applied according to the procedures in Appendix 2. CE-ESI devices were operated by applying and controlling voltages as described in Appendix3. For the limited proteolysis experiments, bulk fluid flow for sustaining ESI was supplied via electroosmotic pumping and 10% 2-propanol 0.2% acetic acid background electrolyte (BGE) was used. An electrokinetic (EK) injection scheme was used for sample injection.

A 50/50 acetonitrile 1.0% formic acid BGE was used for LC/HC analysis. The pumping channel was coated with PEG_{450} and bulk fluid flow was generated by applying head pressure to the pumping reservoir. A hydrodynamic (HD) injection scheme, as described in Appendix 3, was used for sample manipulation and injection. The samples were injected at 0.75 psi. For this analysis +20kV and +2.5kV were applied to reservoirs 1 and 4, respectively, which resulted in a field strength of approximately 685 V/cm.

5.2.4 Data Analysis

For the limited proteolysis experiments MS analysis was performed using a Waters LCT-Premier (Waters Corporation, Milford, MA) operated according to the parameters listed in Appendix 4. A mass spectrum was generated for each species by averaging mass scans across the width of the peak at its base. Deconvolution of the resulting mass spectra was performed based on maximum entropy analysis using the MaxEnt1 deconvolution algorithm in the MassLynx software as described previously.[3,31–33]

MS analysis of the reduced and alkylated mAbs was performed using a Thermo Exactive Plus EMR orbitrap mass spectrometer (Thermo Scientific, Watham, MA). Data were acquired over a mass range of 1000-3000 m/z at a resolution setting of 17500 with the in-source collision energy set to 80 and the S-lens RF at 80. Note that extended mass range (EMR) mode was not used for this analysis. A mass spectrum was generated for each species by averaging mass scans across the width of the peak. Integrated peak areas were generated using the Xcalibur software (Thermo Scientific) and deconvolution of the mass spectra was performed using Protein Deconvolution 3.0 software (Thermo Scientific, Watham, MA).

5.3 Results and Discussion

5.3.1 Analysis of Infliximab via Papain Digestion

Figure 5.2 shows the separation of an Infliximab papain digestion using a 23 cm APS-PEG_{450} device with a 10% 2-propanol 0.2% acetic acid background electrolyte. Each peak is labeled with the associated deconvoluted mass. No intact antibody is detectable indicating the digestion was complete. The triplet of peaks corresponding to the lysine variants of the Fc region is apparent as the first three peaks in the electropherogram. The MWs of these species differ by

approximately 128 Da, which is in agreement with the expected mass shift for the truncation of a C-terminal lysine. The resolution between the C-terminal lysine charge variants is greater when the Fab region of the antibody is removed. Intact analysis resulted in a resolution of 1.2 between C-terminal lysine variants. This was increased to 1.4 after digestion with papain. The deconvoluted and labeled mass spectra of the Fc fragments is given in Figure 5.3. The differences in mass due to glycan variants within a specific Fc fragment are easily seen in the deconvoluted mass spectrum. There are also a significant number of phosphate adducts detected as a mass increase of ~98 Da. It appears that phosphate ions from the digestion conditions remain associated with the mAb fragments despite buffer exchanging these samples to 0.2% acetic acid. This could potentially be alleviated by carrying out the digestion in a volatile buffer, such as ammonium bicarbonate or ammonium acetate.

Peaks four and five are thought to correspond to Fab fragments because they lack the characteristic mass pattern associated with glycan structures. Deconvolution of the mass spectrum corresponding to the most abundant Fab fragment is provided in the Figure 1 inset. Aside from the phosphate adduct there are no other major mass species detected that could be attributed to post translational modifications or degradation. The mass shift between this Fab species and the minor acidic Fab variant is 367 Da. The remaining features of the electropherogram have associated masses of ~23 kDa. This is approximately half the mass of an Fc or Fab fragment so it is thought that these features are the result of the fragments dissociating into light and heavy chain pieces during the separation. This hypothesis is supported by the presence of a long trail of 23 kDa species indicating that the dissociation is occurring during the separation rather than in the sample solution.

5.3.2 Analysis of mAb-D via Papain Digestion

mAb-D is an IgG-2 that has been engineered with a second glycosylation site in the Fab region in addition to the highly conserved glycosylation site in the Fc domain. The glycans at this site become sialylated creating a very complex charge heterogeneity profile, and microfluidic CE-MS analysis of intact mAb-D does not result in significant resolution between the charge variants of the molecule (Figure 5.4a). However, the mass spectrum is not homogeneous across the width of the peak indicating that some degree of separation is occurring in the CE domain, and in the deconvoluted spectra (Figure 5.4b), the presence of sialylated glycans can be detected by mass shifts of ~291 Da between species. Thus, a middle-up approach to analyzing this molecule could increase the amount of information generated for this mAb.

mAb-D was digested with papain in the presence of cysteine to produce Fc and Fab fragments of the mAb. Because the glycan structures in the Fab region are sialylated, the Fab fragments should separate based on charge due to these residues in addition to any other modifications that change the net charge. Microfluidic CE-MS analysis of the fragmented mAb is provided in Figure 5.5a. Several peaks are detected in the electropherogram and deconvolution of the mass spectra associated with these species aided in their identification. The higher mobility fragments were identified as Fc fragments with the main isoform at a mass of 52310 Da. Different glycan structures on the Fc glycosylation site can be detected in the deconvoluted spectra for the Fc species. There are several minor variants of the Fc fragments separated in the CE domain. The basic variant at 52253 Da differs by a mass of 57 Da while the acidic variants at 52324 Da and 52538 Da differ by 14 Da and 228 Da, respectively. The 14 Da mass shift between the main isoform and the first acidic variant is similar to that of oxidation. A reduction in electrophoretic mobility has been seen with oxidized peptides, so it is possible that this Fc

species is an oxidized variant. The identity of the remaining basic and acidic variants is not immediately apparent. The mass shifts do not agree with any common protein modifications. It has been noted in the literature that limited proteolysis via papain can be subject to variability in the cleavage site on the mAb. Thus, it is possible that these variants are due to inconsistencies in the digestion of the mAb. The Fab fragments are present in the latter half of the electropherogram and are slightly lower in mass than the Fc fragments. Figure 5.5b shows the deconvoluted mass spectra for the labeled Fab fragments and identified glycoforms of the Fab fragments. The addition of sialic acids is detected by mass shifts of 291 Da between glycoforms and a reduction in electrophoretic mobility due to the added negative charge. The addition of up to 2 sialic acids is detected from the CE separation and mass spectral information.

As is obvious from Figure 5.5a, the peaks corresponding to the Fab domain are significantly broader than those of the Fc domain. Also, overlap between the Fab glycoforms is apparent in the deconvoluted spectra. To better assess the peak shapes of the Fab species, extracted ion electropherograms were generated for the most abundant glycoforms differing in sialylation levels and are overlaid in Figure 5.6. The peaks appear as doublets with no immediately apparent reason why. Since the deconvoluted masses are consistent between the Fab peaks, a possible explanation is that the Fab fragments are assuming different conformations in solution. These structural conformations would have to be different enough to induce a significant change in the hydrodynamic radius and, thus, electrophoretic mobility. This explanation could also account for the poor peak shape of the Fab fragments. If the Fab fragments exist in a variety of different structural conformations, then they could exhibit a variety of electrophoretic mobilities corresponding to the conformations. This would manifest as apparent band broadening in the CE domain.

Between the Fc and Fab fragment peaks there are species that do not appear to be from either domain. This is based on the appearance of the raw mass spectra. Figure 5.7 compares the raw mass spectra of the Fc main isoform, Fab-2 peak, and the unknown species. Both the Fc and Fab species appear at much higher m/z values while the unknown species appear at much lower values. This could simply indicate higher charging on the molecule due to greater denaturation or disruption of the fragment's structure. However, as discussed before this is not ideal as it can lead to band broadening or multiple peaks for one species.

Limited proteolysis with papain digestion generated smaller mAbs fragments that were separated via CE-MS. This generated information about the different regions of the mAb that was not apparent at the intact level. Glycoform information was generated for the Fc and Fab regions separately. However, the different Fc charge variants detected during analysis do not appear to be due to common protein modifications. It is not apparent whether these modifications are characteristic of the analyte or caused by the digestion process. Additionally, the Fab fragments do not cleanly separate, complicating data interpretation. While this analysis approach was successful in generating more resolved mAb species and general information about modification localization, the overall result is not ideal. Using a more specific protease to cleave the mAb, such as the IdeS protease, could make the digestion more reproducible and improve data interpretation.

5.4 Reduction and Alkylation of mAbs.

Around the same time the limited proteolysis approach was being explored, reduction and alkylation of the mAbs was being evaluated as an alternative middle-up technique. Once optimized, this strategy was found to be faster, easier, and to produce more reliable results.

Recent studies analyzing reduced mAbs via CE-MS reported issues with maintaining solubility of the LC and HC.[30] Initially, similar problems were encountered during sample processing because the mAb fragments had to be desalted and acidified to make them compatible with EK injections. It appeared that this process caused most of the HC species to aggregate and precipitate out of solution. However, once the HD based injection strategy was developed, these desalting steps were eliminated. It was then determined that the liberated polypeptide chains remain relatively stable when kept in a neutral or slightly basic aqueous solution and then analyzed using a BGE with fairly high levels of organic modifier and acid. In this case, 50/50 acetonitrile/water with 1% formic acid was found to be optimal in terms of separation resolution and MS signal quality.

5.4.1 Analysis of a Reduced and Alkylated mAb-B.

mAb-B is a relatively simple IgG-2. Prior analysis of the intact mAb via microfluidic CE-MS revealed three main charge variants of the mAb and that the glycoform heterogeneity is fairly low.[34] Thus, this molecule was chosen for developing the method for analyzing reduced and alkylated mAbs using microfluidic CE-ESI technology. Reduced and alkylated mAb-B was analyzed via microfluidic CE-MS. Approximately 1.3 nL of sample was injected which corresponds to 317 pg of mAb. The resulting electropherogram is provided in Figure 5.8a. Analysis of the reduced mAb was complete in less than 3 minutes. As listed in Table 5.1, migration times of the species are reproducible with less than 1% relative standard deviation.

Several peaks are present in the resulting electropherogram that correspond to LC and HC species. Deconvolution of the mass spectra generated masses that facilitated the identification of species in the electropherogram. At approximately 23.5 kDa, the earliest

migrating species was identified as mAb-B LC. There are no other peaks detected in the electropherogram that would indicate net charge altering modifications to the LC, but minor species (<5%) differing in mass are present in the deconvoluted spectrum (Figure 5.8b). The heavier mass species in the deconvoluted spectrum could be attributed to potassium or phosphate adducts on the LC. The lighter mass species at 23592 Da is 44 Da lighter than the main LC variant. A loss of 44 Da is characteristic of a decarboxylation event. This can change the net charge of a molecule due to loss of a carboxylic acid group, but under the acidic conditions used for this analysis these groups are likely to be protonated so a change in net charge may not be observed.

The remaining species in the electropherogram are HC variants. Deconvolution of the main isoform mass spectrum reveals several glycoforms of the HC as indicated in Figure 5.8b with the most abundant being the G0F glycoform. The basic variant of the HC differs in mass by 18 Da from the main isoform. This mass shift is indicative of pyroglutamic acid formation at the N-terminus and the decrease in electrophoretic mobility agrees with this assignment. This type of modification was also identified in this molecule at the intact level using microfluidic CE-MS as reported previously.[34] The two acidic HC variants differ in mass from the main isoform by 1 Da and 2 Da, respectively, and also decrease in electrophoretic mobility. This indicates the modification induces a decrease in net charge and is most likely caused by deamidation. Deamidated forms of mAb-B were not detected at the intact level using microfluidic CE-MS. Most likely this is due to the low abundance of these species and the limited resolving power of the MS instrument.

5.4.2 Analysis of Reduced and Alkylated mAb-D.

Approximately 1 nL of reduced/alkylated mAb-D sample solution was injected. This equates to ~245 pg of mAb reduced. The microfluidic CE-MS analysis of reduced and alkylated mAb-B is provided in Figure 5.9a and 8b. Several peaks are present in the electropherogram that correspond to the LC and variants of the HC. Their migration times and electrophoretic mobilities can be found in

Table 5.2. A single LC peak was detected at 2.24 minutes with the most abundant species at a mass of 24000 Da. Minor mass modifications of the LC were detected in the deconvoluted mass spectrum. The -44 Da and +37 Da variants identified in mAb-B were also detected in mAb-D. The 23941 Da variant is 59 Da lighter than the main LC species and is likely due to an unalkylated cysteine. The minor 24164 Da variant is 164 Da heavier than the main species and could be attributed to glycation of the LC. The 24128 Da variant is not as easily identified. A 128 Da mass shift is often indicative of a lysine residue. This type of modification would also be accompanied with a change in electrophoretic mobility due to the extra positive charge, but no mobility shift is seen for this species. However, the presence a glutamine residue at the N-terminus would result in a similar mass shift, but not induce a change in net charge. Further experiments are needed to identify this LC variant.

As mentioned above, the HC of mAb-D is expected to bear sialylated glycans. Glycoforms of the HC differing in the amount of sialylation should be easily separated in the CE domain because sialic acids cause a reduction in net charge. Six individual HC species were detected as discrete peaks in the electropherogram (Figure 5.9a). Deconvolution of the mass

spectra for the HC peaks revealed significant glycoform heterogeneity (Figure 5.9b). This is to be expected as the measured masses are a function of both the Fc and Fab glycans present on the HC. Table 5.3 lists the detected glycoforms of the mAb-D HC and their assignments based on mass and changes in electrophoretic mobility. Prior characterization of this molecule determined that sialylation only occurs on the Fab glycans, which facilitated glycoform identification.[35] Mass shifts of 291 Da were detected between the most abundant HC peaks indicating that the reduction in electrophoretic mobility is due to the addition of sialic acids. Overall, 16 glycoforms of the mAb-D HC were identified with up to 3 sialic acids on the Fab glycan structures. It is worth noting that some combinations of glycan structures are identical in mass and thus cannot be differentiated without further analysis. An additional HC variant migrating at 2.48 minutes is 3 Da heavier than the most abundant glycoform and has a lower electrophoretic mobility. This variant accounts for ~2.0% of the unmodified glycoform and is most likely due to deamidation of the HC.

5.4.3 Analysis of Reduced and Alkylated ADC.

mAb-B was conjugated with a peptide drug molecule using lysine based chemistry described previously[36] to create the antibody drug conjugate, ADC-B. Briefly, a conjugation event is characterized by a mass increase of 3145 Da and a decrease in net charge due to the reaction with the lysine side chain. Analysis of mAb-Ac at the intact level using the previously described microfluidic CE-MS method determined a maximum drug to antibody ratio (DAR) of 4 with an average DAR of 1.7.[34] However, information about where conjugation occurred on the mAb structure was not generated through intact analysis. Reducing the ADC to its light and heavy chains can provide insight into the general localization of the drug loads. Thus, ADC-B

was reduced, alkylated, and analyzed via microfluidic CE-MS. An injection volume of ~1.3 nL was used corresponding to ~317 pg of ADC. The resulting electropherogram is provided in Figure 5.10. The separation profile is similar to that of mAb-A though there are now additional species corresponding to conjugated LC and HC. Table 5.4 lists the migration times and electrophoretic mobilities of the separated LC and HC species. After deconvolution to obtain masses, it was evident that a majority of the drug loads are conjugated to the LC. The conjugation chemistry used to create ADC-B is nonspecific and the more solvent accessible lysine residues are preferentially conjugated. Based on this, it can be surmised that although there are nearly twice as many lysine residues in the HC of mAb-B, the majority are not accessible for conjugation due their orientation within the overall mAb structure. Of the LC species detected, 14.6% are unconjugated while 81.4% and 4.0% are singly and doubly conjugated, respectively. Comparatively, only a small amount of the HC is conjugated (1.4%). These percentages can be used to calculate the average DAR of ADC-B using Equation 4.1[37]:

$$DAR_{avg} = 2 \times \frac{\sum nA\%_{LC} + \sum nA\%_{HC}}{100} \tag{4.14}$$

where *n* is the number of drug loads and *A%* is the area percent for the given LC or HC species. The average DAR was calculated to be 1.8, which agrees very well with the average DAR obtained through intact analysis of ADC-B.[34]

Although both the LC and HC are conjugated with the same drug load, the mobility shift due to conjugation is quite different for the two polypeptide chains. Conjugation of the LC results in a decrease in electrophoretic mobility of ~0.2×10^{-4} cm^2/Vs while conjugation of the HC only decreases the electrophoretic mobility by ~0.04×10^{-4} cm^2/Vs. This is not surprising as the

mass of the drug load is ~13% of the mass of the LC but only ~6% of the mass of the HC; it is reasonable to expect this to increase its hydrodynamic radius, and thus decrease its electrophoretic mobility. However, the mobility shift caused by conjugation of the HC is perhaps lower than would be expected based on the mobility shift seen with the LC. In fact, the conjugated HC co-migrates with the deamidated form of the HC indicating that the mobility shift between the two variants is not significantly different. The reason for this is not readily apparent and could be due to the conformation of the HC in solution. If the HC is tightly folded with the drug load it is possible that the hydrodynamic radius is not significantly affected and the mobility shift is dominated by the reduction in net charge.

5.4.4 Analysis of Reduced and Alkylated ADC-C.

In the previous chapter a cysteine linked ADC denoted at ADC-C was analyzed at the intact level. The average DAR calculated did not agree with the average DAR calculated by collaborators at Pfizer (3.52 at UNC versus 4.55 at Pfizer). There was also evidence of degradation and the highest level of conjugation, DAR 8, was not detected via microfluidic CE-MS analysis. To further assess the potential degradation of this molecule, ADC-C was reduced and alkylated and analyzed via microfluidic CE-MS. The resulting electropherogram is provided in Figure 5.11. The LC separates in the CE domain based on the number of drug loads conjugated to it, while only one main HC peak is detected. Deconvolution of the mass spectrum associated with the HC peak reveals that conjugated HC species are present, but the CE resolution is limited. The inset of Figure 5.11depicts overlaid extracted ion electropherograms for the various conjugated HC species. Although it is slight, there is a shift in migration time due to conjugation of the HC. Based on the integrated peak areas, the HC is 14.6% unconjugated,

while 35.2% bears a single drug load, 25.5% bears two, and 24.7% bears three. The LC is 26.0% unconjugated, while 74.0% bears one drug load. The average DAR can be calculated using these distributions and Equation 5.1. For this analysis, the average DAR was calculated to be 4.69. This value is in better agreement with the data provided by Pfizer for this molecule. This value confirms that DAR-8, which was not detected at the intact level via microfluidic CE-MS (Chapter 4, Figure X), is present in the ADC-C sample. This also supports the hypothesis that some level of degradation is occurring before or during analysis. Since conjugated LC and HC were present in the filtrate when the ADC-C stock was filtered, it seems likely that DAR-8 is becoming unstable in the formulation buffer.

5.5 Conclusions

This work demonstrates middle-up analysis of mAb fragments using microfluidic CE-MS. The initial strategy to achieve this focused on limited proteolysis of the mAbs via papain digestion to generate Fc and two Fab fragments. For Infliximab, reducing the size of the analyte molecule increased the resolution between the C-terminal lysine variants. For the doubly glycosylated mAb-D, differences in the Fc and Fab glycan structures could be detected in the deconvoluted mass spectra and differentiated in the CE domain based on the degree of Fab glycan sialylation. However, there were charge variants of both fragments detected in the CE separation of both mAbs that were not readily identified. It is possible that irreproducibility in the cleavage site on the mAbs resulted in some of the anomalous species detected. Utilizing a more specific protease could alleviate these problems and make this approach more reliable and informative.

Analysis of the reduced and alkylated mAbs proved to be much more successful. The LC and HC of the mAbs analyzed were baseline resolved in less than 3 minutes with excellent reproducibility. Additionally, the method described here not only resulted in efficient CE separations, but also high quality mass spectra that facilitated the identification of modifications to the polypeptide chains. Two variants of the mAb-B LC were identified in the deconvoluted spectrum along with adducts of the main LC variant. Four peaks associated with the HC were separated and identified as pyroglutamic acid variants and deamidated forms of the HC, the latter of which were not detected at the intact level. Glycoforms of the HC were also identified in the deconvoluted spectrum.

This method also proved successful for analyzing more complex antibody based therapeutics. Identification of sixteen glycoforms of the doubly glycosylated mAb-D was facilitated by both the CE separation and mass spectral data. The HC glycoforms separated in the CE domain based on the number of sialic acids in the glycan structures. Additional glycoform modifications that do not induce a change in net charge were identified in the deconvoluted mass spectra of the HC species. Analysis of the LC and HC of ADC-B provided information on the general localization of the conjugation sites on the mAb structure. The drug loads preferentially reacted with lysine residues on the LC implying that these residues are more solvent accessible than the lysine residues of the HC. The average DAR was also calculated and found to agree well with the average DAR calculated from intact analysis of the ADC. Analysis of ADC-C confirmed the presence of a higher level DAR species, DAR-8, that was not detected during intact analysis, indicating that the species most likely degraded in the formulation buffer.

The results presented here demonstrate the feasibility of using microfluidic CE-MS for characterizing reduced and alkylated mAbs. After the initial reduction and alkylation, minimal

sample preparation is necessary for analysis of the mAb samples. The analysis times are significantly shorter than many chromatography or electrophoresis based analyses indicating that this method has the potential to be a simple, rapid technique for mAb characterization. Also, elevated temperatures that could be detrimental to the mAbs are not required to achieve efficient separations. The same device design has been used for intact analysis of mAbs and ADCs simply by changing the BGE composition. Thus, the same microfluidic CE-ESI device can be used for multiple levels of mAb characterization.

5.6 Figures and Tables

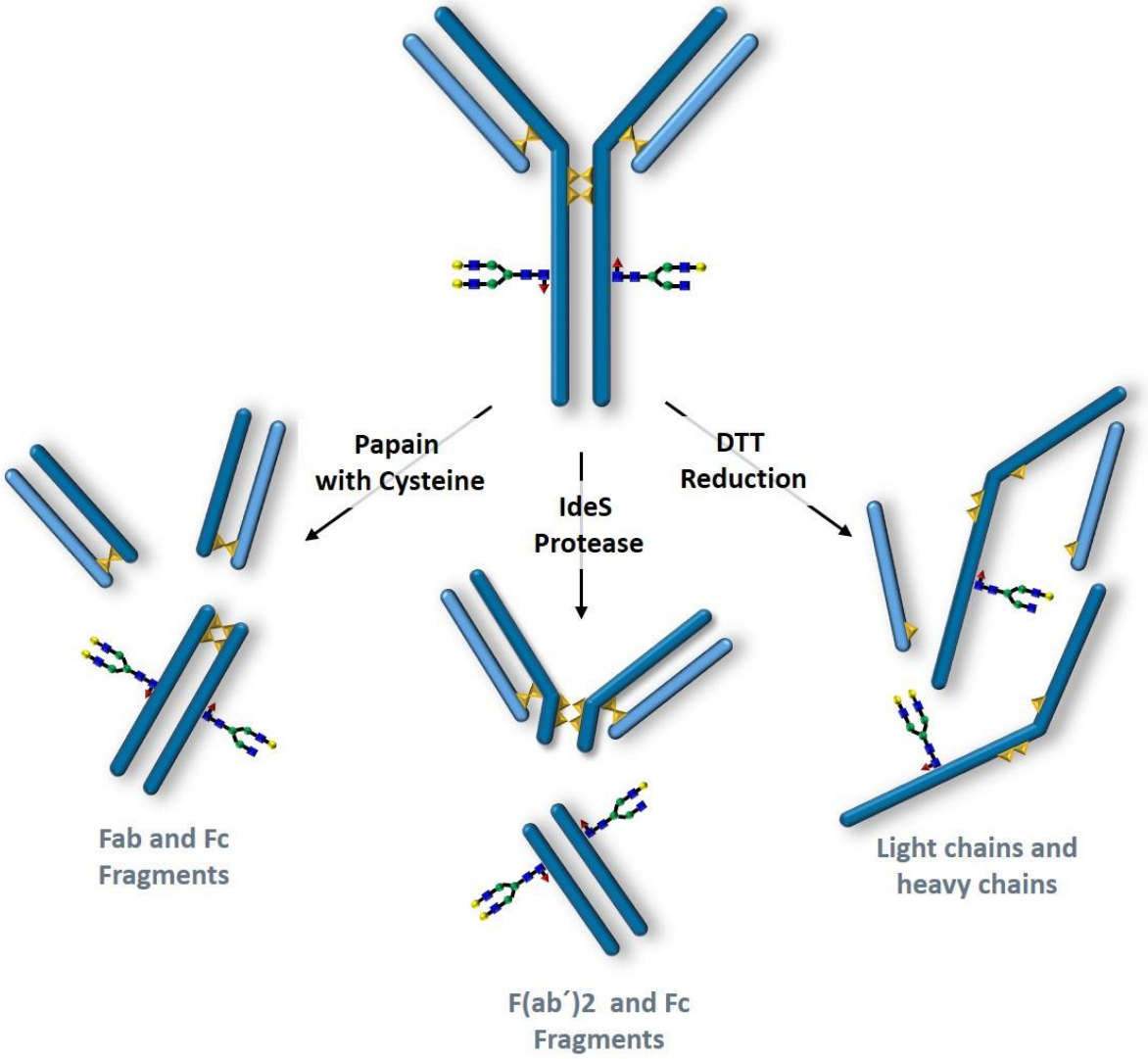

Figure 5.1: mAb fragments generated using chemical and enzymatic sample processing for middle-up and middle-down analysis.

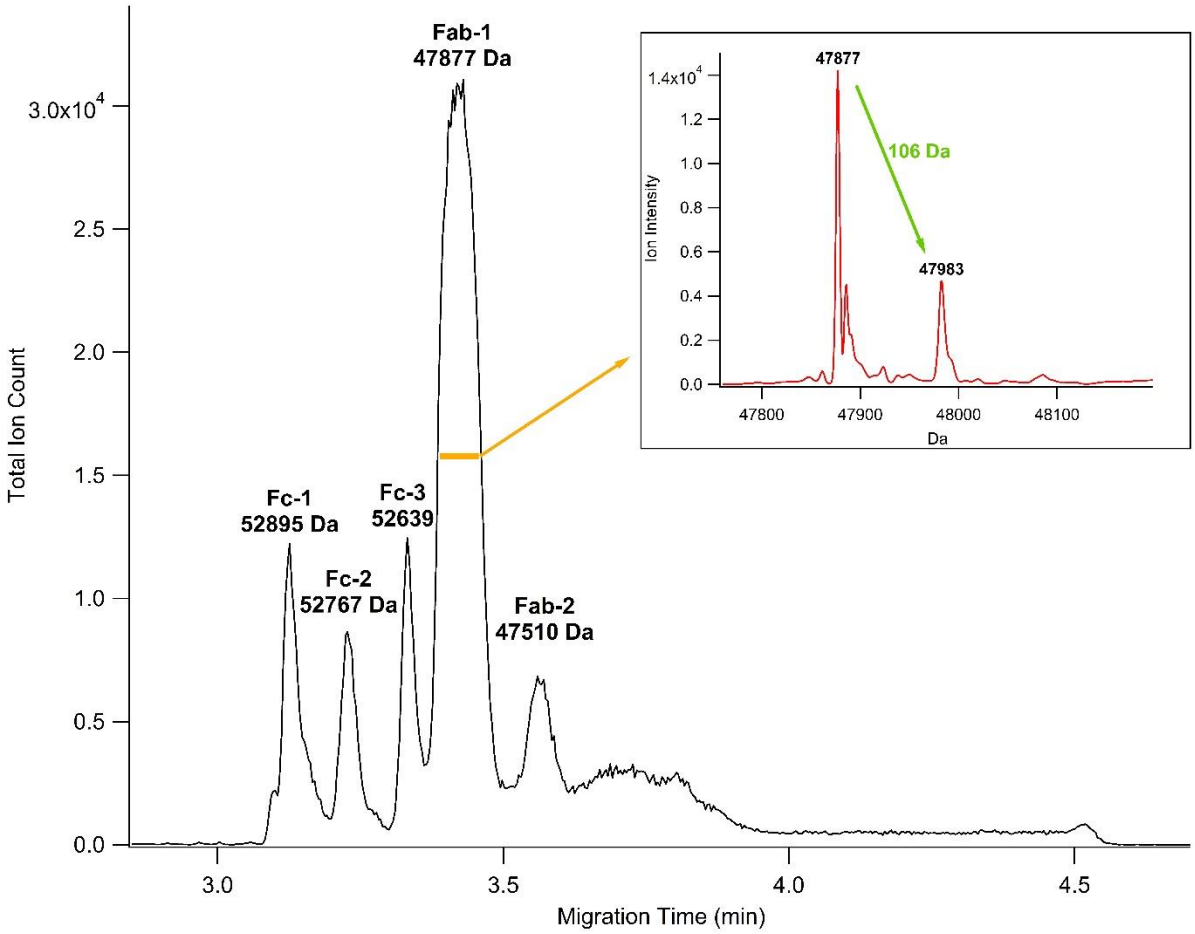

Figure 5.2: Electropherogram showing the separation of 5 mg/mL Infliximab papain digestion in 10% 2-propanol 0.2% acetic acid using a 23 cm APS-PEG_{450} coated device. The inset shows the deconvoluted mass spectrum for the most abundant Fab species. Instrument: Waters LCT-Premier

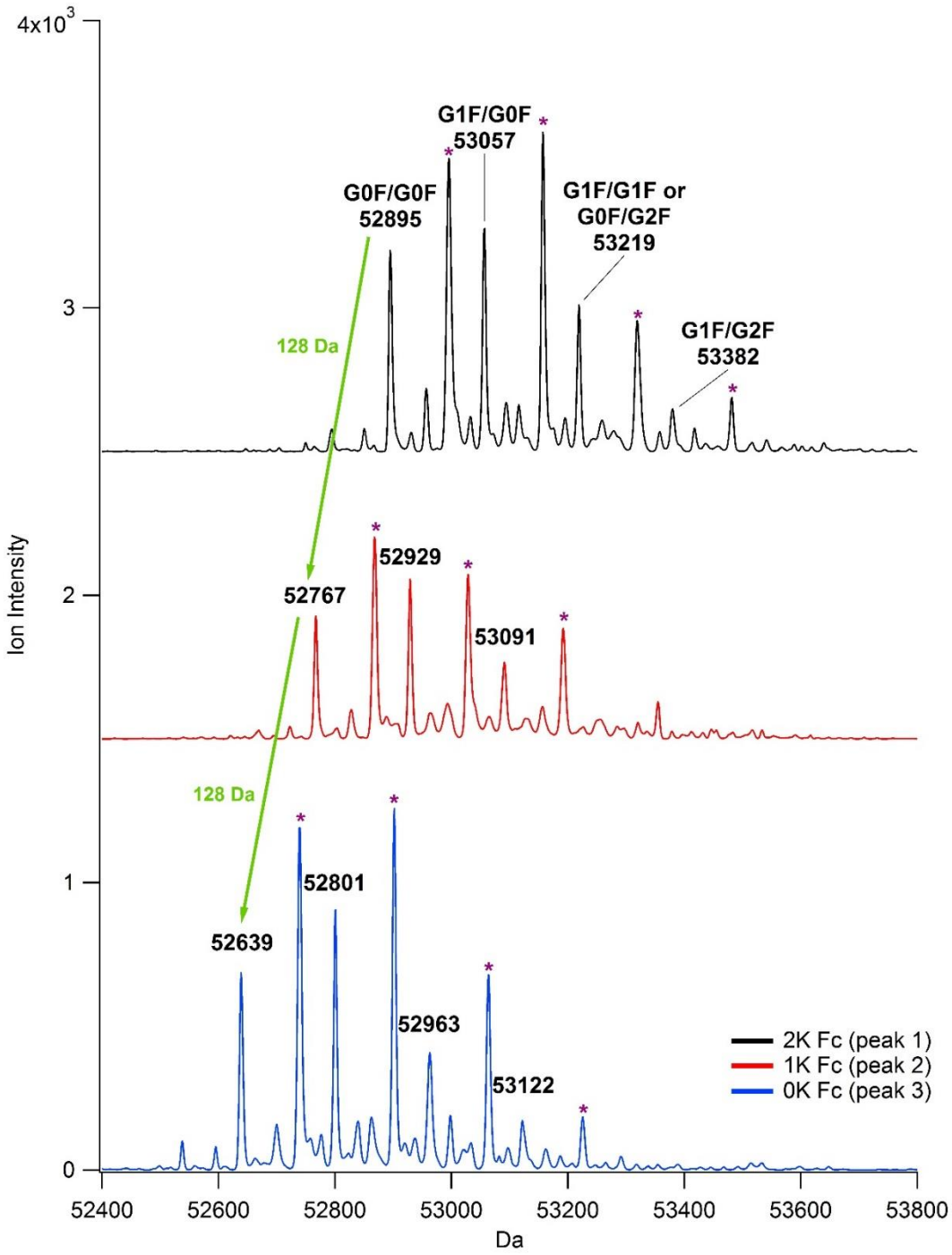

Figure 5.3: Deconvolution of the mass spectra associated with the Fc fragments separated in the CE domain. The mass shift of 128 Da between the C-terminal lysine variants is easily detectable. Glycoforms of the Fc fragments are also apparent in the deconvoluted spectra. (*) indicates a phosphate adduct.

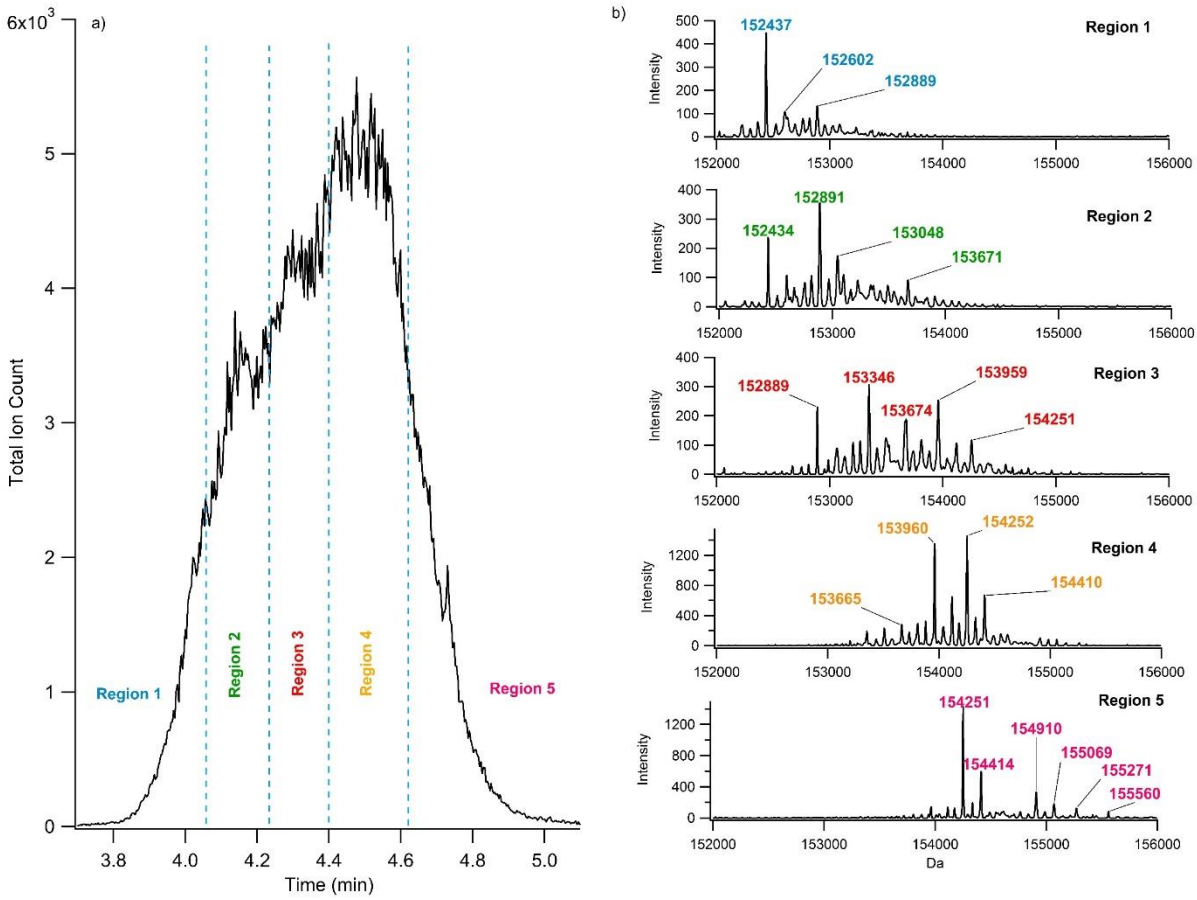

Figure 5.4: Intact charge variant separation of mAb-D via microfluidic CE-MS. a) Electropherogram generated from the CE separation of mAb-D. b) Deconvolution of the mass spectra associated with the marked regions in the electropherogram.

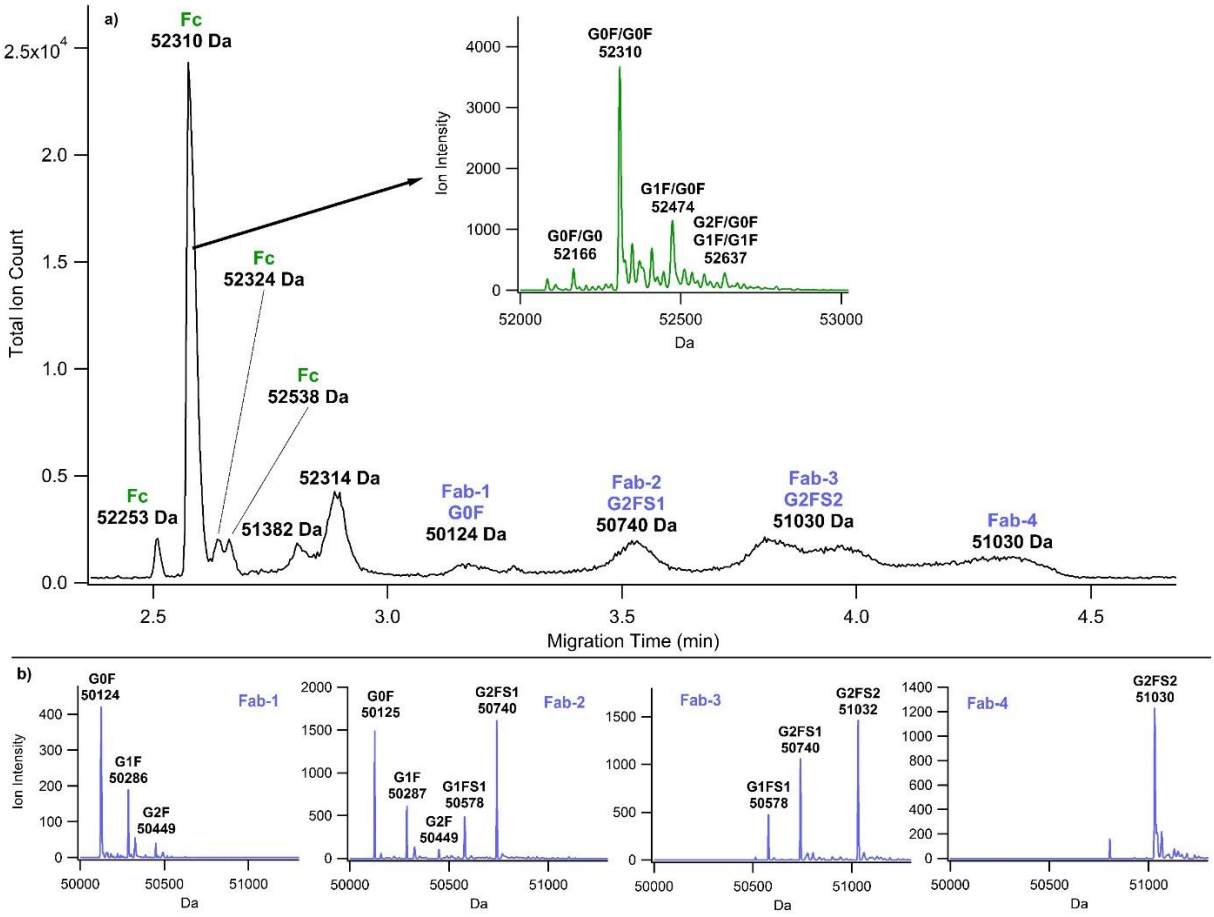

Figure 5.5: Analysis of papain digested mAb-D. a) Electropherogram resulting from the CE separation of the mAb fragments. The Fc fragments migrate faster than the Fab fragments. The inset shows the deconvolution of the most abundant Fc species. b) Deconvolution of the mass spectra associated with the Fab fragment peaks. Glycoforms of the Fab fragments are labeled in the spectra. Instrument: Waters LCT-Premier

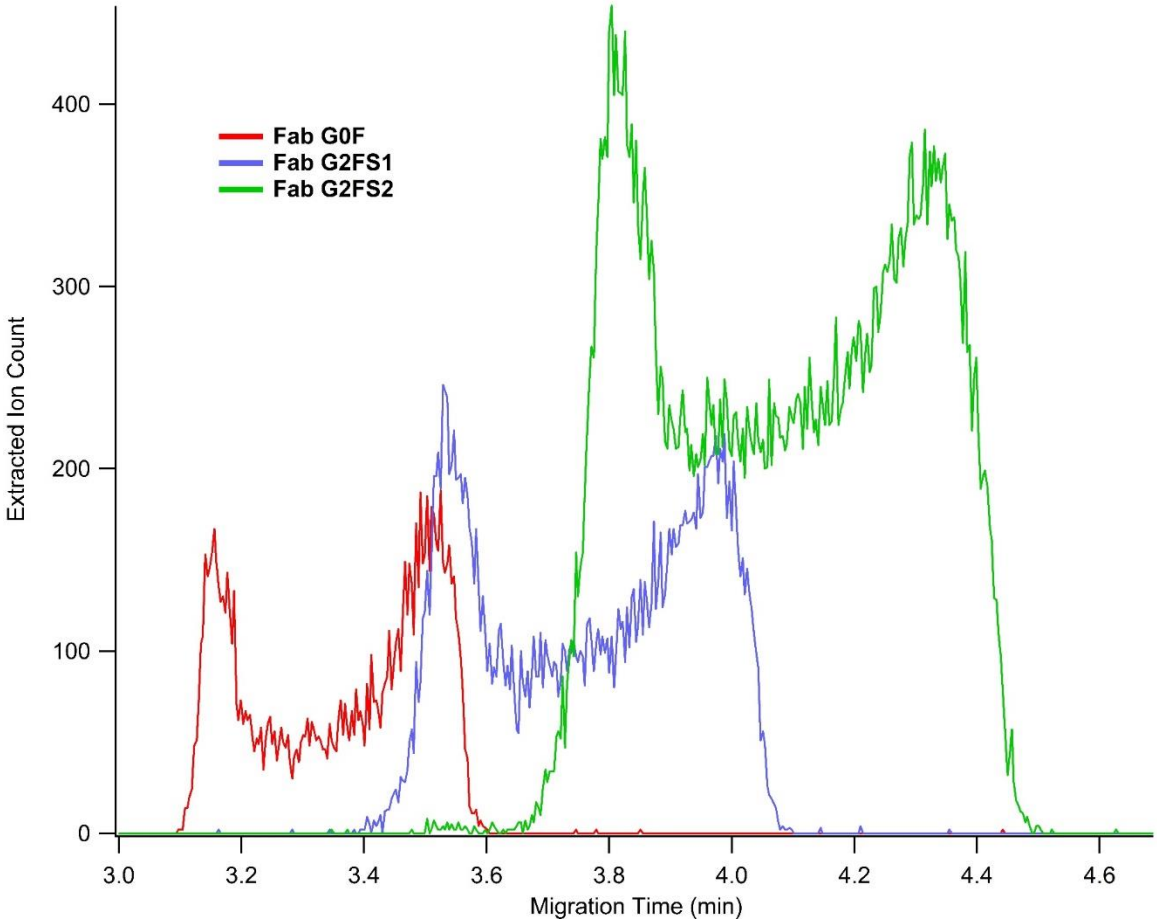

Figure 5.6: Extracted ion electropherograms for the most abundant Fab glycoforms that differ in the degree of glycan sialylation. The peaks appear as doublets rather than single discrete bands.

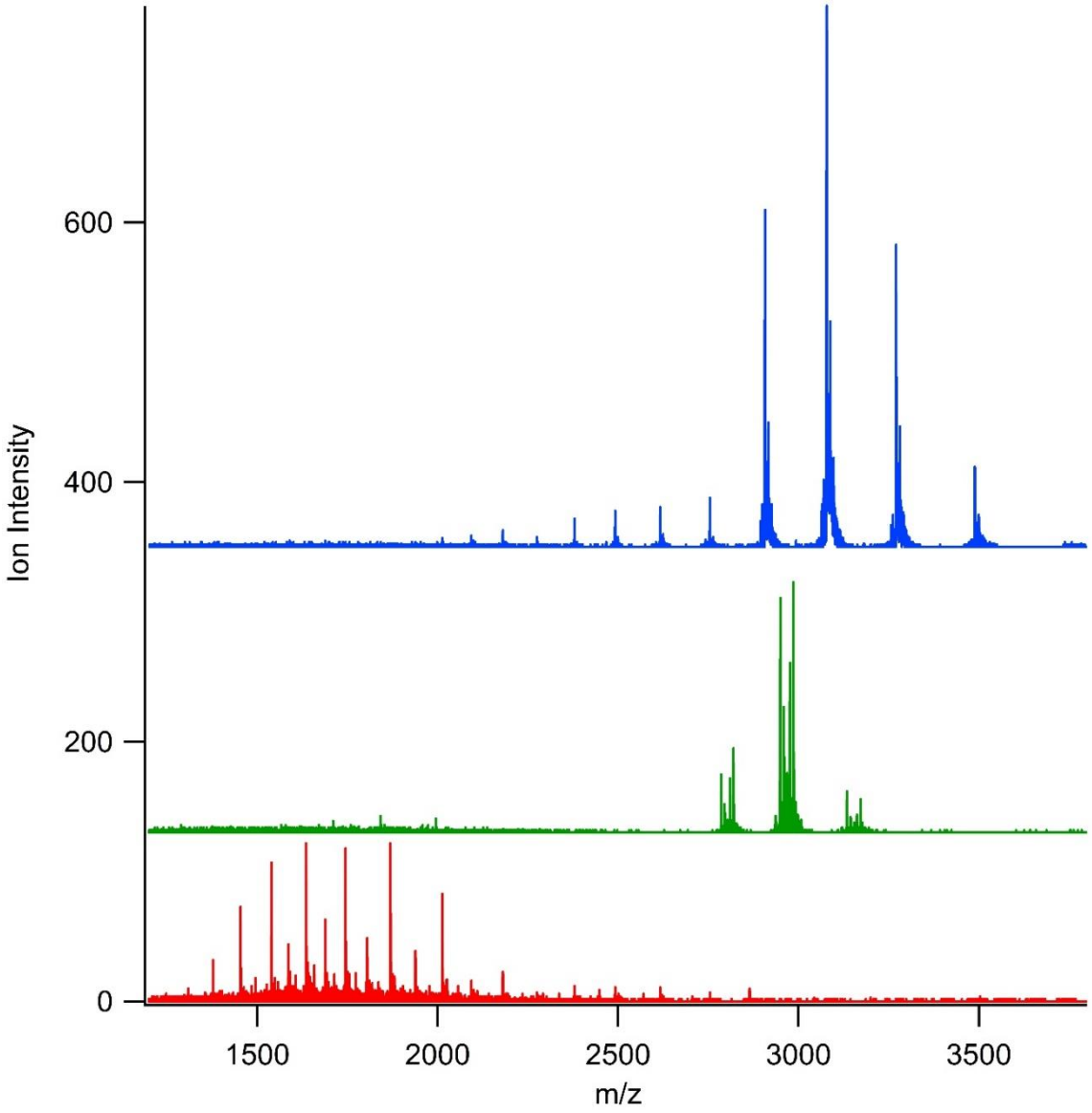

Figure 5.7: Comparison between the raw mass spectra for the most abundant Fc fragment, Fab-2 fragment, and unidentified fragments that migrate between the two. The unidentified fragments appear to be more highly charged.

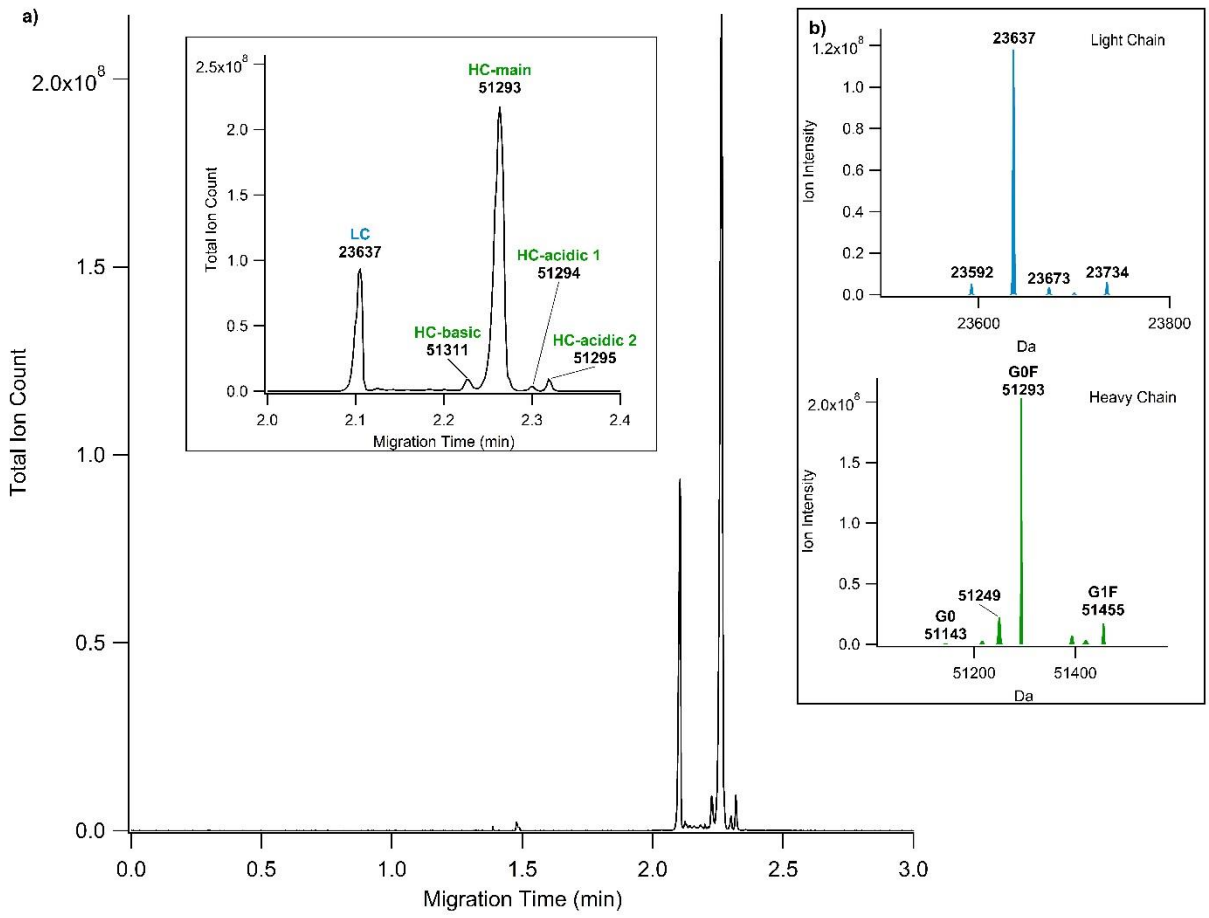

Figure 5.8: Microfluidic CE-MS analysis of reduced and alkylated mAb-B. a) Separation of the LC and HC of mAb-B. Several modifications to the HC are separated including deamidations and pyroglutamic acid formation. The inset shows an expanded view of the separation window with labeled peaks. b) Deconvolution of the mass spectra associated with the main LC and HC peaks in the electropherogram.

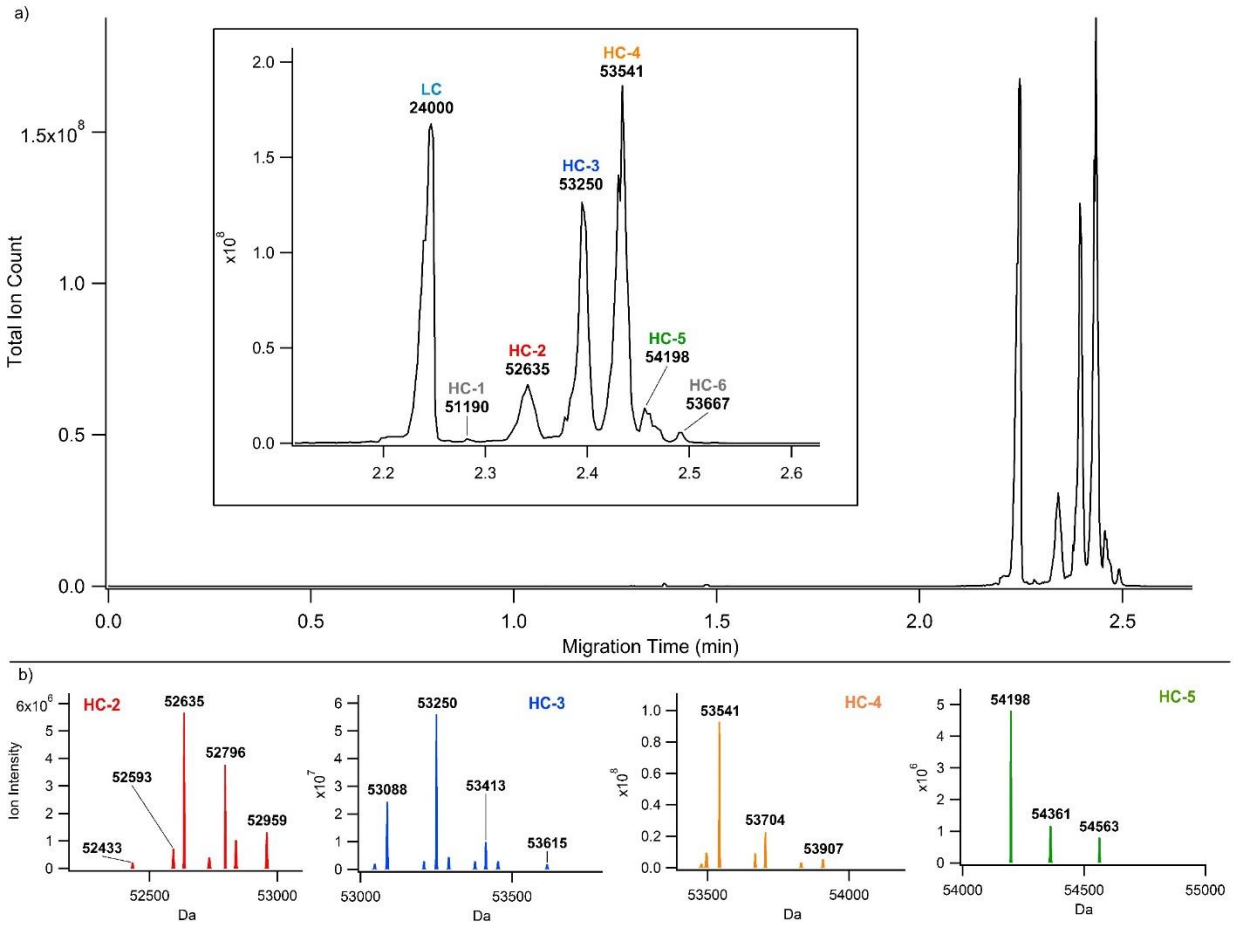

Figure 5.9: Microfluidic CE-MS analysis of mAb-D. a) Electropherogram generated from the microfluidic CZE separation of reduced/alkylated mAb-D. The inset shows an expanded view of the separation window with labeled peaks. Six different HC variants are separated. HC-2 through HC-5 separate based on different levels of glycan sialylation. b) Deconvolution of the mass spectra associated with HC-2 through HC-5. Additional glycoforms are present within the different levels of sialylation due to heterogeneity among the Fc and Fab glycans.

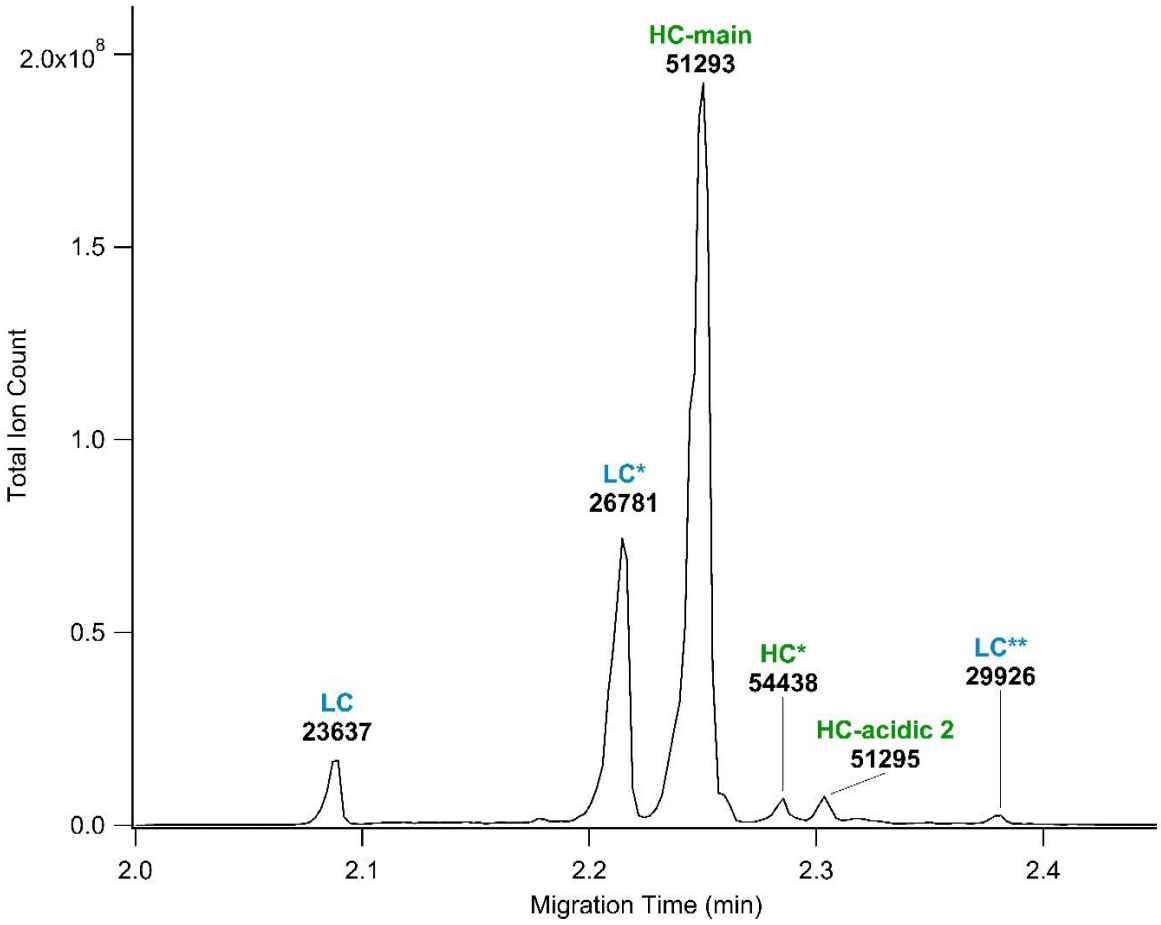

Figure 5.10: Electropherogram resulting from microfluidic CE-MS analysis of reduced and alkylated ADC-B. In comparison to the results from mAb-B, additional LC and HC species are detected corresponding to the addition of a drug load to the polypeptide chain. An (*) indicated the presence of a drug load.

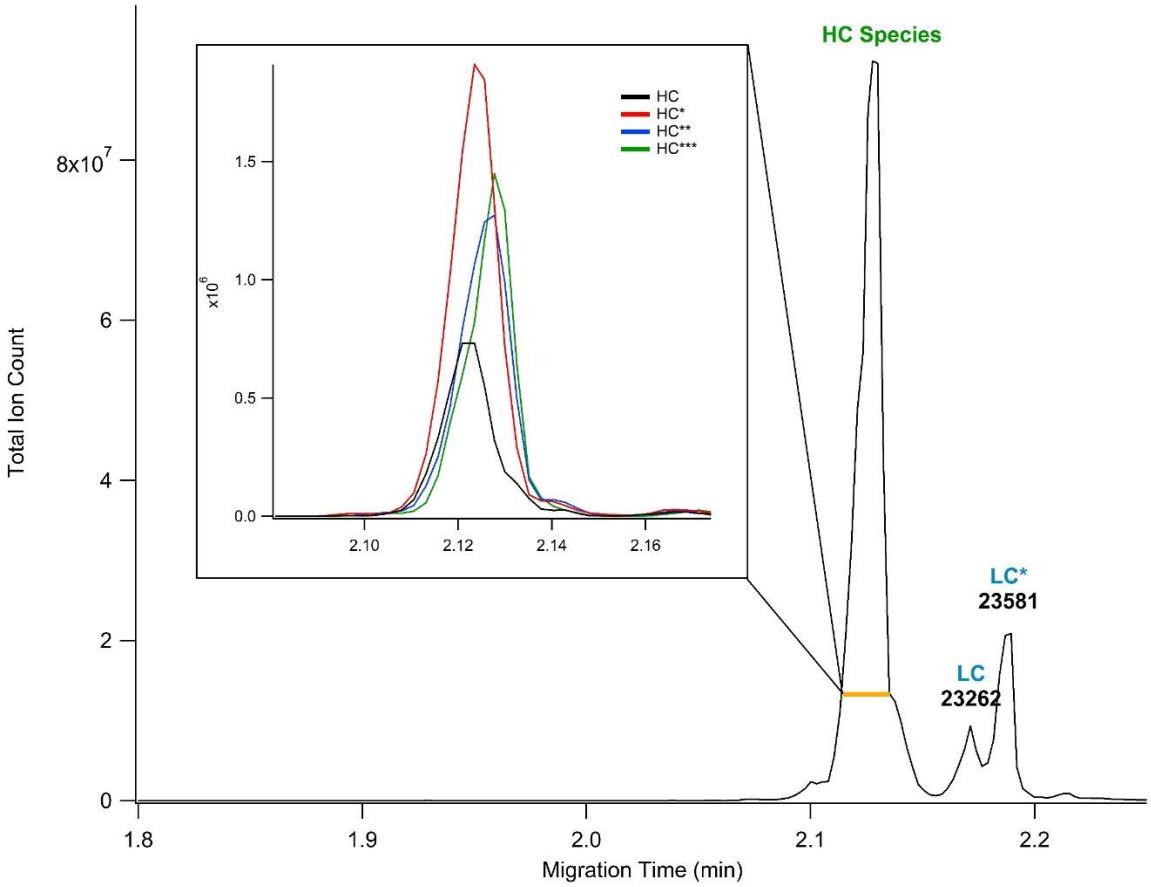

Figure 5.11: Microfluidic CE-MS analysis of reduced and alkylated ADC-C. The inset shows overlaid extracted ion electropherograms for the conjugated HC species.

Table 5.1: Peak migration times and electrophoretic mobilities associated with LC/HC species of mAb-B. Measurements were generated from four replicate runs.

Species	Migration t (min)	RSD	μ_{EP} ($cm^2/V\ s$)
LC	2.10 (±0.01)	0.80%	2.81×10^{-4}
HC-basic	2.22 (±0.02)	0.88%	2.66×10^{-4}
HC-main	2.26 (±0.02)	0.86%	2.61×10^{-4}
HC-acidic 1	2.29 (±0.02)	0.89%	2.57×10^{-4}
HC-acidic 2	2.31 (±0.02)	0.88%	2.55×10^{-4}

Table 5.2: Peak migration times and electrophoretic mobilities associated with LC/HC species of mAb-B. Measurements were generated from three replicate runs.

Species	Migration t (min)	RSD	μ_{EP} ($cm^2/V\ s$)
LC	2.23 (±0.01)	0.37%	$2.64x10^{-4}$
HC-1	2.27 (±0.01)	0.38%	$2.59x10^{-4}$
HC-2	2.33 (±0.01)	0.38%	$2.53x10^{-4}$
HC-3	2.38 (±0.01)	0.40%	$2.47x10^{-4}$
HC-4	2.42 (±0.01)	0.39%	$2.43x10^{-4}$
HC-5	2.45 (±0.01)	0.40%	$2.41x10^{-4}$
HC-6	2.48 (±0.01)	0.44%	$2.38x10^{-4}$

Table 5.3: Assigned glycoforms of the mAb-B HC.

Migration Time (min)	Glycoform Mass (Da)	Fc/Fab
2.27	51190	A2G1F/aglyco
2.33	52433	A1G0F/A2G1F or A2G1F/A1G0F
2.33	52593	A1G0F/A2G2F or A2G2F/A1G0F
2.33	52635	A2G0F/A2G1F or A2G0F/A2G0F
2.33	52796	A2G0F/A2G2F or A2G1F/A2G1F
2.33	52959	A2G1F/A2G2F or A2G2F/A2G1F
2.38	53088	A2G0F/A2G2FS1 or A2G1F/A2G1FS1
2.38	53250	A2G1F/A2G2FS1 or A2G2F/A2G1FS1
2.38	53413	A2G2F/A2G2FS1
2.38	53615	A2G0F/A3G3FS1 or A2G1F/A3G2FS1
2.42	53541	A2G1F/A2G2FS2
2.42	53704	A2G2F/A2G2FS2
2.42	53907	A2G1F/A3G3FS2 or A2G2F/A3G2FS2
2.45	54198	A2G1F/A3G3FS3
2.45	54361	A2G2F/A3G3FS3
2.45	54563	A2G1F/A4G4FS3 or A4G2F/A4G4FS3

Table 5.4: Peak migration times and electrophoretic mobilities associated with LC/HC species of mAb-B. Measurements were generated from four replicate runs.

Species	**Migration t (min)**	**RSD**	**μ_{EP} (cm^2/V s)**
LC	2.10 (±0.02)	1.14%	2.81 $x10^{-4}$
LC*	2.22 (±0.03)	1.20%	2.65 $x10^{-4}$
HC-main	2.26 (±0.03)	1.20%	2.61 $x10^{-4}$
HC*	2.30 (±0.03)	1.23%	2.57 $x10^{-4}$
HC-acidic 2	2.32 (±0.03)	1.26%	2.55 $x10^{-4}$
LC**	2.39 (±0.03)	1.27%	2.47 $x10^{-4}$

REFERENCES

(1) Fekete, S.; Guillarme, D.; Sandra, P.; Sandra, K. *Anal. Chem.* **2016**, *88* (1), 480–507.

(2) Fornelli, L.; Ayoub, D.; Aizikov, K.; Beck, A.; Tsybin, Y. O. *Anal. Chem.* **2014**, No. 86, 3005–3012.

(3) Zhang, Z.; Pan, H.; Chen, X. *Mass Spectrom. Rev.* **2009**, *28*, 147–176.

(4) Ayoub, D.; Jabs, W.; Resemann, A.; Evers, W.; Evans, C.; Main, L.; Baessmann, C.; Wagner-Rousset, E.; Suckau, D.; Beck, A. *MAbs* **2013**, *5* (5), 699–710.

(5) Beck, A. *Glycosylation Engineering of Biopharmaceuticals*; Beck, A., Ed.; Humana Press: New York, 2013; Vol. 988.

(6) An, Y.; Zhang, Y.; Mueller, H. M.; Shameem, M.; Chen, X. *MAbs* **2014**, *6* (4), 879–893.

(7) Chevreux, G.; Tilly, N.; Bihoreau, N. *Anal. Biochem.* **2011**, *415* (2), 212–214.

(8) Leblanc, Y.; Romanin, M.; Bihoreau, N.; Chevreux, G. *J. Chromatogr. B Anal. Technol. Biomed. Life Sci.* **2014**, *961*, 1–4.

(9) Moorhouse, K. G.; Nashabeh, W.; Deveney, J.; Bjork, N. S.; Mulkerrin, M. G.; Ryskamp, T. *J Pharm Biomed Anal* **1997**, *16* (4), 593–603.

(10) Lau, H.; Pace, D.; Yan, B.; McGrath, T.; Smallwood, S.; Patel, K.; Park, J.; Park, S. S.; Latypov, R. F. *J. Chromatogr. B Anal. Technol. Biomed. Life Sci.* **2010**, *878* (11-12), 868–876.

(11) Bondarenko, P. V; Second, T. P.; Zabrouskov, V.; Makarov, A. a; Zhang, Z. *J. Am. Soc. Mass Spectrom.* **2009**, *20* (8), 1415–1424.

(12) Kleemann, G. R.; Beierle, J.; Nichols, A. C.; Dillon, T. M.; Pipes, G. D.; Bondarenko, P. V. *Anal. Chem.* **2008**, *80* (6), 2001–2009.

(13) Yan, B.; Valliere-Douglass, J.; Brady, L.; Steen, S.; Han, M.; Pace, D.; Elliott, S.; Yates, Z.; Han, Y.; Balland, A.; Wang, W.; Pettit, D. *J. Chromatogr. A* **2007**, *1164* (1-2), 153–161.

(14) Yang, J.; Wang, S.; Liu, J.; Raghani, A. *J. Chromatogr. A* **2007**, *1156* (1-2), 174–182.

(15) Wagner-Rousset, E.; Janin-Bussat, M. C.; Colas, O.; Excoffier, M.; Ayoub, D.; Haeuw, J. F.; Rilatt, I.; Perez, M.; Corvaïa, N.; Beck, A. *MAbs* **2014**, *6* (1), 173–184.

(16) Lim, A.; Reed-Bogan, A.; Harmon, B. J. *Anal. Biochem.* **2008**, *375* (2), 163–172.

(17) Lynaugh, H.; Li, H.; Gong, B. *MAbs* **2013**, *5* (5), 641–645.

(18) Firth, D.; Bell, L.; Squires, M.; Estdale, S.; McKee, C. *Anal. Biochem.* **2015**, *485*, 34–42.

(19) Vlasak, J.; Ionescu, R. *MAbs* **2011**, *3* (3), 253–263.

(20) Fekete, S.; Guillarme, D. *LC-GC Eur.* **2012**, *25* (10), 540–550.

(21) Rustandi, R. R.; Wang, Y. *Electrophoresis* **2011**, *32* (21), 3078–3084.

(22) Rustandi, R. R.; Washabaugh, M. W.; Wang, Y. *Electrophoresis* **2008**, *29* (17), 3612–3620.

(23) Lee, H. G. *J. Immunol. Methods* **2000**, *234* (1-2), 71–81.

(24) Taga, A.; Kita, S.; Nishiura, K.; Hayashi, T.; Kinoshita, M.; Sato, A.; Suzuki, K.; Kodama, S.; Kakehi, K. *J. Sep. Sci.* **2008**, *31* (5), 853–858.

(25) Guo, A.; Han, M.; Martinez, T.; Ketchem, R. R.; Novick, S.; Jochheim, C.; Balland, A. *Electrophoresis* **2008**, *29* (12), 2550–2556.

(26) Biacchi, M.; Gahoual, R.; Said, N.; Beck, A.; Leize-Wagner, E.; François, Y.-N. *Anal. Chem.* **2015**, *87* (12), 6240–6250.

(27) François, Y.-N.; Biacchi, M.; Said, N.; Renard, C.; Beck, A.; Gahoual, R.; Leize-Wagner, E. *Anal. Chim. Acta* **2016**, *908*, 168–176.

(28) Haselberg, R.; de Jong, G. J.; Somsen, G. W. *J. Chromatogr. A* **2007**, *1159* (1-2), 81–109.

(29) Haselberg, R.; de Jong, G. J.; Somsen, G. W. *Electrophoresis* **2013**, *34* (1), 99–112.

(30) Zhao, Y.; Sun, L.; Knierman, M. D.; Dovichi, N. J. *Talanta* **2016**, *148*, 529–533.

(31) Redman, E. A.; Batz, N. G.; Mellors, J. S.; Ramsey, J. M. *Anal. Chem.* **2015**, *87* (4), 2264–2272.

(32) Berger, S. J.; Chen, W. *Waters Corporation Application Note*. 2008, p Number APNT10094155.

(33) Ferrige, A. G.; Seddon, M. J.; Green, B. N.; Jarvix, S. A.; Skilling, J. *Rapid Commun. Mass Spectrom.* **1992**, *6*, 707–711.

(34) Redman, E. A.; Mellors, J. S.; Starkey, J. A.; Ramsey, J. M. *Anal. Chem.* **2016**, *88* (4), 2220–2226.

(35) Mellors, J. S.; Black, W. A.; Chambers, A. G.; Starkey, J. A.; Lacher, N. A.; Ramsey, J.

M. *Anal. Chem.* **2013**, *85*, 4100–4106.

(36) Doppalapudi, V. R.; Huang, J.; Liu, D.; Jin, P.; Liu, B.; Li, L.; Desharnais, J.; Hagen, C.; Levin, N. J.; Shields, M. J.; Parish, M.; Murphy, R. E.; Del Rosario, J.; Oates, B. D.; Lai, J.-Y.; Matin, M. J.; Ainekulu, Z.; Bhat, A.; Bradshaw, C. W.; Woodnutt, G.; Lerner, R. a; Lappe, R. W. *Proc. Natl. Acad. Sci.* **2010**, *107* (52), 22611–22616.

(37) Ducry, L. *Antibody-Drug Conjugates*; Springer: New York, NY, 2013.

CHAPTER 6: EVALUATION OF TRANSIENT ISOTACHOPHORESIS INTEGRATED WITH MICROFLUIDIC CAPILLARY ELECTROPHORESIS-MASS SPECTROMETRY FOR BOTTOM-UP PROTEIN MAPPING

6.1 Introduction

Bottom-up proteomics has long been the go-to method for quantifying proteins in biological samples.[1–3] The basic premise is an enzyme is used to cleave proteins into smaller peptide fragments that are then separated and identified via mass spectrometry (MS). As compared to top-down proteomics,[4–8] this approach has achieved prevalence due to the relative ease with which peptides are analyzed using both separation techniques and mass spectrometry. A variant of this technique in which only one protein is analyzed is called bottom-up mapping. Mapping experiments generate site-specific information about modifications to the protein structure. In the realm of biopharmaceuticals, this can be extremely useful for identifying whether modifications have occurred at sites known to affect drug safety and efficacy. While this type of experiment is typically performed using liquid chromatography-mass spectrometry (LC-MS), the analysis could benefit from using microfluidic capillary electrophoresis-mass spectrometry (CE-MS). Due to the lack of stationary phase all injected peptides (both hydrophobic and hydrophilic) migrate through the capillary.[9] This combined with the high efficiency separations achieved with microfluidic CE generates the potential for achieving better characterization of the protein.

A typical bottom-up mapping workflow uses the following steps: The protein is first denatured using chemicals and/or heat to disrupt the folding structure. The disulfide bonds are

reduced using reagents, such as dithiothreitol (DTT), and the cysteine residues are alkylated to prevent disulfide bond scrambling (randomized formation of disulfide bonds). The chosen enzyme is added and the protein/enzyme solution is incubated for several hours.[10] A variety of enzymes can be used that differ in the location at which they sever the protein's backbone.[11–14] For instance, trypsin, which is one of the most frequently used enzymes, cleaves proteins at the C-terminal side of lysine and arginine residues. The resulting peptide fragments are then separated and identified based on tandem MS/MS analysis. As illustrated in Figure 6.1, this involves analyzing the parent peptide ion and then fragmenting that ion further in the mass spectrometer. The parent peptides tend to fragment along the peptide backbone and the fragments are classified by which side of the cleavage site bears the positive charge. If the charge remains on the C-terminal side the ions are classified as a_n, b_n, or c_n ions and if the charge remains on the N-terminal side of the cleavage site the ions are classified as x_n, y_n, or z_n ions.[15] This fragmentation is necessary to elucidate the differences between parent peptides with the same or very similar elemental compositions. Using specialized computer software, the masses of the parent and fragment ions are compared to theoretical proteolytic masses and used to confirm the identity of the parent peptide and any residues modified with post translational modifications (PTMs).[1,2,16] The identified peptides and detected modifications are then used to assess the original protein.

In bottom-up mapping experiments, detecting and identifying peptide fragments that span the entire sequence of the protein is necessary. The degree to which this is achieved is called sequence coverage and a sequence coverage of >90% is desirable.[17] The achieved sequence coverage is partly dependent on the accurate identification of the peptides. A sufficient amount of MS signal intensity must be obtained for the parent peptide ion to confidently detect the

fragments of that ion. As illustrated in Figure 6.1, the signal intensity for the parent ion is divided between the fragments, so the signal intensity will be lower than that of the parent ion.

RPLC-MS is well established as the workhorse technique for performing bottom-up analysis. RPLC benefits from the ability to load a large amount of sample onto the head of the column.[2,3] This focuses the peptides into a narrower sample plug before separation on the column. Thus, a tremendous amount of concentration enhancement can be obtained with little loss in separation efficiency. The injection volumes for capillary electrophoresis (CE) analysis, however, are limited by the small dimensions of the capillary or microfluidic channels. As mentioned in Chapter 1, the total column volume of a capillary used for CE can easily be less than 10 µL. This is close to a typical injection volume used for RPLC. Therefore, to achieve comparable results for bottom-up mapping with CE-MS, concentration enhancement techniques must be used to bolster the loading capacity of the system.

There are numerous demonstrations in the literature of concentration enhancement techniques for CE.[18–22] These generally involve exploiting the effects of conductivity mismatches between the sample and separation background electrolyte (BGE). One such technique is transient isotachophoresis (tITP).[19,23–28] This technique involves hydrodynamically injecting a bolus of sample containing a large amount of a high mobility ion called the leading electrolyte. The leading electrolyte should have a higher mobility than the analyte ions and be at a concentration that makes the conductivity of the sample higher than that of the separation BGE (Figure 6.2).[23] The difference in field strengths between the sample region and the rest of the capillary cause analyte ions to focus into a narrow band at the trailing boundary of the injection plug. As the leading electrolyte migrates out of the sample region, the conductivity reduces to match that of the BGE and zone electrophoresis separation of the analyte ions occurs.[23] Using

tITP a very large volume of sample can be injected into the capillary with the focusing effects preserving the separation efficiency. This strategy has been used with CE-MS systems and resulted in very high sequence coverages for mAb-based therapeutics.[9,29–31]

This approach, however, is not possible with gated electrokinetic (EK) injections that until recently had been the main injection strategy used with our devices. As will be discussed further, the electrophoretic mobility based bias prevents adequate injection of analyte ions from high conductivity samples. As mentioned in Chapter 1, an alternative hydrodynamic (HD) based injection scheme was recently developed for use with microfluidic CE-ESI devices. This approach facilitates the injection of sample solutions of higher conductivity than the BGE; and tITP can be performed to enhance the sample loading capabilities. This chapter evaluates the concentration enhancement effects of tITP and the advantages of using it to assist in protein mapping experiments via microfluidic CE-MS.

6.2 Experimental

6.2.1 Materials and Reagents.

Deionized water was generated with a Nanopure Diamond water purifier (Barnstead International, Dubuque, IA). Optima LC/MS grade 2-propanol, acetonitrile, formic acid, and acetic acid were obtained from Fisher Scientific (Fairlawn, NJ). The silane coating reagent 3-(aminopropyl)di-isopropyl-ethoxysilane (APDIPES) was purchased from Gelest (Morrisville, PA) and the methyl-terminated polyethylene glycol n-hydroxy succinimide ester (NHS-PEG_{450}) was purchased from Nanocs Inc. (Boston, MA). Trichloro-(1H,1H,2H,2H-perfluorooctyl)-silane and dithiothreitol (DTT) was purchased from Sigma-Aldrich (St. Louis, MO). The MassPrep

phosphorylase b protein digest was purchased from Waters Corporation (Milford, MA). The monoclonal antibody (mAb) was provided by Biogen (Cambridge, MA).

6.2.2 Lys-C Digestion of mAbs.

150 μg of mAb was denatured and reduced in 100 μL of a 250 mM TRIS buffer at pH 8 with 8M guanidine HCl and 100 mM DTT. The solution was incubated at room temperature with gentle shaking for approximately 30 minutes. The reduced and denature mAb was diluted to 335 μL with 50 mM sodium phosphate buffer pH 7.2. To achieve an enzyme to substrate ratio of 1:10, 15 μg of rLys-C was added to the mAb solution. The digestion was allowed to proceed overnight at room temperature. Sample clean-up was performed using Waters Oasis HLB solid phase extraction (SPE) cartridges. After the cartridges were conditioned, the digestion solution was acidified with formic acid and passed through the cartridge. The extraction bed containing adsorbed peptides was washed twice with 250 μL of a 0.1% formic acid solution and eluted with 750 μL of 75% acetonitrile, 24.75% water, 0.25% formic acid. The eluted peptides were dessicated using a vacuum centrifuge. For analysis, the digests were reconstituted in 100 μL of 100 mM ammonium acetate in 50/50 acetonitrile/water with 1% formic acid.

6.2.3 Device Preparation and Operation.

The APS-PEG_{450} surface coating was used for this analysis and applied according to the procedures in Appendix 2. Bulk fluid flow for sustaining ESI was supplied via electroosmotic pumping. An aqueous solution of 50/50 acetonitrile/water with 1% formic acid was used for all analyses. CE-ESI devices were operated by applying and controlling voltages as described in Appendix 3. For analysis using HD injections, +20kV and +1.5kV were applied to reservoirs 1

and 4, respectively, which resulted in a field strength of approximately 685 V/cm. The samples were injected at 2 psi. Gated EK injections were performed using the voltages in Table 6.1.

6.2.4 Data Analysis.

MS analysis was performed using a Waters Synapt G2 quadrupole time-of-flight mass spectrometer (Waters Corporation, Milford, MA) operated in sensitivity mode with the source at 105 °C. Data were acquired with a 0.1 s scan time. MS/MS analysis of the peptides was achieved using a process specific to Waters instrumentation called MS^E. A collision energy of 32 was used for the high energy fragmentation. Processing of the MassPrep phosphorylase b digestions was performed using Biopharmalynx 1.3.2 (Waters Corporation, Milford, MA) and processing of the Lys-C enzymatic digestions was performed in Proteinlynx Global Server (PLGS) 3.0 (Waters Corporation, Milford, MA). A minimum of 3 fragments was required for positive peptide fragment identification with the false discovery rate set to 4.

The Waters MS^E approach differs from other types of MS/MS analysis in that all of the ions entering the collision cell are fragmented rather than isolating certain parent ions for fragmentation. This involves alternating the data acquisition between low and high fragmentation energies and then matching the parent ions to their fragments based on chromatographic peak shape. The acquisition rate is, therefore, a critical component of data acquisition and interpretation. There must be enough low and high energy data points to achieve sufficient signal for the parent and fragment ions, and to fit the ions to a peak in the separation. The widths of RPLC peaks (~10-15 seconds) are well aligned with the timescale of an MSE experiment, but the narrow peaks of a microfluidic CE separation (<5 seconds) challenge the acquisition rate of the MS instrument.

6.3 Results and Discussion

6.3.1 Comparison between gated EK and HD injection.

As mentioned in Chapter 1, a limitation of gated electrokinetic injections is electrophoretic mobility based bias. For samples with analytes that span a wide range of electrophoretic mobilities, this can be a significant issue. This bias is more evident when gated EK injections are compared to hydrodynamic flow based injections, which are not subject to electrophoretic mobility based bias. Figure 6.3 correlates the peak areas for amino acids injected electrokinetically ($PeakArea_{EK}$) and hydrodynamically ($PeakArea_{HD}$) to migration time. By plotting the areas as a ratio ($PeakArea_{EK}/PeakArea_{HD}$) versus migration time the bias of the EK injection can be assessed. A slope close to zero would indicate little bias in the injection. The slope of the points is negative, however. While the ratio for the most mobile amino acid is close to 1 (indicating that the amounts injected are relatively similar) as the mobility of the amino acids decreases, the ratios steadily decrease to approximately 0.2. Thus, significantly less of the lower mobility amino acids are injected using a gated EK injection.

A more extreme case of bias is seen with the gated EK injections when the conductivity of the sample matrix is significantly higher than that of the BGE. As mentioned in the introduction, conductivity mismatches between the sample matrix and separation BGE have often been exploited to perform concentration enhancement. Typically, this involves using a BGE that is of higher conductivity than the sample matrix. When voltage is applied sample ions focus at the boundary of the two solutions until the conductivity of the focused band matches that of the BGE.[18,20] However, due to the need to maintain MS ionization efficiency and compatibility, CE-MS BGEs are often of lower conductivity than those used with fluorescence or

optical detection methods thus limiting the practical range of BGE conductivities. This often creates a situation opposite to that of many concentration enhancement techniques. When derived from physiological solutions, the sample conductivity can be much higher than that of BGE due to salt ions, such as sodium and phosphate. These are generally at a higher concentration than the analyte ions and also have a higher electrophoretic mobility. Figure 6.4a depicts what happens when a gated EK injection is attempted with a high conductivity sample. To mimic the presence of salts from a physiological sample 100 mM NaCl was added to the amino acid sample. Very little of the amino acids are injected, but a large band of sodium is detected (as sodium formate clusters) indicating that these sample matrix ions are preferentially injected. Without further processing to desalt the sample, this is an unsuitable approach. However, since there is no bias when the sample is injected hydrodynamically, all of the amino acids are injected and easily detected (Figure 6.4b). The sodium is still present but it is well resolved from the analyte ions so as not to interfere. Thus, a HD injection strategy can facilitate the analysis of biological samples that have inherently high levels of salts without the need for additional desalting steps. Additionally, it shows the feasibility of some concentration enhancement techniques not possible with the gated EK injection method.

6.3.2 Utilizing tITP as a concentration enhancement technique for microfluidic CE-MS

Another limitation regularly encountered with gated EK injections is limited loading capacity due to the small channel sizes. For certain applications, such as bottom-up proteomics, this impedes the analysis quality since sufficient signal intensity is required for successful peptide identification. Figure 6.5 shows the separation of a MassPrep tryptic digest of the protein phosphorylase b using a gated EK injection. The black trace shows the low energy analysis

separation with no fragmentation and the red trace was collected at high collision energy to fragment the peptides for identification. While the efficiency of the separation is very high (black trace), the low signal intensity for the peptide fragments analyzed under MS^E conditions makes identification problematic. In fact, a sequence coverage of only 35% was obtained through this analysis. A larger sample plug can be injected but at the cost of reduced performance levels as band broadening decreases the separation resolution between the peptide fragments. Figure 6.6 shows the relationship between the average injection volume, sequence coverage, and peak capacity for analyzing the phosphorylase b digestion using gated EK injections. Peak capacity is a metric used for describing the ability of a technique to separate a complex mixture. It is based on the average width of the peaks at base or half height and the separation window, and roughly defines how many peaks can be separated within the separation window. In this work peak capacity is calculated using the following equation

$$n_c = 1 + \frac{\overline{FWHH}}{t_{final} - t_{initial}} \tag{6.15}$$

where $\overline{FWHH}$ is the average peak width at half height and t_{final} and $t_{initial}$ are the first and last eluting analytes that define the separation window. The peak capacity decreases with increasing injection volume and the maximum sequence coverage obtained is still only 71%. With this analysis strategy, injecting even more sample would simply result in broad, unresolved peaks that would be difficult to identify using proteomics software.

As mentioned above, a major advantage of the HD injection method is that concentration enhancement and analyte focusing techniques can be more easily incorporated onto the microchip format. To take advantage of the tITP effects, the conductivity of the sample must be

higher relative to that of the BGE. This can be done by adding a salt, such as ammonium acetate, or relying on the innate salt content of the sample, such as with physiological solutions. To evaluate the impact of utilizing tITP, a standard peptide mix was analyzed with and without a salt added to the sample solution. Figure 6.7 shows the results obtained with increasing injection volumes for peptides diluted in BGE and peptides diluted in BGE with 100 mM ammonium acetate added. As seen in Figure 6.7a, increasing the injection volume when the sample is diluted in BGE quickly results in significant band broadening due to the large size of the injection plug. When tITP is employed, however, by adding100 mM ammonium acetate to the sample matrix, the results are starkly different. As evident in Figure 6.7b, the efficiency of the separation is maintained despite the increase in injection volume and a much higher signal intensity is also achieved. This is due to the focusing effects of tITP. The high conductivity of the sample plug and the resulting low field strength in the plug region cause the analyte ions to focus into a narrow band on the trailing boundary between the BGE and sample plug (Figure 6.2). These effects can be easily visualized by plotting the width at half height in relation to the injection volume. Figure 6.8 shows the relationship between the width at half height and injection volume for three of the seven peptides in the mixture. Without the focusing effects of tITP, the peaks broaden rapidly as the injection volume increases (circles). When tITP is taken advantage of, the peak widths remain relatively constant despite increasing the injection volume (diamonds).

A noticeable effect of tITP is an increase in migration times with increasing injection volume due to the duration of the focusing step. During the focusing step, the high mobility salt ions migrate out of the high conductivity region. This process continues until the local conductivity matches that of the bulk BGE and the focused analyte ions separate via zone electrophoresis. As the injection volume increases, the time to match conductivities also

increases. Experimentally, we have seen that both the injection volume and the conductivity difference between the sample and BGE affect the delay in migration time. Further experiments are needed to better characterize this phenomenon.

To determine the effect tITP has on the performance of bottom-up mapping, the MassPrep phosphorylase b digest was analyzed again. The digest was diluted with 100 mM ammonium acetate in 50/50 acetonitrile/water with 1% formic acid. Figure 6.9 shows the relationship between injection volume, sequence coverage, and peak capacity when tITP is used. Because a greater amount of sample is injected without a significant loss in separation efficiency, a higher overall signal intensity is realized and improved peptide identification. The microfluidic CE-MS separation of approximately 6.5 nL of phosphorylase b digest is provided in Figure 6.10. The top trace shows the low energy peptide analysis and the bottom trace is the high energy fragmentation electropherogram. The signal obtained for the fragmented peptides is significantly better than what was achieved without tITP (Figure 6.5). This results in more confident identification of the peptides and a higher degree of sequence coverage.

6.3.3 Evaluation of microfluidic CE-MS for mapping an IgG-2 mAb

To assess the performance of microfluidic CE-MS bottom-up mapping for biopharmaceuticals an IgG-2 mAb was digested with Lys-C using a digestion protocol provided by collaborators at Biogen. The digestion was reconstituted with a 100 mM ammonium acetate in 50/50 acetonitrile/water with 1% formic acid BGE. A 2.14 nL injection of the digest resulted in the electropherogram in Figure 6.11. The analysis was complete in less than 10 minutes with a peak capacity of 172. The data was processed using PLGS and sequence coverages of 95.8% and 95.1% were obtained for the LC and HC, respectively.

Table 6.2 lists the detected peptides from the microfluidic CE-MS analysis. There were several theoretical peptides that were not identified by PLGS, but masses that agree with most of the missing peptide fragments can be found in the raw data. These species are denoted by an asterisk in the CE migration time column. Thus, these peptide fragments were present in the microfluidic CE-MS separation, but were not properly identified by the software. Also of note are the number of peptides detected in the microfluidic CE-MS data that bear either oxidized or deamidated residues. Because the digestion protocol provided by Biogen relied heavily on MS incompatible components (TRIS buffers, guanidine, etc.) the digest solutions were processed via SPE to remove these components and then reconstituted in BGE with ammonium acetate. It is likely that this process artificially induced these degradation products in the peptides. Fortunately, this problem can be assuaged by using digestion buffers and components that are MS compatible, such as ammonium bicarbonate buffer and Waters Rapigest surfactant.

Overall, the analysis of the Lys-C digested mAb via microfluidic CE-MS resulted in a sequence coverage of greater that 95%. The analysis was complete in less than 10 minutes, which is approximately 6x faster than the RPLC-MS method used by collaborators. While this technology may not replace RPLC-MS for performing in-depth characterization of biomolecules, the speed at which this type of data can be collected potentially makes this method amenable to high throughput characterization.

6.4 Conclusions

The work presented here demonstrates the advantages of incorporating tITP into microfluidic CE-MS methods. Using the well-established gated EK injection technique for analysis has significant limitations in terms of sample loading and the composition of the sample

solution. If the sample conductivity is significantly higher than that of the BGE, little of the analyte ions are injected as the bias favors small, high mobility salt cations. Using the HD injection technique to perform tITP circumvents this limitation by performing an unbiased injection and utilizing the high conductivity of the sample solution to achieve analyte focusing and concentration enhancement. Thus, a very large sample volume can be injected with little effect on the efficiency of the CE separation. This approach increased the success of bottom-up mapping experiments performed via microfluidic CE-MS. For a commercially available phosphorylase b tryptic digest standard, the sequence coverage increased from a maximum of ~75% with gated EK injection to 85% with tITP via HD injection. Further success was seen with analyzing a Lys-C digestion of an IgG-2. A sequence coverage of 95% was achieved in less than 10 minutes. For many of the microfluidic CE-MS peptides that were not identified by the software, corresponding masses were detected in the raw data indicating that they were in fact present in the data. This suggests that bottom-up mapping with the microfluidic CE-MS system could be comparable to RPLC-MS analysis, but significantly faster. Further experimentation is needed to fully assess the advantages and limitations of the system in comparison to RPLC-MS.

6.5 Figures and Tables

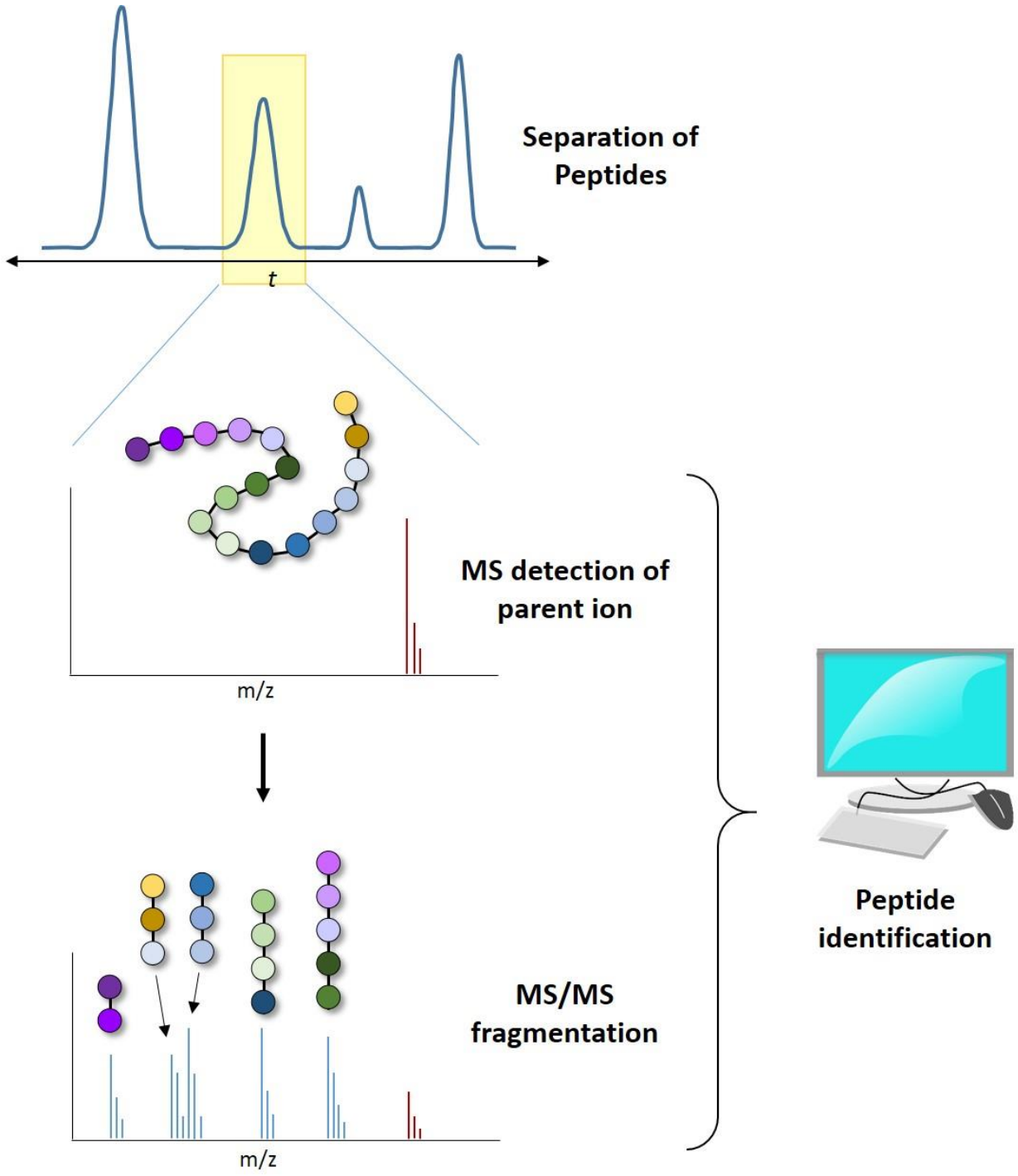

Figure 6.1: Bottom-up mapping workflow involving peptide separation with MS/MS analysis and data processing.

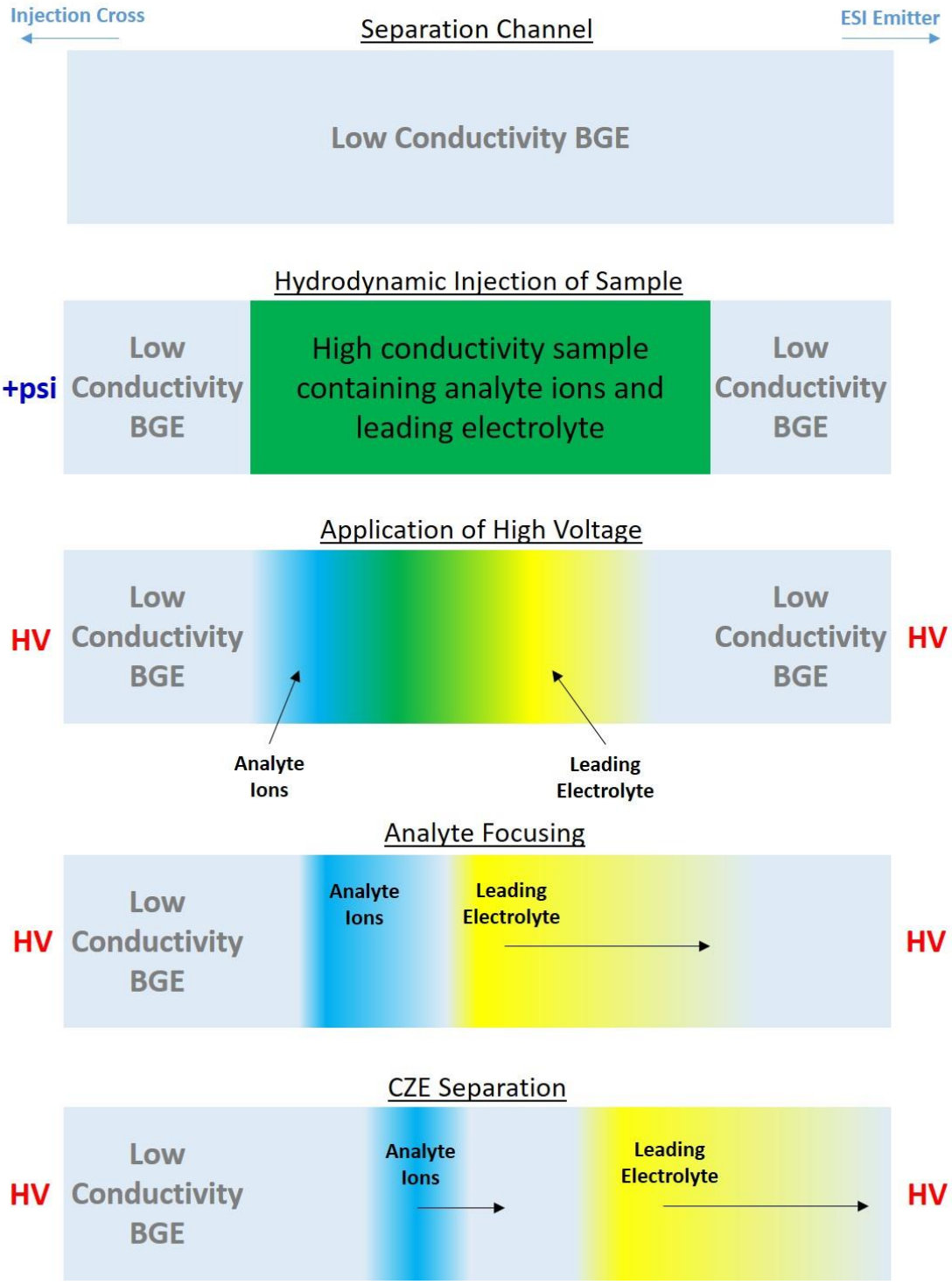

Figure 6.2: Cartoon illustration of tITP. Analytes focus at the trailing end of the sample plug until the conductivity of the plug matches that of the BGE and the zone electrophoresis separation occurs.

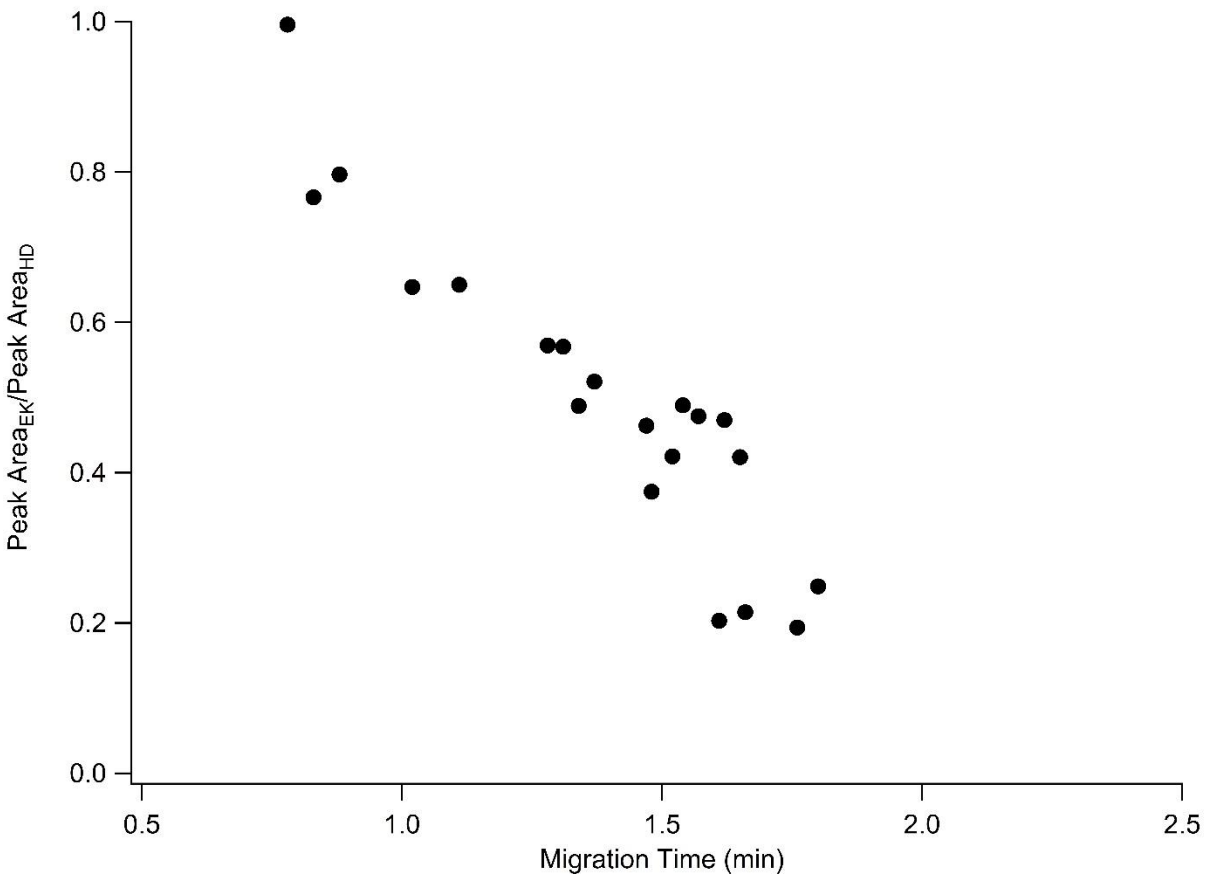

Figure 6.3: Plot of the ratio of amino acid peak areas from separations using gated EK injection and HD injection versus migration time. The negative trend indicates that the peak areas are decreasing with decreasing electrophoretic mobility for the analysis using gated EK injections. This reflects the bias of the gated EK injection.

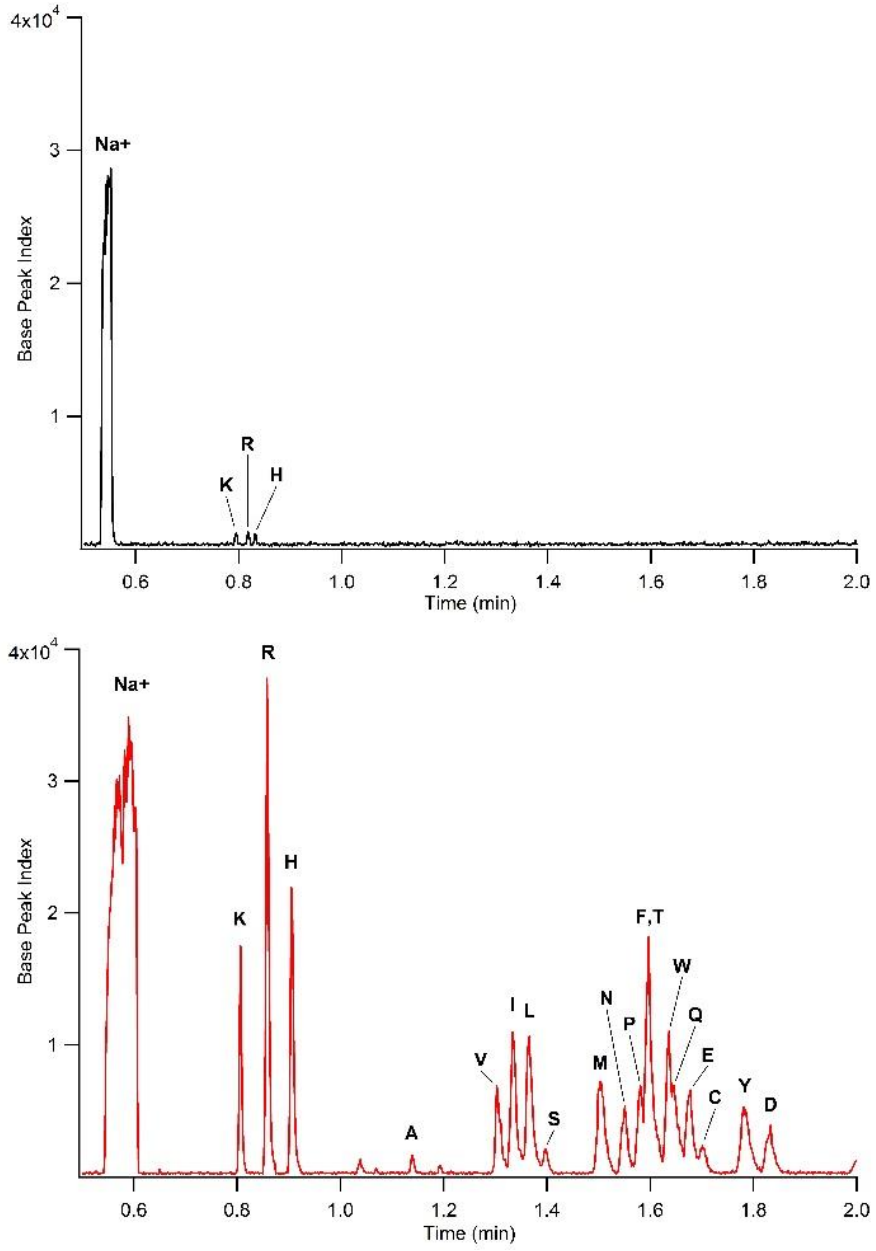

Figure 6.4: Microfluidic CE-MS analysis of high conductivity samples using a) gated EK injection and b) HD injection. 100 mM sodium chloride was added to the amino acid mixture. Using the gated EK injection very little of the amino acids are injected due to electroosmotic mobility bias. Using the unbiased HD injection, all of the amino acids and the sodium ions are detected. Note that a device with a 10 cm separation channel was used for this analysis.

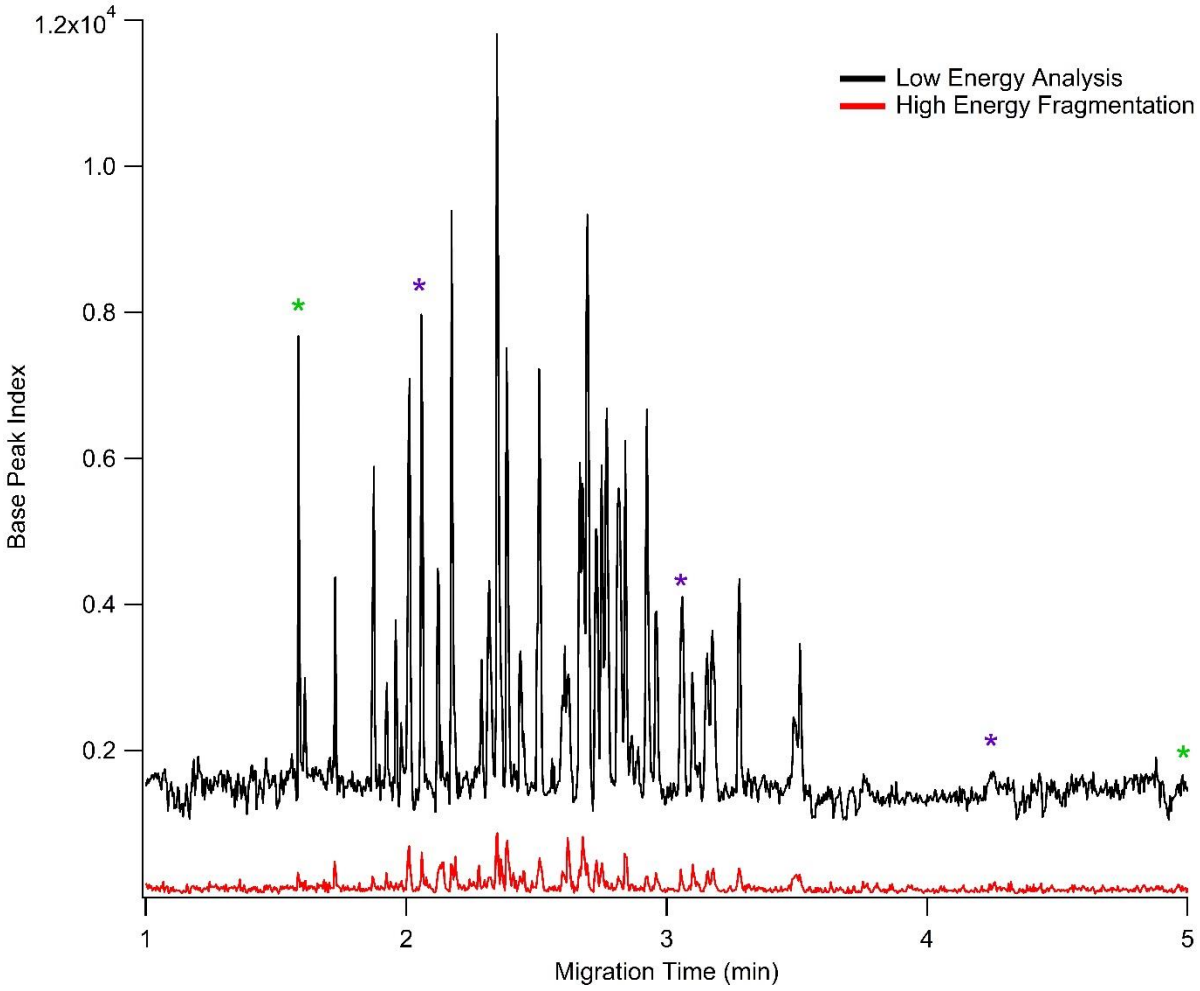

Figure 6.5: Microfluidic CE-MS analysis of a MassPrep phosphorylase b tryptic digest using gated EK injection. The red trace shows the high energy fragmentation of the peptides in the black trace. (*) indicates peaks used to calculate peak capacity. While all marked peaks were used to calculate the average peak width, green asterisks define the separation window.

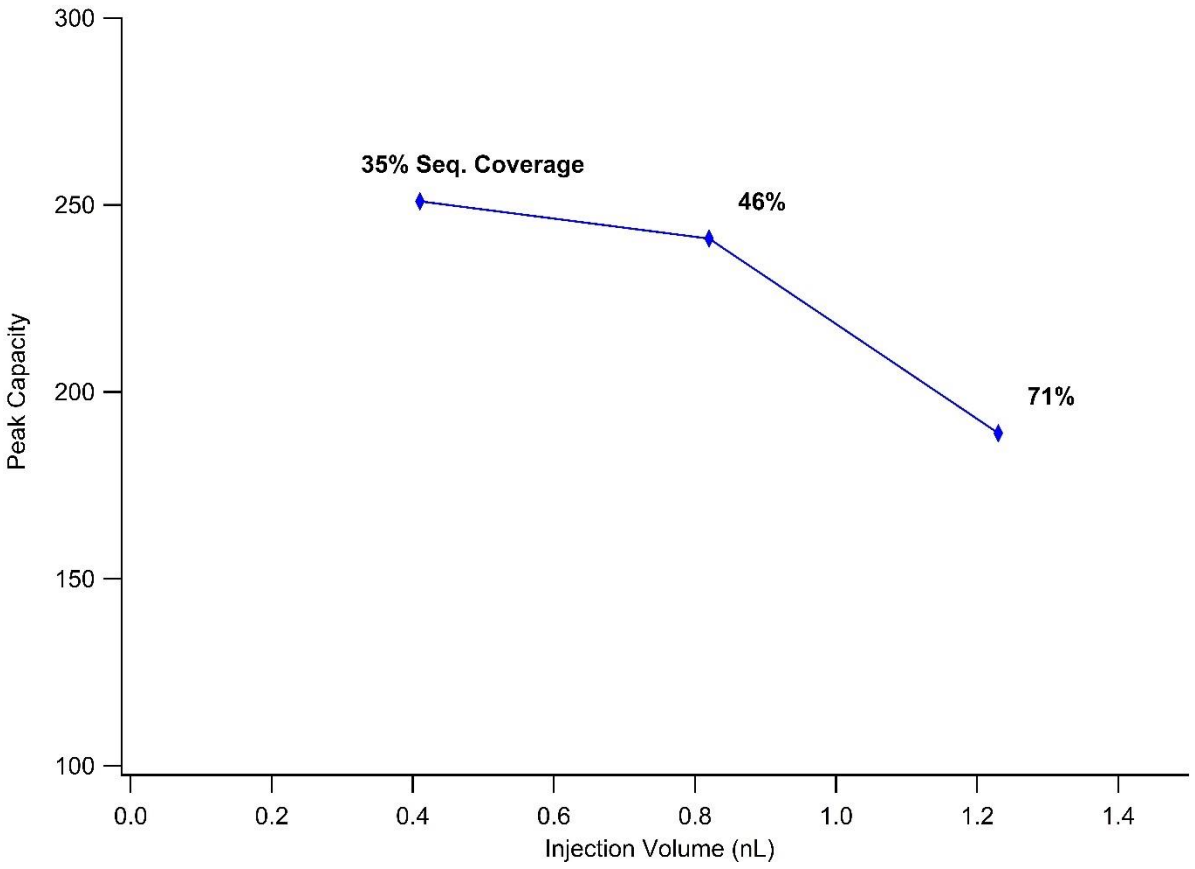

Figure 6.6: Relationship between peak capacity, sequence coverage, and injection volume for analysis of the MassPrep phosphorylase b digestion using gated EK injection. Increasing the injection volume improved the sequence coverage to 71%, but band broadening reduces the peak capacity.

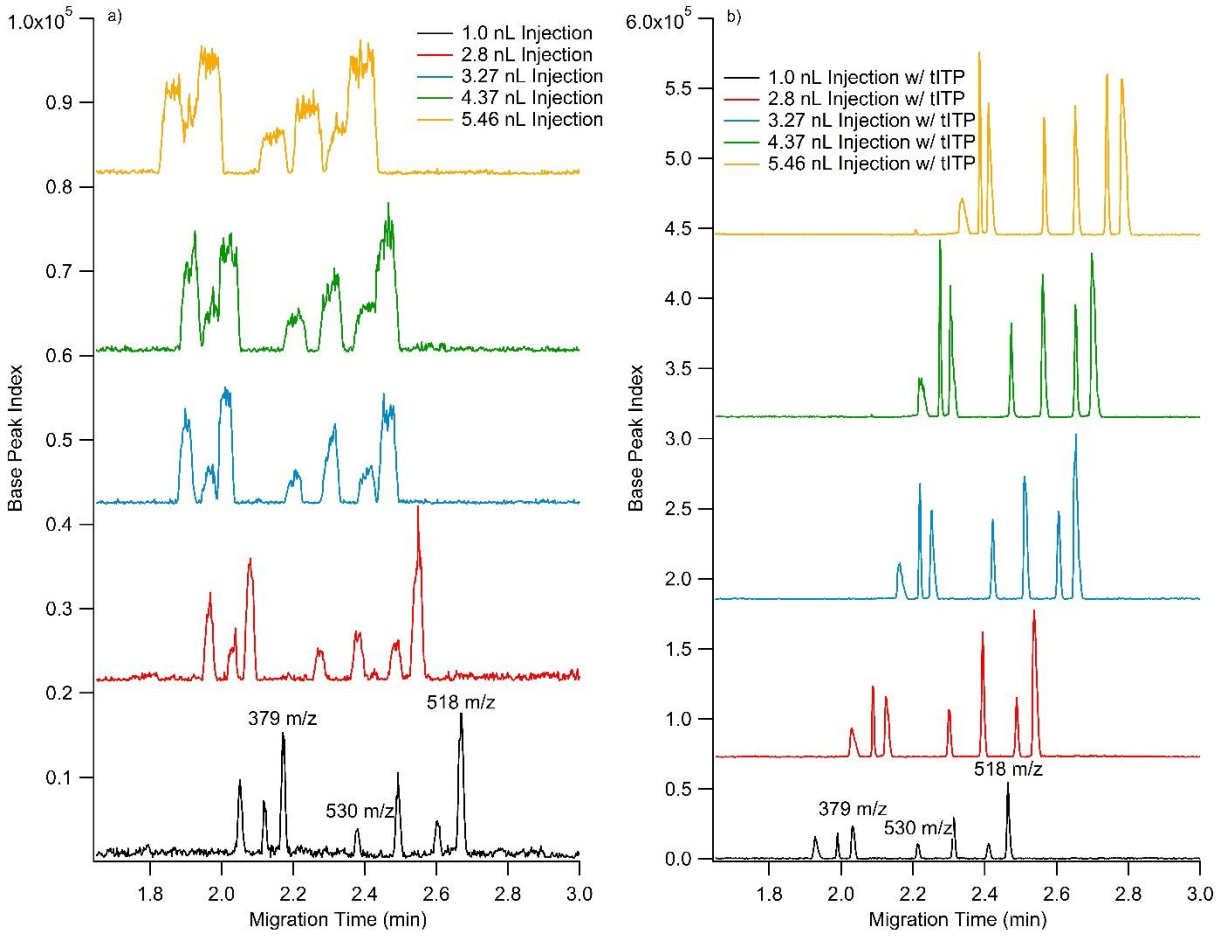

Figure 6.7: Microfluidic CE-MS analysis of peptide standards using HD injection. a) Increasing injection volumes of peptides diluted in BGE. The peaks rapidly broaden with increasing injection volume. b) Increasing injection volumes of peptides diluted in BGE with 100 mM ammonium acetate added to take advantage of tITP. The focusing effects of tITP preserves the efficiency of the CE separation despite the increase in injection volume.

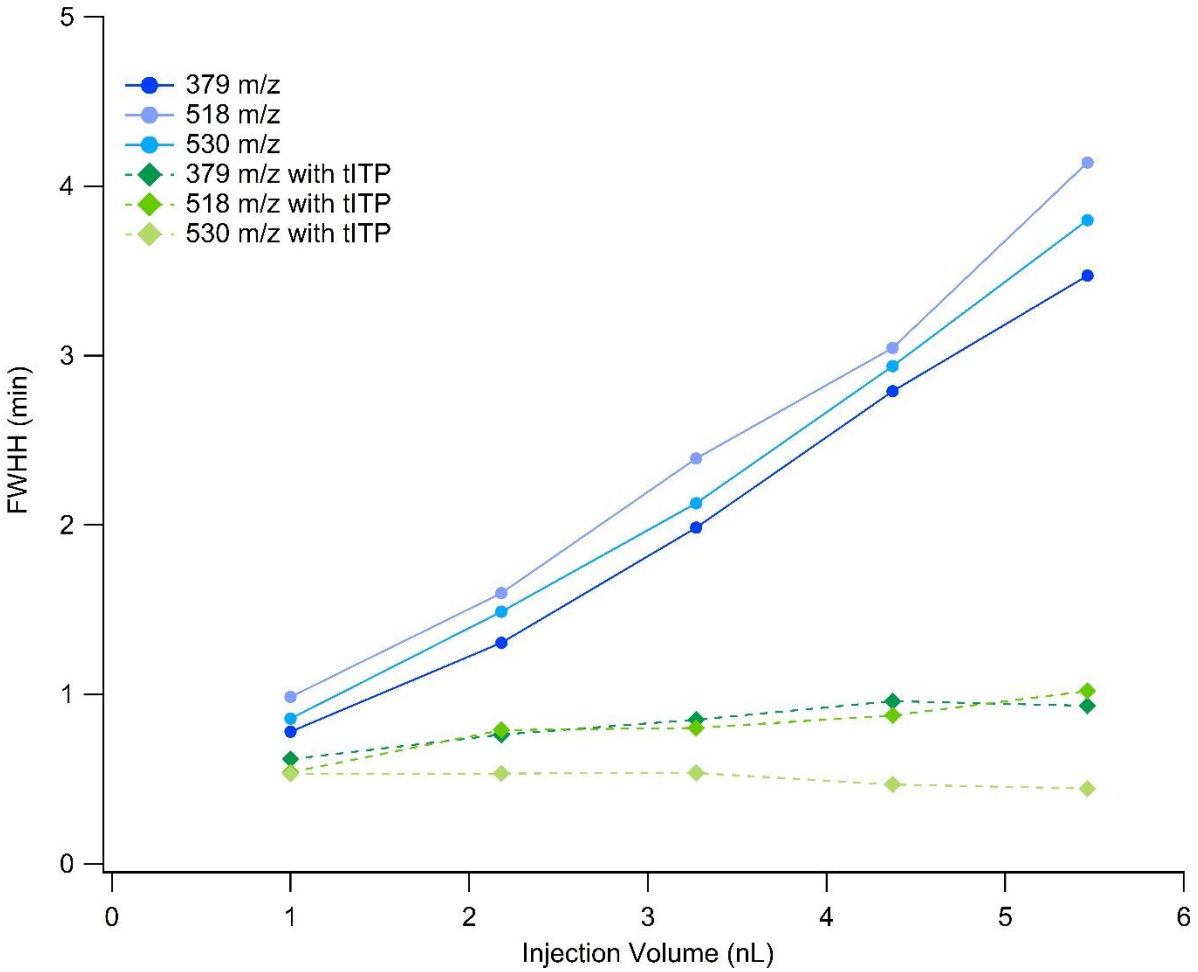

Figure 6.8: Plot of the FWHH versus injection volume for three of the peptides in the standard mixture. Without focusing (circles), the peaks broaden quickly, but with focusing (diamonds) the width remains fairly constant with increasing injection volume.

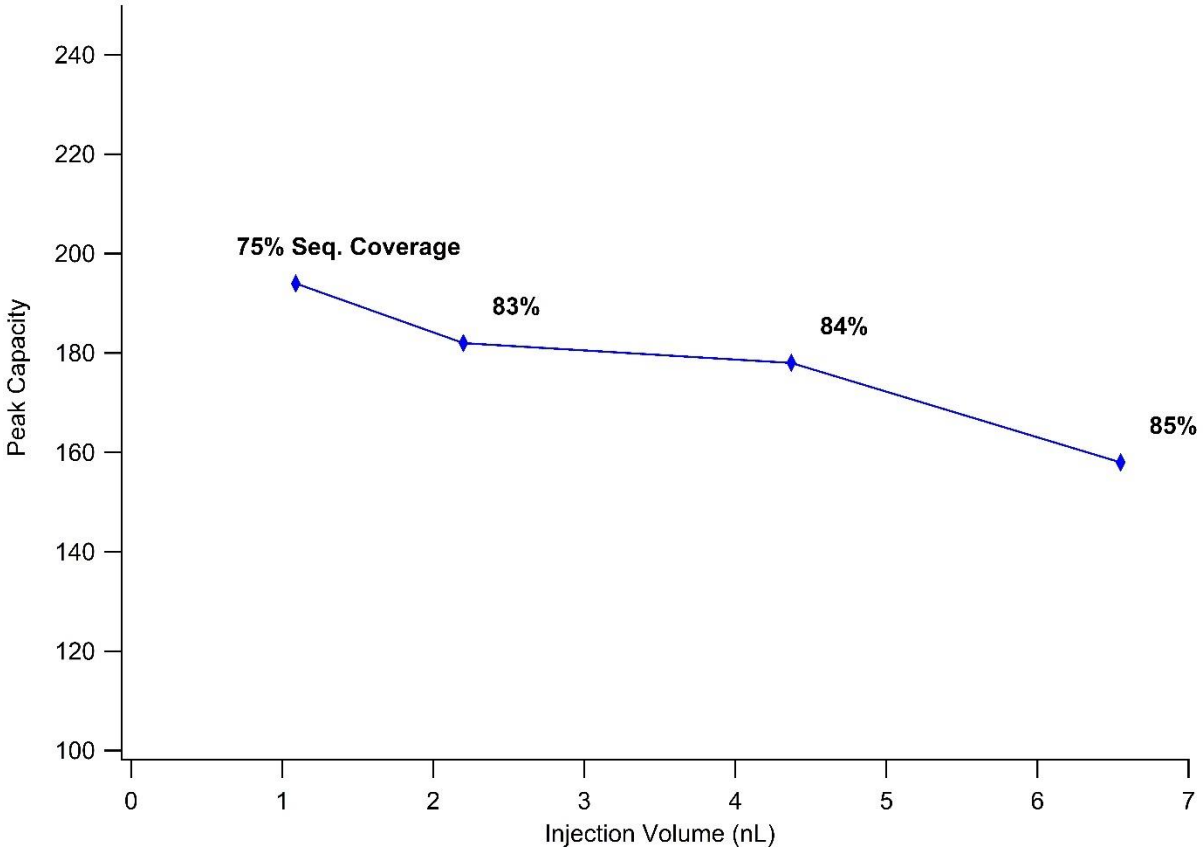

Figure 6.9: Relationship between peak capacity, sequence coverage, and injection volume for analysis of the MassPrep phosphorylase b digestion using HD injection with tITP. A higher degree of sequence coverage is obtained using this approach than with gated EK injection even though the peak capacity of the separation decreases due to compression of the separation window.

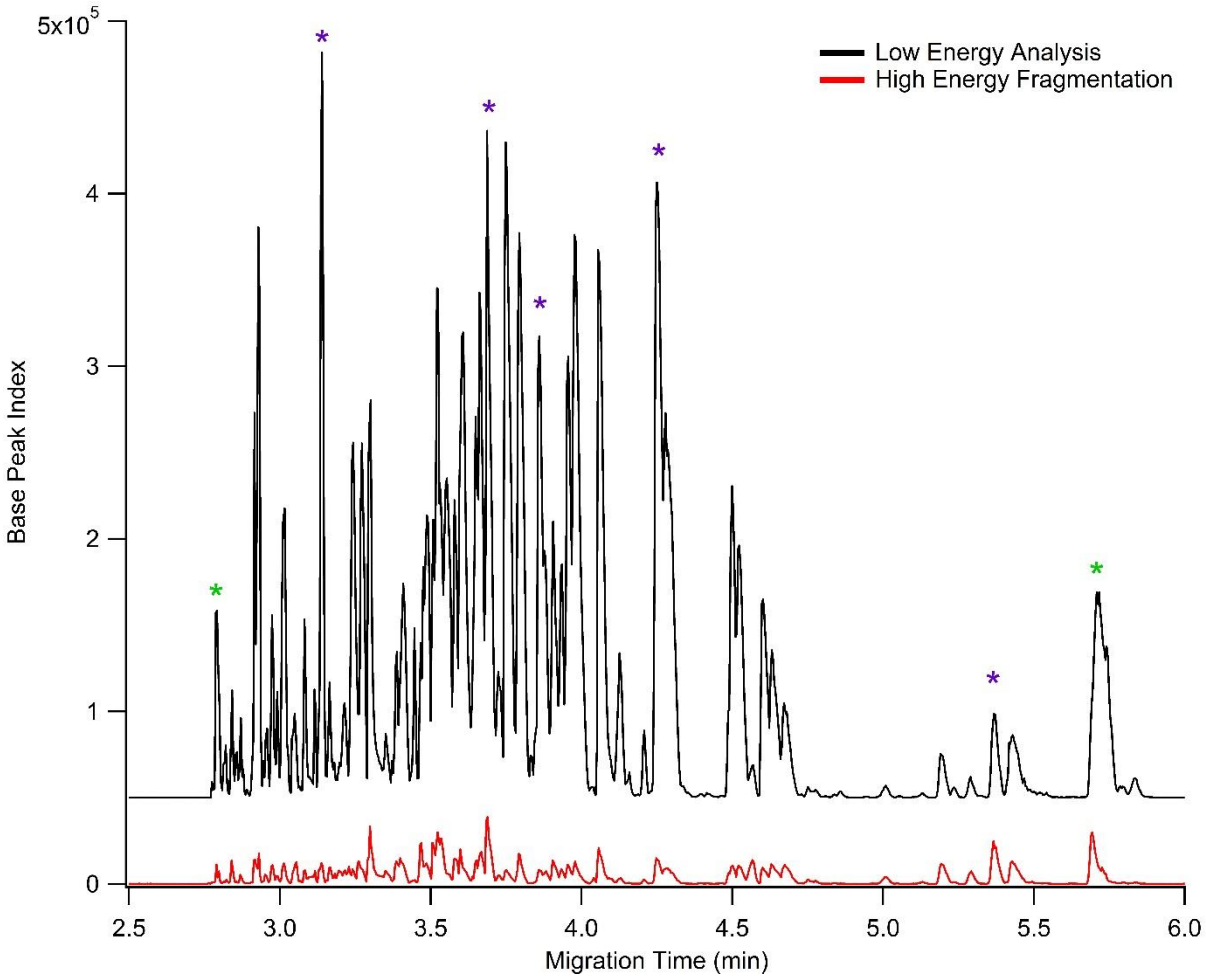

Figure 6.10: Analysis of MassPrep phosphorylase b using HD injections with tITP. The signal obtained for the fragmented peptides (red trace) is significantly higher than that obtained from gated EK injection. This facilitates the identification of the digest peptides and increases the sequence coverage. (*) indicates peaks used to calculate peak capacity. While all marked peaks were used to calculate the average peak width, green asterisks define the separation window.

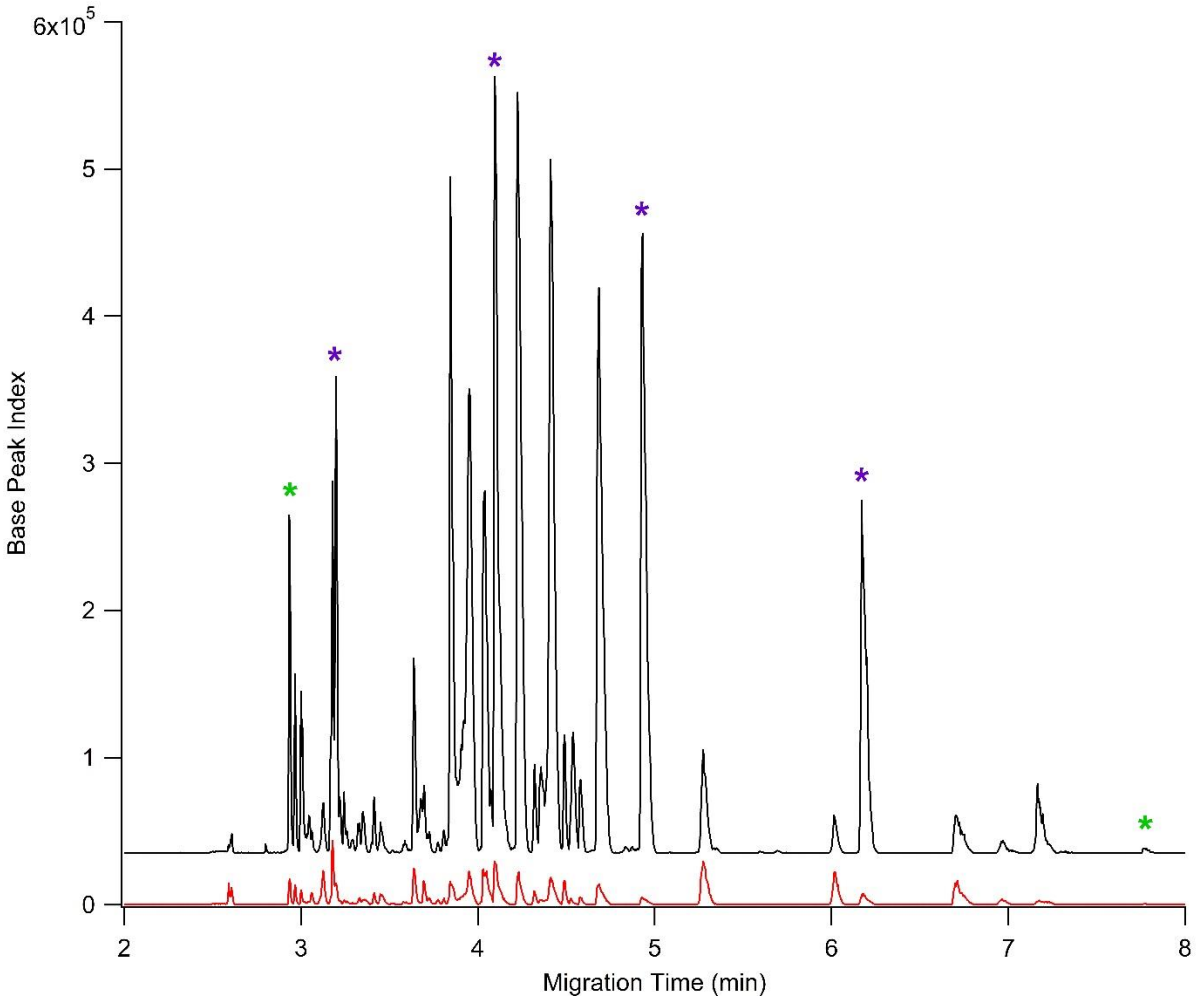

Figure 6.11: Microfluidic CE-MS analysis of a Lys-C digestion of a biotherapeutic mAb. The bottom electropherogram shows the high energy fragmentation of the digestion peptides. This analysis was complete in less than 10 minutes and resulted in a sequence coverage of approximately 95%. (*) indicate peaks used to calculate peak capacity. While all marked peaks were used to calculate the average peak width, green asterisks define the separation window.

Table 6.1: Voltages applied to perform gated EK injections.

	Applied Voltage (kV)	
	Gate	**Inject**
S	20	20
B	20	19
SW	18	19
EO	2	2

Table 6.2: Identified peptides from the microfluidic CE-MS analysis of a Lys-C digestion of a biotherapeutic mAb.

Peptide ID	Start Residue	End Residue	CE Migration Time
KH1	1	43	3.59
KL1-KL2	1	42	4.36
KH1(pQ)	1	43	/*
KH1, 1 oxidation M34	1	43	3.60
KL1-KL3	1	45	3.85
KL1-KL3, oxidation M4	1	45	3.88
KH2-KH3	44	58	3.88
KH2	44	57	5.34
KL4	46	103	7.77
KH3-KH4	58	65	/*
KH4	59	65	4.32
KH4-KH5	59	76	2.94
KH5	66	76	2.93
KH6	77	116	3.20
KH6, oxidation M35	77	116	3.22
KH6, oxidation M7	77	116	3.25
KH6, oxidation M7, M35	77	116	3.26
KH6, deamidation N8	77	116	3.52
KH6, deamidation N1, oxidation M7	77	116	3.54
KL5	104	107	/*
KL6	108	126	4.42
KL6-KL7	108	145	3.95
KL6-KL7, glycation	108	145	4.02
KH7	117	128	4.87
KH7-KH8	117	140	4.69
KL7	127	145	4.23
KH8	129	140	4.84
KH9	141	154	4.93
KL8	146	149	/*

KL9	150	169	6.71
KH10-KH11	155	217	5.28
KH10-KH11	155	212	/*
KL10	170	183	6.18
KL11	184	188	/*
KL12-KL13	189	207	3.19
KL13	191	207	4.10
KL14	208	214	4.04
KH13	221	225	/*
KH15-KH16	230	255	3.95
KH17, 1 oxidation	256	281	4.49
KH17	256	281	4.53
KH17-KH18, deamidation N38	256	281	3.20
KH17-KH18, deamidation N28	256	281	3.36
KH17-KH18, deamidation N28	256	281	3.85
KH17-KH18	256	281	3.92
KH18	282	295	3.85
KH19-KH20+BiNA0-1Gal	296	324	3.64
KH19-KH20+BiNA0	296	324	3.78
KH19-KH20+BiNA0-2Gal	296	324	3.64
KH19-KH20+BiNA0-2Gal-GlcNAc	296	324	3.64
KH19-KH20	296	324	3.17
KH19-KH21	296	327	3.03
KH19-KH20, deamidation N9	296	324	3.09
KH24	334	341	4.12
KH25	342	345	/*
KH27	346	367	3.29
KH27, glycation, oxidation M20	346	367	4.69
KH27-KH28, oxidation M18	348	367	3.68
KH27-KH29	348	367	3.71
KH28	368	377	4.54
KH28-KH29	368	399	5.60
KH29	378	399	6.97
KH29-KH30	378	416	3.13
KH30	400	416	6.02
KH31	417	421	/*
KH31-KH32	417	446	3.02
KH31-KH32, oxidation M19	417	446	3.05
KH32	422	446	3.00
KH32, oxidation M14	422	446	3.04
KH33	447	453	7.17

**indicates peptides that were not identified by PLGS, but corresponding masses were detected in the processed data.*

REFERENCES

(1) Han, X.; Aslanian, A.; Yates, J. R. *Curr. Opin. Chem. Biol.* **2008**, *12* (5), 483–490.

(2) Yates, J. R.; Ruse, C. I.; Nakorchevsky, A. *Annu. Rev. Biomed. Eng.* **2009**, *11* (1), 49–79.

(3) Zhang, Y.; Fonslow, B. R.; Shan, B.; Baek, M.-C.; Yates, J. R. *Chem. Rev.* **2013**, *113* (4), 2343–2394.

(4) Siuti, N.; Kelleher, N. L. *Nat. Methods* **2007**, *4* (10), 817–821.

(5) Kellie, J. F.; Tran, J. C.; Lee, J. E.; Ahlf, D. R.; Thomas, H. M.; Ntai, I.; Catherman, A. D.; Durbin, K. R.; Zamdborg, L.; Vellaichamy, A.; Thomas, P. M.; Kelleher, N. L. *Mol. Biosyst.* **2010**, *6* (9), 1532–1539.

(6) Sun, L.; Knierman, M. D.; Zhu, G.; Dovichi, N. J. *Anal. Chem.* **2013**, *85*, 5989–5995.

(7) Han, X.; Wang, Y.; Aslanian, A.; Fonslow, B.; Graczyk, B.; Davis, T. N.; Yates, J. R. *J. Proteome Res.* **2014**, *13* (12), 6078–6086.

(8) Kelleher, N. L.; Lin, H. Y.; Valaskovic, G. A.; Aaserud, D. J.; Fridriksson, E. K.; McLafferty, F. W. *J. Am. Chem. Soc.* **1999**, *121* (4), 806–812.

(9) Lew, C.; Gallegos-Perez, J.-L.; Fonslow, B.; Lies, M.; Guttman, A. *J. Chromatogr. Sci.* **2015**, *53* (3), 443–449.

(10) Gundry, R. L.; White, M. Y.; Murray, C. I.; Kane, L. A.; Fu, Q.; Stanley, B. A.; Van Eyk, J. E. In *Current Protocols in Molecular Biology*; John Wiley & Sons, Inc.: Hoboken, NJ, USA, 2009; Vol. Chapter 10, p Unit10.25.

(11) Biringer, R. G.; Amato, H.; Harrington, M. G.; Fonteh, A. N.; Riggins, J. N.; Hühmer, A. F. R. *Brief. Funct. Genomic. Proteomic.* **2006**, *5* (2), 144–153.

(12) Swaney, D. L.; Wenger, C. D.; Coon, J. J. *J. Proteome Res.* **2010**, *9* (3), 1323–1329.

(13) Choudhary, G.; Wu, S.-L.; Shieh, P.; Hancock, W. S. *J. Proteome Res. 2* (1), 59–67.

(14) Bian, Y.; Ye, M.; Song, C.; Cheng, K.; Wang, C.; Wei, X.; Zhu, J.; Chen, R.; Wang, F.; Zou, H. *J. Proteome Res.* **2012**, *11* (5), 2828–2837.

(15) Hoffman, E. de; Stroobant, V. *Mass Spectrometry Principles and Applications*, Third.; John Wiley & Sons, Inc.: West Sussex, England, 2007.

(16) Cole, R. B. *Electrospray Ionization Mass Spectrometry: Fundamentals, Instrumentation, and Applications*; John Wiley & Sons, Inc.: New York, 1997.

(17) Meyer, B.; Papasotiriou, D. G.; Karas, M. *Amino Acids* **2011**, *41* (2), 291–310.

(18) Šlampová, A.; Malá, Z.; Pantůčková, P.; Gebauer, P.; Boček, P. *Electrophoresis* **2013**, *34* (1), 3–18.

(19) Breadmore, M. C.; Thabano, J. R. E.; Dawod, M.; Kazarian, A. a; Quirino, J. P.; Guijt, R. M. *Electrophoresis* **2009**, *30* (1), 230–248.

(20) Landers, J. P. *Handbook of Capillary Electrophoresis*, 2nd ed.; CRC Press: New York, NY, 1997.

(21) Li, S. F. Y. *Capillary Electrophoresis: principles, practice and applications*; Elsevier Science: Amsterdam, 1993.

(22) Hirokawa, T.; Okamoto, H.; Gas, B. *Electrophoresis* **2003**, *24* (3), 498–504.

(23) Foret, F.; Szoko, E.; Karger, B. L. *J. Chromatogr. A* **1992**, *608* (1-2), 3–12.

(24) Stegehuis, D. S.; Irthu, H.; Tjaden, U. R.; Van Der Greef, J. *J. Chromatogr. A* **1991**, *538* (2), 393–402.

(25) Larsson, M.; Lutz, E. S. *Electrophoresis* **2000**, *21* (14), 2859–2865.

(26) Busnel, J.-M.; Schoenmaker, B.; Ramautar, R.; Carrasco-Pancorbo, A.; Ratnayake, C.; Feitelson, J. S.; Chapman, J. D.; Deelder, A. M.; Mayboroda, O. A. *Anal. Chem.* **2010**, *82* (22), 9476–9483.

(27) Bahga, S. S.; Santiago, J. G. *Analyst* **2013**, *138* (3), 735–754.

(28) Abdul Keyon, A. S.; Guijt, R. M.; Bolch, C. J. S.; Breadmore, M. C. *J. Chromatogr. A* **2014**, *1364*, 295–302.

(29) Gahoual, R.; Burr, A.; Busnel, J.-M.; Kuhn, L.; Hammann, P.; Beck, A.; François, Y.-N.; Leize-Wagner, E. *MAbs* **2013**, *5* (3), 1–12.

(30) Whitmore, C. D.; Gennaro, L. a. *Electrophoresis* **2012**, *33* (11), 1550–1556.

(31) Zhao, S. S.; Chen, D. D. Y. *Electrophoresis* **2014**, *35* (1), 96–108.

CHAPTER 7: CONCLUSIONS AND FUTURE DIRECTIONS

7.1 Summary of Work

The aim of this work was to develop and optimize a microfluidic CE-MS platform for the separation and characterization of intact mAb based biotherapeutics. Maximizing the separation resolution between protein variants in the CE domain was vital to the success of this type of analysis. By developing unique surface chemistry to treat the microfluidic channels, a MS compatible system for analyzing intact proteins was created.

A covalently bound two-layer surface coating based on an aminopropylsilane (APS) and polyethylene glycol (PEG_{450}) reagent was developed specifically for enhancing resolution between protein variants. This coating was selected because it suppresses the electroosmotic flow (EOF) to near zero, which should increase the separation resolution. Additionally, this coating proved effective in preventing protein adsorption to the channel wall further improving the separation. Initially, the utility of this approach was demonstrated by analyzing abundant blood proteins from whole blood lysate. Intact protein charge variants differing by as little as 1 charge unit were separated. This facilitated the quantitation of hemoglobin and albumin glycation in whole blood. The calculated levels of glycated hemoglobin agreed with HbA1c levels measured using a commercial HbA1c immunoassay. Coupling this analysis to high pressure mass spectrometry detection could lead to clinical applications for the CE-MS device.

The success of the HbA1c analysis suggested that microfluidic CE-ESI devices treated with the APS-PEG_{450} coating could potentially achieve separation of intact charge variants of

larger proteins. The large degree of EOF suppression generated with the APS-PEG_{450} coating meant that many of the complex, MS-incompatible buffer additives used to achieve separation of mAbs with CE-UV systems could be eliminated. This lead to a simple and MS compatible BGE of 10% 2-propanol 0.2% acetic acid that preserves some of the mAb structure in solution. This proved vital to achieving separation of the mAb charge variants. The applicability of the proposed method was demonstrated by analyzing biotherapeutic mAbs and antibody drug conjugates (ADCs). ADCs exhibit additional heterogeneity due to the conjugation of a smaller molecule drug load attached to the mAb structure. Having the CE separation prior to MS analysis not only reduces the necessary resolving power of the MS instrument, it provides two criteria to facilitate identification of variants: electrophoretic mobility shifts and mass shifts. With analysis times of less than 5 minutes, the microfluidic CE-MS platform is also significantly faster than other separation techniques developed for analyzing mAbs and ADCs.

Utilizing similar analysis conditions to those optimized for analyzing the blood proteins, the light chains (LC) and heavy chains (HC) of biotherapeutic mAbs and ADCs were analyzed using a middle-up approach. This is a common characterization strategy that involves reducing and alkylating the disulfide bonds of the molecules to obtain more site-specific information about the modifications to the mAb structure. This approach proved particularly useful for characterizing an especially complex mAb. The mAb was engineered to have multiple glycosylation sites that also became sialylated. Intact analysis did not generate sufficient resolution between the charge variants, but after reduction and alkylation several charge variants of the HC were separated that corresponded to different levels of glycan sialylation. Over 16 different variants of the mAb LC and HC were detected with the CE separation and mass information combined. This middle-up strategy provides an additional level of mAb

characterization than can be accomplished using the same microfluidic CE-ESI device used for intact analysis. Like the intact microfluidic CE-MS characterization, this analysis is also accomplished very rapidly with analysis times of less than 5 minutes.

Although the APS-PEG_{450} surface coating was developed for performing high efficiency intact protein separations, it has also proven useful for analyzing small molecules and peptides. The development of a hydrodynamic (HD) injection strategy to perform transient isotachophoresis (tITP) significantly improved the quality of smaller molecule analysis by injecting larger amounts of sample without experiencing a loss of separation efficiency. This made adding an additional level of mAb characterization feasible: bottom-up peptide mapping. Utilizing tITP for analyzing protein digests increased the achieved sequence coverage for a phosphorylase b tryptic digest from <71% to 85%. The performance of the microfluidic CE-MS system for bottom-up mapping was further evaluated by analyzing a Lys-C digestion of a biotherapeutic mAb. A sequence coverage of approximately 95% was achieved. When compared to results from LC-MS analysis, 82% of the peptides detected in the LC-MS data were also detected in the microfluidic CE-MS data. However, the microfluidic CE-MS analysis was 6 times faster.

The work presented here describes the development of a microfluidic CE-MS system capable of separating and analyzing both small and large intact proteins, peptides, and small molecules. Successful demonstrations of intact charge variant separation, middle-up analysis of LC and HC, and bottom-up peptide mapping of biotherapeutic mAbs were shown. Thus, multiple levels of biotherapeutic mAb characterization can be achieved using the same device. The rapidity with which analysis is completed suggests that these methods could potentially be impactful in a high throughput environment or industrial setting where measurements are tied to

time sensitive processes. Overall, the flexibility of this platform indicates that it can be useful for many different applications outside of what is presented here.

7.2 Future Directions

Future work involving the microfluidic CE-MS platform can span many areas ranging from intact protein separations to metabolomics. Initially, there are still avenues that can be explored to further improve the intact mAb separations and assess the utility of the application in a real-world setting. Some preliminary work in the area has been done through a collaboration with Biogen Idec. While mAbs-based therapies receive a large amount of focus there are smaller proteins and peptides that have been developed to treat various conditions, such as clotting factors, interferons, and erythropoietin.[1] The microfluidic CE-MS platform has proven effective for analyzing smaller proteins (<50 kDa) and would most likely be a significant asset to this class of therapies. Additionally, the bottom-up mapping analysis can be expanded to related techniques, such as hydrogen deuterium exchange (HDX) analysis. Finally, an overarching theme that is developing in the Ramsey lab is microfluidic CE-ESI integration with the miniaturized MS prototypes. It is possible that with further optimization the intact protein separations could be successfully integrated with the miniaturized MS units to create a system that could be deployed in areas where a conventional MS is inappropriate.

7.2.1 Further characterization and optimization of intact mAb separations

Intact mAb separation is perhaps the most unique capability of the microfluidic CE-MS system and additional work in this field could take several paths. The method should be further evaluated for real world applications of intact mAb separations. Some preliminary work in this

area has been done through a collaboration with Biogen Idec. With this project, the technology was evaluated from a manufacturing point of view to determine if it could detect anomalies during mAb production and purification. These anomalies could manifest as additional charge variant peaks or changes in the distribution of existing charge variants or glycoforms. Samples were taken at various manufacturing stages from the bioreactor to the final drug product. Figure 7.1 shows the intact charge variant separation of the biotherapeutic mAb at these stages in the manufacturing process. The only sample preparation needed was dilution of the mAb solution to an appropriate concentration using the separation BGE. For this sample set, no significant changes in the mAb were detected indicating a well-controlled and stable purification process. This preliminary work demonstrates that the microfluidic CE-MS platform could be an asset during mAb production due to the speed and ease of analysis.

While the method presented here for analyzing intact mAbs produces nearly baseline resolved charge variant separations, it is possible that the separation resolution could be improved further to match that of isoelectric focusing. Recently, devices were fabricated with a 35 cm separation channel in an attempt to improve the separation resolution. Figure 7.2 compares the separation generated using a device with a 23 cm separation channel and a 35 cm separation channel. It was found that the increase in channel length increased the resolution between charge variants by a factor of approximately 1.5 though at the cost of longer analysis times. Further improvements in resolution with even longer channels are possible but instrumental concerns, namely using higher voltages to maintain electric fields may limit the usable separation length. An alternative to lengthening the separation channel is to alter the separation BGE. Analyzing proteins under native conditions using native-spray-MS has become a very common technique for characterizing proteins via MS. These experiments involve

infusing the protein in 100 – 200 mM ammonium acetate at pH 4-6. Operating in this pH range could enhance the differences in net charge between mAb and ADC variants and increase the CE separation resolution.

7.2.2 Analysis of other biotherapeutic proteins

While mAbs and ADCs receive a significant amount of attention in the biopharmaceutical industry there are also other types of biomolecules used therapeutically, such as peptides and smaller proteins. In Chapters 2 and 5, the microfluidic CE-MS platform was successfully demonstrated for proteins and mAb fragments in the 15 – 50 kDa mass range. Therefore, the system could be extremely successful for analyzing peptide and small protein biotherapeutics. Figure 7.3 shows the microfluidic CE-MS separation of an ~20 kDa therapeutic glycoprotein. This molecule becomes highly sialylated creating an extremely heterogeneous population of protein glycoforms that differ in both mass and electrophoretic mobility. Some of the identified glycoforms of the protein are labeled with their associated glycan structure. Asterisks indicate deamidated glycoforms. In the CE separation alone, 35 charge variants of the protein as separated and detected as discrete peaks. Additional mass variants that do not separate in the CE domain increase this number even more.

7.2.3 Optimization of hydrogen deuterium exchange analysis

HDX is a technique used to probe the structure of intact proteins. Briefly, the protein is exposed to deuterium which exchanges with hydrogens in the protein backbone. Areas with high levels of deuterium exchange are considered to be the more solvent accessible regions of the protein. Typically, specialized liquid chromatography-mass spectrometry (LC-MS) systems are used for this technique, but HDX analysis is an area where the speed of the microfluidic CE-MS

analysis is an advantage.[2] Initial proof of concept work utilizing microfluidic CE-MS for HDX determined that the efficiency and peak capacity of the CE separations was greater than that of the LC-MS separations and also significantly faster.[3] However, this work was performed before HD injections and tITP were optimized and sample loading was an issue. A much higher concentration of protein was needed to achieve signal intensities and sequence coverages comparable to those of the LC-MS system. With the new injection scheme and concentration enhancement effects of tITP the quality of the HDX data should improve significantly due to the increased loading capacity. The microfluidic CE-ESI devices could then be integrated with a temperature controlled stage to further minimize deuterium back exchange. This could potentially create a system that excels over LC in all aspects of HDX analysis.

7.2.4 Integration with miniaturized MS

A continuing focus within the Ramsey group is interfacing microfluidic CE separations with the miniaturized mass spectrometers. Over the past four years, a significant amount of progress has been made in developing and ESI compatible interface for the miniaturized MS systems. This provides the capability to sample non-volatile analytes ions that are generated through ESI. Metabolite analysis is very well suited for integration with the miniaturized MS because an appropriate mass range is achieved easily using voltages within practical experimental limits. Using a microfluidic CE-ESI method optimized for amino acid analysis interfaced with a miniaturized MS, Gilliland et al. demonstrated that the consumption of metabolites in cell growth media could be monitored and correlated to cell growth progress.[4] As discussed in Chapter 2, preliminary work indicated that interfacing these two systems for analyzing moderately sized intact proteins is possible. Thus, with further optimization it may be

possible to employ this type of miniaturized MS system on the manufacturing floor of biopharmaceutical plants as an alternative to a conventional MS.

7.3 Figures and Tables

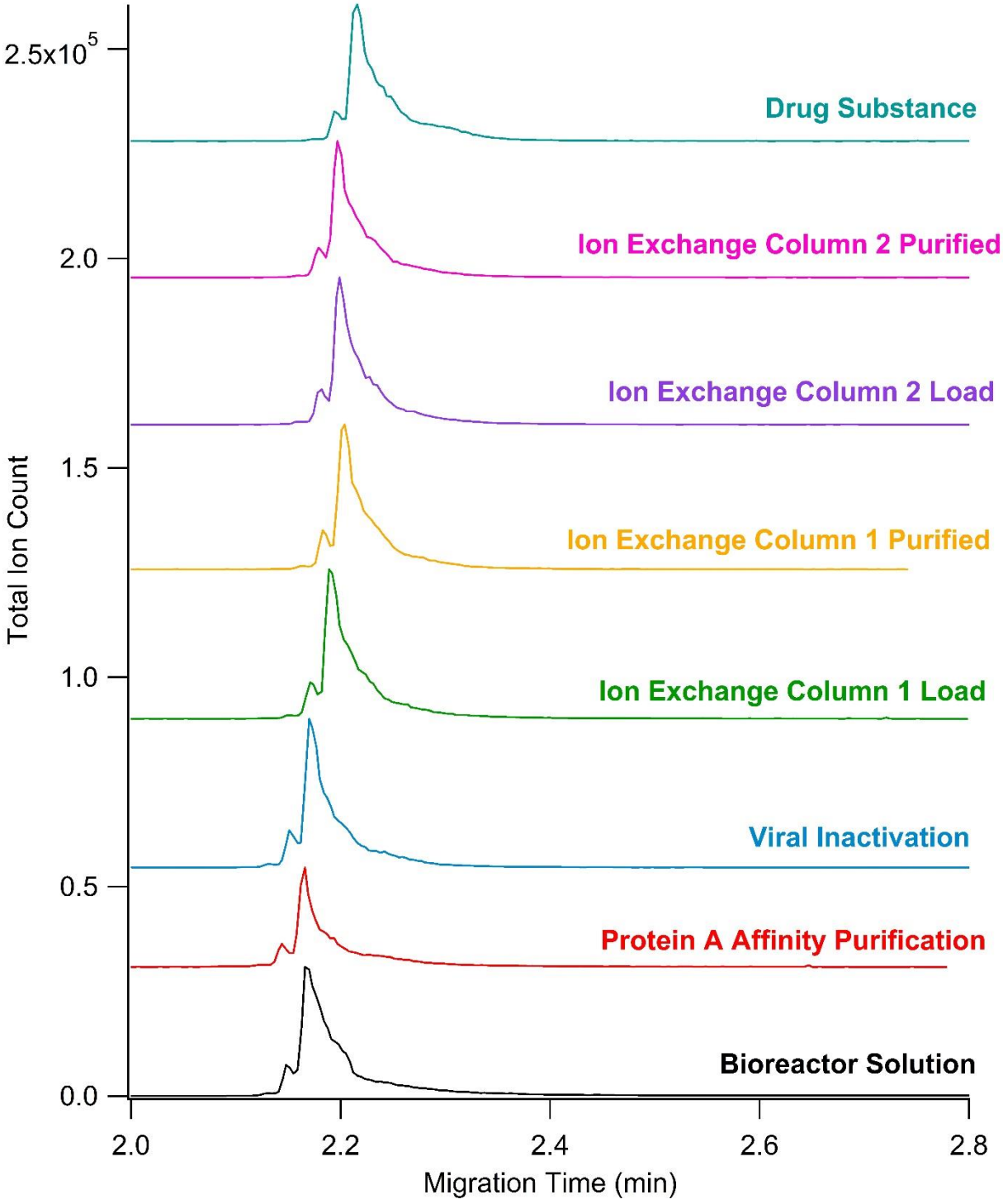

Figure 7.1: Analysis of a biotherapeutic mAb at various stages of production and purification.

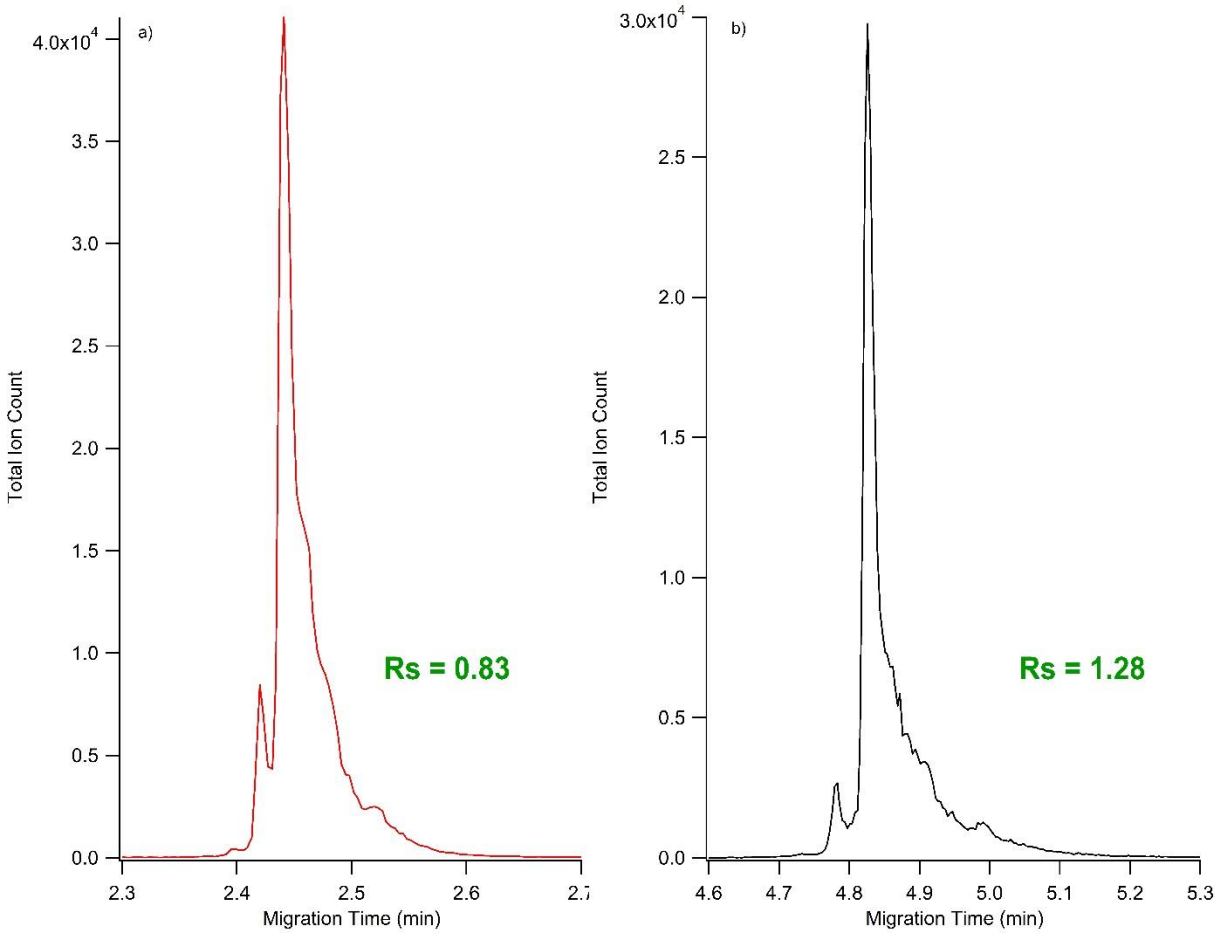

Figure 7.2: Intact charge variant separations via microfluidic CE-MS using a) a device with a 23 cm separation channel and b) a device with a 35 cm separation channel.

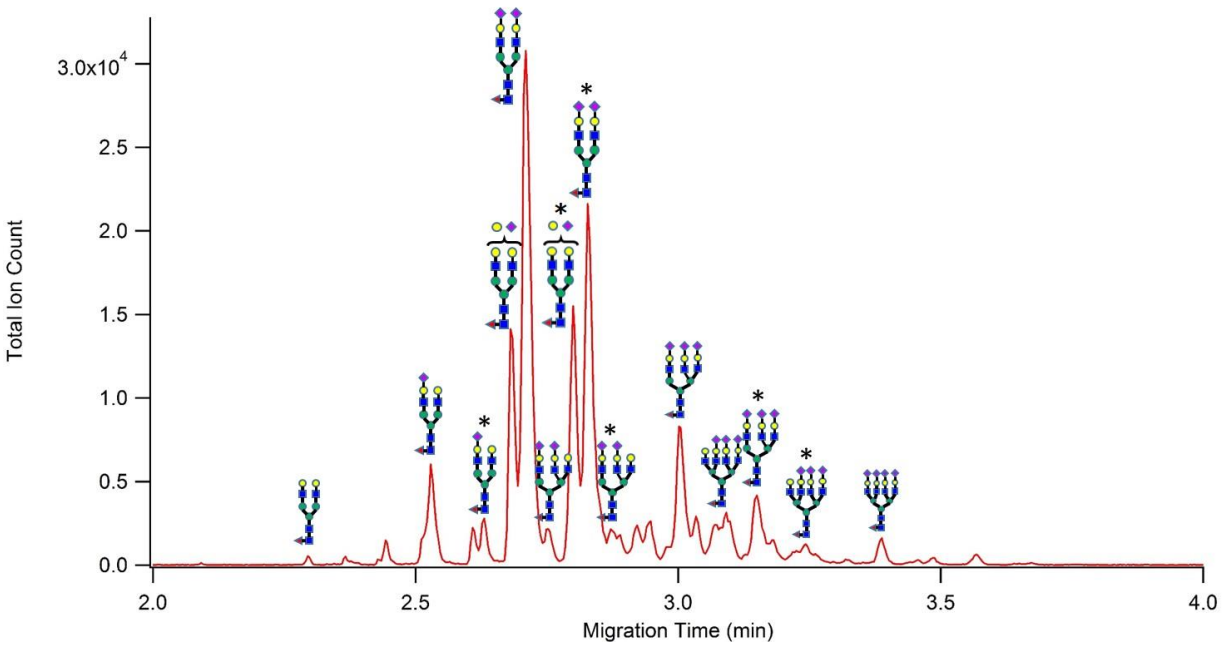

Figure 7.3: Microfluidic CE-MS analysis of a ~20 kDa biotherapeutic glycoprotein. Some identified glycoforms are labeled with their respective glycan structures. (*) indicates a deamidated glycoform of the protein.

REFERENCES

(1) Haselberg, R.; de Jong, G. J.; Somsen, G. W. *Anal. Chem.* **2013**, *85* (4), 2289–2296.

(2) Konermann, L.; Pan, J.; Liu, Y.-H. *Chem. Soc. Rev.* **2011**, *40* (3), 1224–1234.

(3) Black, W. A.; Stocks, B. B.; Mellors, J. S.; Engen, J. R.; Ramsey, J. M. *Anal. Chem.* **2015**, *87*, 6280–6287.

(4) Gilliland, W. M.; Mellors, J. S.; Ramsey, J. M. In *12th Symposium on the Practical Application of Mass Spectrometry in the Biotechnology Industry (CASSS Mass Spec 2015)*; 2015; p poster presentation.

APPENDIX 1: DEVICE FABRICATION

Standard photolithography and wet chemical etching techniques were used to fabricate the CE-ESI and infusion devices. Planar 5”x5” glass substrates were used to fabricate the devices. The type of glass used was either 0.5 mm thick B270 glass (Perkin Elmer, Waltham, MA) or 0.55 mm thick D263 glass (Telic Co., Valencia, CA). The wafers were purchased pre-coated with a layer of chrome and AZ1518 positive photoresist. Device designs were transferred to the glass substrates using a borosilicate mask made in house and photo exposure at 365 nm. The exposed photoresist was developed with AZ 400K developer (Integrated Micro Materials, Argyle, TX). Exposed chrome was removed using Chrome Etchant 1020 (Transene Company, Inc., Danvers, MA) and the device channels were etched into the glass using a HF based buffered oxide etchant (BOE) diluted 1:10 with water. For the D263 glass substrates the etching process was performed at approximately 100 °C. Channels were etched to a depth of approximately 10 µm. Due to the isotropic nature of the etching process this results in channel widths of approximately 70 µm and 25 µm around the tapering of the turns in the separation channel. Inlets to the channels were formed by powder blasting holes through the glass substrate at the channel termini. The remaining photoresist and chrome was removed and a blank 5”x5” substrate was fusion bonded to the etched substrate at 550 °C to form enclosed channels. This results in a total thickness of 1.0 mm or 1.1 mm depending on the glass type. The integrated ESI emitter was formed by dicing the corner of the device to 90° using a precision dicer (Disco Technologies, Santa Clara, CA). The edges of the corner containing the ESI emitter were polished to remove dicing artifacts using 3 µm cerium oxide abrasive lapping paper and a lapping wheel (Ultra Tec, Santa Ana, CA). Buffer reservoirs were formed by attaching 8-mm diameter glass cylinders to

the devices with chemically resistant epoxy (Loctite E-120HP, Henkel Corporation, Germany). The fluid capacity of the reservoirs is approximately 200 µL.

APPENDIX 2: COATING PRODECURES FOR CE-ESI DEVICES

Amiopropylsilane coating

CE-ESI and infusion devices are coated with APDIPES via chemical vapor deposition (CVD) as described previously.[38] Using this strategy multiple devices can easily be coated at one time without deleterious effects on coating quality. Briefly, using a commercial CVD system devices are exposed to the silane reagent under vacuum and at elevated temperatures to ensure volatilization of the reagent. The devices are incubated with the volatilized reagent for ~15 minutes and then the reaction chamber is purged with nitrogen. This process is repeated twice more for a total coating time of about 45 minutes.

PEGylation of APS coating for protein applications

For the separation devices, the injection cross and separation channels are covalently coated with NHS-PEG_{450} through liquid phase PEGylation. For infusion devices, the same PEGylation procedure is used on just the shorter sample channel. A 10 mg/mL solution of NHS-PEG in 100 mM phosphate buffer (pH 7.5) is put in reservoirs 1-3. Flow is maintained through the channels by the application of suction to the ESI emitter and ~50 psi of head pressure to the S, SW, and B reservoirs. Head pressure is applied to the reservoirs via an in-house built apparatus (Figure A2.1). To create an electroosmotic pump, the EO pump channel is not PEGylated. The difference between the strong anodic EOF of the EO pump channel and the weak EOF of the PEGylated separation channel results in pressure-driven flow out of the ESI emitter when voltage is applied to the device. With the low EOF surface coating in the separation channel, the integrated electroosmotic pump is vital to the successful formation of analyte ions; the pumping channel provides continuous fluid flow that is necessary for maintaining stable and

sensitive ESI. A consequence of this is that EOF generated in the pumping channel must be high enough to sustain ESI at the emitter so the field strength and BGE composition must be selected to ensure this. Once the PEGylation process is complete, excess PEG reagent is rinsed from the channels with DI water by thoroughly rinsing all solvent reservoirs and then applying suction to the ESI emitter for 20 min. After the coating procedures are complete, 5 µL of trichloro-(1H,1H,2H,2H-perfluorooctyl)-silane is applied to the ESI emitter to increase the hydrophobicity of the external surface and facilitate ESI. Excess reagent is removed with suction, the liquid is removed from device channels with suction at the tip, and the surface is cured at room temperature for approximately 10 minutes.

Recently, a modification of this coating procedure has been used where all of the channels of the separation device are coated with the NHS-PEG reagent. In doing this, an electroosmotic pump is not created. Instead, ~2 psi of head pressure is applied to reservoir 4 to generate bulk fluid flow for sustaining ESI. This has advantages over the electroosmotic pump strategy in that the volumetric flow rate is not dependent on the EOF that results from the applied field strength or BGE composition. Thus, with pressure driven pumping there is more flexibility in the experimental parameters because the analysis conditions are not tied to the need to generate a certain level of EOF in the pumping channel.

Figures and Tables

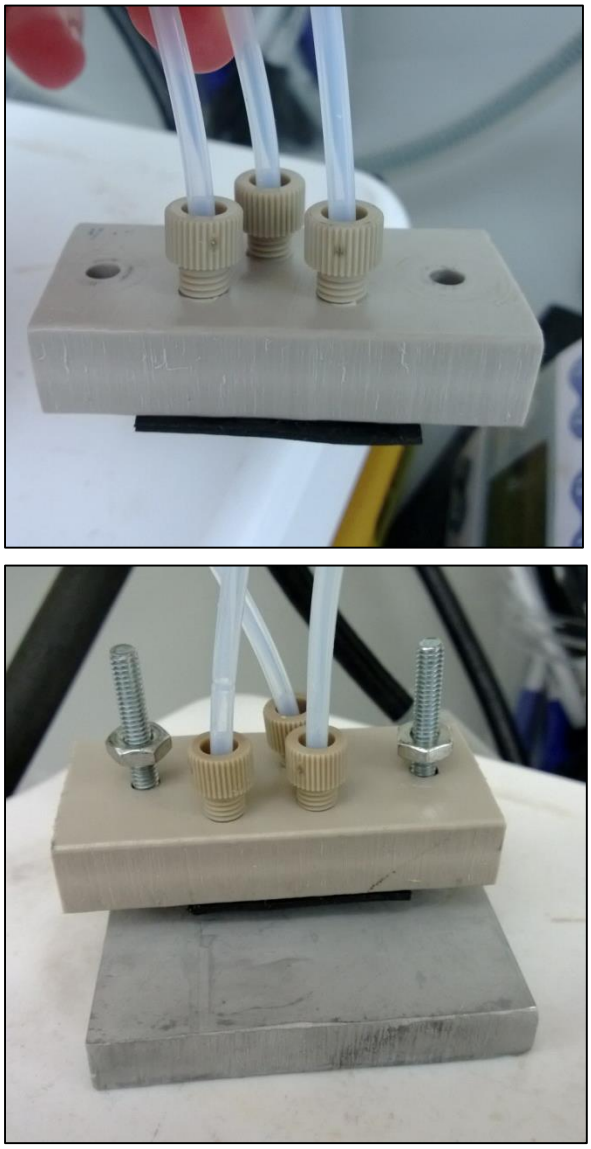

Figure A2.1: In-house built coating apparatus. The microfluidic CE device is sandwiched between the PEEK plate and metal bottom using through screws. The PEEK piece is plumbed to deliver gas pressure individually to reservoirs 1-3 of the device. A viton gasket on the bottom of the PEEK piece insures a gas tight fit.

APPENDIX 3: CE-MS DEVICE OPERATION

Voltage and Pressure Control

CE-ESI and infusion devices are operated by applying voltage to the solvent reservoirs via platinum wire electrodes. The electrodes are powered by an in-house built power supply containing five UltraVolt modules (Ronkonkoma, NY): Three 0 to +35 kV modules to power reservoirs S, B, and SW and two 0 to +10 kV modules to power the EO reservoir and the ESI shield electrode. The voltage output of the power supply is controlled via a custom LabVIEW (National Instruments, Austin, TX) program. Devices are positioned in front of the inlet of the mass spectrometer using a custom built stage as depicted in Figure A3.1. A shield electrode fabricated from single-sided copper clad circuit board (M.G. Chemical, Burlington, Ontario, Canada) is used to isolate the ESI emitter from the electric field generated by the high voltages powering the CE-ESI device. Throughout analysis +500 V is applied to the shield electrode. Data acquisition is accomplished through MassLynx (Waters Corporation) or Xcalibur (Thermo Scientific) software, which is triggered through the LabVIEW program used to control the power supply output.

Operation of Infusion Devices

Infusion-MS devices such as those pictured in Figure A3.2 mimic the use of a syringe pump and pulled tip ESI emitter. The devices are operated by applying approximately +5 kV to the sample reservoir and 0 kV to the BGE reservoir. Upon voltage application the different surface coatings in the two channels create an electroosmotic pump that continuously provides bulk fluid flow for ESI at a rate of 100-200 nL/min. Sample can be placed in one or both of the reservoirs and continuously migrates toward the ESI emitter while voltage is being applied.

Electrokinetic Injection

The typical voltage states used for operating 23 cm APS-PEG_{450} coated devices are given in Table A3.1. Injection of the sample is performed by switching the voltage profile from the gated state to the injection state for 200 ms and back again. The amount of sample injected can be controlled by altering the amount of time the voltages are in the inject state. This injection strategy is rapid, easy to control, and useful for many applications. However, it is not tolerant of samples with much higher conductivity than the BGE, such as those with physiological levels of salts, and desalting sample preparation techniques must be used to make such samples compatible. Additionally, this injection method is biased based on the mobility of the analytes; less of the low mobility analytes are injected. This can become problematic if there is a wide range of analyte mobilites in the sample.

Hydrodynamic Injection

A pressure based injection scheme can also be used for sample manipulation and injection. Hydrodynamic injections are not subject to electrokinetic bias as and can be used for samples with much high salt content, reducing the amount of sample preparation needed for analysis. For this injection strategy voltage is applied to only two reservoirs: the top BGE reservoir and terminal EO pump reservoir. Typical separation voltages for 23 cm APS-PEG_{450} coated devices are +20 kV (BGE reservoir) and +2 kV (EO pump reservoir), but can be optimized for specific applications. Three way valves (Clippard, Cincinnati, OH) are used to precisely control the application and release of ~2 psi of gas pressure to the device. The valves are operated using the same LabView program that controls the power supply. Pressure connections to the reservoirs are made in house using Teflon tubing. Injection of the sample is performed by applying head pressure to reservoirs 1 and 2 simultaneously for the desired

duration. Pressure is then applied to only reservoir 1 for 500-1000 ms to isolate the sample plug in the separation channel and clear sample from the side channels leading to the sample and sample waste reservoirs. Voltages are then applied to reservoirs 1 and 4 to perform the CE separation and generate ESI. The injection volume can be controlled by altering the time that pressure is applied to reservoirs 1 and 2 or by increasing or decreasing the applied pressure. For some applications it may be necessary to apply a small head pressure (~0.5 psi) to reservoir 1 during analysis to isolate the sample and sample waste in their respective reservoirs. Figure A3.3 provides the flow rates in the separation channel resulting from the application of various head pressures to the reservoirs. Data for this plot was generated using a device with a 23 cm separation channel and a 50/50 acetonitrile/water BGE. Flow rates for both the "injection" and "isolation" configurations are provided. This plot can be used to calculate injection volumes for other 23 cm devices when BGEs of similar viscosity are used. If the BGEs differ significantly in viscosity, it is possible that a correction factor could be used to account for this.

Figures and Tables

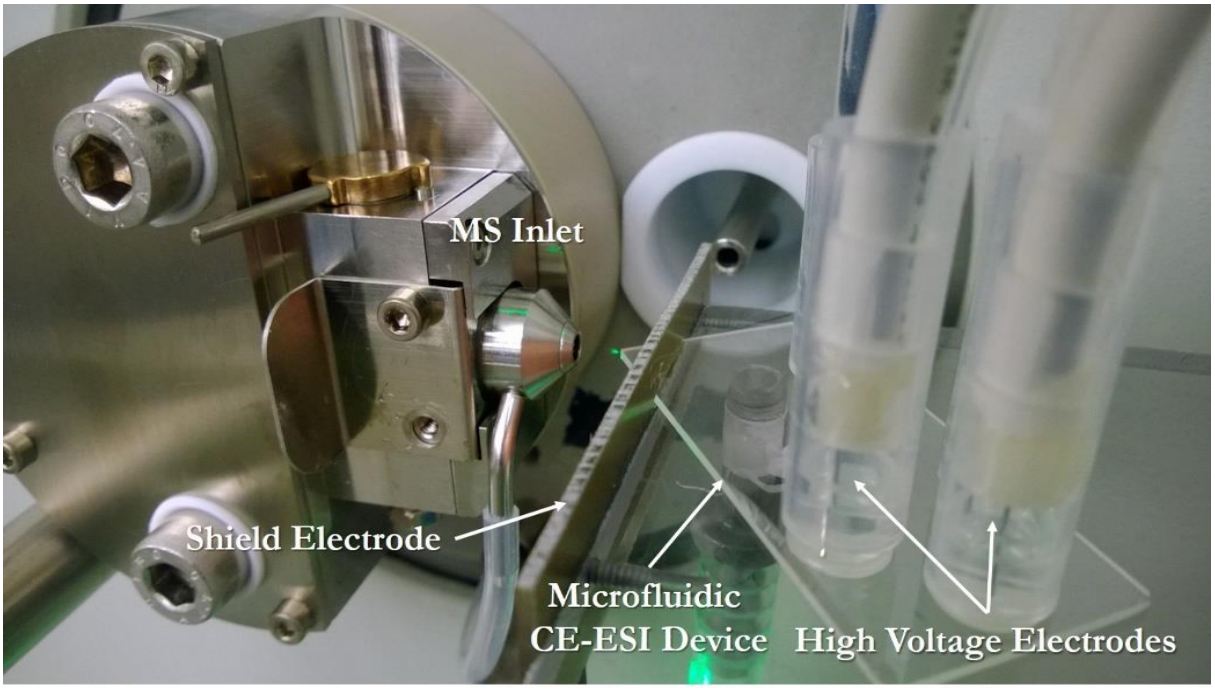

Figure A3.1: Photograph of a microfluidic CE-ESI device positioned in front of the Waters LCT-Premier inlet.

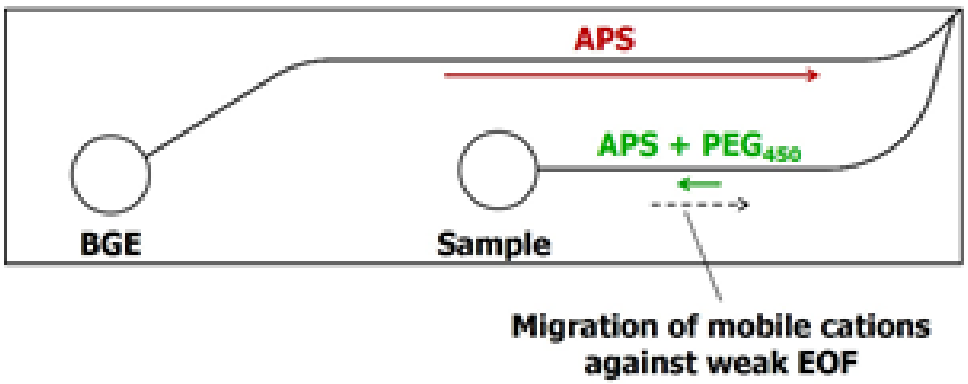

Figure A3.2: Channel schematic for infusion-ESI devices.

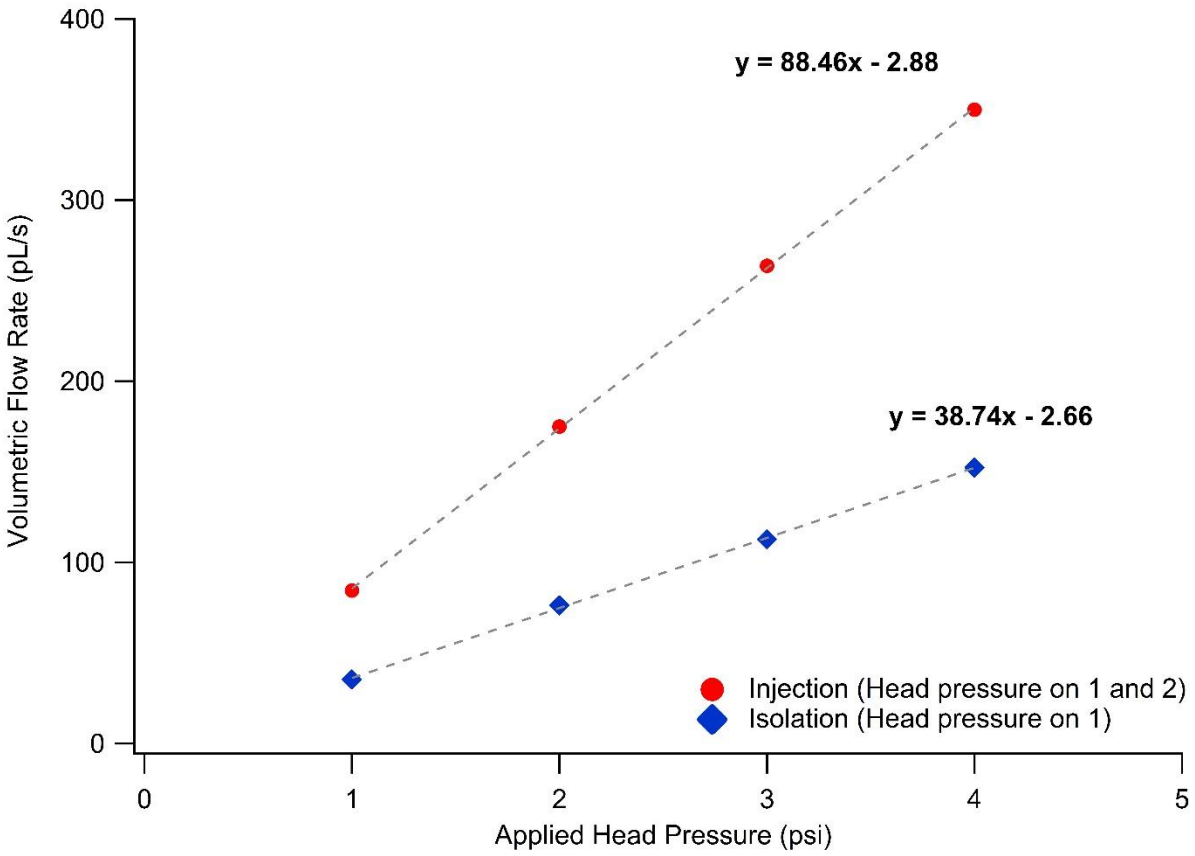

Figure A3.3: Volumetric flow rate versus applied pressure for performing hydrodynamic fluid manipulation on microfluidic CE-MS devices with a 23 cm separation channel and 50/50 acetonitrile/water based BGE.

Table A3.1: Representative voltage scheme for sample handling on the CE-ESI device.

	Applied Voltage (kV)	
	Gate	**Inject**
S	18	18
B	18	17
SW	16	17
EO	2	2

APPENDIX 4: INSTRUMENT SETTINGS FOR INTACT ANTIBODY ANALYSIS

The optimal ion transfer parameters for large, intact proteins are often very different than those needed for small molecules or peptides. However, most commercial mass spectrometers have been optimized for the size range needed for bottom-up proteomics due to the popularity of this technique in many areas of research. This makes analyzing intact proteins using these instruments difficult or impossible without adjusting the ion transfer settings or even the hardware of the MS instrument.[1–3] Recently, some commercial instrument vendors have started developing MS instrumentation or upgrades that optimize the instrument for intact protein analysis. Some of these include the Thermo Exactive Plus with Extended Mass Range (EMR) mode, the qExactive with Protein Mode, and Waters qTofs with a low frequency quadrupole[1], and a high mass Q-Tof upgrade offered by MS Vision.[2] For the work presented here, the available MS instrumentation was limited to a Waters LCT-Premier Tof, a Waters Synapt G2 qTof, and much later a Thermo Exactive Plus EMR. Below are the optimized ion transfer parameters for each instrument evaluated for intact mAb analysis.

Waters LCT-Premier

The LCT-Premier proved to generate superior performance for mAb analysis over the Synapt G2. This can partly be attributed to the simplicity in the ion optics of the instrument. The schematic of the LCT-Premier is provided in Figure A4.1 below. The LCT lacks a quadrupole so ion transfer is mainly accomplished through an ion guide and hexapoles.[1,4] Although the mass resolution is modest, with the CE separation prior to MS analysis a number of species can still be identified.

Method Parameters:

Scan duration (secs): 0.200 (can be adjusted)
Inter Scan Delay (secs): 0.010
Start and End Time(mins): Variable
Ionization mode: ES+
Data type: Accurate Mass
Function type: TOF MS
Mass range: Variable

Instrument Parameters:

Polarity	ES+
Analyzer	V Mode
Sample Cone (V)	30
Source Temp (C)	105
Ion Guide One	*180*
Aperture 1 Voltage	30
Ion Energy (V)	*100*
Aperture 2 Voltage	2
Hexapole DC Voltage	6
Aperture 3 Voltage	5
Acceleration (V)	200
Y Focus (V)	0
Steering (V)	0
Tube Lens (V)	190
Attenuated Z Focus (V)	500
Normal Z Focus (V)	65

**italicized settings indicate those that seemed to have the most impact on the quality of the intact mAb data*

Waters Synapt G2

As seen in Figure A4.2, the Synapt G2 utilizes many more ion optic components than the LCT-Premier. In part, this is due to the quadrupole and ion mobility spectrometry capabilities of the instrument. In order to optimize the ion transfer of intact mAbs, the source backing pressure had to be elevated from to 6-7 mbar by restricting the vacuum in that region. This had a significant impact on the signal intensity. However, the Synapt G2 in our lab is mostly optimized for performing bottom-up proteomics applications and is not equipped with a low frequency quadrupole. This limits the upper m/z threshold to 3000 in the quadrupole settings, so higher mass ions in the <4000 m/z range may not be as well transferred. As seen in Figure A4.3, despite optimizing the ion transfer for the intact mAbs, the Synapt G2 did not match the LCT-Premier in terms of sensitivity. If the instrument was equipped with a low frequency quadrupole the ion transfer could be further enhanced to match that of the LCT.

Method Parameters:

Scan duration (secs): 0.100 (can be adjusted)
Inter Scan Delay (secs): 0.0240
Start and End Time(mins): Variable
Ionization mode: ES+
Analyzer mode: Sensitivity Mode
Mass range: Variable

Instrument Parameters:

Polarity	ES+
Analyzer	Sensitivity Mode
Source Temperature (°C)	150
Sampling Cone	*200*
Extraction Cone	*10*
Ion Energy	10
Trap Collision Energy	6

Transfer Collision Energy	0
Collision Energy	4
Backing Pressure (mbar)	*7.76*
Source Pressure (mbar)	$3.39x10^{-3}$
Sample Plate Pressure (mbar)	$1x10^{-6}$

*italicized text indicates parameters that vary most from normal operation of the instrument for peptide/small molecule analysis.

Thermo Exactive Plus EMR

The ion optics for the Exactive Plus EMR are depicted in Figure A4.4. The main difference between normal operation and EMR mode on the Exactive Plus is where the ions are trapped before entering the mass analyzer. [1,4,3] When analyzing smaller molecules, they are trapped in the C-trap before entering the orbitrap for mass analysis. In EMR mode, high mass ions pass through the C-trap and are trapped in the HCD cell which can be operated at higher pressures. The higher trapping pressures collisionally cools and stabilizes the ions and also results in more complete desolvation.[3] This is vital to successfully analyzing large intact proteins.

Method/Instrument Parameters:

SID Energy: 80
CE: 40
Resolution: 17,500
Microscans: 1
Maximum Ion Injection Time: 50 ms
AGC Target: 5e6
S-lens RF: 100
Capillary T: 200
Trapping Pressure: 6
C-trap Charge Detection: off
Mass Range: 1000-3000 m/z (variable)

The trapping pressure and the SID energy were determined to have the most impact on the signal intensity and resolution of the intact mAb mass spectra. Figure A4.5 shows the effect increasing the SID energy has on the signal intensity for intact mAb separations. This data was taken on a Thermo qExactive operating in protein mode, but the same trend follows for the Exactive Plus EMR. Without any SID energy, the signal intensity is very low and the charge state peaks of the mAb are quite wide indicating insufficient desolvation. However, as the SID energy is raised the signal intensity and resolution of the mass spectra drastically increases also.

Figures and Tables

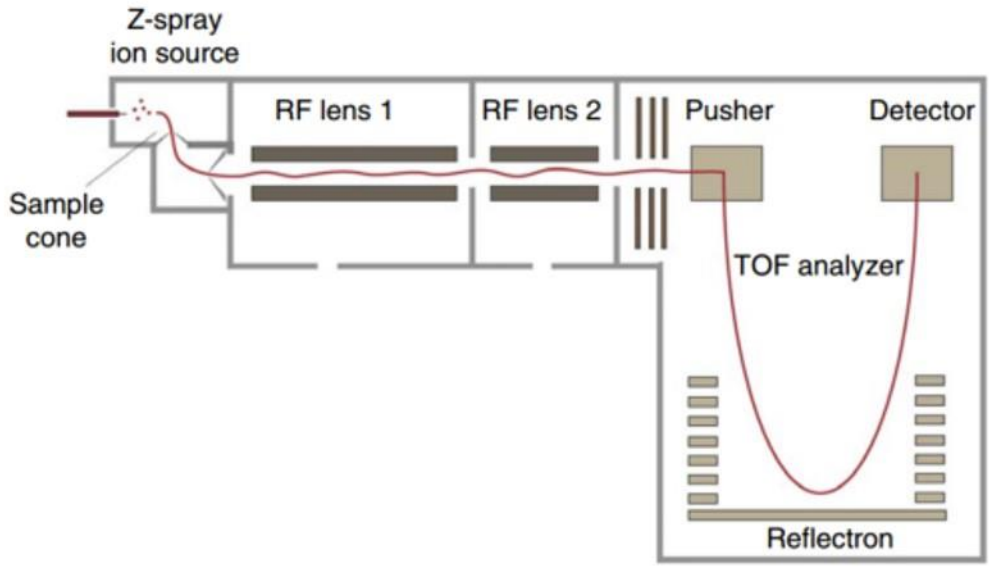

Figure A4.1: Ion optics of the LCT-Premier.[4] RF lens 1 and 2 refer to hexapoles. The instrument has fairly simple ion optics which facilitates the transfer of high mass ions.

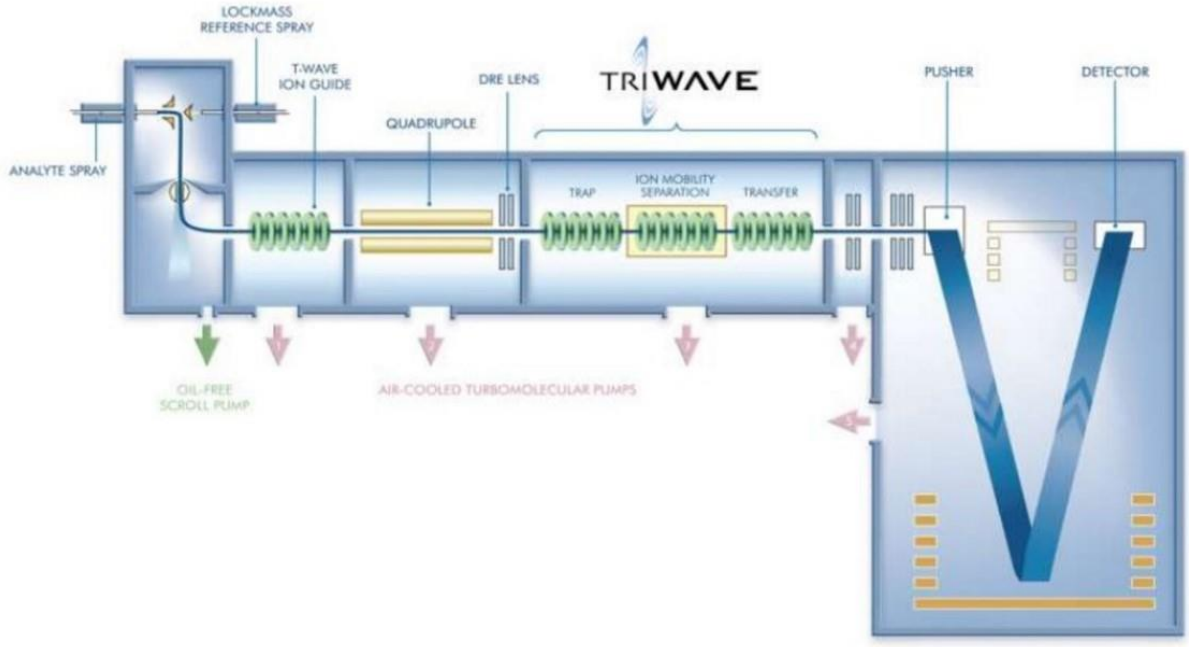

Figure A4.2: Ion optics of the Waters Synapt G2. The Synapt G2 has a quadrupole before the mass analyzer which provides the option of performing MS/MS experiments. However, if the quadrupole is not capable of using lower frequency RF, it can limit the transfer of high mass ions.

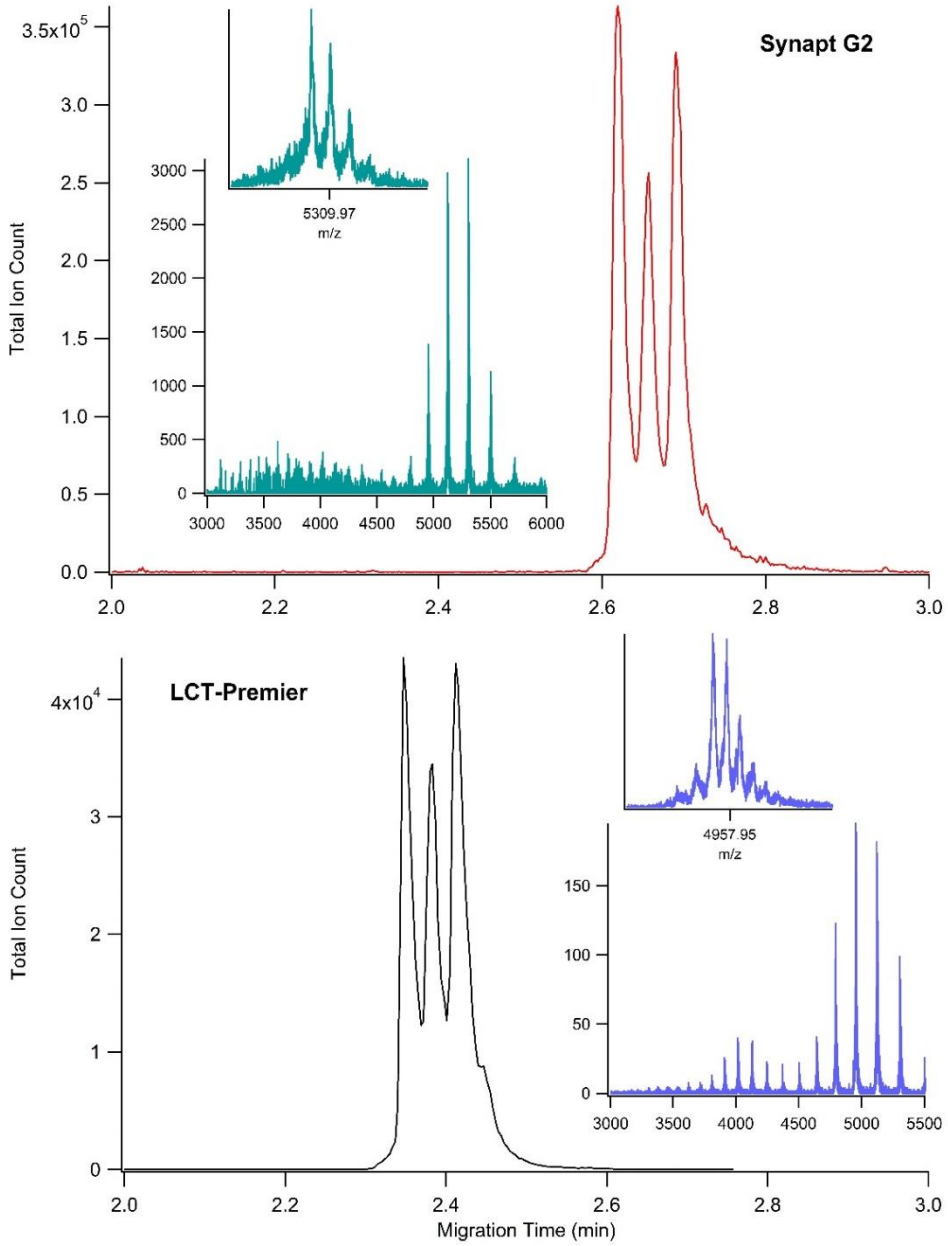

Figure A4.3: Comparison between the LCT-Premier and the Synapt G2 for intact mAb analysis. The results obtained on both instruments are similar, but the sensitivity of the Synapt G2 does not match that of the LCT. Although there is glycoform definition within the charge states of the G2 mass spectrum, some of the minor species are not detected. The insets show the raw mass spectra for the third main variant and a zoomed in view of the most abundant charge state in the spectrum.

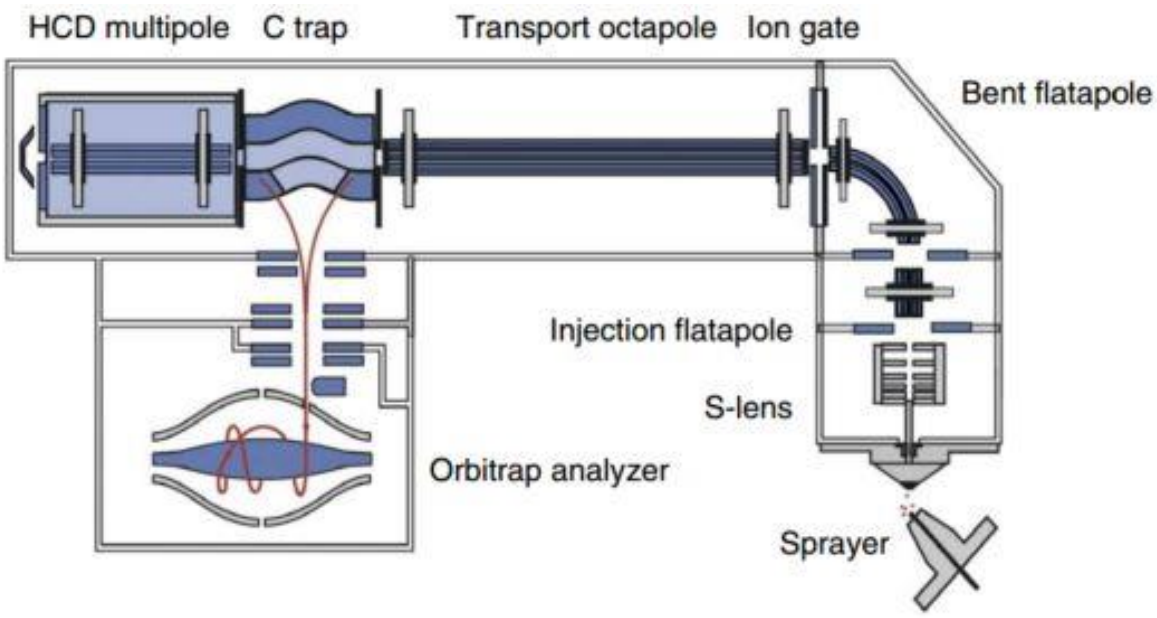

Figure A4.4: Ion optics of the Exactive Plus.[4] In EMR mode the ions are trapped in the HCD cell which is typically at elevated trapping pressures. They are then transferred to the orbitrap for mass analysis.

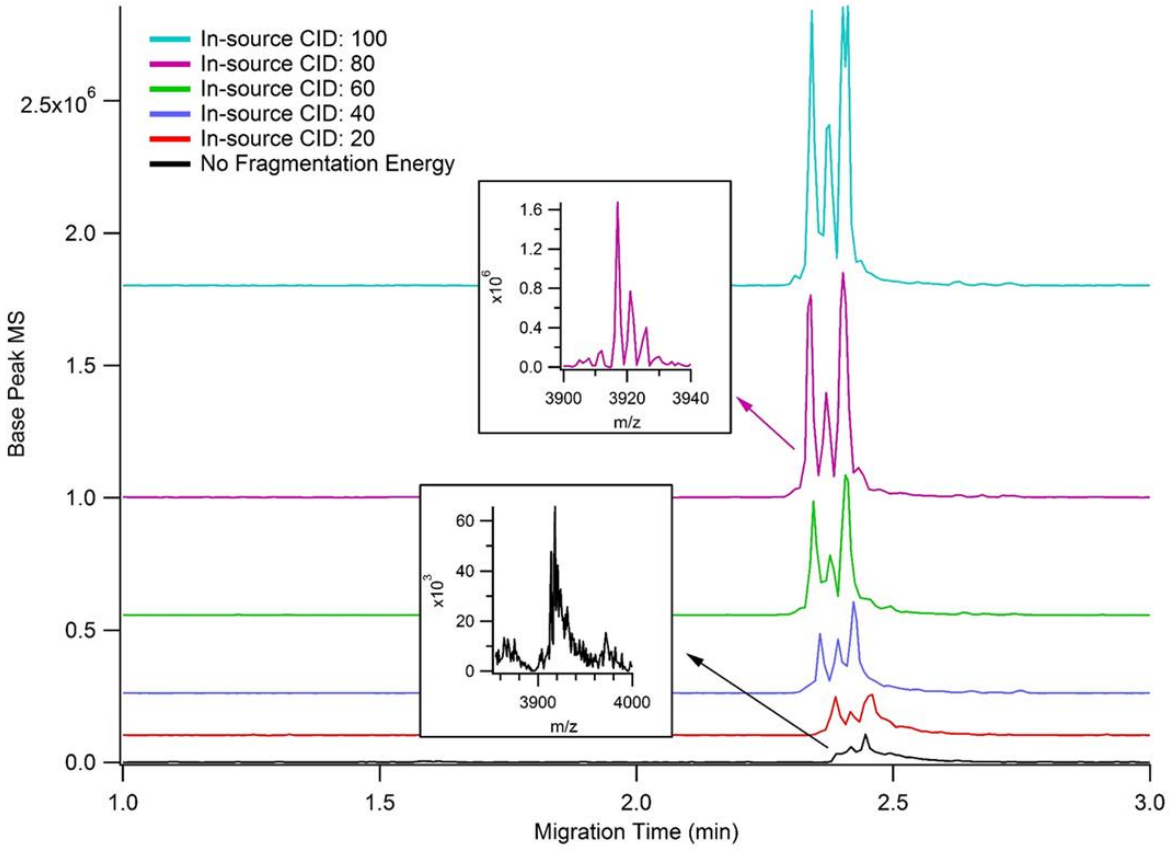

Figure A4.5: Effect of SID energy on signal intensity in Thermo orbitrap instruments. At elevated trapping pressures, the quality of the resulting mass spectra significantly increases with elevated SID energy.

REFERENCES

(1) Thompson, N. J.; Rosati, S.; Heck, A. J. R. *Methods* **2014**, *65* (1), 11–17.

(2) Commandeur, J.; Sons, M.; Connolly, T.; Wortel, N.; Vision, M. S.; Ab, N. L. High-mass Q-ToF upgrade for MS / MS studies of intact non-covalent complexes http://msvision.eu/technologies/ms-vision-high-mass-q-tof (accessed Feb 1, 2016).

(3) Rose, R. J.; Damoc, E.; Denisov, E.; Makarov, A.; Heck, A. J. R. *Nat. Methods* **2012**, *9* (11), 1084–1086.

(4) Rosati, S.; Yang, Y.; Barendregt, A.; Heck, A. J. R. *Nat. Protoc.* **2014**, *9* (4), 967–976.